REPORT NO.
UCB/EERC-80/38
SEPTEMBER 1980

EARTHQUAKE ENGINEERING RESEARCH CENTER

INELASTIC SEISMIC ANALYSIS OF LARGE PANEL BUILDINGS

by
VAHID SCHRICKER
GRAHAM H. POWELL

Report to Sponsor:
National Science Foundation
Grant No. PFR-7908257

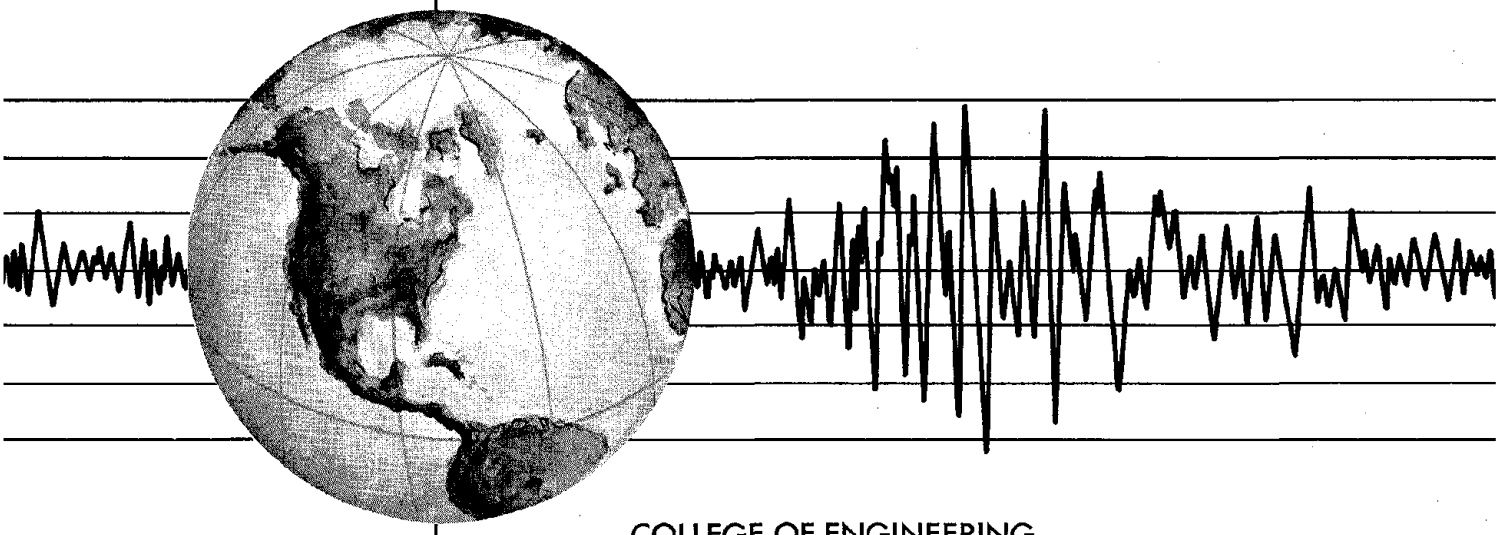

COLLEGE OF ENGINEERING

UNIVERSITY OF CALIFORNIA · Berkeley, California

For sale by the National Technical Information Service, U.S. Department of Commerce, Springfield, Virginia 22161.

See back of report for up to date listing of EERC reports.

50272-101

REPORT DOCUMENTATION PAGE	1. REPORT NO. NSF/RA-800198	2.	3. Recipient's Accession No. PB81 154338

4. Title and Subtitle
Inelastic Seismic Analysis of Large Panel Buildings

5. Report Date
September 1980

6.

7. Author(s)
V. Schricker and G. H. Powell

8. Performing Organization Rept. No.
UCB/EERC-80/38

9. Performing Organization Name and Address
Earthquake Engineering Research Center
University of California, Berkeley
Richmond Field Station
47th Street & Hoffman Boulevard
Richmond, Calif. 94804

10. Project/Task/Work Unit No.

11. Contract(C) or Grant(G) No.
(C)
(G) PFR-7908257

12. Sponsoring Organization Name and Address
National Science Foundation
1800 G Street, N.W.
Washington, D.C. 20550

13. Type of Report & Period Covered

14.

15. Supplementary Notes

16. Abstract (Limit: 200 words)

Large panel structures behave differently from frame and monolithic wall structures because of the distinct planes of weakness in the horizontal and vertical joints between panels. These joints may slide and open during shaking, producing large localized changes in the bending and shear stiffnesses. Special modelling techniques are thus needed for analysis of the inelastic dynamic response.

A mathematical model for inelastic seismic analysis of two-dimensional large panel structures is described. The wall panels are idealized either by elastic beam-type elements or by two-dimensional finite elements. The joints are idealized by nonlinear spring elements, with a variety of possible force-deformation relationships. FORTRAN subroutines for several panel and joint elements have been developed and incorporated into the computer program DRAIN-2D. To account for the large, sudden changes in stiffness in the mathematical model a modified step-by-step integration strategy has also been incorporated into the DRAIN-2D program.

Using DRAIN-2D, a parameter study has been carried out on a multi-story, single-bay, large panel wall to determine the influence of design and analysis assumptions on the computed nonlinear response, considering both slip and opening at the joints.

This report contains a review of the behavior of joints in large panel structures, a description of the modelling procedure and the DRAIN-2D elements, and a detailed discussion of the parameter study.

18. Availability Statement: Release Unlimited	19. Security Class (This Report)	21. No. of Pages
	20. Security Class (This Page)	22. Price

INELASTIC SEISMIC ANALYSIS OF LARGE PANEL BUILDINGS

by

Vahid Schricker
Graduate Student

and

Graham H. Powell
Professor of Civil Engineering

Report to
National Science Foundation
under Grant No. PFR-7908257

Report No. UCB/EERC-80/38
Earthquake Engineering Research Center
College of Engineering
University of California
Berkeley, California

September 1980

ABSTRACT

Large panel structures are used extensively in seismic regions, yet relatively little is known about their performance during earthquakes, particularly their ability to survive very strong shaking. Large panel structures behave differently from frame and monolithic wall structures because of the distinct planes of weakness in the horizontal and vertical joints between panels. These joints may slide and open during shaking, producing large localized changes in the bending and shear stiffnesses. Special modelling techniques are thus needed for analysis of the inelastic dynamic response.

A mathematical model for inelastic seismic analysis of two-dimensional large panel structures is described. The wall panels are idealized either by elastic beam-type elements or by two-dimensional finite elements. The joints are idealized by nonlinear spring elements, with a variety of possible force-deformation relationships. FORTRAN subroutines for several panel and joint elements have been developed and incorporated into the computer program DRAIN-2D. To account for the large, sudden changes in stiffness in the mathematical model a modified step-by-step integration strategy has also been incorporated into the DRAIN-2D program.

Using DRAIN-2D, a parameter study has been carried out on a multi-story, single-bay, large panel wall to determine the influence of design and analysis assumptions on the computed nonlinear response, considering both slip and opening at the joints. The results show that nonlinear joint behavior has a large effect on the computed response and that the response depends substantially on the modelling assumptions. An important

conclusion from the study is that if the joint design is such that the shear strength decreases with increasing slip, undesirable concentration of deformation in a few joints may result.

This report contains a review of the behavior of joints in large panel structures, a description of the modelling procedure and the DRAIN-2D elements, and a detailed discussion of the parameter study.

ACKNOWLEDGEMENTS

The research described in this report was performed under the sponsorship of the National Science Foundation, Grant No. PFR-7908257. The support of the National Science Foundation is gratefully acknowledged.

Invaluable assistance was provided by Mary Carol Randall and Linda Calvin in typing the report and Gail Feazell, Amy Pertschuk, and Mary Edmunds-Boyle in drafting the figures.

The principal author particularly wishes to thank his wife, Lili, for her patience, understanding and encouragement.

TABLE OF CONTENTS

Table of Contents (Continued) Page

Table of Contents (Continued) Page

Table of Contents (Continued) Page

Table of Contents (Continued) Page

1. INTRODUCTION

1.1 GENERAL

Large panel buildings have been used for many years in zones of seismic risk such as Japan, the Soviet Union, Yugoslavia and Romania. A survey of destructive earthquakes in the Soviet Union [37] has shown that while many brick and some frame buildings failed or were severely damaged, most large panel buildings suffered only cracks in the joints between panels. In some large panel structures, however, significant joint deformations and local joint damage were observed. Fintel's report [17] on the March 1977 Romanian earthquake (Richter magnitude 7.2) indicates that large panel buildings withstood the shaking with minimum distress. Velkov [29] has also reported the satisfactory performance of large panel structures during the Romanian earthquake, and has suggested wider application of these structures for tall buildings in seismic zones. In spite of this successful record, relatively little is known about the performance of large panel buildings in earthquakes. This is particularly true of the structural systems likely to be used in the United States.

Under external loads, large panel structures behave quite differently from frame and monolithic wall structures, because of the distinct planes of weakness in the horizontal and vertical joints between panels. These joints may slide and open during shaking, producing large localized changes in the bending and shear stiffnesses of individual walls. Special modelling techniques are thus required for analysis.

Comprehensive reviews of the design and analysis of large panel

structures, with particular emphasis on applications in the United States, have been published by Zeck [68], Frank [34], Fintel, Schultz and Iqbal [32], Kripanarayanan and Fintel [69], and Becker and Llorente [48]. Earlier studies of these structures can be found in textbooks by Lewicki [51] and Polyakov [35]. Hawkins [70] has surveyed the state-of-the-art on earthquake resistance of precast concrete structures, and has reviewed several test results on joints between large panels.

The structural behavior of large precast panel buildings depends on the relative strengths and stiffnesses of the panels and joints. It is generally accepted that earthquake-induced damage will usually occur in the joints, while the panels will remain essentially elastic. Modelling of the inelastic behavior of joints is thus particularly important.

1.2 OBJECTIVE

The first purpose of the study described in this report has been to develop a mathematical model for inelastic seismic analysis of two-dimensional large panel structures. A second objective has then been to study the earthquake response of large panel structures with a variety of joint force-deformation relationships under a variety of ground motions, to determine the influence of design features on the structural behavior.

In the mathematical model, the wall panels are idealized by elastic beams and by two-dimensional finite elements, and the joints are idealized by nonlinear spring elements with a variety of force-deformation relationships. Several panel and joint elements have been developed, and incorporated into the computer program DRAIN-2D [45, 65]. Modifications have been made to DRAIN-2D to improve the step-by-step solution strategy for cases with large, sudden stiffness changes. A parameter

study has been carried out on a multi-story, single-bay, large panel wall, to determine the influence of design and analysis assumptions on the computed nonlinear response.

The results show that inelastic joint behavior has a large effect on the computed response, and that the response depends a great deal on the joint force-deformation relationship. An important conclusion is that joints which lose strength as they deform can produce undesirable response characteristics.

1.3 REPORT CONTENTS

Chapter 2 contains a survey of available test data on the behavior of joints under cyclic loads. The important features of the behavior of joints of different types are identified, with a view to constructing mathematical models.

Chapter 3 discusses idealization procedures for large panel structures. Previous analytical work is reviewed, and the mathematical model used in this report is described. The computer program DRAIN-2D is briefly reviewed, and a weakness in its simple step-by-step dynamic analysis strategy is identified. A modified strategy which has been added to the program is described.

In Chapter 4, detailed descriptions of the mathematical models for two panel elements and seven joint elements are presented. Chapter 5 presents the results of the parameter study on a multi-story large panel wall. Particular attention is directed to studying the effect of joint characteristics on the computed inelastic response. Concluding remarks are presented in Chapter 6.

Appendix A presents details on the modified step-by-step strategy. Appendix B describes recommended computer programming logic for elements

with multi-linear force-deformation relationships. Element user's guides are presented in Appendix C.

2. JOINTS IN LARGE PANEL STRUCTURES

2.1 GENERAL

The joints in large panel structures transfer shear and normal forces from one panel to another. In a strong earthquake, the joints may deform by sliding, opening, cracking and crushing. Ideally, they should be designed to provide a balance of strength and ductility, so that the strength of the connected panels is neither exceeded nor underutilized, and so that deformations of the joints are not excessive. From the point of view of both analysis and design, the joints are the most critical areas.

The problems of joint design are not considered in this report. Rather, the purpose of the report is to develop a procedure for estimating the forces and deformations in joints with specific properties.

A typical horizontal joint is subjected to complex force distributions, consisting, in general, of all of the forces shown in Fig. 2.1.1. However, for the analyses described in this report, it is assumed that the only significant forces are the shear force, F_s, and the bearing force, F_n. The joint models described in Chapter 4 allow for slip under force F_s and opening or crushing under force F_n. Because the force-deformation characteristics of joints vary substantially with the design of the joint, several different joint models have been developed.

2.2 UNREINFORCED WET JOINTS

"Wet" connections are made by casting or packing mortar between the panels after they are erected. Figure 2.2.1 shows the cross section of a typical horizontal connection ("platform" connection) used in U.S. practice. The joint is under compression due to gravitational loads or

posttensioning, so that shear can be transferred by friction between the panels and the joint. The frictional shear strength is essentially the coefficient of friction multiplied by the compressive force on the joint. If the induced shear force exceeds this value, slip can occur. The strength can be increased by adding shear keys and by passing vertical reinforcing through the joint. The initial strength may also exceed the frictional strength because of bond between the panels and the joint mortar.

Verbic [6] investigated the inelastic behavior of wet connections of the type used in the Yugoslavian "Vranica" building system. Horizontal connections were first subjected to vertical compressive loads, and then deformed cyclically (displacement controlled tests) under horizontal loads. The vertical load was kept constant during each test. Because the shear force was applied above the level of the joint, the bending moment on the joint plane was not zero.

Figure 2.2.2 shows the behavior of an unreinforced connection with only the panel self weight producing vertical load. The figure shows an abrupt initial loss of strength presumably due to loss of bond. For subsequent loading the joint exhibits elastic-plastic-strain-hardening behavior, with degradation of the "strain hardening" stiffness under repeated loading. This stiffness loss can be attributed to polishing of the joint surfaces, and to accumulation of loose sand particles which facilitate sliding.

For an unreinforced joint with added vertical load, the behavior is as shown in Fig. 2.2.3. The joint again exhibits initial strength loss followed by degradation of the "strain hardening" stiffness. However, the initial strength loss is now a substantially smaller proportion of the total strength, and the overall behavior is of essentially elastic-per-

fectly-plastic type.

For design and analysis, the coefficient of friction in the joint is an important parameter. For the Verbic tests, Fig. 2.2.4 shows the initial maximum strength as a function of the vertical pressure (line "A"). If it is assumed that the bond strength is a constant, the proportion of the strength which results from friction can be found (line "B"). From this line the effective friction coefficient ranges from 0.96 for small vertical load to 0.66 for the maximum considered in the tests. For a similar situation, Brankov and Sachanski [7] have suggested a friction coefficient of 0.4, which may further decrease with cyclic loading and higher bearing loads. Fintel, Schultz and Iqbal [32] report that coefficients of friction specified by design codes vary from 0.2 to 0.8, with a value of 0.7 commonly used for static load design of precast prestressed joints.

The initial bond strength and the subsequent strain hardening stiffness are also important parameters. If a connection has strong initial bond, substantial loss of strength can occur when the bond fails [6, 21]. Possible types of behavior are shown in Fig. 2.2.5. The analyses described in Chapter 5 indicate that strength loss can lead to undesirable behavior during an earthquake. On the other hand, if the strain hardening stiffness is substantial, a joint will gain strength as it deforms, which can lead to more desirable seismic response.

From the available test results, many aspects of joint behavior are not clear. These aspects include (1) the amount of initial bond strength; (2) whether this strength can be relied on, or whether shrinkage can break the bond; (3) the "strain hardening" stiffness and the degradation of this stiffness under cyclic loading; and (4) the magnitude of the

coefficient of friction. More tests are needed before the load transfer mechanisms in even simple unreinforced joints can be identified sufficiently clearly to allow rational analysis.

2.3 KEYED JOINTS

In wet connections, the panel edges may be plain, grooved, or keyed (castellated), as shown in Fig. 2.3.1. Keyed edges are often used in vertical connections, and provide increased shear resistance through interlocking of the keys.

Most tests on keyed connections have considered only monotonically increasing load [9,10,11,21]. Figure 2.3.2 shows typical behavior for a keyed vertical joint with different key characteristics under increasing load. The figure indicates that keys can provide substantial strength but that strength is lost as the keys fail. The connection failure may be shearing or crushing of the keys, or by diagonal tension cracks in the joint mortar. The "residual" shear resistance, after failure of the keys, depends on friction or, for reinforced keyed connections, on both friction and the strength of the reinforcing bars crossing the joint.

The addition of reinforcement across a keyed joint greatly improves its ductility, and after failure of the keys the residual shear resistance depends a great deal on the amount of reinforcement [10]. The maximum strength of a keyed connection depends on the shape and dimensions of the keys and the spacing between them [9,10]. However, the residual strength of the connection depends much less on the geometry of the keys [21].

Lacombe and Pommeret [21] tested keyed joints under cyclic loads (force controlled tests). In these tests, the connection was subjected

to cyclic loading equal to a specific fraction of the joint strength obtained under monotonic loading. The results showed progressively decreasing stiffness, as indicated in Fig. 2.3.3. The hysteresis loops for cyclic loading are "pinched", indicating low energy absorbing capability. It was observed that the cyclic loading did not affect the residual strength of the connection. After failure of the keys, the cyclic behavior of the connection depended on the amount of tranverse reinforcement and on the compressive load normal to the joint.

Santhakumar, et al. [13] performed cyclic load tests on vertical keyed connections with transverse reinforcement. The tests showed loss of strength and reduction in the joint stiffness of 70% as diagonal cracks formed in the joint.

Velkov, et al. [12] have described tests on both horizontal and vertical connections used in a modification of the French "Balency" system. The tests were force controlled with repeated (not reversed) loading. The joints were reinforced, and were tested both with and without imposed compressive force normal to the joint. It was concluded that panels with keyed edges had joint strengths and ductilities more than 50 percent larger than panels without keys. Nevertheless, it was concluded that keyed joints with zero applied compressive force did not exhibit great ductility. When compressive force was added, both the shear resistance and the ductility were greatly increased.

As for unreinforced wet joints, more tests are needed on keyed joints before their behavior can be understood and a sound mathematical model for seismic response can be developed.

2.4 REINFORCED WET JOINTS

If a wet joint is reinforced, its behavior is significantly affected

by the reinforcing bars which cross the joint. In reinforced wet joints, reinforcing bars pass through the joint perpendicular to the joint plane. The reinforcement may consist of continuous bars grouted in place, bars which project from the panels and are welded in the joint region, or stirrups which interlock in the joint region and are connected by longitudinal bars through the projecting loops. The area of reinforcement is usually only a small proportion of the joint area.

The reinforcement provides additional strength, partly by dowel action and partly by aggregate interlock and "shear friction" [2,41, 56]. The aggregate interlock and shear friction mechanisms have been termed "interface shear transfer" (IST) by Gergely, White, et al. [15,16]. The shear friction resistance results from the development of tension in the reinforcement as the joint deforms. The tension produces an equal normal compression (clamping force) on the joint surface, and hence increases the friction. The maximum normal compression which can be developed is governed by the area and yield strength of the reinforcement.

Most shear tests of reinforced joints have been performed for conventional reinforced concrete, in order to determine the shear strength of beams and walls after tension cracks develop [14,15,16,18,42,55], and to determine the behavior of construction joints [2,3,20]. In these tests, the amount of reinforcement crossing the joint is substantially larger than for typical joints between large panels. Also, the effects of aggregate interlock are larger for rough cracks than for the relatively smooth joints between precast panels. Nevertheless, the behavior is qualitatively similar.

Shear tests on reinforced concrete are typically carried out by pre-cracking the test specimen and then applying shear force. Typical

results obtained from such tests are shown in Figs. 2.4.1 and 2.4.2.

The diagrams in Fig. 2.4.1 wre obtained by Mattock using load-controlled tests [2,3]. They show that they hysteresis loops change shape as the shear force and the number of load cycles increase. The initial loop is of essentially elastic-plastic-strain-hardening type. However, under cyclic loading the stiffness degrades, and near failure the hysteresis loop has a characterisitc "pinched" form. In the regions AB and A'B' (Fig. 2.4.1), the specimen has low stiffness, and develops only small shear resistance. In this region the reinforcement develops little or no clamping action, because the crack is open. The resistance in this region results mainly from aggregate interlock, which decreases and deteriorates as the concrete surrounding the reinforcing bars becomes damaged. Beyond points B and B' the reinforcement develops tension force, providing a clamping action which increases both the friction and aggregate interlock effects. This results in a rapid increase in stiffness and strength. Under cyclic loading, deterioration of the concrete leads to progressive extension of the regions AB and A'B'.

Mattock's work [20] on the effect of reinforcing bar size on shear transfer has shown that the contribution of dowel action is relatively small, and that the transfer of shear across a crack is primarily due to friction and aggregate interlock. Tests reported by Paulay, et al. [41] on shear transfer across construction joints similarly indicate that the contribution of dowel action can be ignored for design purposes.

Mattock's tests also showed that the shear strength available under cyclic loading is less than under monotonic loading. Becker and Llorente [48] have suggested that strength loss under earthquake

loading should be taken into account by assuming a smaller friction coefficient than would be appropriate for static loading.

Shear tests on cracked reinforced concrete have also been conducted by White, Gergely and others at Cornell University. Figure 2.4.2, obtained by Laible, White, and Gergely [59], shows two hysteresis loops in a series of loops obtained by cycling at constant load. In these tests the reinforcing bars were placed outside the specimen to eliminate dowel action. Substantial deterioration of stiffness takes place as the number of cycles increases, and there is a progressive increase in displacement. At each load level, most of the degradation occurred in the first few cycles, with relatively stable loops for later cycles. Jimenez, Gergely and White [54] concluded that the interface shear transfer mechanism carried between 65 and 80 percent of the total applied shear, with the remainder carried by dowel action.

In all of the above tests, there was no compressive force imposed normal to the cracks. Tests results reported by the Portland Cement Association [55] on isolated shear walls indicate that the presence of vertical force adds simple friction to the "shear friction", and hence the hysteresis loops become "fatter".

The only cyclic load tests on large panel joints with reinforcement appear to be those of Verbic [6]. The behavior of the unreinforced joints in this test series were considered in Section 2.2. Typical results for reinforced joints are shown in Figs. 2.4.3 and 2.4.4.

In the Vranica system, continuity is provided by grouted unstressed reinforcement passing vertically through the panels and joints. The amount of reinforcement in the Verbic tests was only 0.33% of the wall area. No attempt was made to break bond on the joint surface be-

fore the tests. The tests were displacement controlled, with four complete cycles of deformation at each displacement level.

Figure 2.4.3 shows the results for a joint with only the self weight of the panel providing vertical bearing force. The figure shows an abrupt initial loss of strength when bond is broken, followed by further loss of strength as the cyclic deformation increases. This behavior is similar to that obtained for an unreinforced joint (Fig. 2.2.2). However, Fig. 2.4.3 shows a larger initial strength compared with the unreinforced joint (550 vs. 90 kN). The reinforced joint also developed greater shear resistance after several loading cycles, and greater "strain hardening" than the unreinforced joint (for example, in the last cycle, 40 kN increasing to 200 kN in Fig. 2.4.3, versus 30 kN increasing to 40 kN in Fig. 2.2.2). As in the tests on cracked reinforced concrete specimens, the stiffness degraded under cyclic loading.

Figure 2.4.4 shows the result for a joint with substantial imposed vertical load. The initial strength is approximately 900 kN, compared to 600kN for the similar unreinforced joint (Fig. 2.2.3). Also, the reinforced joint has greater subsequent resistance and greater "strain hardening" (for example, 750kN increasing to 900kN in Fig. 2.4.4 compared with 600kN with no increase in Fig. 2.2.3).

Qualitatively, when bearing force is not present, the behavior of a reinforced joint exhibits high initial resistance, which deteriorates dramatically as cycling increases. In a typical cycle, the hysteresis loop has the pinched shape characteristic of "shear friction" behavior, but the stiffness gain at the end of the loop is less dramatic than in the reinforced concrete tests. For the case with a large bearing force,

the behavior tends to be dominated by "simple" friction, with less dramatic changes in the shapes of the hysteresis loops. Also, with large bearing forces, there are relatively small differences in behavior between reinforced and unreinforced joints.

Yeroushalmi and Harris [43] conducted a series of small scale tests (1/16 scale) on panels with wet vertical joints under both monotonically increasing and cyclically reversing shear loads. Reinforcement was provided in horizontal joints above and below the test section. Bond was not broken before the test began. The tests were load-controlled, with the shear force increased in each load cycle until the joint failed. The results under monotonic loading showed an abrupt mode of failure, associated with sudden loss of bond strength. The results under cyclic loading showed progressive reductions in strength and stiffness. The behavior again appeared to be dominated by bond, with sudden failure and no noticeable "shear friction" type of behavior. Because of their small scale, the behavior of these joints may not be representative of full scale joints.

2.5 DRY JOINTS WITH MECHANICAL CONNECTORS

In dry joints, the panels are connected through steel plates in the panels. Anchorage may be provided by shear studs or by embedded reinforcing bars, and the plates may be connected by bolting or welding. Figure 2.5.1 shows a typical dry connection. Vertical joints in the United States are almost all of the dry type.

Connection failure can take place in the plate-to-plate connection, in the embedded bars, or in the concrete around the insert. Failure in the plate-to-plate connection is likely to be brittle, and would normally be avoided.

Spencer and Neille [5] investigated the behavior of a commonly used type of welded connection under cyclic shear (displacement-controlled tests). Figure 2.5.2 shows a typical connection detail. The measured load-deflection relationship for a single connection is shown in Fig. 2.5.3. For cyclicing below about 85% of the monotonic strength, there was no degradation of stiffness. For cycling above this force level, the behavior was as shown in Fig. 2.5.3. This is typical "shear friction" behavior, with stiffening at the end of each cycle, and progressive degradation of stiffness and strength as the cyclic deformation increases. After each increase in displacement, the displacement amplitude was typically held constant for three or four cycles. It was observed that under constant amplitude cycling, both the stiffness and strength decreased for a few cycles before the hysteresis loop stabilized. At this level of loading, identified as the "stability limit", no further degradation occurred. Spencer and Neille constructed a "yield" envelope, based on the strength observed for the first cycle in each series, and a "stability" envelope based on the stability limits (Fig. 2.5.3).

The first observable damage in each connection was crushing of the concrete at the end of the connection angle. As cyclic loading progressed, there was continued crushing and spalling of the concrete above and below the angle, and growth of tension cracks. Although no observations could be made, it was presumed that the concrete failed around the studs, allowing the studs to deform. This would explain both the steadily degrading stiffness and the hardening characteristics observed in each cycle. The connections typically failed completely by fracturing of the studs, close to the welds connecting them to the connection angles.

Spencer and Neille concluded that these connections have considerable capacity to deform beyond their yield points, and that they should have satisfactory performance in earthquake, if properly designed and detailed.

In a later report, Neille [39] identified three mechanisms for the transmission of shear forces through joints of this type, namely 1) friction between the plates and the concrete; 2) bearing of the end of the plate on the concrete, and 3) bearing between the embedded studs and the concrete. From a series of tests designed to separate these effects, he concluded that the two bearing mechanisms were dominant. It is interesting to note that tests on cracked reinforced concrete have indicated that "shear friction" effects are dominant and that bearing (dowel action) effects are relatively small [54,20,41].

In order to provide more explicit control over energy absorption capability, Pall and Marsh [40] have proposed the use of additional clearance in the slotted holes of bolted connections for the "Descon/ Concordia" system [4]. In these joints the connection plates are bolted together with high strength bolts. When the bolt holes are slotted, the joints can be designed so that movement first occurs by sliding between the plates. The slot clearance limits the amount of slip. If the deformation exceeds the clearance, the subsequent behavior would presumably be similar to that observed by Spencer and Neille.

Experimental results from tests on such limited-slip bolted joints are shown in Fig. 2.5.4. For monotonic loading, the behavior is essentially rigid plastic, with strength and stiffness increase after the bolt reaches the end of the slotted hole. Under cyclic loading deformations which are less than the available clearance, the behavior is

again essentially rigid-plastic, but with strength changes from cycle to cycle. The strength of the joint depends on surface finish between the connecting plates. Under cyclic deformation, there was substantial degradation of the friction resistance for the mill scale, sand blasted and painted surfaces. However, for the "metalized" surface the effective friction coefficient increased with increased cycling.

These tests indicate that friction bolted joints have desirable ductility characteristics with good capacity for energy absorption. It should be possible to control the strength and energy dissipation characteristics by appropriate choice of joint surface and clearance for the slotted holes. The reserve of strength after the movement exceeds the available clearance; this is probably an advantage. Finally, since there is no yielding of material in the joint, there should be minimum need for repairs following an earthquake.

2.6 JOINT OPENING

Under gravity load only, a horizontal connection will be completely under compression. As the wall is subjected to horizontal load, opening between the wall panels and the joint will occur if the tensile stresses due to bending of the walls exceed the initial compressive stresses. Additional resistance to these tensile stresses may be provided by transverse reinforcing bars across the joint or by posttensioning bars. It may not be economically feasible to restrain the joint opening completely. Moreover, restraining joint opening may be unwise, because opening can significantly reduce the forces in the structure.

When a connection opens, there will be increased bearing and shear stresses on that portion of the connection which remains closed.

This could lead to a crushing failure of the connection, or to splitting failure of the panel corners [8,35,48]. Thus, the joints must be designed to have adequate crushing resistance, and the panel corners must be sufficiently reinforced to prevent splitting under combined bearing and shear stresses.

There appear to be no experimental results available on the characteristics of joints under tension, or on the behavior of joints with opening under combined bearing and shear forces. It may be noted, however, that experiments [52,53] on the strength of platform type horizontal joints under compressive loads indicate that a typical joint has much smaller strength and stiffness than a typical wall panel (less than 50 percent).

2.7 SUMMARY

From the review of joint behavior presented in this Chpater, it can be seen that the behavior is complex, and that several different types of behavior are possible. However, the following important aspects of behavior can be identified.

(1) In unreinforced wet joints, the shear transfer is dominated by friction developed under the bearing forces due to gravity or post-tensioning.

(2) The magnitude of the coefficient of friction has not been definitely determined. Values ranging from 0.2 to 0.8 have been reported. The effective coefficient of friction reduces under cyclic loading.

(3) Keyed joints develop higher initial shear strength than plain joints, but lose strength as the keys fail. The strength loss may be gradual or sudden, depending on the

design.

(4) Substantial initial shear strength appears to be developed by bond. When the bond resistance is overcome, the strength drops suddenly. It is not clear whether shrinkage or other effects could break the bond.

(5) Under cyclic loading, keyed joints and joints with bond are weaker than under monotonic loading.

(6) Reinforced joints under small bearing forces exhibit "shear friction" behavior, characterized by "pinched" hysteresis loops. The stiffness degrades substantially under cyclic loading.

(7) In reinforced joints under larger bearing forces, simple friction behavior is combined with the "shear friction" behavior. With large bearing forces, the simple friction dominates.

(8) Dry joint without slotted holes have behavior which is qualitatively similar to that of reinforced wet joints. Dry joints with slotted holes exhibit essentially rigid-plastic behavior, with change in shear strength under cyclic loading. The strength may decrease or increase, depending on the surface preparation of the joint plates.

(9) There is a lack of information on the opening and crushing characteristics of joints. The joints will generally be weaker than the adjacent panels. However, failure of the panel corners under combined bearing and shear forces may be possible.

3. IDEALIZATION OF LARGE PANEL STRUCTURES

3.1 GENERAL

A large panel structure can be regarded as a shear wall structure with weak pre-cracked planes at the horizontal and vertical joints. The behavior of a large panel structure will be different from that of monolithic shear wall, however, because of localized deformations in the joints.

Monolithic shear wall structures have been analyzed by a variety of methods, using beam and frame idealizations [33,35,49], continuous-medium idealizations for coupled walls [50], and detailed finite element idealizations [36]. A similar range of techniques can be used for analyzing large panel structures. However, relatively few analyses of large panel structures have been reported.

3.2 IDEALIZATION PROCEDURES

Macleod [33], Fintel, et al. [32], Frank [34], and Becker and Llorente [48] have outlined modelling and analysis techniques for structural walls, including large panel structures. The possible methods include the following.

1. Beam Model - The structure is modelled as a cantilever beam with mass either uniformly distributed or lumped at the floor levels. Both flexural and shear deformations may be considered. Flexibility in horizontal joints can be accounted for by introducing short, flexible beams to model the joint regions.

2. Continuous Medium Model - For walls connected by vertical joints or by spandrel beams, the joints or beams can be modelled as a continuous medium in pure shear [51]. Mueller and Becker [57] have used an extended version of this method to obtain an explicit expression for the funda-

mental period of precast walls and coupled shear walls.

3. Frame Model - An equivalent frame, consisting of beam and column members, can be used to approximate a shear wall structure. The procedure is used widely for coupled shear wall analysis [58,64] and can be applied to some types of large panel structures [33]. The method is more versatile than the previous two methods, with the capability of modelling doors and windows, as well as horizontal and vertical joints [33,35]. The technique has been applied to obtain the nonlinear static [1] and dynamic [40] response of large panel structures, by assuming inelastic material characteristics for the members.

4. Finite Element Model - Finite element idealizations with 2D or 3D elements can be used if frame idealizations using 1D beam elements are inadequate. This method has been used in modelling the dynamic response of shear walls (e.g. [36]) and large panel structures [8,31,34,37,38]. This is the most versatile, but also the most expensive, procedure.

3.3 IDEALIZATION USED FOR THIS REPORT

The term "finite element" can be interpreted to include a variety of structural elements, not just conventional finite element for analysis of plane stress, 3D solids, plate bending, etc. A beam element is a type of finite element, and hence a frame idealization using 1D beam elements can be regarded as a finite element model. The mathematical model used in this report is of finite element type, using a variety of special purpose 1D and 2D elements.

For analysis, a precast panel wall or building is modelled as an assemblage of elastic panel elements connected by inelastic joint elements (Fig. 3.3.1). Each horizontal or vertical joint is modelled by one or more elements, with force-displacement relationships chosen

to model the actual behavior of joints under cyclic loading. A wall panel is idealized using either a single element with properties which model the overall behavior of the panel, or by dividing it into plane stress finite elements.

The effects which may exert significant influence on the structural response of large panel buildings are as follows:

1. Elastic and inelastic panel deformations, including crushing and cracking of the concrete, and including the effects of door and window openings.
2. Elastic and inelastic joint deformations, including sliding, opening, and crushing.
3. Thermal, shrinkage, and creep deformations of panels and joints.
4. Foundation flexibility, including deformation of the foundation structure and of the underlying soil.
5. Deformations of floor diaphragms. Such deformations are complex, especially in floors consisting of precast planks.
6. Large displacement effects, leading to significant changes of geometry either of the overall structure or of individual panels or joints.

In this report only a few of the above effects are considered. In particular, the following assumptions have been made in constructing the mathematical model.

1. A single wall can be isolated from the complete building.
2. The wall is a 2D structure, loaded in its own plane.
3. The panels are linearly elastic, so that nonlinear behavior occurs only in the joints.

4. The joints have zero thickness.
5. The modes of deformation at the joints include only sliding, gap opening, and crushing.
6. Displacements, of the whole structure and of individual joints, are sufficiently small that the geometry remains unchanged.
7. The effects of shrinkage, creep, and thermal expansion are negligible.
8. Energy may be dissipated only by hysteretic damping in the joint elements and by viscous damping in the panel elements.

The following additional assumptions have been made for the analyses described in this report. These assumptions have been made to limit the range of parameters to be studied, and are not a necessary part of the mathematical model.

1. The panels are solid, with no door or window openings.
2. A single-bay wall is considered, with horizontal joints only.
3. Masses are lumped at the floor levels.
4. Only the horizontal component of ground motion is considered.
5. Posttensioning bars, where used, are elastic.
6. The foundation is rigid.

3.4 PREVIOUS ANALYSES

Analyses of large panel structures assuming joints with elastic properties have been reported in References 12, 34, 60 and 62. Analyses considering inelastic joint properties have been reported in References 1, 7, 8, 12, 31, 40, 60, 62, and 26. Both static loads [1,12,31,62] and earthquake ground motions [7,8,12,34,40,60,62] have been considered.

Similar analyses, but with application to monolithic walls, have been reported in References 19, 33, 61, and 63.

In all cases, the panels themselves have been assumed to be elastic, and have been idealized using beam elements or 2D finite elements. Several different joint models have been described, using 1D spring elements [1,26,31,40,44] and 2D finite elements [8,34], with both linear and nonlinear force-deformation relationships.

Joints with simple friction resistance have been modelled using bilinear shear-slip relationships [26,44]. Becker et al. [44] used an elastic-plastic relationship between shear stress and shear strain, with strength dependent on the bearing stress on the joint. Schwin and Mehlhorn [31] modelled the behavior of the joints by two spring "boxes" as shown in Fig. 3.4.1a. The strength of the shear spring depended on the normal stress in the joint. The variation of shear strength with normal stress was as shown in Fig. 3.4.1b.

Neille [39] modelled the behavior of welded stud connections [5] by combining a trilinear action-deformation model (an extension of classical elastic-plastic behavior with strain hardening) with a stress-strain model for concrete adopted from work by Karsan and Jirsa [66]. A degrading strength characteristic was implemented using a quadratic function for the relationship between load decrement and maximum deflection, fitted to experimental data points by the method of least squares. Neille obtained very good agreement between the calculated behavior of his analytical model and the measured behavior for static cyclic loads. Muller and Becker [57] have modelled the same test data [5] using the simpler degrading force-deformation relationship shown in Fig. 3.4.2. Muller and Becker have also used re-

lationships as shown in Fig. 3.4.3.

The mechanisms of shear transfer across a crack in reinforced concrete structure have been modelled by a few researchers. Aktan [19] has suggested a hysteretic model with four linear segments to model shear transfer across a crack in shear walls, as show in Fig. 3.4.4. This model permits changes in the hysteresis loop with increasing crack width, but does not allow stiffness degradation under cyclic loading. Jimenez, Gergely and White [54] developed mathematical models for interface shear transfer and dowel action. They have proposed a multi-linear idealization for the hysteresis loops of each mechanism, with stiffness coefficients obtained from test data. The shapes of the loops change with the number of load cycles and are dependent on the crack width. Gates [30] has propsed a model for general degrading systems. The model incorporates an elastic element, an elastic-plastic element, and an element with cracking and crushing type of behavior, acting in parallel. The type of behavior which results is shown in Fig. 3.4.5

Joint opening has been modelled by Llorente [8] and by Powell and Schricker [26], using elements with zero strength in tension and a finite strength in compression.

3.5 JOINT MODELS DEVELOPED FOR THIS REPORT

Elements to model several types of joint behavior have been developed in the current study. The behavior modelled includes: (1) simple friction, with and without degradation of the friction coefficient; (2) strength loss following failure of shear keys; (3) "shear friction" behavior; (4) gap opening in tension; (5) joint crushing in compression; and (6) combined gap opening and sliding. Types of behavior which have not been modelled include the effect of variable

gap opening on "shear friction" response, and the effect of variable gap opening on the behavior of shear keys.

Seven different joint elements have been developed, as follows.

1. Simple friction element, with constant shear strength.
2. Friction element with a degrading friction coefficient. The shear strength reduces as slip accumulates.
3. Gap element, allowing opening of a joint in tension and either elastic or inelastic behavior in compression.
4. Combined gap-friction element, in which the shear strength is proportional to the bearing force.
5. Key element, with more-or-less sudden strength loss, to model failure of a joint key.
6. Shear friction element, with the characteristic pinched hysteresis loop, and with options for stiffness and strength degradation.
7. Stop element, which allows a limited amount of slip, then develops resistance against further movement.

These elements may be used singly or in combination. They allow a variety of simple and complex force-deformation relationships to be specified. Details of the models are presented in Chapter 4.

3.6 DRAIN-2D IMPLEMENTATION

DRAIN-2D [45,65] is a computer program for the analysis of inelastic plane structures subjected to earthquake motions. The program consists of a series of "base" subroutines, to which subroutines for structural elements of a variety of types may be added. The program features and limitations are as follows.

The structure must be idealized as a 2D assemblage of discrete

elements connected at nodes. Analysis is by the Direct Stiffness Method, with the nodal displacements as unknowns.

2. Each node may possess up to three displacement degrees of freedom. Degrees of freedom may be specified to be deleted or combined.
3. The structure mass is assumed to be lumped at the nodes, so that the mass matrix is diagonal.
4. Viscous damping effects may be included, if desired. Damping coefficients proportional to mass, initial elastic stiffness and/or tangent stiffness can be specified.
5. Static loads may be applied prior to the dynamic loading, but no inelastic deformation is permitted under these loads.
6. The earthquake excitation is defined by time histories of ground acceleration. All support points are assumed to move identically and in phase.

The DRAIN-2D program uses a simple step-by-step solution strategy, in which the structure tangent stiffness matrix is modified at the end of any step in which the tangent stiffness changes for one or more structural elements. The constant average acceleration method (Newmark β = 1/4) is used for the step-by-step analysis. A change of stiffness in any element in any time step introduces an equilibrium unbalance at the end of the step. Unbalanced loads are eliminated by applying corrective loads in the following time step to restore the equilibrium. There is no equilibrium iteration within the time step, and a constant time step is retained throughout the analysis.

If large stiffness changes occur, the unbalanced forces may be large, and inaccurate or unstable numerical results may be obtained.

Large unbalanced forces occur most often in elements with stiffening behavior, for example when a gap closes. To help avoid instability, a modified step-by-step technique has been incorporated into the program. This technique eliminates the unbalanced forces, and permits stable response be computed with substantially larger time steps than is possible with the original DRAIN-2D program. The technique is described in Appendix A.

The DRAIN-2D program has also been modified to avoid the need to store the complete time histories for the ground acceleration records in core. This has been done by blocking the time histories and saving the blocks on a scratch file. This procedure significantly reduces the required storage for a dynamic analysis.

4. MATHEMATICAL MODELS FOR PANELS AND JOINTS

4.1 GENERAL

In this chapter several mathematical models are developed for idealizing the behavior of the wall panels and joints. Beam elements and rectangular finite elements are included to model the panels. The joint elements consist of nonlinear springs placed parallel and normal to the joint surfaces.

The modes of deformation for a joint have been assumed to be sliding and opening. These two deformations are assumed to be uncoupled in most cases, but one element which allows for coupling is described.

Each joint element is assigned a fairly simple force-displacement relationship. However, complex relationships can be obtained by placing two or more elements in parallel in a single joint. A variety of composite elements can be constructed by this process.

The force-displacement relationship of each nonlinear element is assumed to be multi-linear. Such relationships provide the analyst with flexibility in defining the joint behavior, and also have advantages from the computer programming point of view. Some computer programming aspects are considered in Appendix B.

4.2 PANEL ELEMENT: MODIFIED BEAM MODEL

4.2.1 GENERAL CHARACTERISTICS

In many analyses, it will be reasonable to idealize a complete panel as a single structural element in which the overall extensional, flexural, and shear stiffnesses of the panel are modelled. The modified beam model provides this type of idealization.

Figure 4.2.1a shows a large panel with an opening. An effective centroidal axis can be found, such that an axial force applied along

the axis produces no bending. The panel is idealized as shown in Fig. 4.2.1b, with four nodes and eight degrees of freedom. It consists of a beam element (with nonzero axial, flexural, and shear stiffnesses), placed along the effective centroidal axis and connected to the nodes by flexurally rigid links. These links enforce a plane section condition along the top and bottom edges of the panel.

The panel is assumed to have three uncoupled primary modes of deformation as shown in Fig. 4.2.2a. The element stiffness is defined by its rigidities in extension (effective EA), bending (effective EI), and shear (effective GA'), respectively. The element has two secondary modes of deformation (Fig. 4.2.2b) for which zero stiffnesses are assumed. These deformation modes plus three rigid body modes (Fig. 4.2.2c) make up the eight degrees of freedom of the element. It should be noted that the third mode of deformation in Fig. 4.2.2a is shown as pure shear with no flexure. This feature of the element is considered further in Section 4.2.2.

Panels will typically be arranged in a complete structure as indicated in Fig. 4.2.3. Horizontal joint elements will connect nodes on horizontal planes (e.g. nodes 5, 6, 9, 10) and vertical joint elements will connect nodes on vertical planes (e.g., nodes 2, 3, 6, 7). The vertical displacements of pairs of nodes on horizontal planes (e.g., pairs (5,9), (6,10)) may be made equal, indicating rigid vertical connection, or may be connected by "gap" elements which allow separation when tension develops. The same applies for horizontal displacements at pairs of nodes on vertical planes.

It should be noted that the top and bottom edges of the panel are assumed to remain straight, whereas the vertical edges are allowed to

bend. This may be important for multi-bay walls, because it allows incompatibility at vertical panel edges to develop, for example as illustrated in Fig. 4.2.4. The compatibility is improved if each wall panel is modelled by several elements as shown in Fig. 4.2.5. It should also be noted that rotational displacements of the nodes are not restrained by either the panel or joint elements, and must usually be constrained to be zero (Zero Displacements option in the DRAIN-2D User's Guide).

The mass of each panel must be lumped at its nodes. This permits a reasonable representation of the translational inertia (both vertical and horizontal) of the panel, but overestimates its rotational inertia. This is an inherent error of this panel model, but should not be serious in most cases. If it is believed that the rotational inertial will substantially affect the dynamic response, each panel should be divided into several elements to provide a more accurate representation of the mass distribution in the panel.

If the assumptions on which this panel element is based are not reasonable for any given structure, a more refined idealization will be necessary, in which a single building panel is divided into several structural elements. The panel element based on a finite element forumlation (Section 4.3) can be used in such cases.

4.2.2 DISCUSSION OF PANEL STIFFNESS

The displacement degrees of freedom, r_1 through r_8, are shown in Fig. 4.2.1b. The primary modes of deformation, as shown in Fig. 4.2.2a, involve (1) vertical extension; (2) uniform bending; and (3) "racking" in shear. These three modes of deformation are believed to model the most important deformation characteristics of a typical panel. The stiffnesses associated with each mode (i.e., effective extensional,

flexural, and shear stiffnesses) must be determined by experiment or by separate calculations, and entered as data to the computer program. These effective stiffnesses must take account of doors, windows, thickness variations, etc.

Panel edges ij and kl (Fig. 4.2.1) are assumed to remain straight (analogous to plane sections remaining plane in simple beam theory). Compatibility violations between adjacent panels due to bending of lines ik and jl are assumed to be acceptable (Fig. 4.2.4). It will typically be specified that $r_1 = r_2$ and $r_3 = r_4$ (i.e., no extension of lines ij and kl), using the Equal Displacements option in the DRAIN-2D User's Guide. These displacements need not be made equal if the analyst desires otherwise, but it should be noted that the element has zero stiffness for extension of ij and kl.

The stiffness matrix in terms of the three primary modes of deformation is assumed to be

$$\underline{k}_d = \begin{bmatrix} \frac{EA_e}{h} & & \\ & \frac{EI_e}{h} & \\ & & \frac{GA'_e}{h} \end{bmatrix} \qquad (4.2.1)$$

in which A_e = effective area for vertical extension; I_e = effective moment of inertia for symmetrical bending; A'_e = effective shear area for racking; E = Young's modulus; G = shear modulus; and h = panel height.

These stiffnesses are referred to the effective centroidal axis (Fig. 4.2.1). The extensional and symmetrical bending modes are uncoupled because of the way in which this axis is defined. The racking

mode is not necessarily uncoupled from the other modes, but it should be reasonable to make this assumption in most cases.

For single bay walls, the racking deformation will be associated with both shear force and bending moment in the wall. The stiffness GA'_e/h is an effective stiffness, which must account for both shearing and flexural deformations. For a beam deformed as shown in Fig. 4.2.6 (antisymmetrical bending plus shear), the flexibility will be

$$f = \frac{h^3}{12EI} + \frac{h}{GA'} \tag{4.2.2}$$

in which I = actual moment of inertia and A' = actual shear area. The third stiffness term in matrix $\underline{k}_d$ should therefore be

$$\frac{GA'_e}{h} = \frac{1}{f} \tag{4.2.3}$$

For a beam with a rectangular section, a depth (i.e, panel width) d, and Poisson's ratio 0.15, the ratio of shear to bending flexibilities is

$$\left(\frac{h}{GA'}\right) \Big/ \left(\frac{h^3}{12EI}\right) = 2.3 \left(\frac{d}{h}\right)^2 \tag{4.2.4}$$

For a panel with d/h = 3, typical of U.S. practice, this ratio is 20.7, indicating that shear flexibility dominates, and the antisymmetrical bending flexiblity can be ignored. In narrower panels, A'_e should be calculated from Eq. 4.2.3, accounting for the bending flexibility. Pollner et al. [1] have used a modified beam model similar to that described herein, but assuming that the bending flexibility dominates.

For multi-bay panels, racking deformation will be associated with

more complex loadings, involving not only bending and shear from the panels above and below, but also shear forces from other panels on either side. In this case, the effective racking stiffness will more closely approach that based on shear deformations only.

The discussion in this section emphasizes that this is a simplified panel model which may not be sufficiently accurate in some cases.

4.2.3 THEORY

The uncoupled element actions, $\underline{Q}$, and deformations, $\underline{q}$, are shown in Fig. 4.2.7. The vectors $\underline{Q}$ and $\underline{q}$ are conjugate (that is, $\frac{1}{2}\underline{Q}^T\underline{q}$ = strain energy). The basic stiffness relationship is

$$\begin{Bmatrix} Q_1 \\ Q_2 \\ Q_3 \end{Bmatrix} = \underline{k}_d \begin{Bmatrix} q_1 \\ q_2 \\ q_3 \end{Bmatrix} \tag{4.2.5}$$

where $\underline{k}_d$ is given by Eq. 4.2.1.

The relationship between the nodal displacements, $\underline{r}$, and element deformations, $\underline{q}$, is:

$$\begin{Bmatrix} q_1 \\ q_2 \\ q_3 \end{Bmatrix} = \begin{bmatrix} 0 & 0 & 0 & 0 & \frac{b}{d} & \frac{a}{d} & -\frac{b}{d} & -\frac{a}{d} \\ 0 & 0 & 0 & 0 & -\frac{1}{2d} & \frac{1}{2d} & \frac{1}{2d} & -\frac{1}{2d} \\ \frac{b}{d} & \frac{a}{d} & -\frac{b}{d} & -\frac{a}{d} & -\frac{h}{2d} & \frac{h}{2d} & -\frac{h}{2d} & \frac{h}{2d} \end{bmatrix} \begin{Bmatrix} r_1 \\ r_2 \\ r_3 \\ r_4 \\ r_5 \\ r_6 \\ r_7 \\ r_8 \end{Bmatrix}$$

or:

$$\underline{q} = \underline{a}\,\underline{r} \tag{4.2.6}$$

Hence, the (8 x 8) element stiffness matrix, $\underline{K}$, is given by

$$\underline{K} = \underline{a}^T \underline{k}_d \underline{a} \qquad (4.2.7)$$

The computer program prints out top and bottom moments, shear force and axial force in the element, as shown in Fig. 4.2.8. These actions are defined as follows:

$$M_{top} = -(Q_2 + \tfrac{1}{2} hQ_3)$$

$$M_{bottom} = Q - \tfrac{1}{2} hQ$$

$$F_{shear} = Q_3$$

$$F_{axial} = Q_1$$

4.2.4 ADVANTAGES AND LIMITATIONS OF MODIFIED BEAM MODEL

The advantages of the modified beam model are as follows:

1) The model is computationally efficient, requiring fewer elements and degrees of freedom than the more "exact" finite element model considered in Section 4.3.
2) The model can be used for panels with openings and for sandwich, hollow core, and ribbed panels as well as solid panels, because the effective values of EA_e, EI_e, and GA'_e, are specified. The finite element model is less flexible in this respect.

The limitations of the model are as follows:

1) The panel top and bottom edges are assumed to remain straight, which is not necessarily correct.
2) The model must be used cautiously for multi-bay walls, because incompatibility is allowed along vertical edges.
3) The effective shear area, A'_e, must be chosen with care, because it must account for both shear and antisymmetrical bending deformations.

4.3 PANEL ELEMENT: FINITE ELEMENT MODEL

4.3.1 GENERAL CHARACTERISTICS

Although the modified beam panel element models the dominant overall modes of deformation of a wall panel, it assumes that the horizontal joint planes remain flat. For cases in which joint opening occurs, Llorente [8] has observed that the joint surface distorts significantly. If distortion of the surface occurs, the gap opening is progressive (Fig. 4.3.1a), whereas the rigid plane assumption predicts sudden opening over the entire joint width (Fig. 4.3.1b).

To allow for more refined modelling of panels, a rectangular finite element has been included in the computer program. This element allows single panels to be subdivided into several elements, for example as shown in Fig. 4.3.2. This type of idealization not only allows for distortion of horizontal joint surfaces, but also improves the compatibility along vertical joints.

For the greatest computational efficiency with this type of panel idealization, it is advantageous to use substructuring, by condensing the complete panel stiffness matrix down to a stiffness matrix in terms of joint nodes only. This option is not provided in the present version of the program.

Each element is assumed to be elastic and isotropic. If the panel is of ribbed or sandwich type, appropriate values of Young's modulus and Poisson's ratio must be specified.

4.3.2 THEORY

The element is a plane stress four-node rectangular element with eight displacement degrees of freedom. The element has the five modes of deformation shown in Fig. 4.3.3 plus three rigid body motions. The

formulation of the element sitffness is well known (e.g. [47]) and will not be repeated here.

If desired, a uniform initial stress pattern may be specified for each element, to represent the effects of gravity and/or posttensioning. These stresses are added to the calculated stresses for each element at each time step. Because the element is assumed to be linear and elastic, the stresses have no effect on its stiffness.

4.4 SIMPLE FRICTION JOINT ELEMENT

4.4.1 GENERAL CHARACTERISTICS

If a joint is unreinforced or has very little reinforcing, its behavior in shear is dominated by friction. The tests by Verbic [6] suggest an elastic-plastic shear-slip relationship for constant compressive force normal to the joint.

The element described in this section has a friction strength equal to μF_n, where μ is the coefficient of friction and F_n is the compressive force on the joint, both assumed to remain constant. Degradation of the friction coefficient can be considered using the element described in Section 4.5. Variation of the compressive force can be considered using the element described in Section 4.7.

Each simple friction element must be connected to four nodes, two on one panel and two on an adjacent panel. For a horizontal joint, the nodes must be as shown in Fig. 4.4.1a, and for a vertical joint as shown in Fig. 4.4.1b. The joint element restrains relative sliding between the panels, with a force-slip relationship as shown in Fig. 4.4.2. The initial shear stiffness, k_s, will typically be large. The stiffness after slip commences, k_h, will typically be small or zero. The unloading stiffness is equal to the initial stiffness, which is in agreement with

experimental data. If desired, the element can be used in parallel with other elements to obtain more complex behavior (see Chapter 5).

The element (joint) thickness must be zero, as indicated in Fig. 4.4.1, otherwise the solution will violate equilibrium.

4.4.2 UNLOADING BEHAVIOR

Because the stiffness k_s will typically be large, the joint stiffness increases a great deal when a slipping element reverses. This can lead to numerical stability problems in the DRAIN-2D program. The problem is illustrated in Fig. 4.4.3a, where it can be seen that the state determination procedure can lead to a large unbalanced force. To avoid this problem, an option is provided to assume behavior as shown in Fig. 4.4.3b on unloading. With this option, the element stiffness is assumed to change at the end of the step, and there is no unbalanced force. The use of this option is generally recommended.

4.4.3 ELEMENT STIFFNESS

The element has four displacement degrees of fredom, as shown in Fig. 4.4.4, and one deformation degree of freedom. The element deformation is given by:

$$q = \frac{1}{2}(r_1 + r_2) - \frac{1}{2}(r_3 + r_4) \qquad (4.4.1)$$

which is the average slip across the joint, or:

$$q = \underline{a}\,\underline{r} \qquad (4.4.2)$$

where the displacement transformation matrix is

$$\underline{a} = 1/2 < 1 \quad 1 \quad -1 \quad -1 > \qquad (4.4.3)$$

The basic stiffness relationship between the element action, Q, and

deformation, q, is

$$Q = kq \tag{4.4.4}$$

in which k is the tangent shear stiffness (k_s or k_n). Hence, the tangent stiffness matrix is

$$\underline{K} = \underline{a}^T \underline{k}\, \underline{a} = \frac{k}{4} \begin{bmatrix} 1 & 1 & -1 & -1 \\ 1 & 1 & -1 & -1 \\ -1 & -1 & 1 & 1 \\ -1 & -1 & 1 & 1 \end{bmatrix} \tag{4.4.5}$$

4.5 FRICTION JOINT ELEMENT WITH DEGRADING STRENGTH

4.5.1 GENERAL CHARACTERISTICS

If the behavior of a joint is dominated by friction, its behavior may be substantially influenced by polishing of the joint surfaces under cyclic loading [6,7], with a progressive reduction in the coefficient of friction. The joint model described in this section allows for decrease of the friction force as the joint accumulates slip. The reduction may be caused by polishing of the joint or by the accumulation of sand and aggregate particles in the joint, which tend to roll and facilitate slippage.

A multi-linear relationship is assumed between the friction coefficient and the accumulated joint slip (sum of the absolute values of the slip excursions), as shown in Fig. 4.5.1. This type of relationship permits modelling of either sudden loss or gradual degradation of joint strength.

4.5.2 ELEMENT STIFFNESS

The element stiffness is the same as for the simple friction element (Section 4.4). The stiffnesses k_s and k_h are assumed not to be affected by the strength degradation.

4.5.3 STATE DETERMINATION

For analysis, the bilinear force-slip characteristic of the simple friction element is decomposed into two components, one elastic and one elastic-plastic, as shown in Fig. 4.5.2. The degrading strength feature is then applied to the elastic-plastic component. For any step of the step-by-step analysis, the friction strength is first assumed to be constant, equal to the strength at the beginning of the step. The slip (if any) and hence the accumulated slip are calculated. The element strength is then obtained at the end of the step, using the specified degrading characteristic (Fig. 4.5.1). Because of this adjustment there is an equilibrium error at the end of the step. The unbalanced force is calculated and applied in the following step to restore equilibrium. This implies a shear-slip relationship as shown in Fig. 4.5.3.

4.6 GAP ELEMENT

4.6.1 GENERAL CHARACTERISTICS

A gap element is a spring with zero length, placed normal to the joint surface. A finite stiffness is assigned to the element in compression (typically large) and a zero stiffness is assigned in tension. Hence, the element allows a gap to develop between the connected panels.

The element force-deformation relationship is as shown in Fig. 4.6.1. For a horizontal joint, the element provides this relationship between vertical force and relative vertical displacement between the nodes. For a vertical joint, the relationship is between horizontal force and dis-

placement. The relationship allows for nonlinear behavior in compression (joint crushing), with the joint bearing surfaces yielding as the normal compressive force increases. The element has options to unload elastically or to unload inelastically, as shown.

Compressive deformation is assumed to be positive. The element may be preloaded to represent gravity and/or posttensioning effects. Separation occurs when any added tension force exceeds the preload.

Gap elements may be placed in horizontal or vertical joints. An element may connect four nodes as shown in Fig. 4.6.2, in which case the distance between the connected lines must be zero. Alternatively, an element may connect two nodes directly, in which case the nodes must have identical coordinates.

Three-node connectivity may also be specified if desired, as shown in Fig. 4.6.3. This figure illustrates a horizontal joint between two adjacent panels, one idealized with a single modified beam element and the other with several rectangular finite elements. The joint is modelled with five gap elements, each connecting one node in the lower panel to the two nodes on the upper panel. This modelling can be used to enforce an essentially straight upper edge on the lower panel, in order to satisfy displacement compatibility between the panels.

A real joint will actually be of finite thickness, with finite compressive stiffness. It is desirable to model the deformability of the joint as accurately as possible, by calculating the compressive stiffness from the actual joint geometry and mechanical properties. Numerical errors may occur if excessively stiff gap elements are specified.

4.6.2 PANEL TILTING

If a horizontal joint develops a gap, the upper panel tilts relative to the lower panel. When modified beam elements are used for the panels, it will be natural to place a gap element at each end of the joint (Fig. 4.6.4a). If a gap opens, the assumption is then that the panels pivot about the corner point, as shown.

It has been emphasized [8,48] that joint opening takes place progressively, rather than suddenly, and that the assumption that plane joint sections remain plane may be substantially incorrect. To consider the true mechanism of joint opening, it is necessary to use a finite element panel model, with several elements across the joint. Distortion of the joint plane, and progressive joint opening, can then be modelled. However, this type of idealization is more expensive computationally.

When the modified beam panel element is used, the error in assuming a rigid joint plane can be partially corrected by either moving the assumed pivot points or by modelling the joint with several gap elements. The pivot points can be moved by specifying two gap elements located within the joint rather than at the corners, as shown in Fig. 4.6.4b. A less sudden joint opening can also be obtained by specifying several gap elements along the joint, as shown in Fig. 4.6.4c. In this case, however, the gap elements must be made relatively flexible in compression, otherwise tilting will occur essentially about one corner, and all gap elements will open at essentially the same time.

4.6.3 ELEMENT STIFFNESS

A four-node gap element has four displacement degrees of freedom, as shown in Fig. 4.6.2, and one extensional mode of deformation. The element deformation is given by:

$$q = \left\langle -\frac{b_1}{L_1} \quad -\frac{a_1}{L_1} \quad \frac{b_2}{L_2} \quad \frac{a_2}{L_2} \right\rangle \begin{Bmatrix} r_1 \\ r_2 \\ r_3 \\ r_4 \end{Bmatrix} \tag{4.6.1}$$

where $L_1 = a_1 + b_1$ and $L_2 = a_2 + b_2$; or

$$q = \underline{a}\,\underline{r} \tag{4.6.2}$$

Hence, the element stiffness matrix is:

$$\underline{K} = \underline{a}^T \underline{k}\,\underline{a} = k \begin{bmatrix} \left(\frac{b_1}{L_1}\right)^2 & \frac{a_1 b_1}{L_1^2} & \frac{b_1 b_2}{L_1 L_2} & \frac{a_2 b_1}{L_1 L_2} \\ & \left(\frac{a_1}{L_1}\right)^2 & \frac{a_1 b_2}{L_1 L_2} & \frac{a_1 a_2}{L_1 L_2} \\ \text{Symmetric} & & \left(\frac{b_2}{L_2}\right)^2 & \frac{a_2 b_2}{L_2^2} \\ & & & \left(\frac{a_2}{L_2}\right)^2 \end{bmatrix} \tag{4.6.3}$$

where k is the tangent stiffness of the element (k_1, k_2, k_3, k_4, or zero, Fig. 4.6.1).

A two-node element is obtained by setting $b_1 = b_2 = 0$, and a three-node element by setting either $b_1 = 0$ or $b_2 = 0$.

4.6.4 STATE DETERMINATION

Because of the state determination procedure used in the DRAIN-2D program, substantial unbalances may occur when a gap closes, especially if the time step is long or the element stiffness is high. When gap elements are used, the element stiffnesses should be made as low as possible, the time step should be short, and the results should be examined carefully to ensure that oscillation or divergence of results does not occur following gap closure. A solution strategy which has been added to DRAIN-2D to help avoid numerical problems is discussed in Appendix A.

4.7 COMBINED GAP-FRICTION ELEMENT

4.7.1 GENERAL CHARACTERISTICS

In the simple friction element, it is assumed that the shear resistance is constant, regardless of changes in bearing stress on the joint. In an actual joint, the bearing stress varies with time and with position in the joint, because of bending of the walls and vertical shaking of the building. Hence, the shear strength will also vary. The combined gap-friction element allows the frictional resistance to vary as the bearing stress changes, assuming a constant friction coefficient.

The element combines the gap and friction elements previously described, but modifies the friction element so that its shear strength at any time is equal to the compressive force on the gap element multiplied by the coefficent of friction. The shear strength becomes zero if gap opening occurs. Note that in compression, the shear resistance is assumed to increase in direct proportion to the bearing force. That is, there is no limiting failure envelope of the type assumed by Schwing and Mehlhorn [31].

Each element may be connected to four nodes (two on one panel and two on an adjacent panel, Fig. 4.7.1) or to only two nodes (one on each panel, Fig. 4.7.2). As for the gap element, the position of the element in the joint determines the point about which rotation occurs when gap opening occurs.

4.7.2 ELEMENT STIFFNESS

The four- and two-node elements have eight and four displacement degrees of freedom, respectively, as shown. The composite element consists of separate shear and gap components. There is no coupling between the stiffnesses of the two components, but the strength of the shear component, F_s, is governed by the compressive force, F_n, in the gap component.

The force-deformation characteristics of the components are as shown in Fig. 4.7.3. If q_s is the deformation of the shear component and q_n that of the gap component, the element deformation-displacement relationship for a four-node element is

$$\begin{Bmatrix} q_s \\ q_n \end{Bmatrix} = \begin{bmatrix} \frac{b}{L} & \frac{a}{L} & -\frac{b}{L} & -\frac{a}{L} & 0 & 0 & 0 & 0 \\ 0 & 0 & 0 & 0 & -\frac{b}{L} & -\frac{a}{L} & \frac{b}{L} & \frac{a}{L} \end{bmatrix} \begin{Bmatrix} r_1 \\ r_2 \\ r_3 \\ r_4 \\ r_5 \\ r_6 \\ r_7 \\ r_8 \end{Bmatrix} \qquad (4.7.1)$$

where L = a + b; or:

$$\underline{q} = \underline{a}\,\underline{r} \qquad (4.7.2)$$

Hence, the stiffness matrix is:

$$\underline{K} = \underline{a}^T\,\underline{k}\,\underline{a} \qquad (4.7.3)$$

where

$$\underline{k} = \begin{bmatrix} k_s & 0 \\ 0 & k_n \end{bmatrix} \tag{4.74}$$

and k_s and k_n are the tangent stiffnesses of the shear and gap components, respectively. The relationship for the two-node element is the same, except that:

$$\begin{Bmatrix} q_s \\ q_n \end{Bmatrix} = \begin{bmatrix} 1 & -1 & 0 & 0 \\ 0 & 0 & -1 & 1 \end{bmatrix} \begin{Bmatrix} r_1 \\ r_2 \\ r_3 \\ r_4 \end{Bmatrix} \tag{4.75}$$

4.7.3 STATE DETERMINATION

Frictional slip under varying bearing stress is a complex process. The behavior is particularly complex if shear movement is occurring with an open gap and the gap suddenly closes. The procedure used to determine the state of an element at the end of any time step is not exact, but is believed to be reasonable and has worked well in example analyses. The logic of the procedure is shown in Fig. 4.7.4.

In this procedure, the state of the friction element is first found using the friction strength at the beginning of the step. The state of the gap element is then found, and the friciton strength is updated, based on the new bearing force. Finally the state of the friction element is modified, taking account of the new bearing force. Five different cases can be identified as shown in Fig. 4.7.4. The figure shows the assumption made for each case.

4.8 KEY ELEMENT

4.8.1 GENERAL CHARACTERISTICS

The key element allows modelling of mechanical keys in horizontal or vertical joints. The element can also be used to model connections which have initial adhesion or strong bond.

Each key element can be connected to either two or four nodes on adjacent panels, as for other elements. Elements may be specified at horizontal and/or vertical joints.

The relationship between shear force and shear displacement between the connected nodes is as shown in Fig. 4.8.1. The force-displacement relationship is assumed to be initially elastic (line 1, Fig. 4.8.1). The initial stiffness will usually be specified to be large. At a specified yield strength, the element yields at constant force (line 2). Beyond a specified yield displacement the element loses strength along line 3, simulating failure of the key. When the strength of the element reaches zero, total failure is assumed and the behavior follows line 5. After failure, no further shear resistance is provided by the element.

The failure may be either brittle or ductile, as shown in Fig. 4.8.2. A brittle failure is characterized by a short yield plateau and subsequent steep decline along line 3. A ductile failure is characterized by a longer plateau and slow decline.

In the absence of detailed experimental results, unloading has been assumed to take place along line 4. This assumes partial key failure, with consequent loss of stiffness. Pollner et al. [1] have used a similar force-deformation relationship for the static analysis of vertical joints in large panel walls.

An actual keyed joint will not lose strength completely, after

failure of the key, but will retain frictional strength. A keyed joint will therefore usually be modelled using a key element in parallel with a friction element. Key elements can also be placed in parallel with other element types, to obtain complex degrading strength characteristics. Examples are given in Chapter 5.

4.8.2 NEGATIVE STIFFNESS

It should be noted that the tangent stiffness associated with line 3 (Fig. 4.8.1) is negative. Thus, diagonal terms in the element stiffness matrix become negative, and if line 3 is steep, the structure tangent stiffness matrix may no longer remain positive definite. This may cause computational difficulties, and hence large negative slopes for line 3 should be used with caution.

4.8.3 ELEMENT STIFFNESS

The four-node element has four displacement degrees of freedom and the two-node element has two, as shown in Fig. 4.8.3. The element has one deformation degree of freedom, namely the average relative shear displacement across the joint. The deformation-displacement transformation for a four-node element is

$$q = 1/2 < 1 \quad 1 \quad -1 \quad -1 > \begin{Bmatrix} r_1 \\ r_2 \\ r_3 \\ r_4 \end{Bmatrix} \tag{4.8.1}$$

or:

$$q = \underline{a}\,\underline{r} \tag{4.8.2}$$

The basic action-deformation relationship is

$$Q = kq \tag{4.8.3}$$

in which k is the current tangent stiffness of the element. Hence, the element stiffness matrix is

$$\underline{K} = \underline{a}^T \, k \, \underline{a} \tag{4.8.4}$$

The relationship for the two-node element is the same, except that

$$q = \langle 1 \quad -1 \rangle \begin{Bmatrix} r_1 \\ r_2 \end{Bmatrix} \tag{4.8.5}$$

4.9 SHEAR FRICTION JOINT ELEMENT

4.9.1 GENERAL CHARACTERISTICS

The behavior of reinforced wet joints was described in Section 2.4 and of dry joints in Section 2.5 It was shown that these joints all exhibited "shear friction" behavior characterized by:

1. "Pinched" hysteresis loops, with stiffening behavior near the end of each cycle and a high unloading stiffness.
2. Similar force-displacement relationships for positive and negative shear.
3. Degradation of stiffness and strength as the number of load cycles increases.

The shear friction element has been developed for modelling joints with these characteristics.

Each element must be connected to four nodes, two on one panel and two on an adjacent panel, as shown in Fig. 4.9.1. The element shear deformation is the relative displacement between the connected panels, assumed to be the average displacement of nodes i, j minus the average displacement of nodes k, ℓ.

The element consists of two components in parallel, with force-

displacement relationships as shown in Fig. 4.9.2. Component 1 has an elastic-plastic relationship (Fig. 4.9.2a), to account for simple friction due to applied compressive load on the joint. Component 2 accounts for the "shear friction" mechanism, developing a "pinched" hysteresis loop (Fig. 4.9.2b) after several loading cycles. This loop begins with a low stiffness region (line 1) representing the state in which the reinforcement exerts little or no clamping action on the joint. As slip increases, clamping action develops and the stiffness increases (line 2). After further deformation, the reinforcement yields and the clamping action reaches a limiting value. The strength on this line may be constant or may be specified to increase with displacement (stiffness k_3). The component unloads first along line 4 with a large stiffness, and then along line 5, with a small or zero stiffness. Lines 1 and 5 are both assumed to pass through the origin (no residual slip under zero shear). Under reversed loading, the behavior is similar, and the hysteresis loop is symmetrical.

4.9.2 VARIATION OF FRICTION RESISTANCE

The strength of Component 1 (simple friction) is assumed to be constant, with no strength degradation due joint polishing and no allowance for variation of the bearing force. If joint polishing is important, it can be accounted for by specifying zero strength for Component 1, and placing the shear friction element in parallel with a friction element with degrading strength (Section 4.5). Similarly, if variation of bearing force is important, the shear friction element may be placed in parallel with a combined gap-friction element (Section 4.7).

4.9.3 STIFFNESS DEGRADATION

Joint tests show that the stiffness and strength of reinforced joints both degrade under cyclic loading. The element accounts for degradation effects in the hysteresis loop of Component 2 (shear friction component). The procedure allows for reduction in the stiffness of Line 1 (k_1, Fig. 4.9.2b) and decrease in the maximum strength of the component (F_2, Fig. 4.9.2b). The procedure for stiffness degradation is as follows.

It is assumed that under cyclic loading with constant shear force the stiffness k_1 decreases, while the force F_1 (Fig. 4.9.2b) remains unchanged. That is, there is an increase in the displacement at which the stiffness changes from k_1 to k_2 (Δ_1, Fig. 4.9.2b). The change in Δ_1 is assumed to be based on the maximum deformation in the k_2 and k_3 regions (S_{2m}, Fig. 4.9.3, measured from the end of the current Line 1). Degradation of stiffness k_1 is obtained by adding a proportion of S_{2m} to the deformation Δ_1, to obtain an increased Δ_1 value. The degradation is controlled by a factor α ($\alpha \geq 0$), such that $\Delta_1' = \Delta_1 + \alpha S_{2m}$. The new stiffness k_1 is then given by

$$k_1' = \frac{\Delta_1}{(\Delta_1 + \alpha S_{2m})} \; k_1$$

When α is specified to be zero, no degradation occurs, and k_1 and Δ_1 remain constant.

The degradation process is implemented during load reversal. The increase in Δ_1 begins when the cycle moves from Line 4 to Line 5, and is completed when the cycle returns to the origin. In between these two points, Δ_1 is increased linearly. This gradual degradation is necessary because a complete loop is not necessarily obtained under arbitrary load-

ing. If Δ_1 were increased to Δ_1' immediately the cycle moved to Line 5, incorrect results would be obtained for partial cycling.

The degradation of k_1 affects both directions because Lines 1 and -1 are assumed to have the same slopes. Hence, deformation S_{2m} in the positive direction affects the negative part of the hysteresis loop, and vice versa. The stiffness k_1 is not allowed to become less than k_5. If k_1 reduces to k_5, then Δ_1 is increased as above, but F_1 is also increased, so that k_1 remains constant. The stiffnesses k_2, k_3, k_4, and k_5 all remain constant.

With this procedure, the force-displacement relationship stabilizes in the second cycle for cycling under constant load. This is because S_{2m} is measured from the current value of Δ_1, and hence $S_{2m} = 0$ for the second cycle. The loop will similarly stabilize in the second cycle for constant displacement cycling.

4.9.4 STRENGTH DEGRADATION

A trilinear "strength envelope," as shown in Fig. 4.9.4, has been assumed to define the strength degradation. The strength, F_2, is decreased as Δ_1 increases, as shown. For any current value of k_1, the intersection of Line 2 with the specified strength envelope is found. This defines a new displacement limit Δ_2, and a new strength F_2. With this procedure the hysteresis loop for constant displacement cycling stabilizes in the second cycle, but does not stabilize for constant load cycling.

The multi-linear representation of the strength envelope permits modelling of either sudden loss or gradual degradation of strength.

4.9.5 EXAMPLES

Figure 4.9.5a shows example properties for the simple friction and shear friction components. Figure 4.9.5b shows the force-displacement relationship for the resulting element under four displacement-controlled cycles. It can be seen that the behavior is qualitatively similar to that observed in experiments. Figure 4.9.6b shows loops for similar cycling, but with the simple friction component specified to have zero strength, and a friction element with degrading strength (Section 4.5) placed in parallel with the shear friction component. The properties of the friction element with degrading strength are shown in Fig. 4.9.6a. In this case the loops show a progressive narrowing as the amount of cycling increases. Other examples are considered in Chapter 5.

4.9.6 ELEMENT STIFFNESS

The element has four displacement degrees of freedom, as shown in Fig. 4.9.1, and one deformation degree of freedom. The element deformation is given by

$$q = 1/2 < 1 \quad 1 \quad -1 \quad -1 > \begin{Bmatrix} r_1 \\ r_2 \\ r_3 \\ r_4 \end{Bmatrix} \qquad (4.9.1)$$

or:

$$q = \underline{a}\, \underline{r} \qquad (4.9.2)$$

where $\underline{a}$ is the displacement transformation. Hence, the element tangent stiffness matrix is

$$\underline{K} = \underline{a}^T \underline{k}\, \underline{a} = \frac{k}{4} \begin{bmatrix} 1 & 1 & -1 & -1 \\ 1 & 1 & -1 & -1 \\ -1 & -1 & 1 & 1 \\ -1 & -1 & 1 & 1 \end{bmatrix} \qquad (4.9.3)$$

where k is the basic tangent stiffness at any time, equal to the combined stiffnesses of the simple friction and shear friction components.

4.10 LINK ELEMENT

4.10.1 GENERAL CHARACTERISTICS

The link element is a uniaxial element with finite length, which may be arbitrarily oriented (i.e. not necessarily horizontal or vertical). The element has zero stiffness in tension and a finite stiffness in compression.

The force-displacement relationship is as shown in Fig. 4.10.1. Either one of two unloading paths for the element, namely elastic or inelastic, may be used. For the inelastic option, unloading takes place parallel to the initial elastic stiffness k_1. The element can be preloaded to a specified compression force if desired, or alternatively can be prestrained in tension to give a specified initial clearance. The element can thus function as a prestressed bearing element or as an element with an initial gap.

Each link element must be connected to two nodes, which must not have identical coordinates. For large panel applications, link elements will usually be placed in either horizontal or vertical joints, connecting nodes on adjacent panels.

4.10.2 LINK ELEMENT USE TO MODEL A STOP

A stop in a joint will permit a certain amount of slip and will then develop resistance to constrain further slip. Such behavior could be

produced by a set of unbonded dowels projecting vertically through a horizontal joint, and placed in slots or clearance holes. Joints incorporating such dowels are being tested by the PCA [28]. Similar behavior occurs, together with other types of resistance, in the bolted joints tested by Pall and Marsh [40].

A stop can be modelled by placing a pair of link elements, with initial clearances, between panels as shown in Fig. 4.10.2a. Figure 4.10.2b shows the resulting force-deformation characteristic (assuming elastic behavior).

4.10.3 OTHER COMBINATION OF LINK ELEMENTS

A pair of link elements can also be used to obtain the behavior shown in Fig. 4.10.3. In this case, the elements have no initial gap or preload, and are specified to be elastic-plastic in compression. More complex behavior can also be obtained (Fig. 4.10.4) by specifying a multi-linear relationship in compression for each link element (in this case, $k_2 = 0$).

An element with a characteristic similar to that shown in Fig. 4.10.3 is being investigated by Becker et al [44] to model metal connectors for vertical joints.

4.10.4 ELEMENT STIFFNESS

The link element has four displacement degrees of freedom and one deformation degree of freedom, as shown in Fig. 4.10.5. The relationship between nodal displacement and element deformation is

$$q = \langle \text{Cos}\theta \quad \text{Sin}\theta \quad -\text{Cos}\theta \quad -\text{Sin}\theta \rangle \begin{Bmatrix} r_1 \\ r_2 \\ r_3 \\ r_4 \end{Bmatrix} \qquad (4.10.1)$$

or:

$$q = \underline{a}\,\underline{r} \tag{4.10.2}$$

Hence, the tangent stiffness matrix is determined from

$$\underline{K} = \underline{a}^{T}\, k\, \underline{a} \tag{4.10.3}$$

where k is the element tangent stiffness (i.e. k_1, k_2, k_3, or zero).

5. PARAMETER STUIDES

5.1 GENERAL

A parameter study has been carried out to study the influence of different joint properties and earthquake motions on the computed non-linear response. The force-deformation characteristics of the joints, the distribution of vertical loads in the building, and the earthquake motion have been varied. The study is limited to a 10-story, single bay, large panel wall with horizontal joints only. The maximum amounts of joint slip and opening, and the maximum forces in the structure have been computed.

The purposes of the study are as follows:

1. To study the extent to which forces in the structure are reduced when joint slip and gap opening are permitted.
2. To study the distribution of joint deformations for different vertical load distributions on the wall.
3. To investigate the effect of the joint force-deformation relationship on the response of the wall.
4. To investigate whether the response is sensitive to the assumed ground motion.

It is important to emphasize that the structure properties, especially the joint strengths assumed for the anslysis, are not necessarily representative of real structures. Nevertheless, the behavior modelled is qualitatively similar to that observed in tests, and hence it is believed that the results are qualitatively correct. In particular, if joints with particular force-deformation relationships exhibit undesirable behavior in the analyses, it is believed that they will tend to exhibit similar undesirable behavior in practice,

although the level of seismic excitation necessary to produce such behavior would not necessarily be the same as that used in this study.

The analyses show several ways in which joint behavior can be idealized for analysis. However, these idealizations are not necessarily recommended for use in practical analysis. This is a complex problem which requires much further study.

5.2 STRUCTURE DIMENSIONS AND PROPERTIES

Figure 5.2.1 shows a 10-story, 1-bay, large panel wall, isolated from a cross-wall, large panel system of the type which might be used in an apartment building in the United States. The dimensions and properties are identical to those of a wall studied by Becker [24]. Further details are given in Table 5.2.1.

5.3 MATHEMATICAL MODELS

5.3.1 PANEL IDEALIZATION

The panels have been idealized using both modified beam elements and 4-node finite elements. For the Beam Model (Fig. 5.3.1) each panel is modelled by one modified beam element, whereas for the Finite Element (F.E.) Model (Fig. 5.3.2) each panel is modelled by eight rectangular finite elements.

A "mixed" model has also been studied (Fig. 5.3.3), in which the first four panels from the base are modelled by finite elements and the rest by modified beam elements. For this model, the number of nodes changes from two to five at the junction of the finite elements and the beam elements. To ensure displacement compatibility (horizontal section remains plane after deformation), five gap elements with high stiffnesses were placed at the junction. The horizontal displacements of nodes 61, 65, 66, and 67 (Fig. 5.3.3) were also constrained

to be identical.

The thickness of each horizontal joint in the actual wall is 12 inches. The mathematical model assumes a joint flexibility the same as the actual joint, but assumes that the joint thickness is zero. Thus, the height of each wall panel is 9 feet in the mathematical model, compared with 8 feet for the actual panel. To compensate for this difference, the panel stiffness must be adjusted to assume 6-inch rigid segments at the top and bottom of each panel.

For panels modelled using modified beam elements, the panel cross section stiffnesses in extension (EA) and bending (EI) were increased by the factor 9/8, so that the correct stiffness values EA/h and EI/h, where h = 9 feet, were calculated by the computer program. The panel stiffnesses input to the computer program were thus

$$\frac{9}{8}\ (\ EA\ ) = 9{,}473{,}760\ \text{k.}$$

$$\frac{9}{8}\ (EI) = 454{,}740{,}480\ \text{k.ft}^2$$

As noted in Section 4.2, the effective shear stiffness (GA'_e) must account for both shearing and antisymmetrical bending deformations. This stiffness is given by Eqn. 4.2.3 as

$$GA'_e = \frac{1}{\frac{1}{GA'} + \frac{h^2}{12EI}}$$

However, with the 6-inch rigid segments at the top and bottom of the panel, the stiffness becomes

$$GA'_e = \frac{1}{\frac{1}{\frac{9}{8}(GA')} + \frac{h^2}{\frac{41}{32}(12EI)}} = 3{,}315{,}330\ \text{k.}$$

The factor 9/8 could be used in place of the more accurate 41/32 with negligible loss of accuracy.

For panels modelled using rectangular finite elements, the elastic moduli were first increased by 9/8, and then "fine tuned" as described in the following section.

5.3.2 STIFFNESS MATCH OF PANEL MODELS

For the F.E. and mixed Beam-F.E. models, the elastic moduli of the finite elements were first increased by 9/8 to compensate for the joint width effect. The stiffnesses of the resulting wall models were then compared with the stiffness of the modified beam model, to ensure that equal stiffnesses (and hence essentially identical elastic dynamic properties) were obtained. The stiffnesses were compared for two static loadings, namely lateral force and moment, applied at the roof. The horizontal joints were assumed to be rigid. The computed lateral displacements from the three models were closely similar but not identical. To obtain still closer agreement, the elastic moduli of the rectangular finite elements in the F.E. and Beam-F.E. Models were reduced by 1.4 percent.

In all three models, the masses were lumped at the panel corners only.

5.3.3 DAMPING

Viscous damping is introduced to model dissipation of energy in the wall panels due to miscellaneous causes. Rayleigh damping ($C = \alpha M + \beta K$) corresponding to approximately five percent of critical damping in the first and second modes has been assumed.

The first two periods of vibration of the wall were estimated assuming a cantilever beam with flexural deformations only. The periods

are given [25] by

$$T_1 = 1.787 \frac{ML^3}{EI} = 0.526 \text{ sec.}$$

$$T_2 = 0.283 \frac{ML^3}{EI} = 0.084 \text{ sec.}$$

The values of α and β are then $\alpha = 1.030$ and $\beta = 0.00115$. The actual periods would be somewhat larger than the above values, because of shear deformations.

5.3.4 POSTTENSIONING BARS

In the analyses, vertical loading on the wall was assumed to be provided by gravity alone in some cases and by combined gravity and ungrouted posttensioning bars in others. The posttensioning bars were located as shown in Fig. 3.3.1. The bars were modelled by elastic spring elements connecting the roof to the foundation, with no intermediate connection to the wall. The stiffness of each spring was calculated as

$$k = \frac{EA}{L} = \frac{(30{,}000 \text{ ksi})(0.775 \text{ in}^2)}{(90 \text{ ft})} = 258.3 \text{ k/ft}$$

Each tendon in the actual wall is stressed to a force of 77.2 kips (100 ksi), corresponding to a concrete stress of 201 psi. The prestress was introduced into the analysis by specifying appropriate preload forces on the elements modelling the joints.

5.3.5 INTEGRATION TIME STEP

For all of the inelastic analyses described herein, a time step of 0.001 seconds was used. For cases involving joint slip only, the time step repetition option (see Appendix A) was not used. For cases involving joint opening, experience showed that instability could occur

(although not in all cases), and the time step repetition option was used.

Comparisons of results obtained using different time steps generally showed only small changes in computed response for time steps as large as 0.005 seconds. However, to ensure that correct results were obtained, the value of 0.001 seconds was used.

5.4 APPROXIMATIONS DUE TO MASS LUMPING

5.4.1 GENERAL

In all of the mathematical models, the masses have been lumped at the panel corners only. The masses account for the wall panel mass, the mass of the floor, and the mass of the stairs [34]. The floor and roof masses dominate.

For most of the analyses reported herein, the same values have been specified for both the horizontal (X) and vertical (Y) masses at the mass points. This can lead to potential errors in modelling vertical and rotational effects.

5.4.2 EFFECT OF VERTICAL INERTIA

A problem in modelling the vertical inertia is the amount of floor mass which is assumed to move vertically. If the floor slabs were flexurally rigid, then all of the floor mass would move. However, the floors are actually far from rigid. Therefore, for accurate modelling, it would be necessary to perform 3D analyses, accounting for vertical vibration of the floors.

When gap opening occurs, the panels tilt and vertical displacements of the mass points occur. The inertia forces associated with these displacements could significantly alter the computed response. To assess this effect, a series of analyses with different assumed Y masses has

been carried out. Values equal to the panel mass plus, respectively, 100%, 20% and 0% of the floor and stair masses have been assumed, and the effects on computed gap opening have been determined. The results are discussed in Sections 5.11 and 5.12.

5.4.3 EFFECT OF ROTATIONAL INERTIA

Lumping the panel and floor masses at the corner nodes overestimates the rotational inertia of the panels and may significantly affect the computed response. The effects of rotational inertia have been estimated by studying an elastic wall.

A 10-story cantilever beam (zero width) was analyzed, with its horizontal mass lumped at each floor, and varying amounts of rotational inertia (J) added at the mass points. The beam was assigned a flexural stiffness equal to that of the large panel wall being studied, but shear deformations were ignored. The natural periods of the beam were computed, using the computer program CAL [27], considering the following cases for the rotational mass:

1. No rotational mass ($J = 0$ k.ft.sec^2).
2. Actual panel rotational mass ($J = 32$ k.ft.sec^2).
3. Panel rotational mass for lumped masses at the panel corners ($J = 96$ k.ft.sec^2).
4. Case 3 plus 20% of the floor mass ($J = 226$ k.ft.sec^2).
5. Case 3 plus 100% of the floor mass ($J = 749$ k.ft.sec^2). The masses assumed for most analyses in this report corresponded to this last case.

The calculated values for the first three natural periods are shown in Table 5.4.1. It can be seen that the first period changes little as J is varied, whereas the higher mode periods change by significant amounts.

Because the effects on the first mode period are small, it is probable that overestimation of the rotational mass has minor effects. Nevertheless, further study is desirable.

5.5 EARTHQUAKE RECORDS

For the ground excitation, four earthquake records were used, two real and two artificial, as follows:

1. First 6 seconds of El Centro, N-S component, 1940 record. Peak acceleration = 0.32 g at t = 2.007 sec. Identified herein as "EC" earthquake.
2. First 10 seconds of Pacoima Dam, S16E component, 1971 record. Peak acceleration = 1.17 g at t = 7.740 sec. Identified herein as "PD" earthquake.
3. First 10 seconds of an artificial earthquake generated for an expected peak acceleration of 1.0 g. Peak acceleration = 0.87g at t = 4.760 sec. This record was previously used in a study of reinforced concrete frames by Powell and Row [67], and in an earlier study of large panel walls by Powell and Schricker [26]. The accelerogram simulates strong motion earthquake for firm soil at moderate distance from the epicenter. Identified herein as "AA" earthquake.
4. First 12 seconds of an artificial ground motion, generated at M.I.T. [24] to match the Newmark-Blume-Kapur response spectrum with 2% damping. Peak acceleration = 1.0 g at t = 10.310 sec. Identified herein as "AB" earthquake.

All motions were scaled to produce the same maximum base shear for the Beam Model assuming linear elastic behavior (see Section 5.7). Figures 5.5.1 through 5.5.4 show the acceleration response spectra for the

motions after scaling.

5.6 PARAMETERS TO BE STUDIED

The major parameter varied has been the joint behavior. Several cases with different joint models have been analyzed, and in a few cases the parameters for a given joint model have also been varied. The cases which have been studied are as follows:

1. Simple friction joint. The friction coefficient and strain hardening ratio have been varied (μ = 0.2 and 0.6, k_h/k_s = 0, 0.001 and 0.002).
2. Friction joint with degrading strength. The friction coefficients have been specified to degrade from 0.6 to 0.2 as slip accumulates. The effect of local weakness (in one story) has also been studied.
3. Friction joint with stops. To prevent excessive slip, stops have been added in parallel with friction joints (with and without degradation of the friction coefficient). The stop stiffness has also been varied (values of 0.2 and 2.0 percent of the initial shear stiffness).
4. Keyed joint. The effect of sudden strength loss has been studied.
5. Joints with shear friction behavior. The effect of strength and stiffness degradation of shear friction type has been studied.
6. Joint gap opening with no slip. The effects of elastic and inelastic gap opening have been studied.
7. Joint opening with slip. The effects of elastic gap opening combined with slip have been studied for uncoupled behavior

(separate friction and gap elements), and coupled behavior (combined gap-friction element).

In addition, limited stuides have been carried out considering the following parameters:

8. Panel modelling. The differences between beam and finite element models have been studied.
9. Y-mass (vertical inertia). The effect of the assumed Y-mass on slip and gap opening has been studied.
10. Small changes in panel stiffness. The sensitivity of the response to small changes in the panel stiffness has been studied.

The following parameters have also been varied in order to determine the influence and sensitivity of design assumptions on the computed response:

a) Distribution of vertical load on the joints over the building height. For most cases, two assumptions were made, namely (1) pure gravity (identified as "G" cases); and (2) combined gravity and posttensioning load (identified as "GP" cases). The assumed vertical load distributions are shown in Fig. 5.6.1.

b) Ground motion. For most cases, all four earthquake records were used, although fewer earthquake motions were considered for some studies. Only horizontal ground excitation was considered.

5.7 SELECTION OF EARTHQUAKE INTENSITY

The Beam Model was subjected to all of the earthquakes described in Section 5.5, assuming linear elastic behavior for the joints. The Y-mass was assumed to be equal to the X-mass. An integration time

step of 0.005 sec. was used for the dynamic analysis (less than 1/100 of the first mode period). The maximum computed base shears are shown in Table 5.7.1. The earthquake motions were then scaled to produce a maximum base shear of 950 k for each motion. This value was close to the base shear obtained using the EC ground motion. After scaling, the peak accelerations of the four motions were as follows:

EC: 0.32g

PD: 0.94g

AA: 0.39g

AB: 0.43g

Table 5.7.2 shows the maximum roof deflections and base moments produced by the scaled motions.

5.8 ELASTIC DYNAMIC RESPONSE

The maximum calculated shears at all stories for the scaled motions are shown in Fig. 5.8.1. These shears are compared with the joint shear strengths assuming simple friction resistance only, for μ = 0.2 and 0.6. The distributions of calculated story shears are similar, except that the PD earthquake gives smaller shear forces in several of the lower joints. The calculated values exceed the friction strengths for all cases except the GP case with μ = 0.6.

The maximum calculated overturning moments at all stories are shown in Fig. 5.8.2. The figure compares these moments with the "stabilizing" moments provided by gravity and prestress. The stabilizing moment at any story is assumed to be the overturning moment required to cause pivoting about the panel corners at that story, equal to the vertical load on the joint, multiplied by half the panel width (12 ft). This moment is an upper bound on the overturning moment which can be

resisted at any story. A moment of this magnitude can never be reached in practice, because it would require infinite bearing stress at the panel corner. It is important to note that the overturning moment required to reach zero compressive stress at one end of the joint is only one third of the full pivoting moment. Joint opening actually begins at this lower moment value. The nature of joint opening is considered in more detail in Section 5.11.

The elastic dynamic response was also caculated for the F.E. Model of the wall, with linear elastic joint elements equivalent to those used in the Beam Model. The response was computed for the EC earthquake only, and very close agreement between the two models was found. Table 5.8.1 compares the maximum values of the roof deflection, base shear, and base moment obtained from the F.E. and Beam Models.

5.9 SHEAR STRENGTH RATIO OF JOINTS

From the elastic response of the Beam Model, a shear strength ratio can be defined for each joint as

$$\text{Strength Ratio} = \frac{\text{Maximum Shear Force on Joint}}{\text{Joint Strength}}$$

where the joint strength is the friction resistance corresponding to the vertical load on the joint. The shear forces and joint strengths are shown in Fig. 5.8.1. The variations of the joint strength ratios over the height of the wall are shown in Figs. 5.9.1 through 5.9.4.

It can be seen that the strength ratios for the GP case using $\mu = 0.6$ are less than unity for all joints. This means that there will be no joint slip for this case. For the G cases, the strength ratios increase towards the top joints. For the GP cases, the ratios are more uniform, and the maximum ratios occur in the middle joints.

This suggests that larger slips will occur in the top joints for the G cases, and in the middle joints for the GP cases. The actual computed joints slips are compared with the joint strength ratios in Section 5.10.

5.10 NONLINEAR DYNAMIC RESPONSE: JOINT SLIPPAGE ONLY

5.10.1 RESULTS IDENTIFICATION

For identifying the results, a code of the following type is used: G/μ or GP/μ, in which G or GP identifies the vertical loading (see Section 5.6) and μ identifies the friction coefficient (0.2 or 0.6). In some cases the earthquake identifier is also used (e.g. G/0.2/EC).

5.10.2 EFFECT OF SIMPLE FRICTION

The simplest mathematical model is one in which the joints are allowed to slide only, with constant friction resistance and no gap opening. To study the effect of simple friction, analyses have been carried out as follows.

1. Beam Model (Fig. 5.3.1), with panel and joint stiffnesses as in Table 5.2.1.
2. Four-node simple friction elements at all joints.
3. Joint strengths corresponding to friction coefficients of 0.2 and 0.6 under the vertical loads of both the G and GP cases.
4. Zero strain hardening for the joint elements and zero degradation of friction coefficient (i.e. constant friction force after slip).
5. All four ground motions.

The effects of the posttensioning bars were ignored, because the stiffening effect of the bars is small when joints are not permitted to

open.

As was noted in Section 5.9, the joints for the GP/0.6 case have sufficient strength to remain elastic. For the other cases, the maximum computed joint slips are shown in Figs. 5.10.1 through 5.10.3. Selected envelope values are shown in Tables 5.10.1 and 5.10.2. The following observations may be made.

1. For the pure gravity (G) cases, the slip tends to be concentrated in the upper joints, although some slip occurs at all levels in most cases. This correlates qualitatively with the distribution of the joint strength ratio (see Section 5.9). The slip is more strongly concentrated in the upper joints for the cases with $\mu = 0.6$ than $\mu = 0.2$. With $\mu = 0.2$, substantial slip also occurs at the base of the wall.
2. For the combined gravity and posttensioning (GP) case, the slip tends to be larger in the middle joints (joints 3 through 6), except that substantial slip occurred at the base with the PD and AB earthquakes. The top joint remained elastic. Again, this correlates qualitatively with the distribution of the joint strength ratio, but the differences in slip are much larger than the differences in strength ratio.
3. Substantial variations in the distribution of slip were produced by different earthquake motions. Sensitivity of the computed response to earthquake motion has also been observed in frame structures [67, 22]. Nevertheless, the distributions of slip are qualitatively similar for different motions.
4. The maximum slips (at the top joints) for the G/0.6 and

G/0.2 cases are of similar magnitude. Usually, it is observed that stronger structures undergo smaller deformations (i.e. have smaller ductility factors). The maximum slips for the G and GP cases are also of similar magnitude.

5. The maximum displacements at the roof are compared for the elastic and inelastic cases in Table 5.10.3. These displacements are of similar value for all cases. Because more of the joints slip in the G/0.2 case, it might be expected that the accumulation of slip over the height of the wall would produce larger roof displacements. However, this is not the case, indicating that the maximum slips do not all occur simultaneously.

6. The maximum base shears and base overturning moments are compared for the elastic and inelastic cases in Tables 5.10.4 and 5.10.5. The base shears are equal to the joint strengths for the G/0.2 and GP/0.2 cases, because slip occurs at the base. The base shears and base moments are substantially lower than the elastic values for all cases. The base moments for the G/0.6 case are considerably larger than for the G/0.2 case, reflecting the fact that the stronger joints transmit larger forces into the structure.

7. A useful indication of the amount of inelastic cycling in a joint is the ratio between the maximum and accumulated slips at the joint, where the accumulated slip is the sum of the absolute values of all slip excursions. The maximum and accumulated slips at selected joints are shown in Tables 5.10.1 and 5.10.2. Table 5.10.6 shows the variaton of the

ratio of accumulated to maximum slip throughout the wall for two earthquakes. A zero ratio indicates that the joint remains elastic; a ratio of unity indicates inelastic excursions in one direction only (possibly only a single excursion); and a large value indicates several excursions with reversal. It can be seen that substantial cycling occurs at most slipping joints, with a particularly large amount at the top joint for the G/0.2/EC case. The ratios for the base joint are close to one.

8. The calculated slip values are large, and probably not acceptable in a real structure.

5.10.3 EFFECT OF POST-SLIP STRENGTHENING

In the analyses of the preceding section, the joint friction strength was assumed to be constant (zero "strain hardening" for the joint). Some tests [28] have indicated stiffening behavior in unreinforced joints following slip. Because of this, an analyst may be inclined to specify non-zero strain hardening for friction elements. To study the effect of specifying strain hardening, analyses have been carried out as follows.

1. Beam Model (Fig. 5.3.1), with panel and joint stiffness as in Table 5.2.1.
2. Four-node simple friction elements at all joints.
3. Joint strengths corresponding to the G/0.2 case only.
4. Joint strain hardening ratios of 0.1% and 0.2% (stiffnesses after slip of 1843.7 and 3687.3 k/ft, respectively).
5. EC and AB motions only.

Note that although the strain hardening ratios are small, the post-slip

stiffnesses are large. For the hardening ratio of 0.1%, a slip of 0.1 inches corresponds to a force increase of 184.4 k, which is a large proportion of the basic slip force. Also, because the same stiffness applies for all joints, regardless of strength, the strength increase after slip is proportionately larger for the weaker joints (near the top of the wall) than for the stronger ones (near the base).

The maximum computed slips are shown in Figs. 5.10.4 and 5.10.5 for the EC and AB motions, respectively. In Table 5.10.7, selected envelope values are shown, and compared with the corresponding values for zero strain hardening. The following points may be noted.

1. For the EC motion, the maximum computed slips tend to reduce as the strain hardening ratio increases, but the behavior is not greatly changed.
2. For the AB motion, the maximum slips are again reduced by strain hardening, but the values are now dramatically lower than for the case with zero strain hardening, and the distribution of slip throughout the wall height is much more uniform. From a practical point of view, the computed behavior is much more desirable with strain hardening than without.
3. The base overturning moments are affected little (less than 10%). The base shears are essentially unchanged for the EC motion, but increased for the AB motion. Note that the maximum base shear is limited to 950 k for the zero hardening case, but can increase with increasing slip for the non-zero hardening cases.
4. The maximum computed slips for the cases with non-zero hardening are of similar magnitude for the two ground motions. How-

ever, the accumulated slips are substantially larger for the AB motion, indicating more inelastic cycling.

These analyses indicate that substantially lower slips are likely to be computed if nonzero strain hardening is specified. The analyst must therefore be extremely cautious when specifying strain hardening. Joint strengths which increase with slip should be specified only if strength increase is actually present in the real structure.

5.10.4 EFFECT OF POST-SLIP WEAKENING

In several tests, reductions in friction resistance have been noted in unreinforced joints subjected to cyclic deformation [6]. This type of behavior is essentially the opposite of the strengthening behavior considered in the preceding section. To study the effect of strength degradation, analyses have been carried out as follows.

1. Beam Model (Fig. 5.3.1), with panel and joint stiffnesses as in Table 5.2.1.
2. Four-node degrading friction element at all joints.
3. Initial friction strengths of the G/0.6 case, but degrading to the strengths of the G/0.2 case. Degradation with accumulated slip as shown in Fig. 5.10.6. Degradation complete with an accumulated slip of 2.0 inches. (This value was chosen arbitrarily).
4. Zero strain hardening for the joint elements.
5. EC, PD and AB ground motions.

The maximum computed slips are shown in Figs. 5.10.7 through 5.10.9, and compared with the computed slips for constant friction strength. For all three ground motions, strength degradation leads to large increases in computed slip at certain joints (particularly the topmost joint), and

to a concentration of slip in only a few joints. The concentration of slip is particularly severe for the PD and AB motions.

This behavior is in contrast to that computed for the case with post-slip strengthening. With strengthening, the computed slips were reduced, and were distributed over more joints. With weakening, the computed slips are increased, and are concentrated in fewer joints.

5.10.5 EFFECT OF LOCAL WEAKNESS

The concentration of the computed slips undoubtedly results from localized losses of strength in a few joints. If a particular joint starts to slip, its friction coefficient will degrade, and because the joint is weaker than the surrounding joints, it will "attract" more deformation. This, in turn, leads to further strength loss, and further concentration of deformation.

To confirm this, analyses have been carried out in which one joint has been deliberately made weaker than the other joints, by specifying a lower friction coefficeint. The analyses were as follows.

1. Beam Model (Fig. 5.3.1), with panel and joint stiffnesses as in Table 5.2.1.
2. Four-node simple friction elements at all joints, with zero strain hardening.
3. G/0.6 strength distribution, except as follows: (a) reduction in strength of joint 1 only (topmost joint) by a factor of 5/6 (16% reduction); (b) same reduction in strength of joint 4 only.
4. EC and AB ground motions.

The maximum computed slips are shown in Fig. 5.10.10, and compared with the computed slips for the basic G/0.6 case. The analyses all show

dramatic increases in computed slip at the weakened joints, with reductions in computed slip at all other joints.

Similar analyses were also carried out for the GP/0.2 case, with 10% strength reduction at (a) joint 4; and (b) joint 10 (the base joint). The computed slips for the AB ground motion are shown in Fig. 5.10.11. Again, the analyses show strongly concentrated deformations.

5.10.6 STRENGTH LOSS THROUGH KEY FAILURE

Section 5.10.4 considered the effect of gradual strength loss through progressive reduction of the friction coefficient. More sudden strength losses can occur, through failure of keys and through loss of initial bond strength [10,21]. To consider more sudden strength loss, each joint was modelled using a key element placed in parallel with a simple friction element. The combined shear-slip relationship is shown in Fig. 5.10.12. Analyses were carried out as follows.

1. Beam Model (Fig. 5.3.1), with panel and joint stiffnesses as in Table 5.2.1.
2. Four-node simple friction elements and two-node key elements at each joint, with properties as shown in Fig. 5.10.13. The friction strengths corresponded to the G/0.2 case with zero strain hardening. The key strengths were the same in all joints, arbitrarily assumed to be equal to the friction strength of the base joint (309.1 k). This means that the joint strengths are relatively higher in the upper joints, compared to the G/0.2 case.
3. EC and AB ground motions.

The maximum computed slips are shown in Fig. 5.10.14. Again, the strength loss leads to severe concentration of the deformations. For

the EC motion, only one joint showed any significant slip, with a very large computed value.

These analyses confirm the earlier conclusion that strength loss will cause concentration of the deformation in a small number of joints. Such a concentration of deformation in a real structure would probably be undesirable.

5.10.7 STIFFNESS DEGRADATION OF SHEAR FRICTION TYPE

Dry joints exhbit "shear friction" behavior under cyclic load, as described in Section 2.5. This behavior is characterized by degradation of both strength and stiffness, with a "pinched" hysteresis loop.

In this section only the stiffness is assumed to degrade. The joints are assumed to have properties similar to those observed in Mattock's tests [2,3] with no strength degradation (see Section 4.9). Analyses were carried out as follows.

1. Beam Model (Fig. 5.3.1), with panel and joint stiffnesses as in Table 5.2.1.
2. Four-node shear friction elements at all joints. The properties of the shear friction component are as shown in Fig. 4.9.5a.
3. Simple fricton strengths corresponding to a friction coefficient of 0.2 under the vertical loads of both the G and GP cases.
4. Joint shear friction strengths of 200 k (this value was chosen arbitrarily).
5. Stiffness degrading factor, α, equal to (a) zero (i.e. no stiffness degradation), and (b) unity.
6. EC and AB motions only.

The maximum computed joint slips are shown in Figs. 5.10.15 through 5.10.18. Selected envelope values are shown in Table 5.10.8. The following observations may be noted.

1. The slip distributions are substantially different from the case in which the joint strength was due to simple friction only (Section 5.10.2). In particular, for the G/0.2 case the maximum slip no longer occurs in the topmost joint.
2. The slip magnitudes are less than for the case with simple friction (except for the G/0.2/EC case, in which the maximum slip was slightly increased). Note that the joint strengths with shear friction are greater than in the simple friction case.
3. Stiffness degradation produced significant changes in the distribution of slip over the building height, but no significant differences in magnitude.
4. Unlike the cases with strength degradation, the slip is not concentrated in only a few joints. That is, stiffness degradation alone does not appear to produce undesirable behavior, of the type observed for the joints with strength degradation.
5. The base shears and base overturning moments are larger than for the case with simple friction. This simply reflects the larger joint strengths.

5.10.8 STRENGTH AND STIFFNESS DEGRADATION OF SHEAR FRICTION TYPE

The preceding section considered only stiffness degradation of shear friction type. To study the effect of both stiffness and strength degradation, analyses were carried out as follows.

1. Beam Model (Fig. 5.3.1), with panel stiffnesses as in Table 5.2.1.
2. Four-node simple friction elements in all joints, with strengths corresponding to the G/0.2 and GP/0.2 cases, elastic stiffnesses of $1.844.10^6$ k/ft as before, and zero strain hardening.
3. Two-node key elements in all joints, with stiffnesses and strengths twice those shown in Fig. 5.10.19a (to represent two dry joints per floor level). These properties were the same for all joints.
4. Four-node shear friction elements in all joints, with strengths and other stiffnesses double those shown in Fig. 5.10.19b. These properties were the same for all joints.
5. All four ground motions.

The behavior of the combined key and shear friction elements under cyclic deformation is as shown in Fig. 5.10.20. The total joint behavior is obtained by adding the simple friction behavior. For the G/0.2 case, the combined joint elements give strengths as follows:

(a) Joint 1: 96.8 k degrading to 57.9 k

(b) Joint 5: 217.3 k degrading to 178.4 k

(c) Joint 10: 368.0 k degrading to 329.1 k

For the GP/0.2 case the corresponding values are

(a) Joint 1: 189.4 k degrading to 150.5 k

(b) Joint 5: 309.9 k degrading to 271.0 k

(c) Joint 10: 460.6 k degrading to 421.7k

The maximum strength loss due to "shear friction" behavior under cyclic loading is 38.9 k for all joints.

The maximum computed slips are shown in Figs. 5.10.21 and 5.10.22. It can be seen that once again the trend is for the deformations to be concentrated in a relatively small number of joints. The concentration is not as severe as for the degrading strength examples in earlier sections. Nevertheless, the behavior would probably be undesirable in a practical structure.

5.10.9 EFFECT OF JOINT STOPS

The analyses described in the preceding sections indicate that undesirable behavior will accompany strength loss in a joint, whether the loss is due to joint polishing, key failure or shear friction behavior. On the other hand, the analyses indicate that strength increase, through postulated strain hardening, will produce a more desirable distribution of joint deformations.

From published tests on the behavior of joints under cyclic load, it appears that strength loss rather than strength gain is more likely to occur. That is, sustained strain hardening is not likely to be present in a typical joint.

Nevertheless, the analyses also indicate that the panel stresses are reduced substantially if joints are allowed to slip. A compromise is needed which will allow slip, but not allow the amount of slip to become excessively large. A possible design solution is to design joints with positive stops, which allow a controlled amount of slip to take place, but then engage and develop resistance against further slip. The bolted joint with slotted holes described by Pall and Marsh [40] would develop this type of resistance. A joint containing stiff steel dowels in clearance holes might also be designed to develop similar characteristics. For design, it would be necessary to determine appropriate

stop clearances and stiffnesses, so that sufficient reduction in panel loads could be obtained without allowing excessive joint deformations.

To investigate the effect of stops for the case with no strength degradation, analyses were first carried out as follows.

1. Beam Model (Fig. 5.3.1), with panel and joint stiffnesses as in Table 5.2.1.
2. Four-node simple friction elements at all joints, with zero strain hardening.
3. Joint strengths corresponding to the G/0.2 and G/0.6 cases.
4. Stops with 0.25 inch clearance, and elastic stiffness k_s (Fig. 5.10.23). These values were chosen arbitrarily.
5. EC and AB ground motions.

Comparisons of the computed slips for the cases with and without stops are shown in Figs. 5.10.24 and 5.10.27. Table 5.10.9 shows selected envelope values.

As expected, the slip is distributed more uniformly throughout the structure compared with the case without stops. Less slip occurs at joints which previously experienced large amounts of slip, and more slip at joints which previously had little or no slip. The joint shears are significantly increased. However, the maximum overturning moments change very little.

In Section 5.10.4, it was shown that joints with degrading friction strength would "attract" large amount of slip. To study the effect of stops in this case, analyses were carried out as follows.

1. Beam Model (Fig. 5.3.1), with panel and joint in Table 5.2.1.
2. Four-node degrading friction elements at all joints, with

zero strain hardening.

3. Initial friction strength corresponding to the G/0.6 case, with degradation to the G/0.2 case as shown in Fig. 5.10.6.
4. Stops with 0.25 inch clearance, and stiffnesses of (a) 0.2% and (b) 2.0% of k_s.
5. EC, PD and AB ground motions.

The maximum computed slips are shown in Figs. 5.10.28 and 5.10.29 and compared with the case without stops. Selected envelope values are shown in Table 5.10.10.

It can be seen that the slips at the critical joints are reduced considerably, and that the distribution of slip throughout the wall height is made more uniform, compared to the case without stops. The effect is substantially larger for the stiffer stops (2.0% of k_s). The stiffer stops lead to significant increases in the base shear and overturning moment, whereas the increases for the more flexible stops are small.

It can be concluded that the undesirable effects of strength degradation in the basic joint can be counteracted if a sufficiently strong stop device can be included in the joint.

5.10.10 SENSITIVITY OF MATHEMATICAL MODEL

To study the sensitivity of the computed slips to changes in the mathematical model, analyses were carried out using the F.E. Model (Figs. 5.3.2) for the case of simple friction with zero strain hardening. The maximum computed slips were all virtually identical to those calculated for the Beam Model (Fig. 5.3.1). This confirms the similarity of the two models for cases involving joint shear deformation only.

To study the sensitivity to changes in the specified panel stiff-

ness, analyses were carried out using the Beam Model, with the panel stiffnesses (EA, EI and GA') changed by (a) + 10% and (b) - 10% for all panels. The joints were of simple friction type with zero strain hardening. The EC and AB ground motions were considered, for the G/0.2 and G/0.6 joint strengths. The maximum computed slips are shown in Figs. 5.10.31 through 5.10.34.

The distributions of slip are all qualitatively similar, but there are significant changes in the slip magnitudes. The changes are larger for the G/0.6 case than for the G/0.2 case. These results indicate that inelastic seismic analyses cannot be relied upon to give precise quantitative results. In practice, it is unlikely that an analyst will be able to determine the stiffness of a panel within 10%. The computed results will generally give a reliable indication of the qualitative effect of an earthquake, but only an approximate indication of the quantitative effect.

Even more important than uncertainties in the modelling of stiffness, however, are the uncertainties in modelling the strength characteristics and in selecting the ground motion. The analyses of the preceding sections have shown that changes in the assumed strengths and motions can produce major changes in the computed response. As a result, a great deal must depend on the engineering judgement of the analyst, both in modelling the structure and in interpreting the results.

Fortunately, the ability of a building to survive an earthquake is unlikely to be affected by subtleties in the reponse, but rather by gross overall considerations. The computed response of a well conceived structure may be quite sensitive to the analysis assumptions, but an analysis is likely to show, qualitatively, that the structure performs

well. Correspondingly, the computed response values for a poorly conceived structure may vary a great deal, but qualitatively the analysis is likely to indicate fundamental weaknesses in the design.

5.10.11 PERMANENT DEFORMATION

Estimates of permanent deformation were made for the G/0.2 case with simple friction elements, for the EC and AB motions. This was done by adding two seconds of zero accelerations to the EC motion and three seconds to the AB motion, and continuing the analysis to the ends of these extended motions. The amounts of slip at the end of the analyses were as follows.

Joint 1, EC motion: 0.379 inch (compared with 0.387 inch maximum).

Joint 2, AB motion: 1.418 inch permanent (compared with 2.338 inch maximum).

5.11 NONLINEAR DYNAMIC RESPONSE: JOINT OPENING ONLY

5.11.1 GENERAL

In the analyses of the preceding Section, it was assumed that only slip would occur at the joints, with no gap opening. Becker and Llorente [8,48] have stated that opening, rather than sliding, is the dominant mode of joint deformation in a large panel building.

The calculated overturning moments for elastic behavior were shown in Fig. 5.8.2 These moments were substantially larger than the stabilizing (pivoting) moments due to gravity and prestress, indicating that gap opening might occur. The overturning moments have also been calculated for the cases in which the joints slip. For the Beam Model with simple friction joints (as considered in Section 5.10.2), the overturning and stabilizing moments are compared in Figs. 5.11.1 and 5.11.2. These figures show that for the G/0.2 and GP/0.2 cases, the calculated over-

turning moments exceed the stabilizing moments only at the base joints, suggesting that little gap opening will occur. For the G/0.6 and GP/0.6 cases, however, the calculated overturning moments are substantially larger than the stabilizing moments at almost all joints, indicating that substantial joint opening can be expected.

It may be noted that the results of the preceding section, assuming joint slip only, are not necessarily invalid. The tendency for joint slip to occur without joint opening will be larger for walls which are shorter or wider than the wall considered here, and also for walls of I or box section in plan, in which the flange walls increase the moment resistance more than the shear strength.

In this section, the behavior is calculated considering only joint opening, with no slip. In Section 5.12, analyses with both opening and slip are considered.

5.11.2 ANALYSIS MODELS

Analyses have been carried out using both the Beam and Finite Element Models, to determine whether the computed response is sensitive to the modelling assumptions. The effects of changing the assumed amount of vertical inertia has also been studied.

In all cases, five gap elements were assumed in each joint, as shown in Fig. 5.11.3. The compression stiffness of the complete joint was divided among the gap elements in proportion to their tributary widths (1/8; 1/4; 1/4; 1/4; 1/8 of total, respectively). The effects of gravity load and presetress were specified as initial compression forces in the elements, also distributed in the above proportions.

For the Beam Model, each horizontal joint is assumed to remain straight (plane sections assumption), and because the gap elements are

very stiff, gap opening tends to occur suddenly across the entire joint width, with the upper panel pivoting about a corner. For the Finite Element Model, however, horizontal sections do not remain plane, and gap opening can occur more progessively. Note, however, that the finite element mesh used in the study is rather coarse. A finer mesh may be necessary for accurate analysis of gap opening effects [8].

In all cases a time step of 0.001 seconds was specified, and the time step repetition option was used.

5.11.3 EFFECT OF ELASTIC OPENING

If the tension force in any gap element due to the earthquake effect exceeds the initial compression force due to gravity load or prestress, the gap begins to open. This occurs when the overturning moment is one third of the stabilizing moment. With the Finite Element Model, significant gap opening can then occur. For the Beam Model, however, with stiff gap elements, virtually no opening occurs until the overturning moment equals the stabilizing moment.

To study the effect of gap opening, analyses have been carried out as follows.

1. Beam Model (Fig. 5.3.1), Finite Element Model (Fig. 5.3.2) and mixed Beam-F.E. Model (Fig. 5.3.3), with panel stiffnesses as in Table 5.2.1.
2. For the Beam and Finite Element Models, five gap elements at each joint, preloaded according to the G and GP vertical load distributions. For the mixed Beam-F.E. Model, five gap elements in joints 6 through 10, but only two elements in joints 1 through 5 (placed at the panel corners). Figure 5.11.4 shows the force-deformation relationship for the gap

elements.

3. Vertical (Y) inertia assumed to be 100% of the horizontal (X) inertia (see Section 5.4 for discussion). The mass is lumped at the panel corners for all three models.
4. For the GP case, posttensioning bars modelled as described in Section 5.3.
5. EC ground motion only. Note that only horizontal ground motion is considered.

The maximum computed gap openings are shown for the G case in Fig. 5.11.5. The distributions of gap opening are quite different for the Beam and Finite Element Models, with the Beam Model predicting smaller openings in the upper joints, and a larger opening at the base. The calculated openings for the mixed Beam-F.E. Model are even smaller than those for the Beam Model in the upper joints, but are close to the Finite Element Model in the lower joints.

It is not difficult to see why substantially different results are computed for the different models. With the Finite Element Model, a gap will begin to open when the load on the outermost gap element reduces to zero. Assuming plane sections remain plane, the moment at this time will be only one third of the moment required to produce full pivoting about one corner of the panel. The gap will then open progressively, accompanied by distortion of horizontal cross sections. With the Beam Model and only two gap elements per joint, gap opening will occur suddenly, when the moment reaches the full pivoting value. For the Beam Model with five gap elements, gap opening will begin at one third of the pivoting moment, but if the gap elements are very stiff, the amount of opening will be very small between the initial opening

and development of the full pivoting moment. The calculated behavior will thus be close to that with only two gap elements per joint.

The results indicate that allowing gradual gap opening will lead to smaller computed gaps, with a more uniform distribution of gap opening throughout the height of the structure. This is to be expected. If the gap opening is sudden, opening will occur first at the joint where the overturning moment first exceeds the pivoting moment. The moment at the pivoting joint will then remain constant, and the moments at other joints will tend also to remain constant. With gradual opening, on the other hand, opening at the most critical joint will occur at a moment well below the pivoting moment, and the moment will continue to increase. The moments at other joints will thus also continue to increase and they also will begin opening at moments well below the pivoting moments. The results for the Finite Element Model are undoubtedly more realistic than those for the Beam Model.

The computed gap openings for the GP case are shown in Fig. 5.11.6, for the Beam and Finite Element Models only. The results show the same trend as the G case. Note that the upper joints for the GP case have larger stabilizing moments than the G case because of the posttensioning, with the result that opening does not occur at these joints.

The maximum calculated moments obtained from the Beam Model are shown in Figs. 5.11.7 and 5.11.8, and compared with the stabilizing (pivoting) moments and the moments calculated when gap openings are not allowed at the joints (i.e. the elastic case). The maximum moments for cases with gap opening would be expected not to exceed the pivoting moments. However, because of vertical inertia at the mass points, the moments for the G case can exceed the pivoting moments by significant

amounts. For the GP case, a further increase occurs because of force increase in the posttensioning bars as the joints open.

Table 5.11.1 compares the maximum roof deflection, maximum gap opening at the base, and maximum base overturning moment for the linear (without gap opening) and nonlinear (with gap opening) cases. The maximum roof deflections do not change substantially when gap opening is allowed. However, the maximum base overturning moments are significantly reduced. Figure 5.11.9 shows how much the story shears are reduced when the joints are allowed to open for the G and GP cases. Both slipping and tilting serve to reduce the forces in the structure by a mechanism similar to base isolation, in which only forces of limited magnitude are permitted to be transferred from the ground to the structure. Joint slipping is an inelastic phenomenon which dissipates energy, whereas panel tilting is essentially elastic.

The maximum computed joint shears obtained from the Beam Model for both the G and GP cases are shown in Fig. 5.11.10, and compared with the joint strengths for the 0.2 and 0.6 friction coefficients (simple friction resistance). The computed shears for the G case are larger than the joint strengths for both friction coefficients; for the GP/0.2 case, the maximum computed shears are larger than the joint strengths only at the top joints; and for the GP/0.6 case the strengths exceed the calculated shears at all joints. This indicates that the assumption of joint opening with zero slip is reasonable for the GP case, but incorrect for the G case. Since the assumption of joint slip with no opening is also incorrect, it is apparent that both slip and opening can be expected to occur in some cases.

5.11.4 EFFECT OF ASSUMED VERTICAL INERTIA

The magnitude of the Y-mass has been varied, in order to study its effect on the computed joint opening. Analyses were carried out as follows.

1. Beam Model (Fig. 5.3.1), with panel and joint stiffnesses as in Table 5.2.1.
2. Five 4-node gap elements at each joint, with compressive stiffnesses as before and preload based on the gravity (G) distribution.
3. Three different values for the vertical (Y) masses as follows: (a) Y-mass = X-mass (X-100% Y case); (b) Y-mass = 30% of X-mass (X-30% Y case); (c) Y-mass = 0 (X-0% Y case). Table 5.11.2 shows the nodal X and Y masses for the three cases.
4. EC ground motion only.

The maximum computed gap openings are shown in Fig. 5.11.11. The envelope values of selected results are shown in Table 5.11.3. The following points may be noted.

1. The results for gap openings are similar in all three cases, except for differences at joint 9. Surprisingly, the gap openings for the case with Y-mass equal to 30% of X-mass do not lie consistently between those for the other cases.
2. The maximum overturning moments reduce with decreasing vertical inertia, as shown in Fig. 5.11.12. Note that when the Y-mass is zero the maximum overturning moments are equal to the pivoting moments, whereas the overturning moments exceed the pivoting moments for nonzero Y-mass. This

demonstrates that the increase is due to vertical inertia forces.

3. The maximum panel shear forces for all three cases are shown in Fig. 5.11.13. Again, the X-30%Y case does not lie consistently between the X-100%Y and X-0%Y cases.

It can be concluded that changes in the assumed Y mass could have significant effects on the computed response. The changes can be attributed to the influence of vertical inertia on the natural period of vibration for configurations with open gaps. The changes in period lead to changes in the computed response. Further study is needed to determine the "correct" amount of vertical inertia to be assumed for analysis.

5.11.5 EFFECT OF INELASTIC JOINT OPENING (JOINT CRUSHING)

When a joint opens, that portion of the joint which remains closed may crush in compression. Thus, the connection does not behave elastically under bearing forces, but yields when the magnitude of the bearing force exceeds the joint compressive strength. The mathematical model used to study inelastic joint opening was as follows:

1. Beam Model (Fig. 5.3.1), with panel and joint stiffnesses as in Table 5.2.1.
2. Five 4-node gap elements at each joint, with compressive stiffnesses as before and preload based on the gravity (G) load distribution.
3. Joint compressive strength corresponding to a mortar strength of 4000 psi. The strength of each inner element is twice that of each outer element, as shown in Fig. 5.11.14.
4. Y-mass equal to X-mass (X-100%Y case).

5. EC ground motion only.

Figure 5.11.15 shows the maximum computed gap openings at the joints, and compares them with the case with elastic joint opening. The following points may be noted.

1. The magnitude of gap opening is reduced substantially at joints 8 and 9, but increased substantially at joint 6. Overall, however, the openings are similar for the elastic and inelastic cases.
2. The analysis showed crushing at joints 7, 8, and 10 only. The calculated compressive deformations for all joints are shown in Table 5.11.4. It can be seen that substantial inelastic deformation occurred only at the base.
3. Figure 5.11.16 shows the maximum overturning moments and compares them with the case with elastic gap opening. The overturning moments are reduced at all stories, presumably because crushing increases the base isolation effect.
4. Figure 5.11.17 shows the computed panel shears for the elastic and inelastic cases. With joint crushing the shear forces are smaller in the upper stories and larger in the lower stories. This can be attributed to changes in the dynamic characteristics of the structure, leading to changes in the shear distribution.

5.11.6 CONCLUSIONS ON JOINT OPENING

In large panel structures, gap opening is likely to occur, and can constitute an important mode of deformation at the joints. Joint opening can significantly reduce the forces in the structure by a base isolation mechanism. However, the analyses indicated no substantial

increase in the roof displacement, larger deformations in the joints being balanced by smaller deformations in the panels.

When posttensioning bars were used, the effect was to increase the stabilizing moments, with the result that gap opening did not occur in the top joints. The results for the GP case indicated smaller joint openings and smaller roof deflections compared with the G case.

The Finite Element Model almost certainly predicts the gap openings more correctly, since this model allows distortion of the panel edges, with gradual gap opening. This model predicts a more uniform distribution of gap opening throughout the height of the wall than the Beam Model. That is, the Beam Model predicts a larger opening at the base and smaller openings at the other joints.

The analyses indicate that the effect of vertical inertia on the calculated joint opening is small, but that there is a significant effect on the panel and joint stresses because of changes in the overturning moments.

A possible danger when joint opening occurs is that the bearing area between panels is reduced, and the compression and shear stresses are thus increased. It has been emphasized by Llorente [8] that the resulting high stresses could cause crushing in the connections or fracturing of the panel corners. There is thus a need for detailed estimation of the deformations and stresses developed when gaps open. The analyses described herein do not provide detailed values.

5.12 NONLINEAR DYNAMIC RESPONSE: COMBINED SLIP AND OPENING

5.12.1 GENERAL

For the G/0.2, GP/0.2 and G/0.6, the analyses of the preceding sections indicate that both slip and gap opening will occur. Analyses

have thus been carried out allowing both of these effects to occur simultaneously. Only the Beam Model has been considered, with only two gap elements per joint. This does not provide accurate results for the amount or distribution of gap opening, but allows comparison of the results obtained with different analysis assumptions.

The properties of the model were as follows.

1. Beam Model (Fig. 5.3.1) with panel stiffnesses as in Table 5.2.1.
2. Two gap elements (at the panel corners) plus simple friction elements in each joint. In some analyses separate gap and friction elements were used, so that the friction strength was independent of bearing force (uncoupled case). In other analyses, coupled gap-friction elements were used.
3. Vertical (Y) inertia assumed to be 100% of horizontal (X) inertia.
4. For the GP case, posttensioning bars modelled as described in Section 5.3.
5. All four ground motions.

5.12.2 UNCOUPLED CASE

For the uncoupled case, the maximum computed joint slips are shown in Figs. 5.12.1 through 5.12.3. Figure 5.12.4 shows the maximum gap openings for the case G/0.6 subjected to the EC motion. Maximum values of selected results are shown in Tables 5.12.1 and 5.12.2. The following observations can be made.

1. A comparison of the slip results with the slips from Section 5.10.1 (which ignored gap opening) shows that when the amount of gap opening is very small (i.e. the G/0.2 and GP/0.2 cases), the slip magnitudes and distributions are affected little by

gap opening (compare Figs. 5.12.1, 5.12.3 with Figs. 5.10.1, 5.10.3).

2. For the G/0.6 case, the gap openings are larger. In this case, the calculated slips with gap opening are much smaller than when gap opening is ignored (compare Fig. 5.12.2 with Fig. 5.10.2). However, the calculated gap openings for this case are similar whether or not slip is allowed (compare Fig. 5.12.4 with Fig. 5.11.8).

5.12.3 COUPLED CASE

In the coupled gap-friction element, the friction resistance is proportional to the bearing force. Because of the vertical (Y) inertia, the total bearing force on any joint can vary somewhat when a gap is open, and hence the friction resistance can also vary. The effect of this variation should, however, be small.

The maximum computed joint slips for the coupled case are shown in Figs. 5.12.5 through 5.12.7. Tables 5.12.3 and 5.12.4 show envelope values of selected results. The following observations can be made.

1. The slip distributions for both the G/0.2 and GP/0.2 cases are very close to the case when the friction elements are uncoupled from the gap elements (compare Figs. 5.12.5, 5.12.7 with Figs. 5.12.1, 5.12.3). However, for the G/0.6 case, the calculated slips increase at most joints (compare Fig. 5.12.6 with Fig. 5.12.2).
2. The maximum gap opening and bearing force at the base joint are similar for the coupled and uncoupled cases, except that the maximum base gap is increased for the GP/0.2 case under the PD and AA earthquakes.

3. The maximum overturning moment at the base remains essentially unchanged. However, the maximum base shear increases in the coupled case, because the strength of the friction component depends on the bearing force in the gap component, and this is increased because of vertical inertia.

5.12.4 EFFECT OF COMPUTATIONAL SCHEME

A possible source of difference between the results for the coupled and uncoupled cases is in the computational scheme. The procedure used to determine the friction resistance for the coupled gap-friction element has been described in Section 4.7. In order to test the consistency of the numerical procedure, analyses have been carried out with zero Y mass. With this assumption, the total vertical force on any joint must remain constant, and hence the friction resistance should be unchanged. The results for the coupled and uncoupled cases should therefore be identical.

Figures 5.12.8 and 5.12.9 show comparisons of maximum computed slips and gap openings for the G/0.6 case, for both the coupled and uncoupled cases, when the nodal Y masses are specified to be zero. It can be seen that the results for the EC earthquake are closely similar, but that the results are substantially different for the AB earthquake.

This comparison indicates that the computed response is sensitive to the computational scheme. Further work is being carried out to explore the reason for this sensitivity, and to improve the computational scheme. In the meantime, the results of gap opening analyses should be interpreted cautiously. In particular, analyses should be carried out for different time steps, to ensure that consistent results are obtained.

6. CONCLUSION

6.1 CONCLUSIONS

This report has explored several aspects of the seismic response analysis of large panel structures, including mathematical modelling, numerical computation, and the influence of various parameters on the computed response. Although the study has been a lengthy one, many questions remain unanswered and much additional work remains before analyses of actual buildings can be carried out with confidence. Conclusions which can be reached from the study are as follows.

(1) More experimental data is needed on the behavior of large panel joints, especially under cyclic loading. So little data is currently available that not even the static strength can be predicted reliably.

(2) The computed responses of a given mathematical model for different ground motions are qualitatively similar. This indicates that inelastic dynamic analysis can be used in design to predict the overall expected response of the structure. In particular, inelastic analysis can assist in identifying design weaknesses which could lead to excessive damage in a strong earthquake. However, inelastic dynamic analysis cannot be expected to give accurate quantitative results.

(3) The computed response can be very sensitive to the assumed post-yield or post-slip behavior. In particular, the computed response is sensitive to the assumed amount of post-slip "strain hardening". Great care must be taken in specifying the post-slip stiffness, otherwise grossly incorrect results can be obtained.

(4) A particularly important conclusion is that undesirable

behavior can be expected if the joints lose strength against slip after initial sliding occurs. If a joint loses strength, the analyses indicate a consistent tendency for slip deformations to be concentrated in the joint which slips first, because it becomes weaker than the surrounding joints. It can be concluded that sound design requires that joints be detailed such that they gain strength after sliding begins.

(5) The analyses also show that if a particular joint is initially weaker than the surrounding joints slip will tend to be concentrated in the weaker joint. This supports the preceding conclusion that joints should be designed to gain strength after sliding begins.

(6) The computed response can be sensitive to the computational procedure and particularly to the time step used in the step-by-step analysis. It is advisable, with the present version of DRAIN-2D, to repeat the analysis with a different time step to ensure that consistent results are obtained.

(7) Both slip and gap opening at joints are effective in reducing the forces induced in the panels of a large panel structure. The reduction is partly due to a base isolation effect and partly due to hysteretic energy absorption in inelastic joints.

6.2 FUTURE WORK

The analyses in this report have placed more emphasis on joint slip than on gap opening. It is recognized, however, that in many cases gap opening may dominate. Work is continuing to incorporate more sophisticated modelling of gap opening into the analysis, in particular by allowing progressive gap opening rather than sudden tilting [48].

Work is also continuing on refining the computational procedure to provide greater economy and reliability, especially for gap opening

analyses in which very large stiffness changes can occur. An improved time stepping scheme, based on work by Hibbitt and Karlsson [71], has been developed and is being incorporated into DRAIN-2D. This scheme has the advantage that the time step is selected automatically by the computer program and is varied, as necessary, during the analysis to achieve a specified degree of accuracy. A modified version of DRAIN-2D incorporating this and other improvements is being prepared.

REFERENCES

1. Pollner, E., Tso, W. K., and Heidebrecht, A. C., "Analysis of Shear Walls in Large-Panel Construction," Canadian Journal of Civil Engineering, Vol. 2, No. 3, Sept. 1975.

2. Mattock, A. H., "The Shear Transfer Behavior of Cracked Monolithic Concrete Subjected to Cyclically Reversing Shear," Report SM74-4, Department of Civil Engineerg, University of Washington, Nov. 1974.

3. Mattock, A. H., "Shear Transfer under Cyclically Reversing Loading Across an Interface between Concretes Cast at Different Times," Report SM77-1, Department of Civil Engineering, University of Washington, June 1977.

4. Shemie, M., "Bolted Connections in Large Panel System Buildings," Journal of the Prestressed Concrete Institute, Vol. 18, Jan/Feb, 1973.

5. Spencer, R. A., Neille, D. S., "Cyclic Tests of Welded Headed Stud Connections," Journal of the Prestressed Concrete Institute, Vol. 21, No. 3, Man/June, 1976.

6. Verbic, B., "Test of Panel Joints in "Vranica" Type Large Panel Building," Institute za Materijale: Konstruckcije, Sarajevo, Yugolsavia, April 1977.

7. Brankov, G., Sachanski, S., "Response of Large-Panel Buildings for Earthquake Excitation in Nonelastic State, "Sixth World Conference on Earthquake Engineering, New Delhi, India, Jan. 1977.

8. Llorente, C., "The Effect of Opening of Horizontal Connections on the Dynamic Response of Precast Panel Buildings," Submitted in partial fulfillment of the requirements for the degree of Master of Science in Civil Engineering at the Massachusetts Institute of Technology, June 1977.

9. Olesen, S.O., "Effects of Vertical Keyed Shear Joints on the Design of Reinforced Concrete Shear Walls," Industrialization in Concrete Building Construction, ACI, Publication No. SP-48, 1975.

10. Hansen, K., Kavyrchine, M., Mehlhorn, G., Olesen, O., Dume, D., and Schwing, H., "Design of Vertical Keyed Shear JOints in Large Panel Buildings," Building Research and Practice, July/August 1974.

11. Cholewicki, A., "Loadbearing Capacity and Deformability of Vertical Joints in Structural Walls of Large Panel Buildings," Building Science, Vol. 6, 1971.

12. Velkov, M. D., Gavrilovic, P., Jurukovski, D., "Seismic Stability of an 18-Story Large Panel Building Constructed in Modified "Balancy" Precast System in Novi Beograd: Analytical and Experimental Study," Sixth European Conference on Earthquake Engineering, Dubrovnik, Yugoslavia, Sept. 1978.

13. Santhakumar, A. R., Swamidenari, A., and Lakshmipathy, M., "Behavior of Joints in Prefabricated Shear Walls for Seismic Zones," Sixth World Conference in Earthquake Engineering, New Delhi, India, Jan. 1977.

14. Ma, S. M., Bertero, V. V., and Popov, E. P., "Experimental and Analytical Studies on the Hysteretic Behavior of Reinforced Concrete Rectangular and T-Beams," EERC Report 76-2, University of California, Berkeley, May 1976.

15. Gergely, P., "Experimental and Analytical Investigations of Reinforced Concrete Frames Subjected to Earthquake Loading," Workshop on Earthquake-Resistant Reinforced Concrete Building Construction, University of California, Berkeley, July 1977.

16. Jimenez, R., Perdikaris, P., Gergely, P., White, R., "Interface Shear Transfer and Dowel Action in Cracked Reinforced Concrete Subject to Cyclic Shear," Proceedings of the National Structural Engineering Conference, ASCE, Vol. 1, Wisconsin, Aug. 1976.

17. Fintel, M., "Performance of Precast Concrete Structures during Romanian Earthquakes of March 4, 1977," PCI Journal, Vol. 22, No. 2, March/April 1977.

18. Smith, J. K., Gergeley, P., White, R. N., "The Effects of Cracks on the Seismic Analysis of Reinforced Concrete Nuclear Containment Vessels," Report No. 368, Department of Structural Engineering, Cornell University, Ithaca, N.Y., April 1977.

19. Aktan, H. M., "A Method to Analyze the Cyclic Behavior of the Slender Reinforced Concrete Shear Walls," Ph.D. Dissertation submitted to the University of Michigan, June 1977.

20. Mattock, A. H., "Effect of Reinforcing Bar Size on Shear Transfer Across a Crack in Concrete," Report SM77-2, Department of Civil Engineering, University of Washington, Sept. 1977.

21. Lacombe, G. and Pommeret, M., "Les Joints Structuraux Dan Les Constructions en Grands Panneaux Prefabriques," Annales de I.T.B.T.P., Gros Oeuvre, No. 18, Paris, Feb. 1974.

22. Kan, C. L., Chopra, A. K., "Linear and Nonlinear Earthquake Responses of Simple Torsionally Coupled Systems," EERC Report No. UCB/EERC 79-03, University of California, Berkeley, Feb. 1979.

23. Paulay, T., Loebes, P. J., "Shear Transfer by Aggregate Interlock," ACI Special Publication No. SP-42, Vol. 1, 1974.

24. Becker, J. M., Private Communications, MIT, Cambridge, Mass.

25. Clough, R. W. and Penzien, J., "Dynamics of Structures," McGraw-Hill, N.Y. 1975.

26. Powell, G. H., Schricker, V., "Ductility Demands of Joints in Large Panel Structures," ASCE Fall Convention, San Francisco, Oct. 1977, Preprint 3022.

27. Wilson, E. L., "CAL78 User Information Manual," Report No. SESM 79-1, University of California, Berkeley, Nov. 1978.

28. Fintel, M., Private Communications, Portland Cement Association, Skokie, Illinois.

29. Velkov, M., "Behavior of Large Panel Building During the Romania Earthquake of March 4, 1977," Seminar on Constructions in Seismic Zones, Bergamo-Udien, Haly, May 1978.

30. Gates, N. C., "The Earthquake Response of Deteriorating Systems," PhD. Dissertation Submitted to the California Institute of Technology, March 1977.

31. Schwing, H. and Mehlhorn, G., "Overall Behavior of Large Panel Shear Walls," Betonwek and Fertigteil-Technik, Heft 5, 1974.

32. Fintel, M., Schultz, D., and Iqbal, M., "PCA Report No. 2: Philosophy of Structural Response to Nromal and Abnormal Loads," Design and Construction of Large-Panel Concrete Structures, Department of Housing and Urban Development, Washington, D.C., Aug. 1976.

33. MacLeod, I. A., "Large Panel Structures," Handbook of Concrete Engineering, Mark Fintel, Editor, Van Nostrand Reinhold Co., N. Y. 1974.

34. Frank, R., "Dynamic Modeling of Large Panel Precast Panel Buildings Using Finite Elements with Substructuring," Report No. R76-36, Department of Civil Engineering, MIT, Cambridge, Mass., Aug. 1976.

35. Polyakov, S., "Design of Earthquake Resistant Structures," Mir Publishers, Moscow, 1974.

36. Petersson, H., Popov, E. P., Bertero, V. V., "Practical Design of R/C Structural Walls using Finite Elements," IASS World Congress on Space Enclosures, Montreal, July 1976.

37. Djabua, S. A., Chachava, T. N., Abashidze, G. G., Djishkariari, N. M., and Koeuoklidoze, G. S., "Research on Seismic Resistance of Large Panel Apartment Buildings," Proceedings of the Sixth World Conference in Earthquake Engineering, New Delhi, India, Jan. 1977.

38. Jabua, J. A., Chachava, T. N., Abashidze, G. G. and Rekvava, P. A., "Some Research and Designing Problems of Earthquake Resistance of Large Panel Buildings," Sixth European Conference on Earthquake Engineering, Dubrovnik, Yugoslavia, Sept. 1978.

39. Neille, D. S., "Behavior of Headed Stud Connections for Precast Concrete Panels under Monotonic and Cyclied Shear Loading," Ph.D. Dissertation Submitted to the University of British Columbia, Structural Research Series, Report No. 20, Vancouver, British Columbia, Oct. 1977.

40. Pall, A. S. and Marsh, C., "Seismic Response of Large-Panel Structures Using Limited-Slip Bolted Joints," Third Canadian National Conference on Earthquake Engineering, McGill University, Montreal, June 1979.

41. Paulay, T., Park, R., and Phillips, M. H., "Horizontal Construction Joints in Cast-in-Place Concrete," Shear in Reinforced Concrete, ACI Special Publication No. SP-42, Detroit 1974.

42. Fiorato, A. E. and Corley, W. G., "Laboratory Tests on Earthquake Resistant Structural Wall Systems and Elements," Workshop on Earthquake-Resistant Reinforced Concrete Building Construction, University of California, Berkeley, July 1977.

43. Yeroushalmi, M. and Harms, H. G., "Behavior of Vertical Joints Between Precast Concrete Wall Panels Under Cyclic Reversed Shear Loading," Structural Models Laboratory, Report No. M78-2, Dept. of Civil Engineering, Drexel University, Philadelphia, March 1978.

44. Becker, J. M., Roesset, J. M., Llorente, C., Lanham, K., "The Seismic Response of Precast Concrete Panel Buildings Considering Connection Behavior," Sixth Europena Conference on Earthquake Engineering, Dubrovnik, Yugoslavia, Sept. 1978.

45. Kanaan, A. E. and Powell, G. H., "General Purpose Comptuer Program for Inelastic Dynamic Response of Plane Structures," Report No. EERC 73-6, Earthquake Engineering Research Center, University of California, Berkeley, April 1873.

46. Hughes, T. J. R., Coughey, T. K., Liu, W. K., "Finite-Element Methods for Nonlinear Elastodynamics Which Conserve Energy," Journal of Applied Mechanics, Vol. 45, June 1978.

47. Przemieniecki, J. S., "Theory of Matrix Structural Analysis," McGraw-Hill, N. Y. 1968.

48. Becker, J. M., Llorente, C., "Seismic Design of Precast Concrete Panel Buildings," Workshop on Earthquake-Resistant Reinforced Concrete Building Construction, Univ. of California, Berkeley, July 1977.

49. Park, T. and Paulay, R., "Reinforced Concrete Structures," John Wiley and Sons, London, 1975.

50. Rosman, R., "Approximate Analysis of Shear Walls Subjected to Lateral Loads," ACI Journal, Vol. 61, No. 6, June 1974.

51. Lewicki, B., "Building with Large Prefabricates," First edition, Elsevier Publications Co., London, 1966.

52. Iyengor, B. and Hariss, H. G., "Behavior of Horizontal Joints in Large Panel Precast Concrete Buildings," Report No. M78-1, Structural Models Laboratory, Dept. of Civil Enginnering, Drexel University, Philadelphia, Feb. 1978.

53. Johal, L. S. and Hanson, N. W., "Horizontal Joint Tests," Design and Construction of Large Panel Concrete Structures, Supplemental Report B., prepared for U. S. Department of Housing and Urban Development, Portland Cement Association, Nov. 1978.

54. Jimenez, R., Gergely, P., White, R. N., "Shear Transfer Across Cracks in Reinforced Concrete," Report 78-4, Cornell University, Department of Structural Engineering, Ithaca, N. Y., Aug. 1978.

55. Oesterle, R. G., Fiorato, A. E., Johal, L. S., Carpenter, J. E., Russell, H. G., Corley, W. G., "Earthquake Resistant Structural Walls-Tests of Isolated Walls," Portland Cement Association, Skokie, Ill., Nov. 1976.

56. Hofbeck, J. F., Ibrahim, I. O., and Mattock, A. H., "Shear Transfer in Reinforced Concrete," ACI Journal, Proceedings, Vol. 66, No. 2, Feb. 1969.

57. Mueller, P., and Becker, J. M., "Seismic Characteristics of Composite Precast Walls," Proceedings of Third Canadian Conference on Earthquake Engineering, Montreal, Canada, June 1979.

58. Wilson, E. L., Doney, H. H., "Thre Dimensional Analysis of Building Systems-TABS," University of California, Berkeley, Report No. EERC/72-8, Dec. 1972.

59. Laible, J. P., White, R. N., Gergely, P., "Experimental Investigation of Seismic Shear Transfer Across Cracks in Concrete Nuclear Containment Vessels," Reinforced Concrete Structures in Seismic Zones, ACI Special Publication, SP-53, 1977.

60. Velkov, M., Simeonov, B., Gavrilovic, P., Jurukovski, D., "Theoretical and Experimental Study of the Precast Large Panel Structural System "SPUZ"," Sixth Europena Conference on Earthquake Engineering, Dubrovnik, Yugoslavia, Sept. 1978.

61. Burnett, E. F. P., Rajendra, R. C. S., "Influence of Joints in Panelized Structural Systems," Journal of the Structural Division, ASCE, Vol. 98, No. ST9, Sept. 1972.

62. Velkov, M., "Earthquake Resistant Design of Twenty-One Story Prefabricated Large Panel Building," Sixth World Conference in Earthquake Engineering, New Delhi, India, Jan. 1977.

63. Petersson, H., "Analysis of Loadbearing Walls in Multistory Buildings," Department of Building Construction, Chalmers University of Technology, Goteborg, Sweden, 1974.

64. MacLeod, I. A., "Analysis of Shear Wall Buildings by the Frame Method," Proceedings of Institution for Civil Engineers, (Great Britain), Vol. 55, Part 2, Sept. 1973.

65. Powell, G. H., "DRAIN-2D Users Guide," Report No. EERC 73-22, Earthquake Engineering Research Center, University of California, Berkeley, Oct. 1973.

66. Karsan, I. D. and Jirsa, J. O., "Behavior of Concrete Under Compressive Loadings," Journal of the Structural Division, ASCE, No. ST12, Dec. 1969.

67. Powell, G. H., Row, D. G., "Influence of Analysis and Design Assumptions on Computed Inelastic Response of Moderately Tall Frames," Report No. EERC 76-11, University of CAlifornia, Berkeley, April 1976.

68. Zeck, U. I., "Joints in Large Panel Precast Concrete Structures," Report No. R76-16, Department of Civil Engineering, MIT, Cambridge, Mass., Jan. 1976.

69. Kripanarayanan, K. M., Fintel, M., "PCA Report No. 3: Wall Panels; Analysis and Design Criteria," Design and Construction of Large-Panel Concrete Structures, Department of Housing and Urban Development, Washington, D. C., Aug. 1976

70. Hawkins, N. M., "State-of-the-Art Report on Seismic Resistance of Prestressed and Precast Concrete - Part 2," PCI Journal, Vol. 23, No. 1, Jan/Feb., 1978.

71. Hibbitt, H. D. and Karlsson, B. I., "Analysis of Pipe Whip," Report NP-1208, Electric Power Research Institute, Nov. 1979.

TABLES

TABLE 5.4.1

EFFECT OF ROTATIONAL INERTIA ON NATURAL PERIODS

	T_1 (sec)	T_2 (sec)	T_3 (sec)
Case 1 (J = 0)	0.5475	0.0878	0.0315
Case 2 (J = 32)	0.5486	0.0890	0.0325
Case 3 (J = 96)	0.5507	0.0914	0.0344
Case 4 (J = 226)	0.5548	0.0957	0.0378
Case 5 (J = 749)	0.5710	0.1112	0.0487

TABLE 5.7.1

ELASTIC MAXIMUM BASE SHEARS FOR UNMODIFIED GROUND MOTIONS

Ground Motion	Maximum Base Shear (k)
EC (.32 g)	946.3
PD (1.17 g)	1178.4
AA (1.0 g)	2417.4
AB (1.0 g)	2228.2

TABLE 5.7.2

ELASTIC MAXIMUM BASE MOMENTS AND ROOF DEFLECTIONS FOR SCALED GROUND MOTIONS

Ground Motion	Roof Deflection (in)	Base Moment (k.ft)
EC	3.93	59757
PD	3.68	50897
AA	4.13	61053
AB	3.73	58165

Note: Base shear = 950 k for all motions.

TABLE 5.8.1

MAXIMUM RESPONSES OF BEAM AND F.E. MODELS. EC MOTION

	Maximum Roof Deflection (in)	Maximum Base Shear (k)	Maximum Base Moment (k.ft)
Beam Model	3.928	950	59757
F.E. Model	3.936	946	57289

TABLE 5.10.1

ENVELOPE VALUES. SIMPLE FRICTION JOINTS. G CASES.

Case	Motion	Maximum Slip (in)	Joint No.	Max. Roof Displ. (in)	Max. Base Shear (k)	Max. Base Moment (k.ft)	Max. Accum. Slip (in)	Joint No.
G/0.2	EC	0.387	1	1.80	309	19090	4.57	1
	PD	1.065 1.203	1 10	5.88	309	19094	12.94 4.27	1 10
	AA	0.867	1	3.43	309	18843	8.00	1
	AB	2.338	1	4.97	309	18466	12.82	1
G/0.6	EC	0.851	2	4.84	782	48188	3.21	1
	PD	1.341	1	3.18	927	44896	7.39	1
	AA	0.763	1	4.54	810	46848	3.85	1
	AB	0.890	2	4.15	877	46348	5.09	1

TABLE 5.10.2

ENVELOPE VALUES. SIMPLE FRICTION JOINTS. GP CASES.

Case	Motion	Maximum Slip (in)	Joint No.	Max. Roof Displ. (in)	Max. Base Shear (k)	Max. Base Moment (k.ft)	Max. Accum. Slip (in)	Joint No.
GP/0.2	EC	0.34	3	2.64	402	26004	1.26	4
	PD	1.66	10	4.07	402	27714	2.91	10
	AA	0.81	5	4.78	402	27539	1.96	4
	AB	0.64	10	3.97	402	26141	1.68	6

TABLE 5.10.3

ROOF DISPLACEMENTS (INCHES).
ELASTIC CASE AND CASES WITH SIMPLE FRICTION JOINTS

Earthquake Motion	Elastic	Inelastic		
		G/0.2	G/0.6	GP/0.2
EC	3.93	1.80	4.84	2.64
PD	3.68	5.88	3.18	4.07
AA	4.13	3.48	4.54	4.78
AB	3.73	4.97	4.15	3.97

TABLE 5.10.4

MAXIMUM BASE SHEARS (k).
ELASTIC CASE AND CASES WITH SIMPLE FRICTION JOINTS

Earthquake Motion	Elastic	Inelastic		
		G/0.2	G/0.6	GP/0.2
EC	950	309	782	402
PD	950	309	927	402
AA	950	309	810	402
AB	950	309	877	402

TABLE 5.10.5

MAXIMUM BASE MOMENTS (k. ft).
ELASTIC CASE AND CASES WITH SIMPLE FRICTION JOINTS

Earthquake Motion	Elastic	Inelastic		
		G/0.2	G/0.6	GP/0.2
EC	59757	19090	48188	26004
PD	50897	19094	44896	27714
AA	61053	18843	46848	27539
AB	58165	18466	46348	26141

TABLE 5.10.6

RATIOS OF ACCUMULATED TO MAXIMUM SLIPS. SIMPLE FRICTION JOINTS.

Joint No.	G/0.2		G/0.6		GP/0.2	
	EC	AB	EC	AB	EC	AB
1	11.81 (max)	5.48	4.07 (max)	5.85 (max)	0.00	0.00
2	9.47	4.99	1.83	2.10	3.22	1.71
3	7.11	6.99 (max)	1.36	1.74	3.11	4.04
4	4.20	5.98	1.04	2.50	4.35 (max)	3.06
5	4.71	4.27	1.00	1.41	3.62	2.55
6	4.33	3.54	1.00	1.58	2.72	3.05
7	2.68	3.47	1.00	1.35	2.48	4.14 (max)
8	2.46	3.13	0.00	1.00	1.93	3.99
9	3.45	3.02	0.00	0.00	3.08	2.04
10	1.33	1.47	0.00	0.00	1.28	1.25

TABLE 5.10.7

ENVELOPE VALUES. FRICTION JOINTS WITH STRAIN HARDENING.

Case	Strain Hardening Ratio	Maximum Slip (in)	Joint No.	Max. Roof Displ. (in)	Max. Base Shear (k)	Max. Base Moment (k.ft)	Max. Accum. Slip (in)	Joint No.
G/0.2/EC	0	0.387	1	1.80	309	19090	4.57	1
	0.1%	0.259 0.367	1 2	2.35	317	17363	3.61 3.81	1 2
	0.2%	0.306	3	2.48	323	17134	3.14	2
G/0.2/AB	0	2.338	1	4.97	309	18466	12.82	1
	0.1%	0.377 0.439	1 3	3.96	365	18981	10.35 4.88	1 3
	0.2%	0.325	4	3.52	402	19182	7.23	1

TABLE 5.10.8

ENVELOPE VALUES. JOINTS OF SHEAR FRICTION TYPE.

Case	Stiffness Degrading Factor	Maximum Slip (in)	Joint No.	Max. Roof Displ. (in)	Max. Base Shear (k)	Max. Base Moment (k.ft)	Max. Accum. Slip (in)	Joint No.
GP/0.2/ EC	α=1	0.285	7	3.42	602	40665	1.21	5
GP/0.2/ AB	α=1	0.524	10	3.01	602	36139	2.14	10
G/0.2/ EC	α=0	0.396	5	2.84	509	33333	1.78	5
	α=1	0.414	6	2.93	509	31567	1.49	5
G/0.2/ AB	α=0	0.324	10	2.78	509	30968	2.65	2
	α=1	0.452	10	3.12	524	29538	3.86	3

TABLE 5.10.9

ENVELOPE VALUES. SIMPLE FRICTION JOINTS WITH STOPS.

Case	Motion	Maximum Slip (in)	Joint No.	Max. Roof Displ. (in)	Max. Base Shear (k)	Max. Base Moment (k.ft)	Max. Accum. Slip (in)	Joint No.
G/0.2	EC	0.394	1	1.84	309	18702	4.30	1
	AB	0.503 0.480	2 1	4.43	344	18501	12.69	1
GP/0.2	EC	0.323	3	2.47	402	26004	1.26	4
	AB	0.396	6	3.96	435	26141	1.64	6

TABLE 5.10.10 - PART A (WITHOUT STOPS)

ENVELOPE VALUES. FRICTION JOINTS WITH DEGRADING FRICTION.

Case	Motion	Maximum Slip (in)	Joint No.	Max. Roof Displ. (in)	Max. Base Shear (k)	Max. Base Moment (k.ft)	Max. Accum. Slip (in)	Joint No.
G/0.6 → 0.2 No Stops	EC	3.751	1	4.14	784	47989	21.33	1
	PD	2.689	1	4.16	927	46808	38.19	1
	AA	4.846	1	4.57	752	36643	32.70	1
	AB	10.256	1	9.73	768	38143	66.88	1

TABLE 5.10.10 - PART B (WITH STOPS)

ENVELOPE VALUES. FRICTION JOINTS WITH DEGRADING FRICTION.

Case	Motion	Maximum Slip (in)	Joint No.	Max. Roof Displ. (in)	Max. Base Shear (k)	Max. Base Moment (k.ft)	Max. Accum. Slip (in)	Joint No.
G/0.6 → 0.2 With Stops (0.2%)	EC	1.046 0.933	2 1	4.10	792	46843	8.44 7.81	1 2
	AB	1.100 0.963	2 1	3.79	754	37955	23.37 19.21	1 2
G/0.6 → 0.2 With Stops (2.0%)	EC	0.416	2	3.80	811	48092	6.32	1
	PD	0.506	1	2.94	927	44464	14.49	1
	AB	0.438	2	3.08	800	41478	13.16	1

TABLE 5.11.1

EFFECT OF GAP OPENING ON ROOF DEFLECTION AND BASE MOMENT

BEAM MODEL. EC MOTION

	Elastic (No Gap Opening)	With Gap Opening	
		G	GP
Maximum Roof Deflection (in)	3.93	4.22	3.68
Maximum Gap Opening at Base (in)	0	0.779	0.665
Maximum Base Moment (k.ft)	59750	23064	32531

TABLE 5.11.2

MASSES USED IN STUDY OF VERTICAL INERTIA EFFECTS

Masses in $k.sec^2/ft$.

	X-100% Y Case		X-30% Y Case		X-0% Y Case	
	X-mass	Y-mass	X-mass	Y-mass	X-mass	Y-mass
Roof	3.54	3.54	3.54	0.948	3.54	0
	4.68	4.68	4.68	1.416	4.68	0
	4.68	4.68	4.68	1.416	4.68	0
	4.68	4.68	4.68	1.416	4.68	0
	4.68	4.68	4.68	1.416	4.68	0
	4.68	4.68	4.68	1.416	4.68	0
	4.68	4.68	4.68	1.416	4.68	0
	4.68	4.68	4.68	1.416	4.68	0
	4.68	4.68	4.68	1.416	4.68	0
	4.68	4.68	4.68	1.416	4.68	0
Base	2.34	2.34	2.34	0.708	2.34	0

TABLE 5.11.3

ENVELOPE VALUES WITH GAP OPENING. EFFECT OF Y MASS.

Case	Mass	Max. Roof Displ. (in)	Max. Base Shear (k)	Max. Base Moment (k.ft)	Maximum Gap (in)	Joint No.
G/EC	X-100%Y	4.22	606	24064	0.7788	10
	X-30% Y	4.69	540	20888	0.8496	10
	X-0% Y	4.76	609	18547	0.9132	10

TABLE 5.11.4

MAXIMUM JOINT COMPRESSIVE DEFORMATIONS

ELASTIC AND INELASTIC JOINTS

Joint No.	Deformation (in) Elastic Joints	Deformation (in) Inelastic Joints
1	0.0048	0.0036
2	0.0060	0.0048
3	0.0096	0.0072
4	0.0120	0.0096
5	0.0144	0.0120
6	0.0168	0.0144
7	0.0180	0.0240*
8	0.0216	0.0252*
9	0.0240	0.0164
10	0.0288	0.2232*

*Joint loaded beyond yield. Yield deformation = 0.0167 in.

TABLE 5.12.1

ENVELOPE VALUES. UNCOUPLED SIMPLE FRICTION AND GAP OPENING. G CASES.

Case	Motion	Max. Slip (in)	Joint No.	Max. Roof Displ. (in)	Max. Base Shear (k)	Max. Base Moment (k.ft)	Max. Accum. Slip (in)	Joint No.	Max. Gap (in)	Joint No.
G/0.2	EC	0.437	1	1.96	309	18599	4.70	1	0.001	10
	PD	1.190	1	6.49	309	18914	13.56	1	0.001	10
	AA	1.000	1	3.58	309	18656	8.93	1	0.001	10
	AB	2.050	1	4.70	309	18298	13.65	1	0	10
G/0.6	EC	0.101	1	3.88	816	26739	0.43	1	0.679	10
	PD	0.419	1	14.48	886	29832	2.49	1	3.530	10
	AA	0.060	1	4.15	556	26763	0.31	1	0.756	10
	AB	0.162	1	5.29	827	27120	1.20	1	1.120	10

TABLE 5.12.2

ENVELOPE VALUES. UNCOUPLED SIMPLE FRICTION AND GAP OPENING. GP CASES.

Case	Motion	Max. Slip (in)	Joint No.	Max. Roof Displ. (in)	Max. Base Shear (k)	Max. Base Moment (k.ft)	Max. Accum. Slip (in)	Joint No.	Max. Gap (in)	Joint No.
GP/0.2	EC	0.377	5	2.71	402	25869	1.528	4	0.0456	10
	PD	1.666	10	4.03	402	25625	1.807	4	0.0192	10
	AA	0.817	5	3.92	402	25886	2.074	4	0.0144	10
	AB	0.693	10	4.07	402	24814	1.750	5	0.026	10
GP/0.6	EC	0	-	3.54	855	35745	0	-	0.691	10
	PD	0	-	4.06	867	32990	0	-	0.688	10
	AA	0	-	4.16	691	31627	0	-	0.698	10
	AB	0	-	4.49	726	35316	0	-	0.822	10

TABLE 5.12.3

ENVELOPE VALUES. COUPLED SIMPLE FRICTION AND GAP OPENING. G CASES.

Case	Motion	Max. Slip (in)	Joint No.	Max. Roof Displ. (in)	Max. Base Shear (k)	Max. Base Moment (k.ft)	Max. Accum. Slip (in)	Joint No.	Max. Gap (in)	Joint No.
G/0.2	EC	0.422	1	1.98	300	18571	4.41	1	0.0001	10
	PD	1.172	1	6.50	314	18892	13.72	1	0.0039	10
	AA	0.997	1	3.55	310	18657	8.99	1	0.0006	10
	AB	2.075	1	4.70	307	18312	13.74	1	0	10
G/0.6	EC	0.314	1	4.03	774	26478	0.54	1	0.677	10
	PD	0.253	1	14.50	1106	29589	1.89	1	3.509	10
	AA	0.148	1	4.21	610	26717	0.32	1	0.752	10
	AB	0.272	1	4.82	905	26242	1.22	1	1.053	10

TABLE 5.12.4

ENVELOPE VALUES. COUPLED SIMPLE FRICTION AND GAP OPENING. GP CASES.

Case	Motion	Max. Slip (in)	Joint No.	Max. Roof Displ. (in)	Max. Base Shear (k)	Max. Base Moment (k.ft)	Max. Accum. Slip (in)	Joint No.	Max. Gap (in)	Joint No.
GP/0.2	EC	0.371	5	2.82	419	26497	1.620	3	0.0554	10
	PD	1.434	10	4.02	439	26385	2.796	10	0.0654	10
	AA	0.798	5	3.91	416	26216	2.051	3	0.1343	10
	AB	0.693	10	3.97	421	25740	1.686	4	0.0287	10
GP/0.6	EC	0.0152	10	3.53	852	35513	0.0634	10	0.689	10
	PD	0.0163	8	4.07	875	32874	0.1316	10	0.686	10
	AA	0.1200	10	4.16	830	31434	0.1141	10	0.696	10
	AB	0.0135	10	4.50	763	35216	0.1684	10	0.830	10

FIGURES

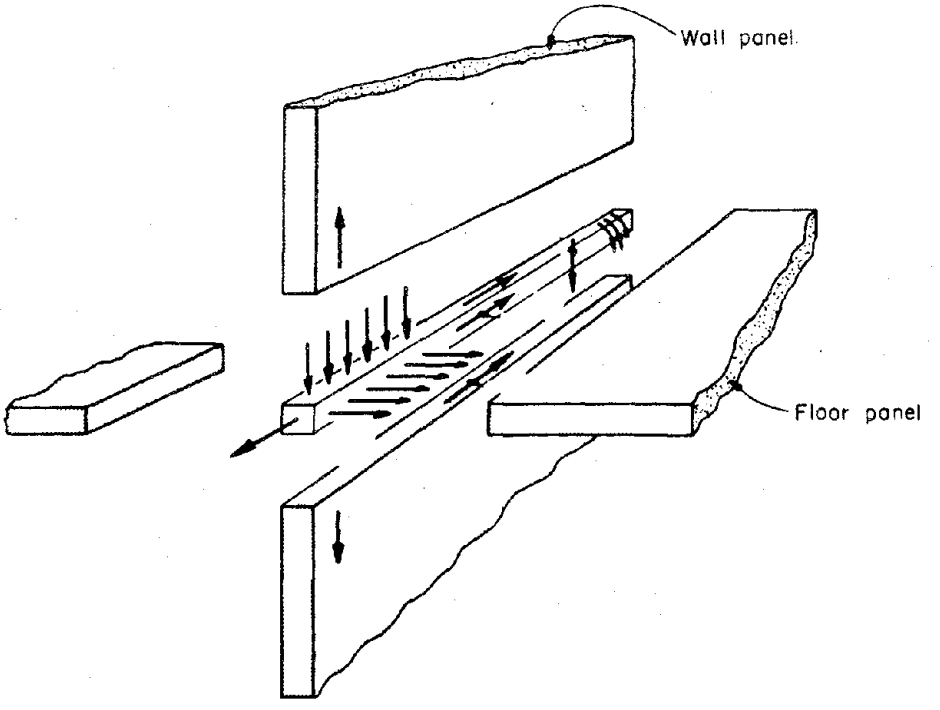

FIG. 2.1.1 FORCES ON TYPICAL HORIZONTAL JOINT [32]

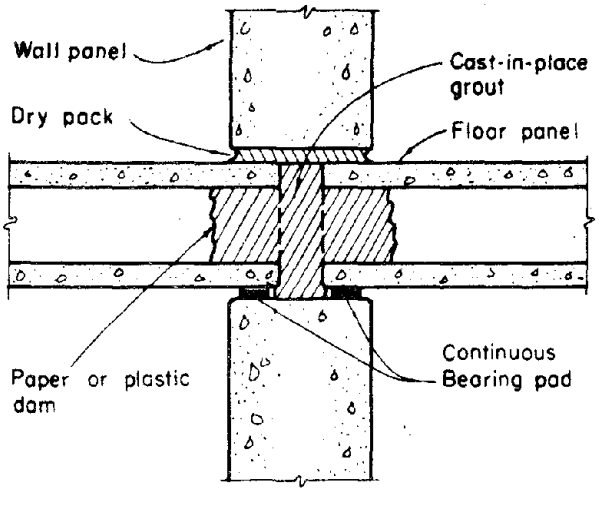

FIG. 2.2.1 "PLATFORM" CONNECTION [32]

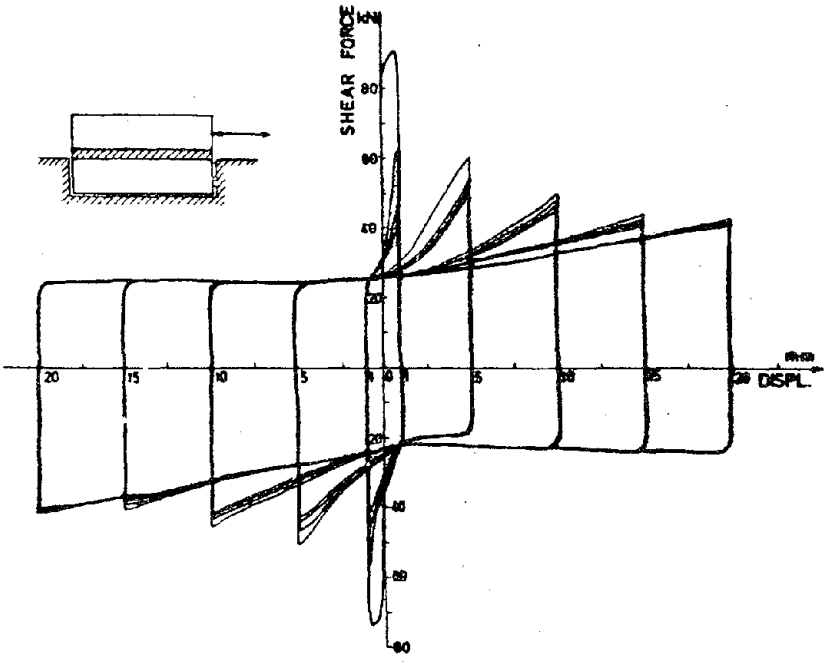

FIG. 2.2.2 LOAD-DEFORMATION RELATIONSHIP FOR UNREINFORCED JOINT WITH NO VERTICAL LOAD [6]

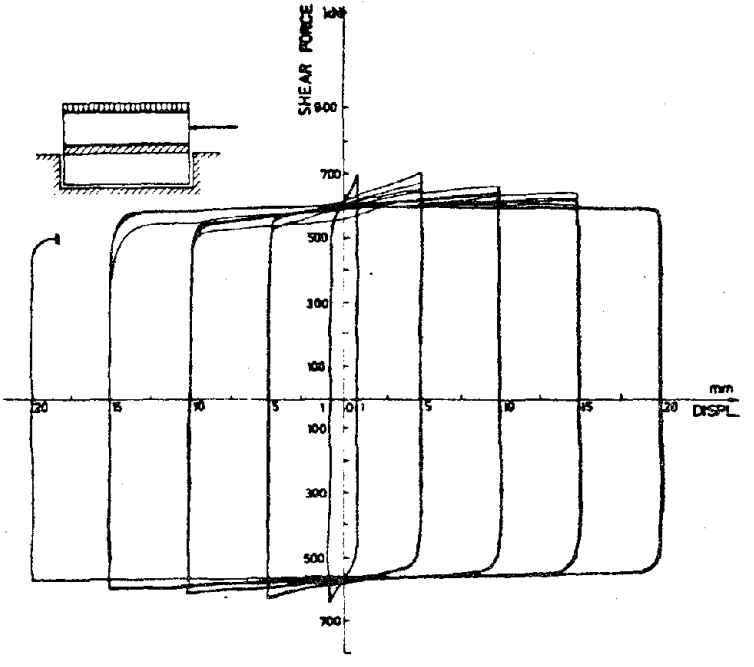

FIG. 2.2.3 LOAD-DEFORMATION RELATIONSHIP FOR UNREINFORCED JOINT WITH VERTICAL LOAD [6]

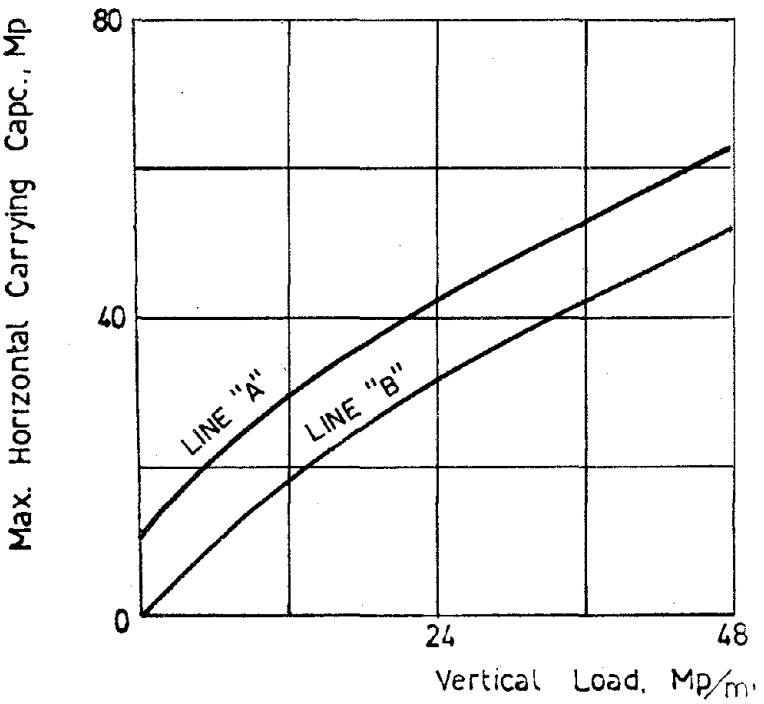

FIG. 2.2.4 JOINT SHEAR STRENGTH [6]

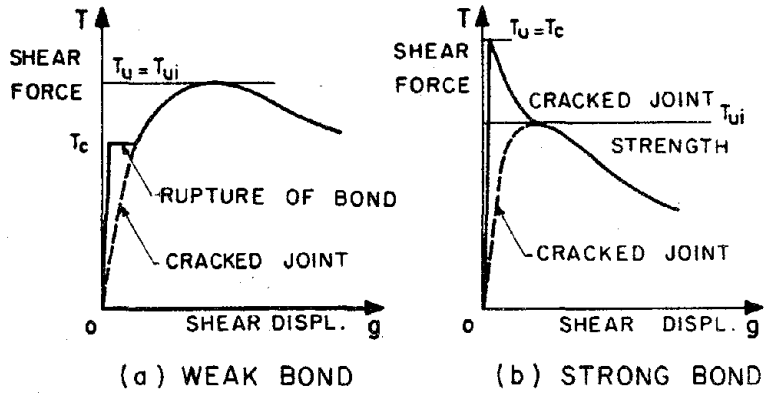

FIG. 2.2.5 EFFECT OF BOND [21]

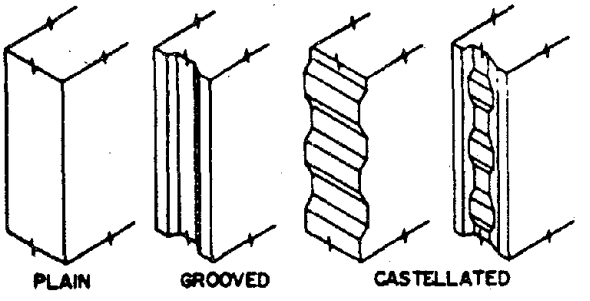

FIG. 2.3.1 PANEL EDGES [48]

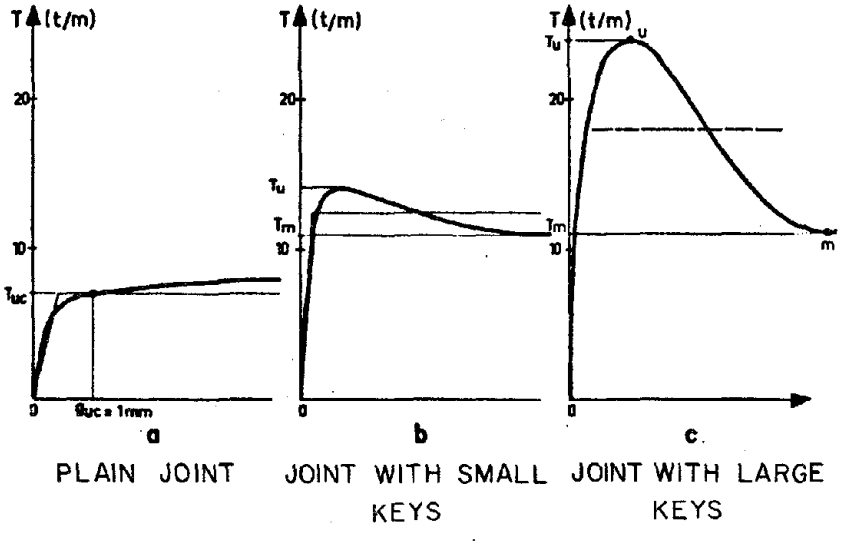

FIG. 2.3.2 FORCE-DISPLACEMENT RELATIONSHIP FOR KEYED JOINTS [21]

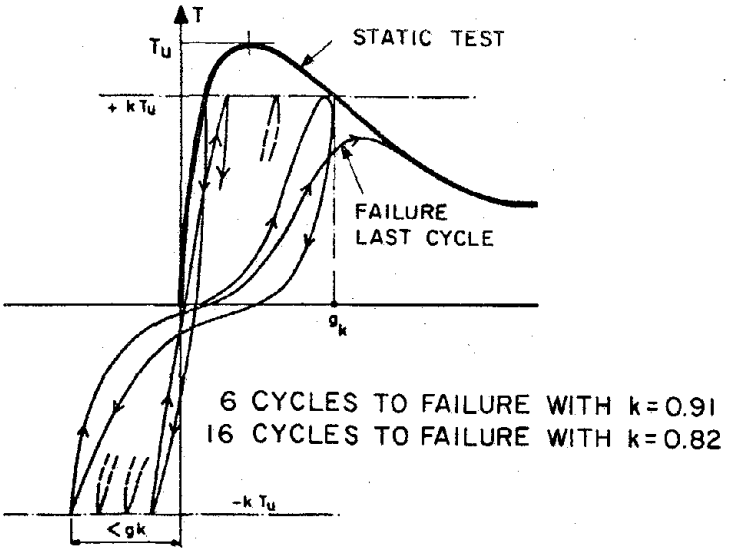

FIG. 2.3.3 LOAD CONTROLLED CYCLIC TESTS ON KEYED JOINTS [21]

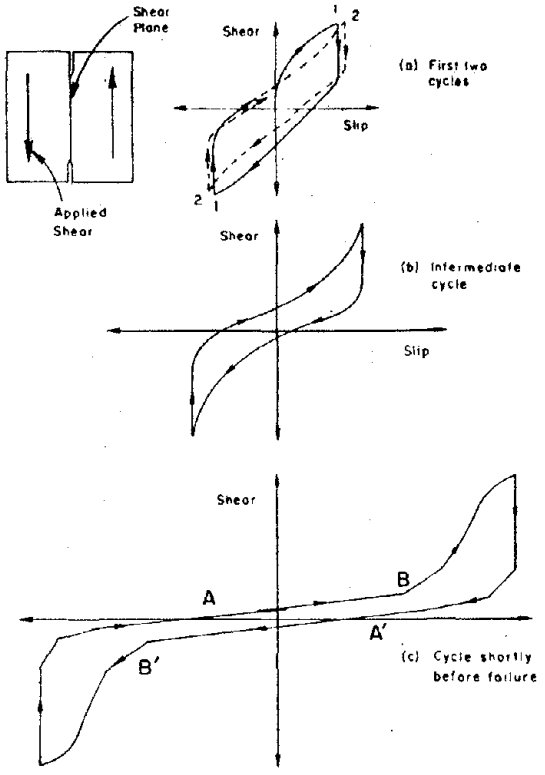

FIG. 2.4.1 SHEAR VERSUS SLIP FOR PRECRACKED R.C. SPECIMEN (MATTOCK [2])

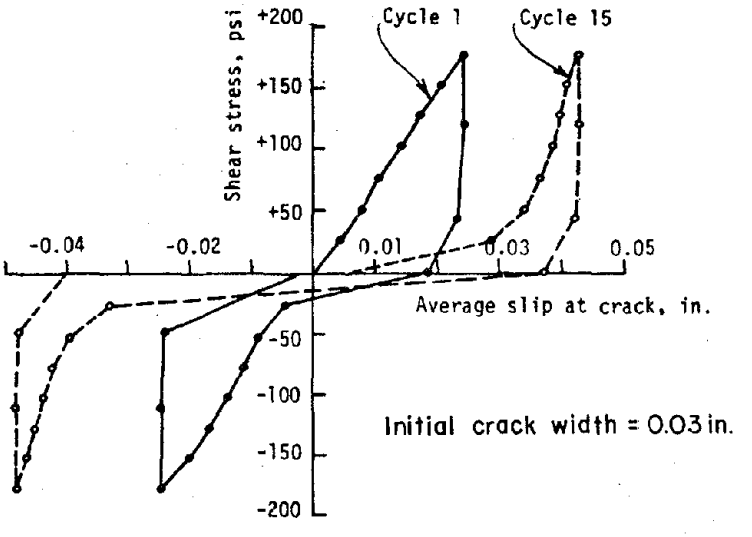

FIG. 2.4.2 SHEAR VERSUS SLIP FOR PRECRACKED R.C. SPECIMEN (LAIBLE ET AL [59])

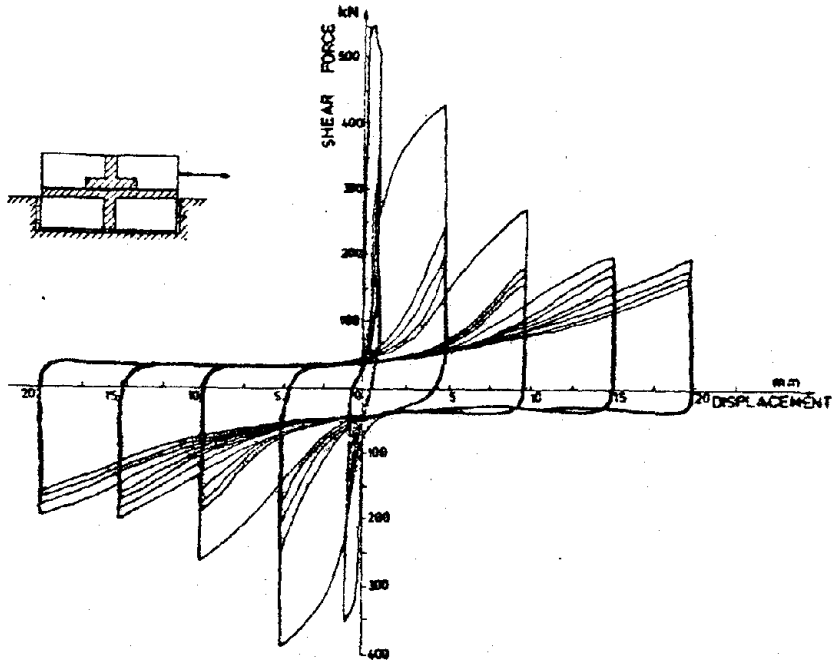

FIG. 2.4.3 LOAD-DEFORMATION RELATIONSHIP FOR REINFORCED JOINT WITH NO VERTICAL LOAD [6]

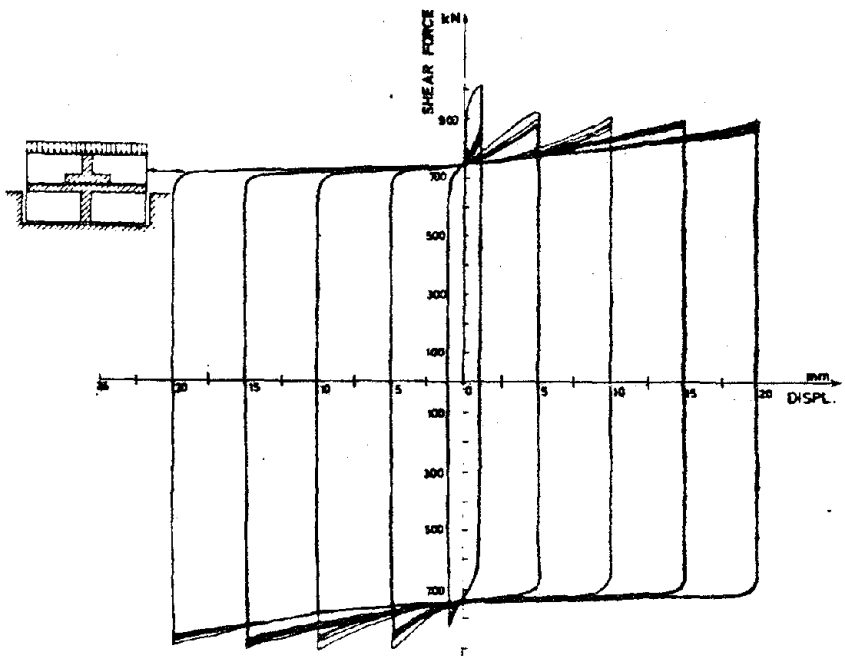

FIG. 2.4.4 LOAD-DEFORMATION RELATIONSHIP FOR REINFORCED JOINT WITH VERTICAL LOAD [6]

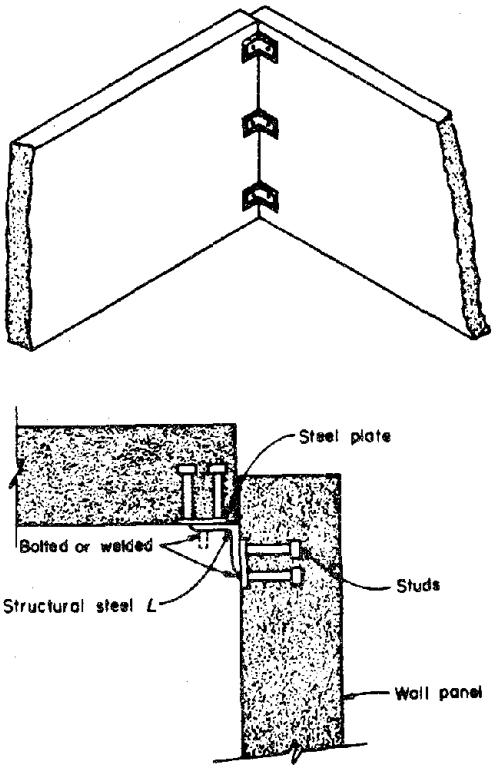

FIG. 2.5.1 TYPICAL "DRY" VERTICAL CONNECTION [32]

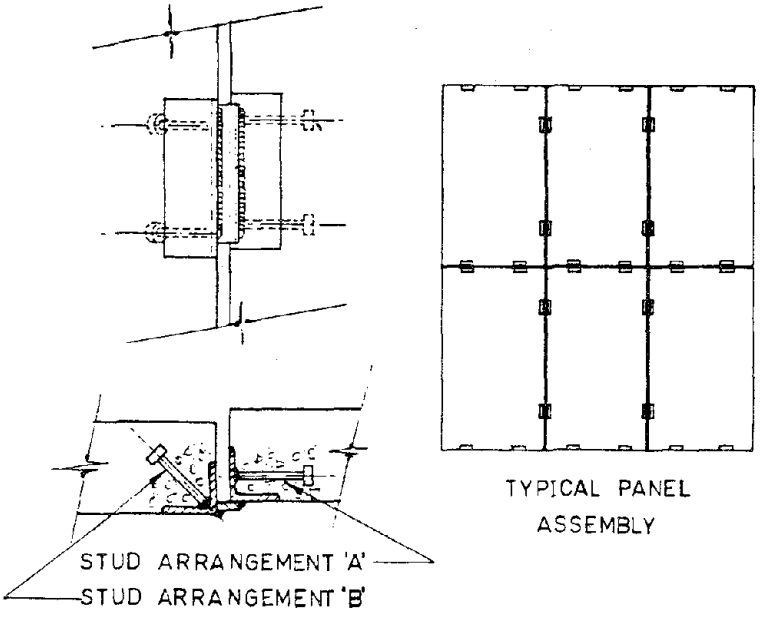

FIG. 2.5.2 HEADED STUD WELDED CONNECTION SHOWING TYPICAL APPLICATION [5]

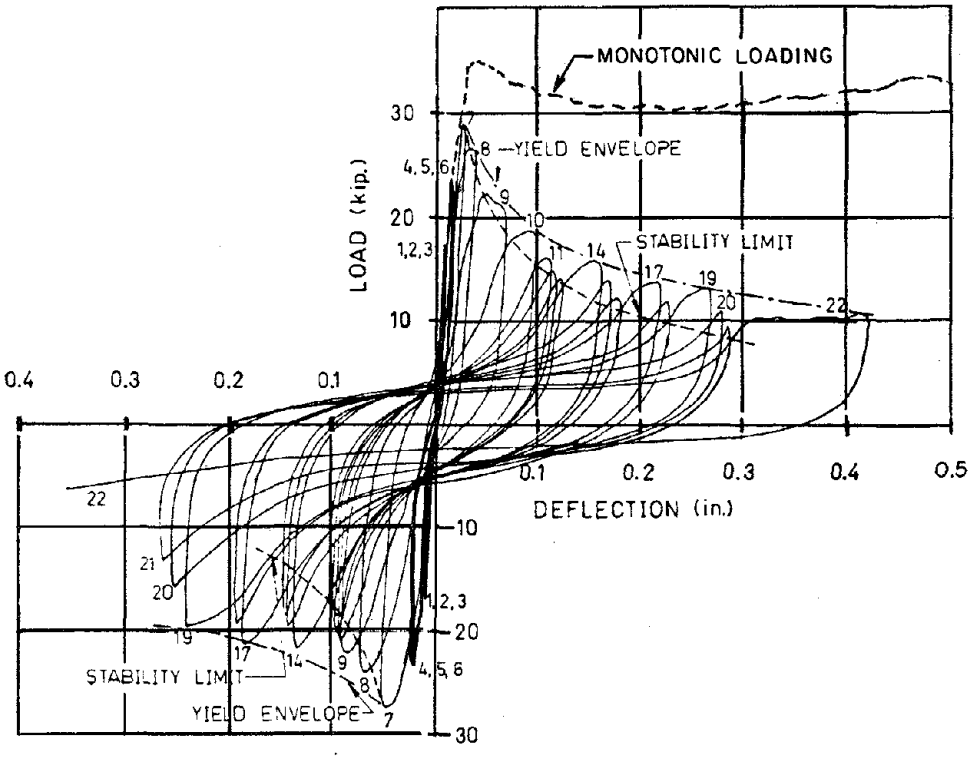

FIG. 2.5.3 LOAD-DEFLECTION LOOPS FOR DRY VERTICAL CONNECTION [5]

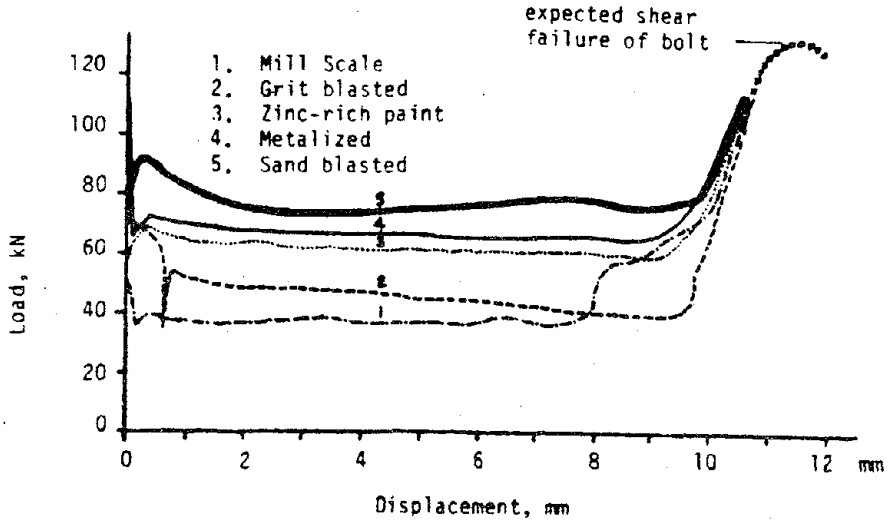

(a) MONTONIC LOADING

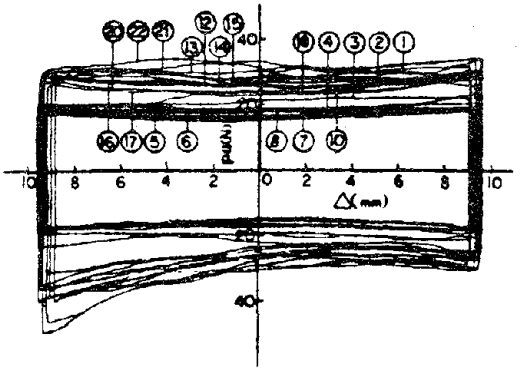

(i) Mill Scale

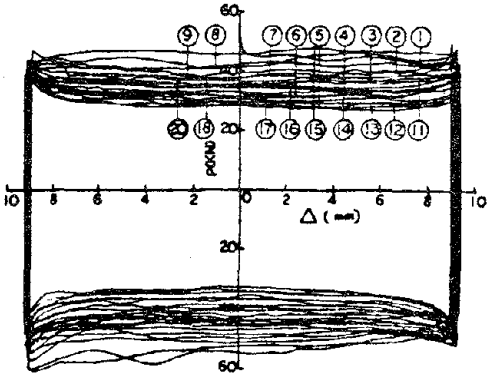

(ii) Sand Blasted

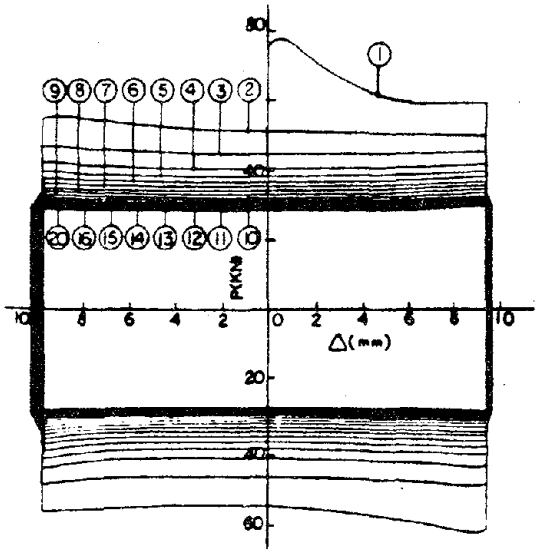

(iii) Inorganic Zinc-Rich Paint

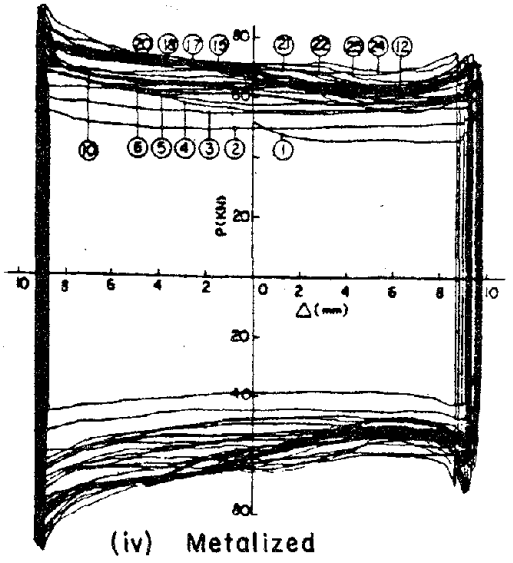

(iv) Metalized

(b) CYCLIC LOADING

FIG. 2.5.4 BEHAVIOR OF DRY JOINTS WITH SLOTTED HOLES [40]

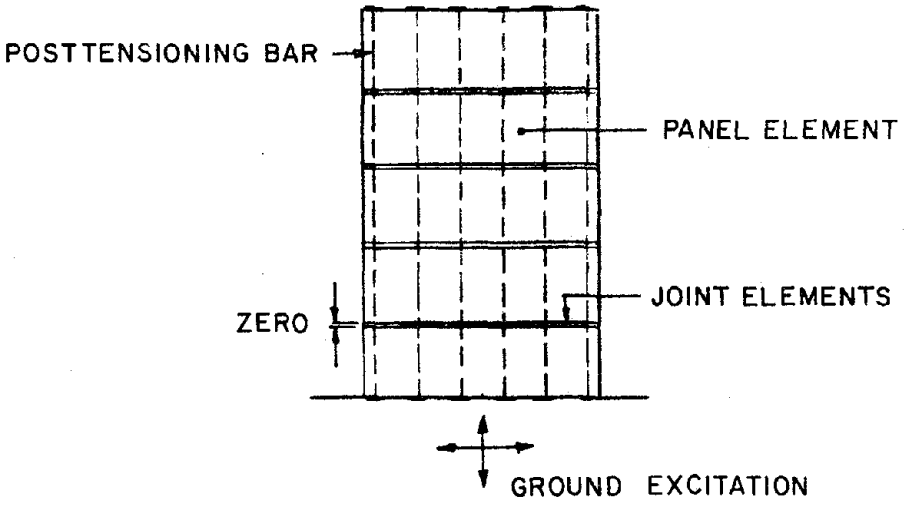

FIG. 3.3.1 MATHEMATICAL MODEL FOR A MULTI-STORY LARGE PANEL WALL

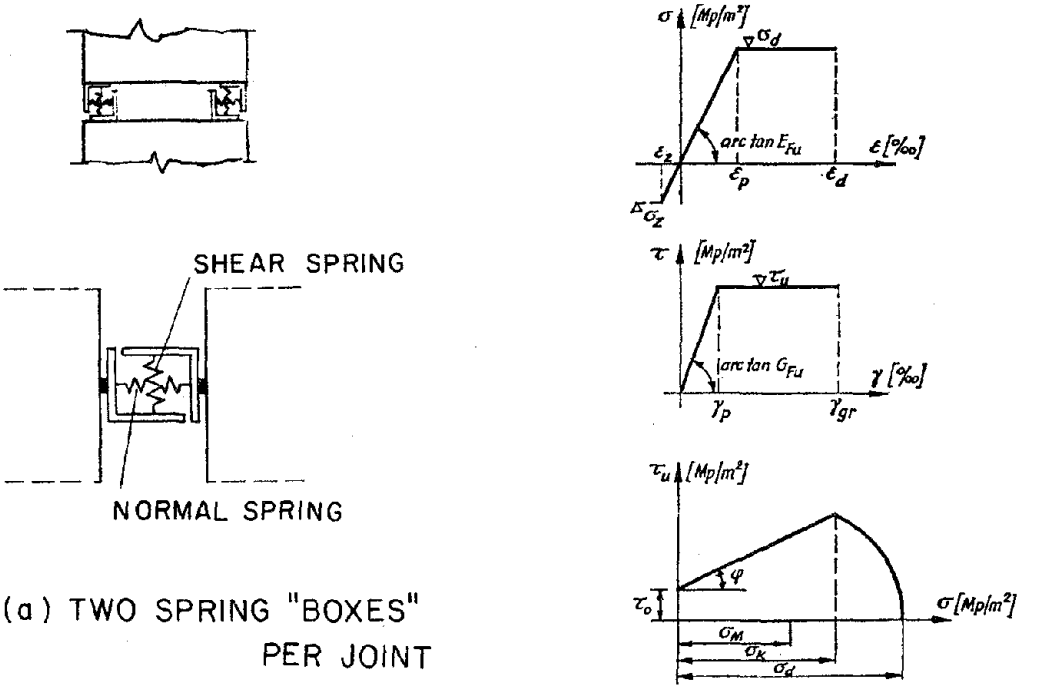

(a) TWO SPRING "BOXES" PER JOINT

(b) RELATIONSHIP BETWEEN SHEAR AND NORMAL STRESSES

FIG. 3.4.1 JOINT IDEALIZATION USED BY SCHWIN AND MELHORN [31]

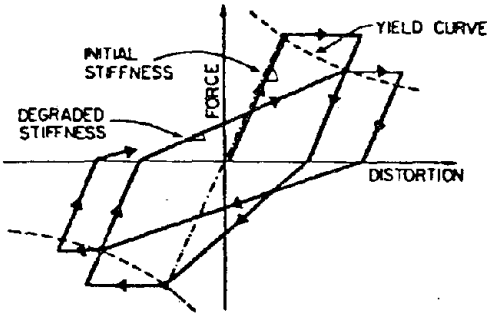

FIG. 3.4.2 MUELLER-BECKER MECHANICAL CONNECTOR MODEL [57]

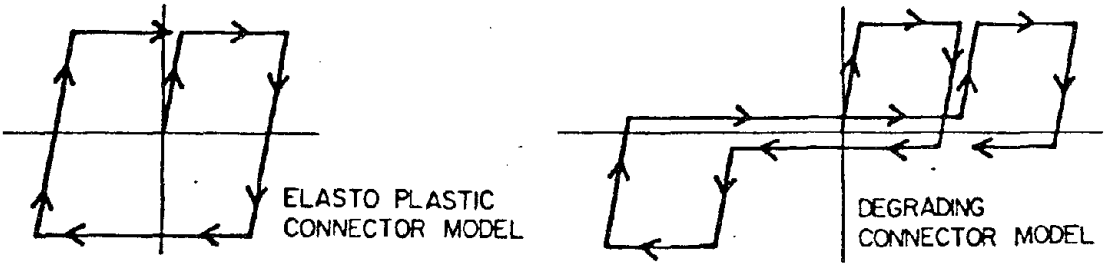

FIG. 3.4.3 MUELLER-BECKER VERTICAL CONNECTOR MODELS [57]

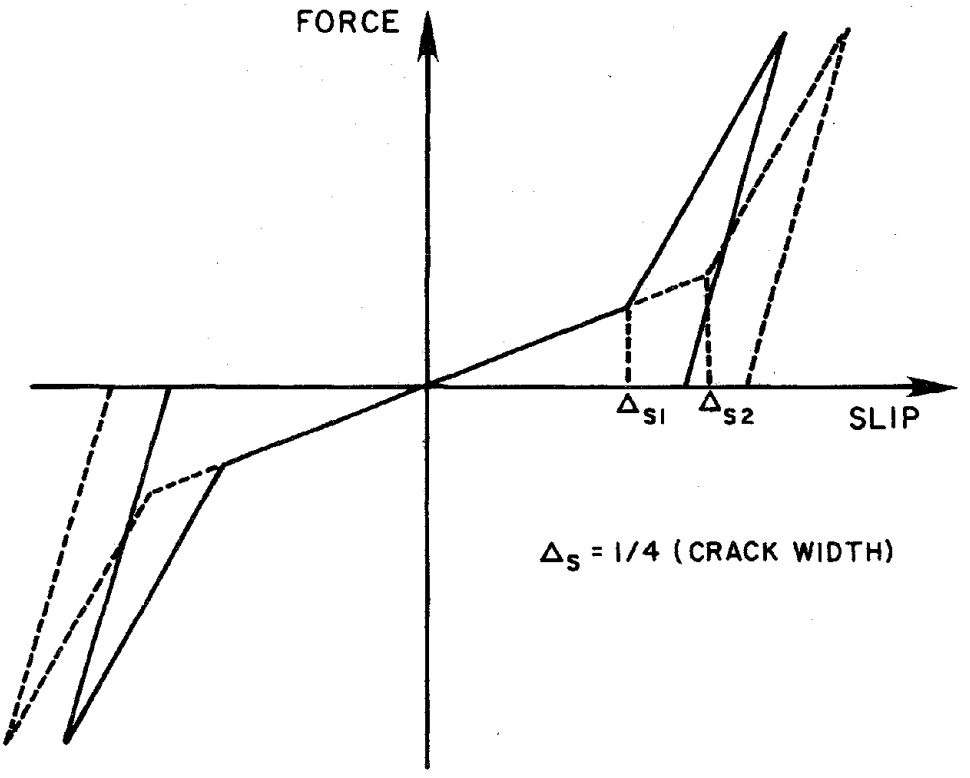

FIG. 3.4.4 AKTAN MODEL FOR SHEAR TRANSFER ACROSS A CRACK [19]

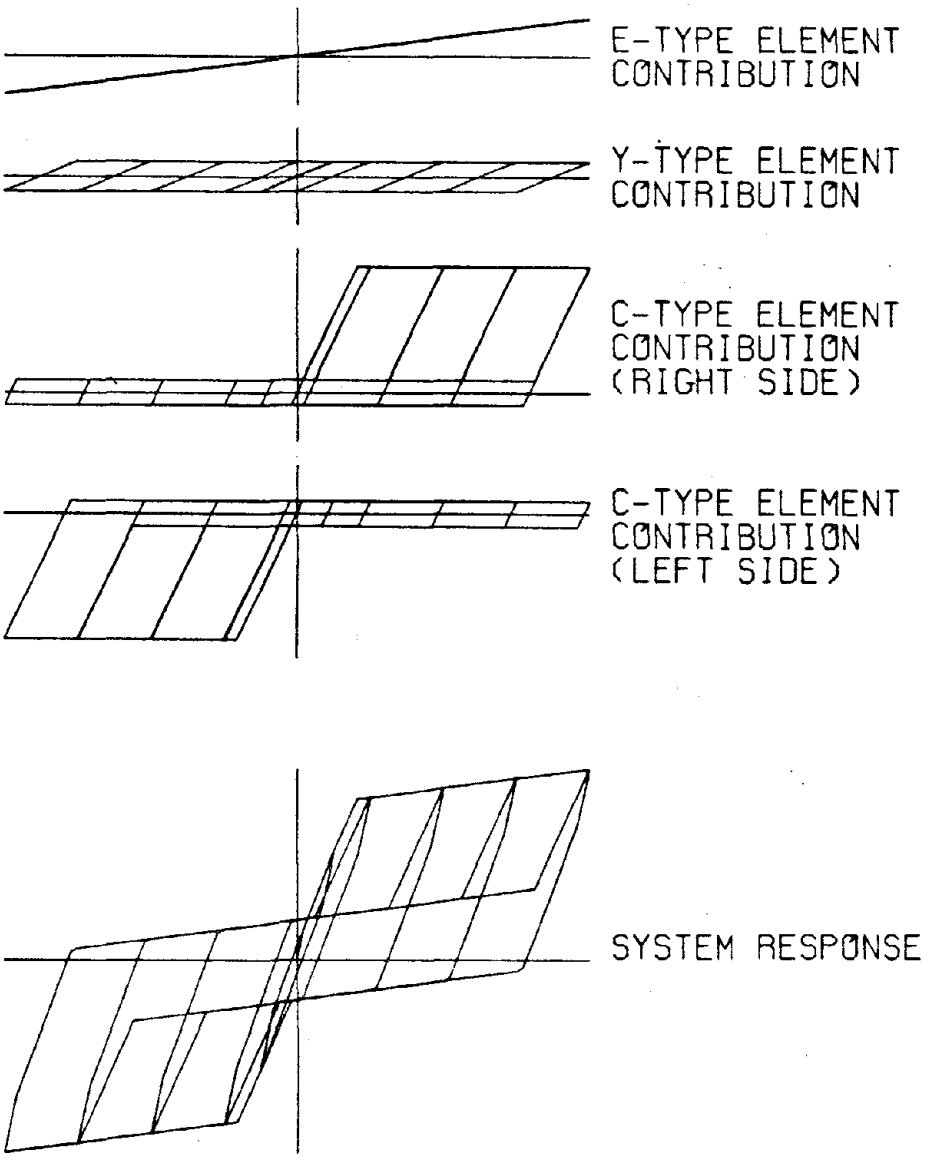

FIG. 3.4.5 GATES MODEL: SUMMATION OF ELEMENT CONTRIBUTIONS [30]

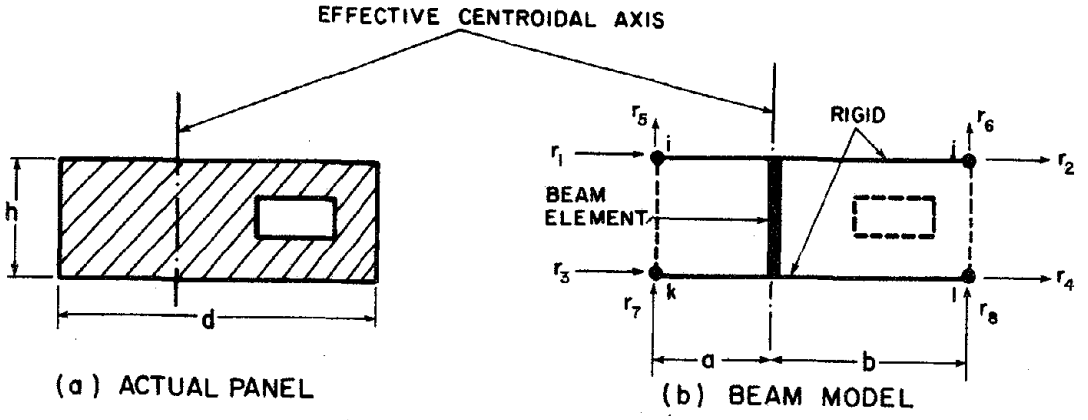

FIG. 4.2.1 PANEL ELEMENT: MODIFIED BEAM MODEL

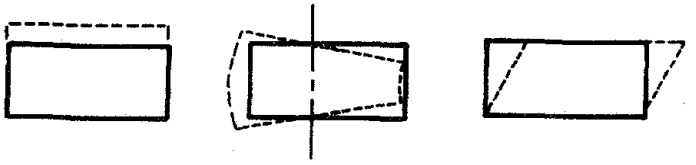

(a) PRIMARY MODES OF DEFORMATION

(b) SECONDARY MODES OF DEFORMATION

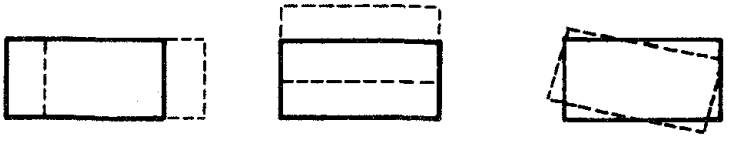

(c) RIGID BODY MODES

FIG. 4.2.2 DEFORMATION MODES

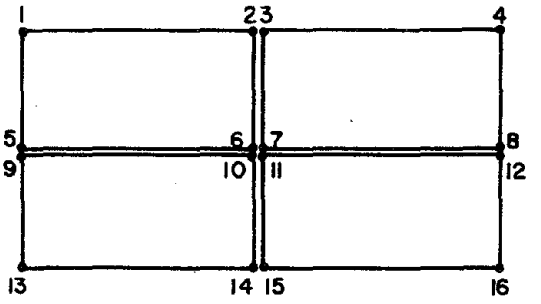

FIG. 4.2.3 TYPICAL ARRANGEMENT OF PANELS

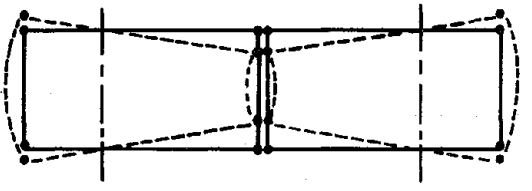

FIG. 4.2.4 INCOMPATIBILITY ALONG VERTICAL CONNECTIONS

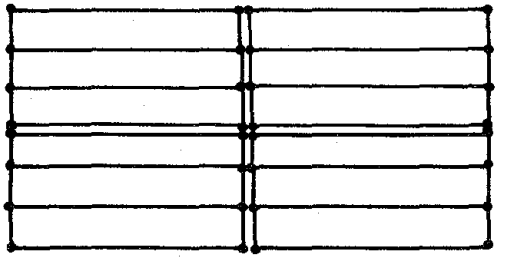

FIG. 4.2.5 SEVERAL ELEMENTS PER PANEL IMPROVES COMPATIBILITY AT VERTICAL EDGES

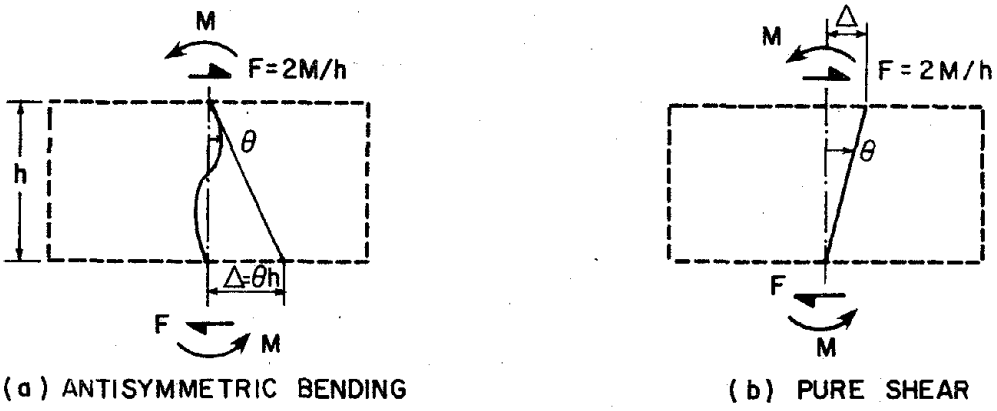

FIG. 4.2.6 BEAM DEFORMATIONS

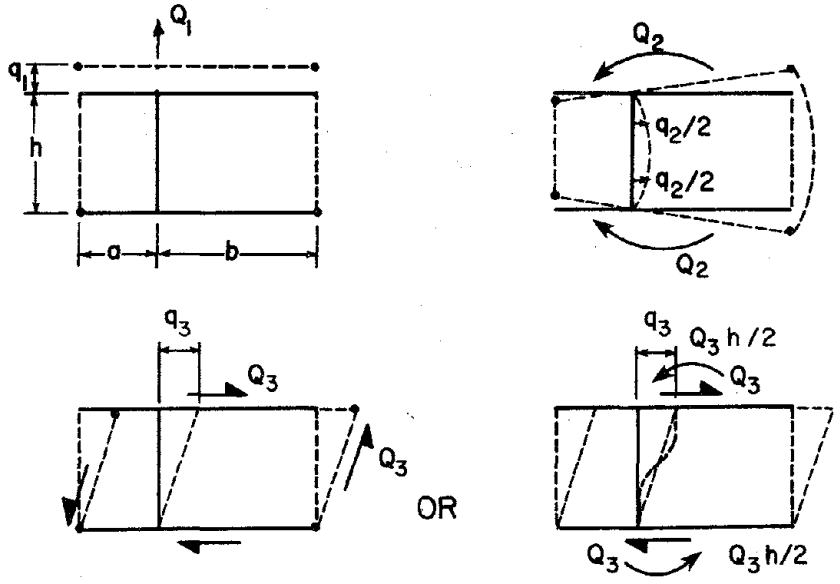

FIG. 4.2.7 POSITIVE ACTIONS AND DEFORMATIONS FOR PANEL ELEMENT

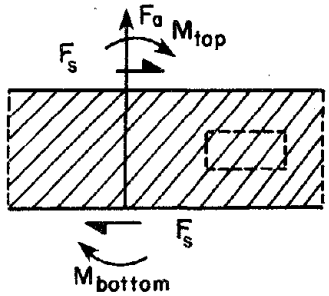

FIG. 4.2.8 OUTPUT ACTIONS FOR PANEL ELEMENT

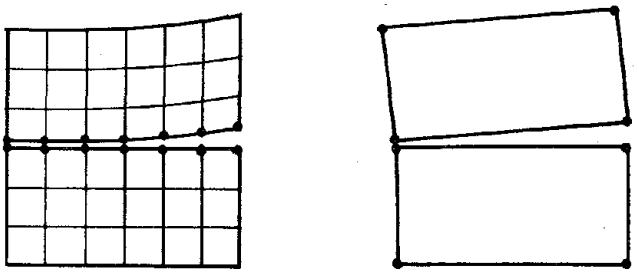

FIG. 4.3.1 GAP OPENING AT HORIZONTAL JOINT

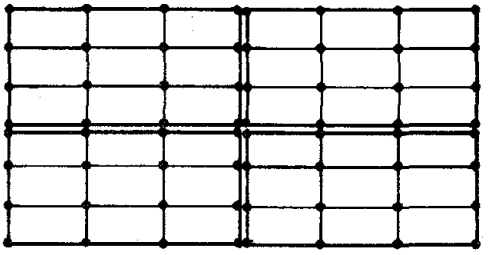

FIG. 4.3.2 FINITE ELEMENT IDEALIZATION OF WALL PANELS

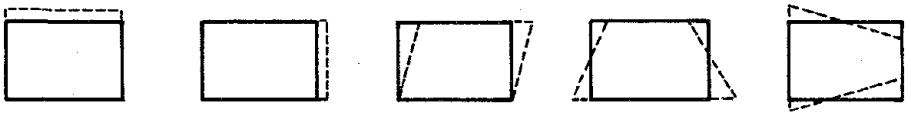

FIG. 4.3.3 MODES OF DEFORMATION

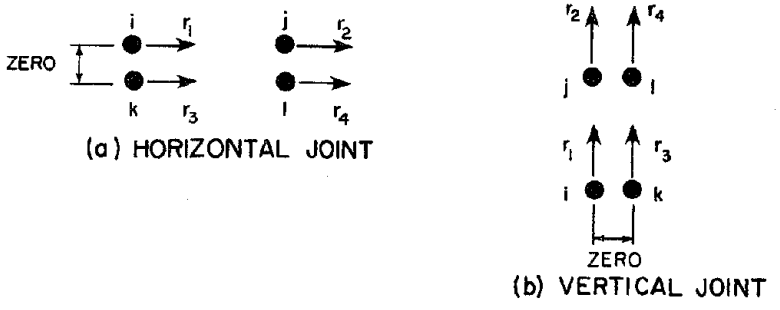

FIG. 4.4.1 ELEMENT DEGREES OF FREEDOM

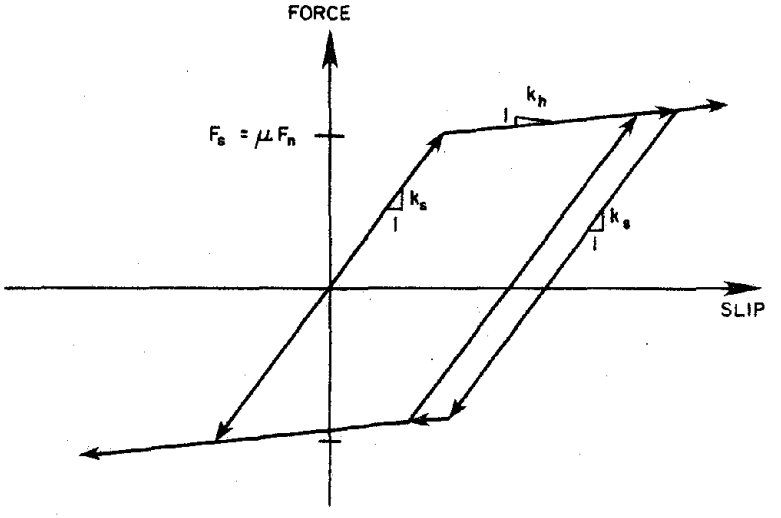

FIG. 4.4.2 FORCE-SLIP RELATIONSHIP

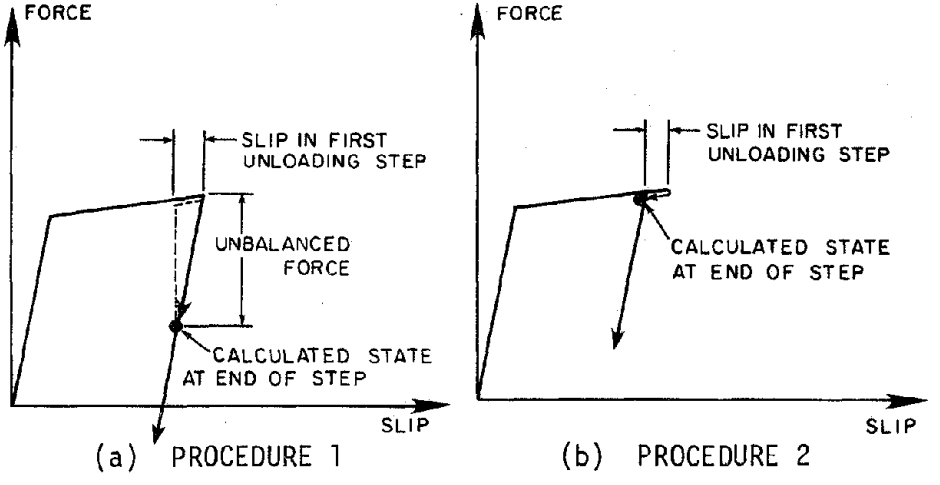

FIG. 4.4.3 STATE DETERMINATION PROCEDURES

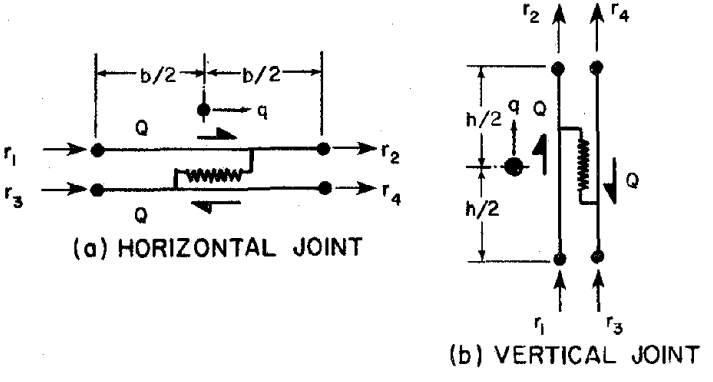

FIG. 4.4.4 POSITIVE SHEAR FORCE AND DEFORMATION

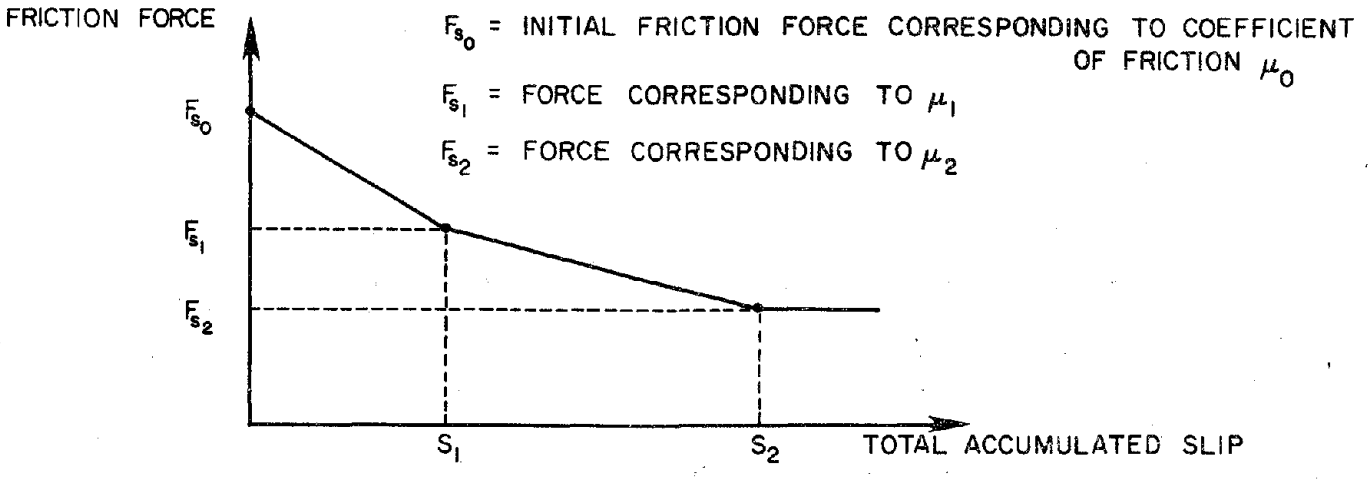

FIG. 4.5.1 DEGRADING STRENGTH CHARACTERISTIC

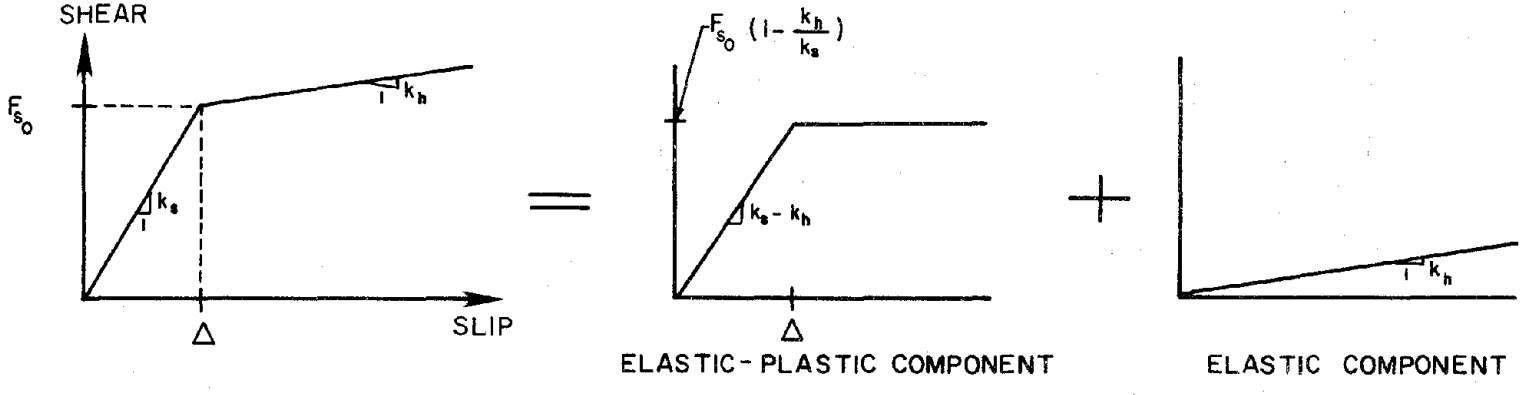

FIG. 4.5.2 DECOMPOSITION OF SHEAR-SLIP RELATIONSHIP

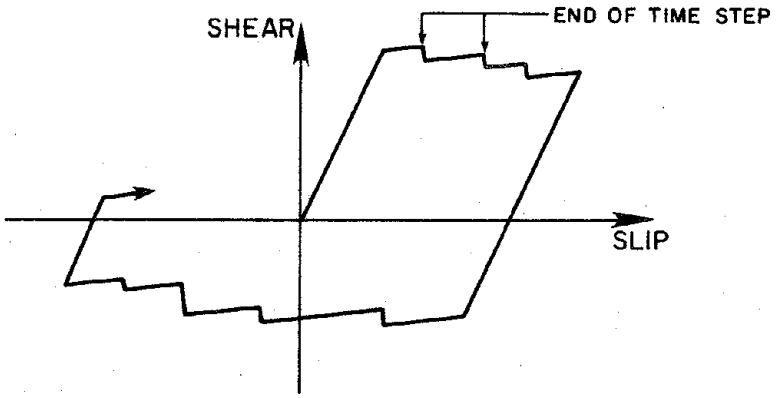

FIG. 4.5.3 IMPLIED SHEAR-SLIP RELATIONSHIP

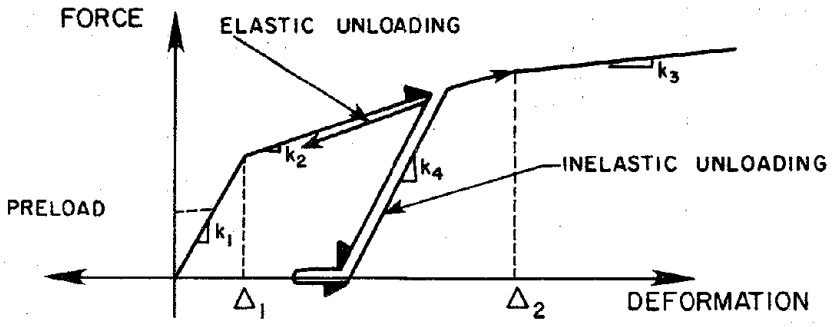

FIG. 4.6.1 GAP ELEMENT FORCE-DEFORMATION RELATIONSHIP

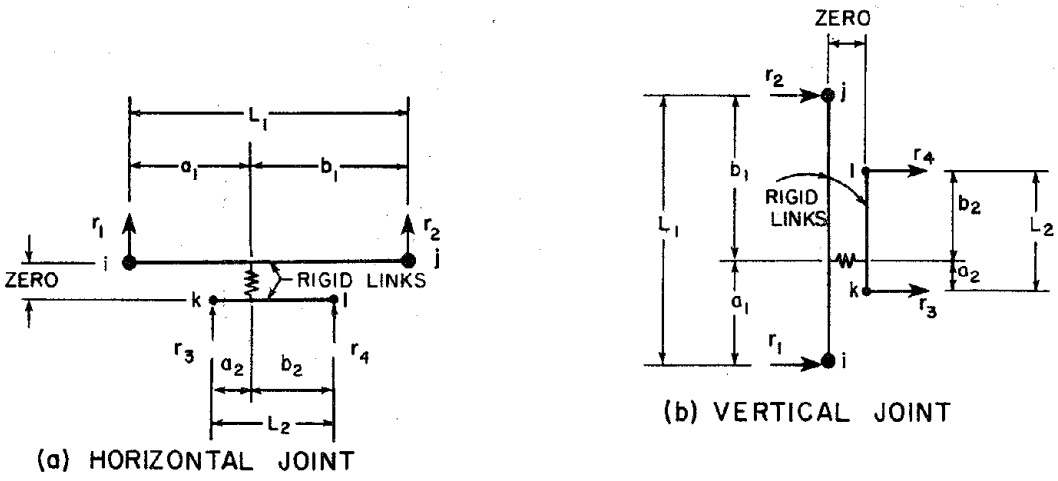

FIG. 4.6.2 GAP ELEMENT DEGREES OF FREEDOM

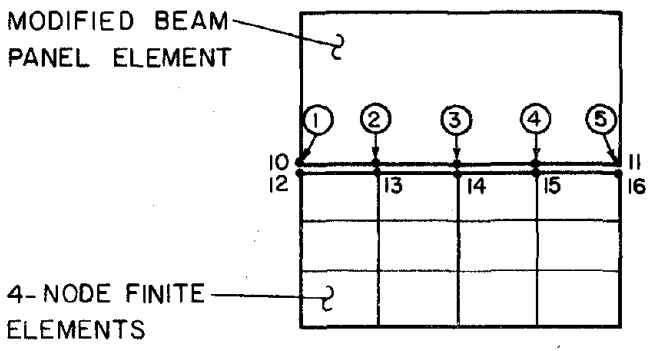

JOINT ELEMENT NO.	MODE NUMBERS i	j	k	l
1	10	10	12	12
2	10	11	13	13
3	10	11	14	14
4	10	11	15	15
5	11	11	16	16

FIG. 4.6.3 MATCHING OF BEAM AND FINITE ELEMENT PANEL MODELS

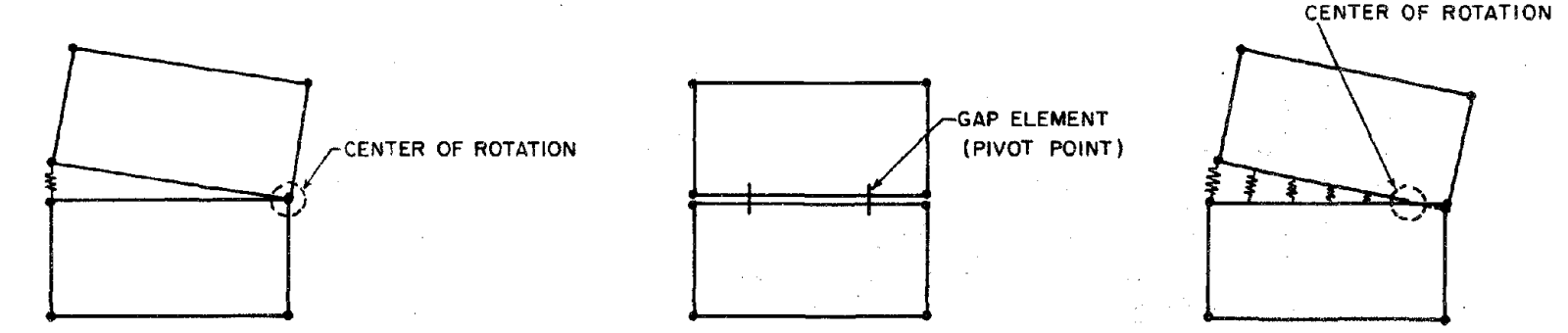

(a) 2 GAP ELEMENT PER JOINT (b) CHANGE OF PIVOT POINT (c) 7 GAP ELEMENT PER JOINT

FIG. 4.6.4 PANEL TILTING

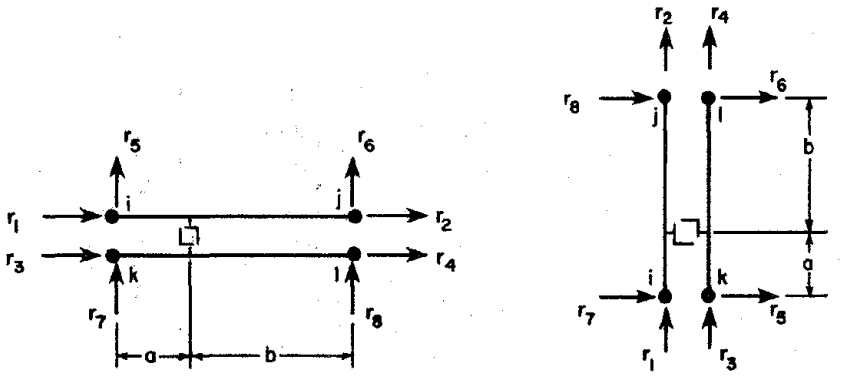

(a) HORIZONTAL JOINT (b) VERTICAL JOINT

FIG. 4.7.1 ELEMENT DEGREES OF FREEDOM: FOUR-NODE CASE

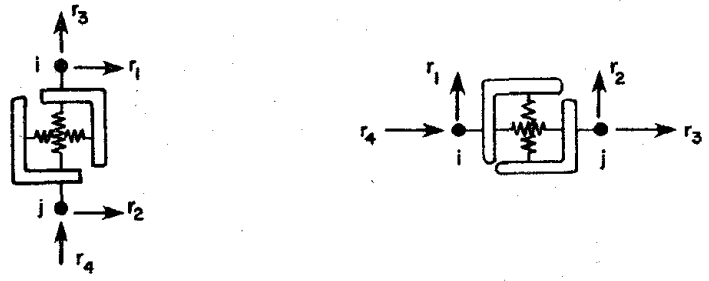

FIG. 4.7.2 ELEMENT DEGREES OF FREEDOM: TWO-NODE CASE

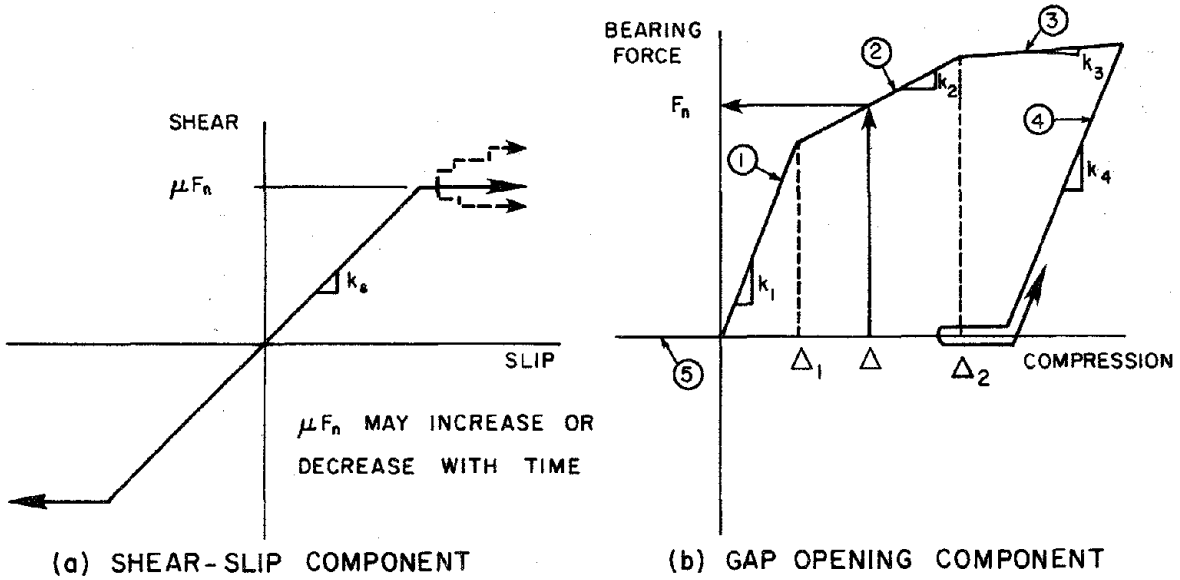

(a) SHEAR-SLIP COMPONENT (b) GAP OPENING COMPONENT

FIG. 4.7.3 FORCE-DEFORMATION RELATIONSHIPS

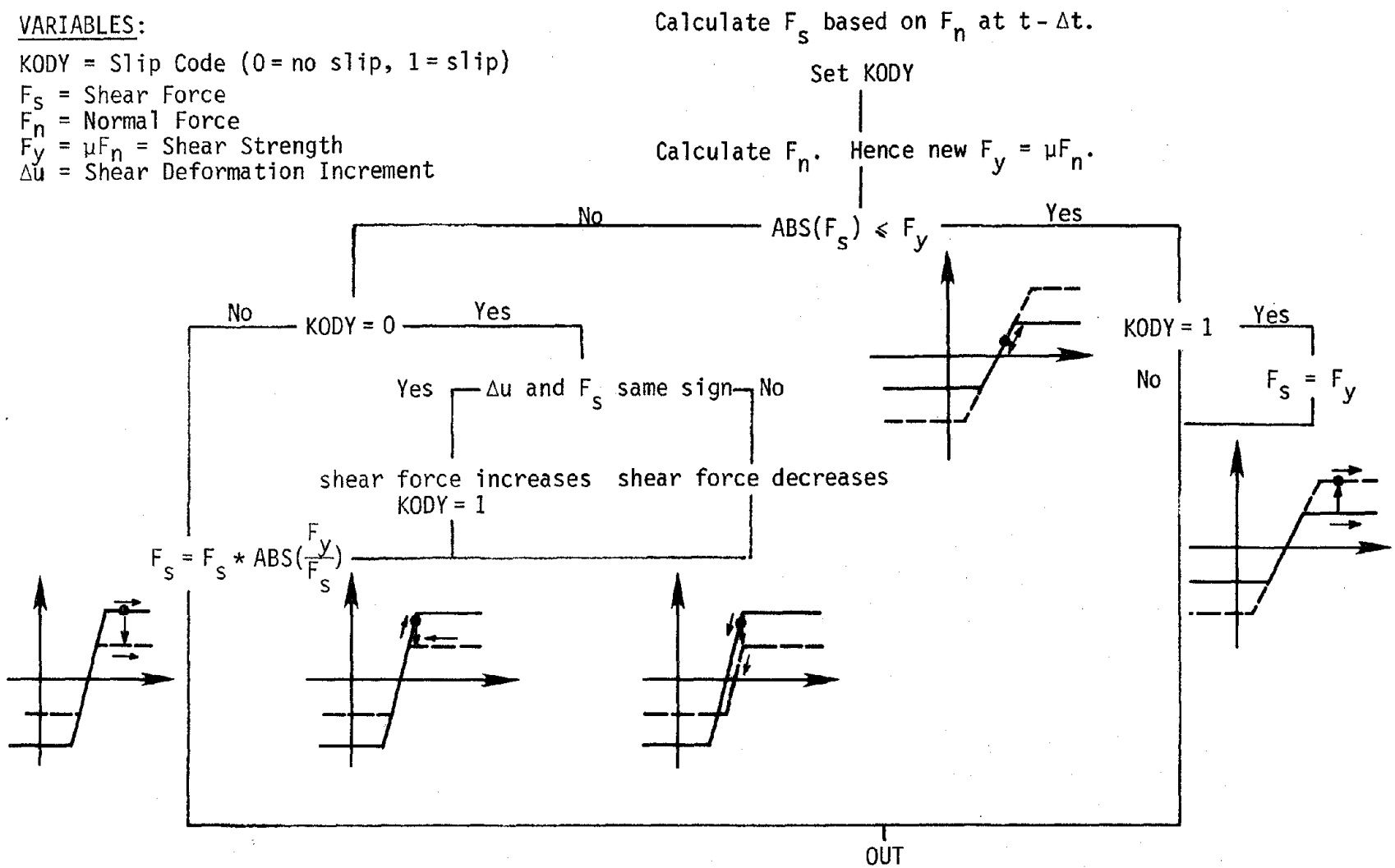

FIG. 4.7.4 LOGIC FOR GAP-FRICTION ELEMENT

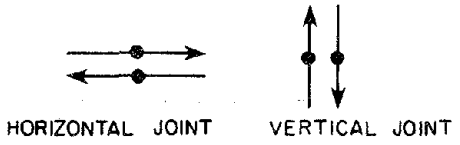

(a) POSITIVE DEFORMATION

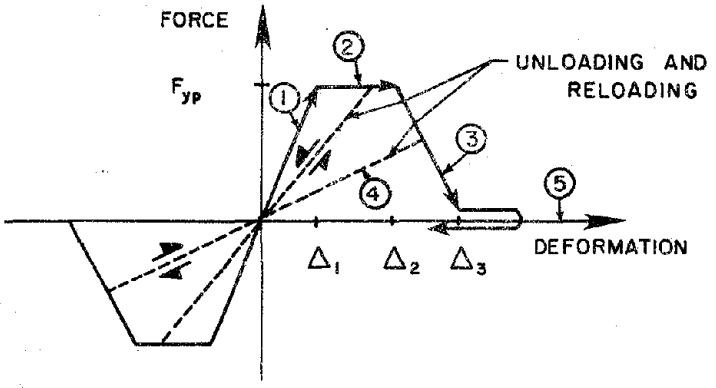

(b) FORCE - DEFORMATION RELATIONSHIP

FIG. 4.8.1 CHARACTERISTICS OF KEY ELEMENT

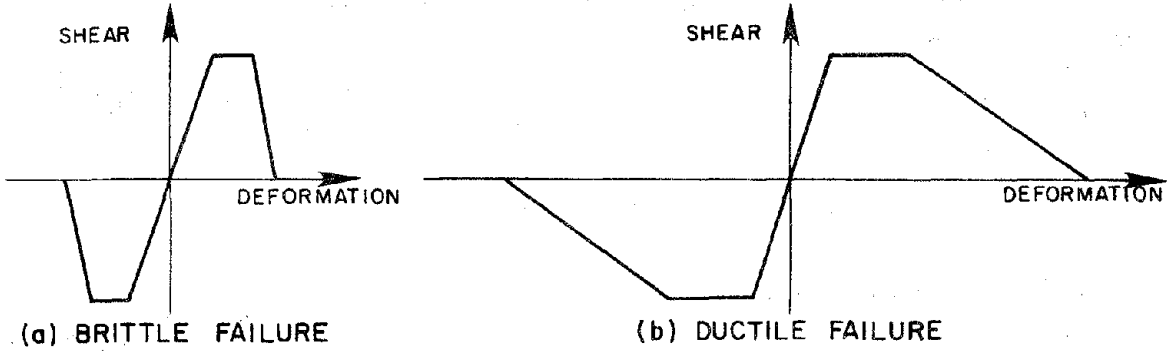

(a) BRITTLE FAILURE

(b) DUCTILE FAILURE

FIG. 4.8.2 BRITTLE AND DUCTILE CHARACTERISTICS

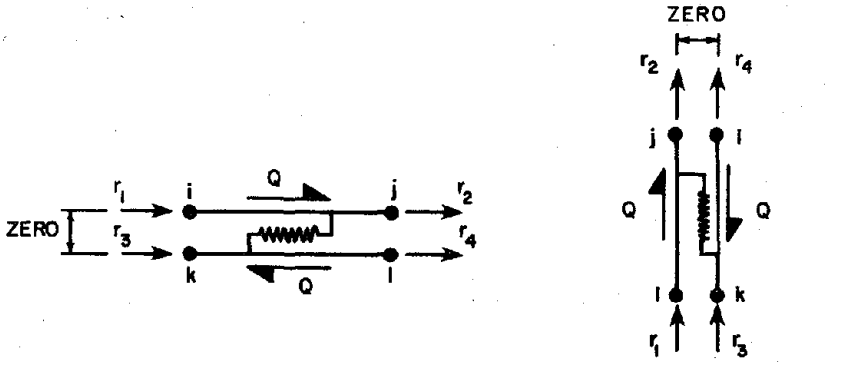

(i) HORIZONTAL JOINT (ii) VERTICAL JOINT

(a) 4 - NODE ELEMENT

(i) HORIZONTAL JOINT (ii) VERTICAL JOINT

(b) 2 - NODE ELEMENT

FIG. 4.8.3 KEY ELEMENT DEGREES OF FREEDOM

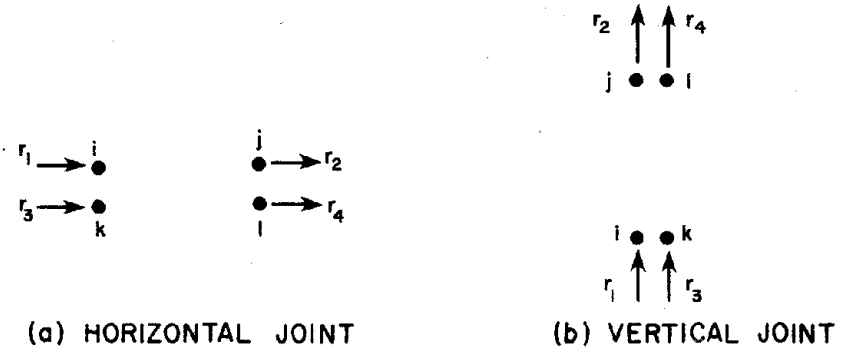

(a) HORIZONTAL JOINT (b) VERTICAL JOINT

FIG. 4.9.1 DEGREES OF FREEDOM FOR SHEAR FRICTION ELEMENT

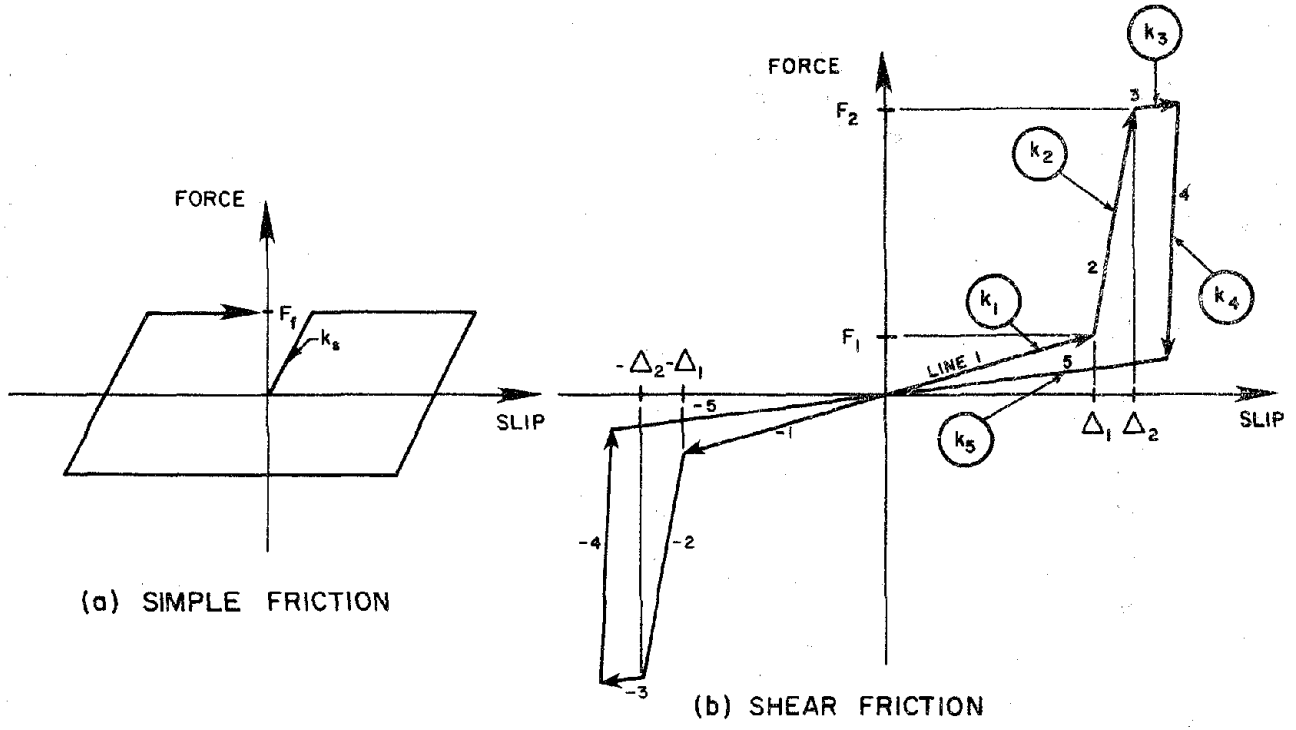

FIG. 4.9.2 SHEAR-SLIP RELATIONSHIPS FOR SHEAR FRICTION ELEMENT

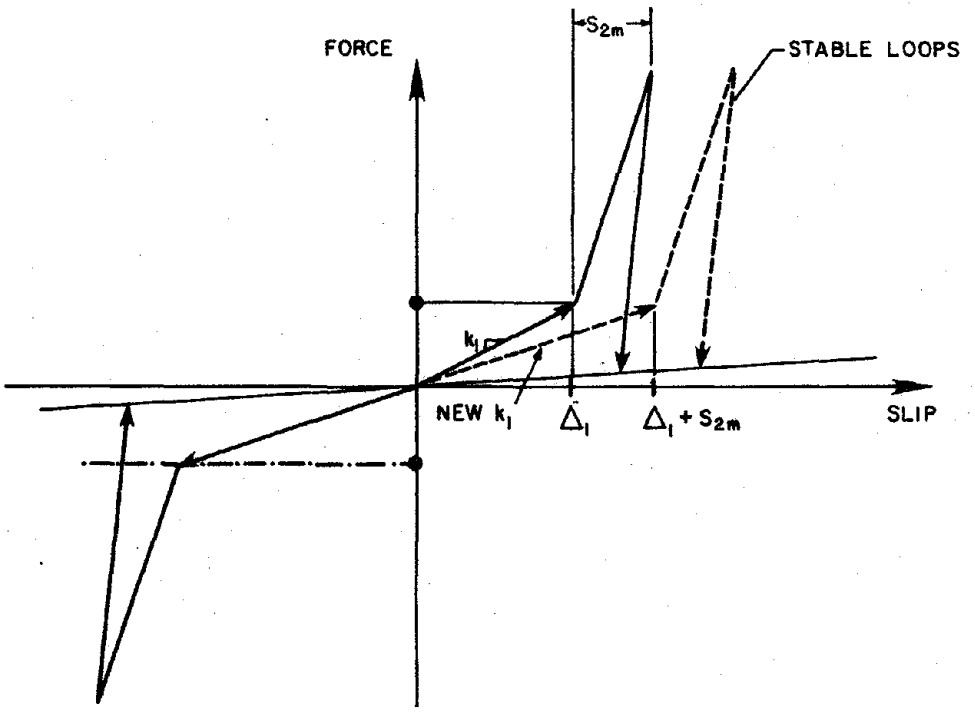

FIG. 4.9.3 STABILIZED HYSTERESIS LOOPS AFTER STIFFNESS DEGRADATION

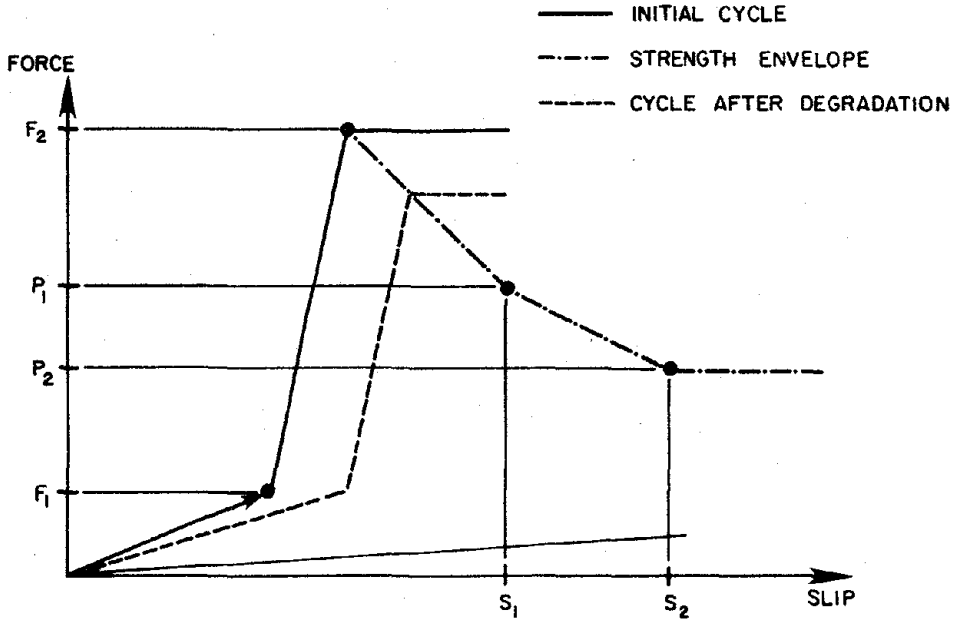

FIG. 4.9.4 STRENGTH ENVELOPE

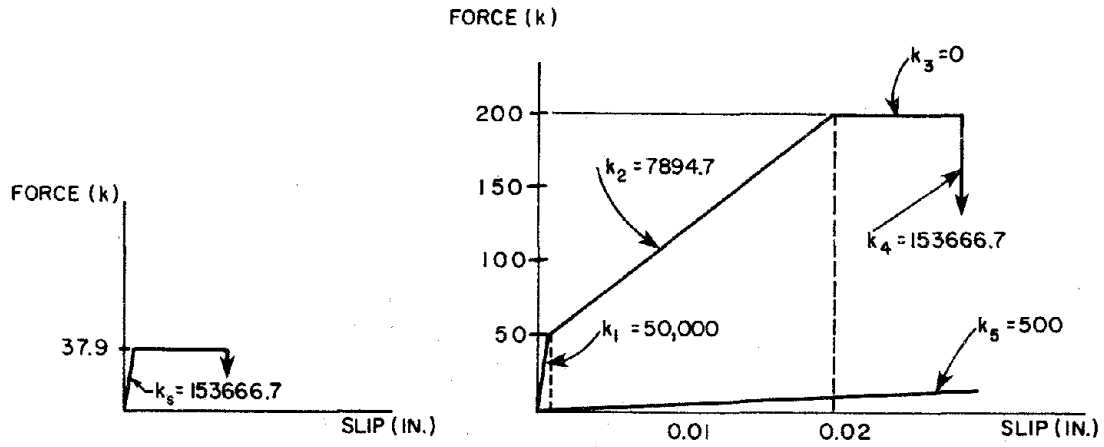

(a) PROPERTIES OF TWO COMPONENTS

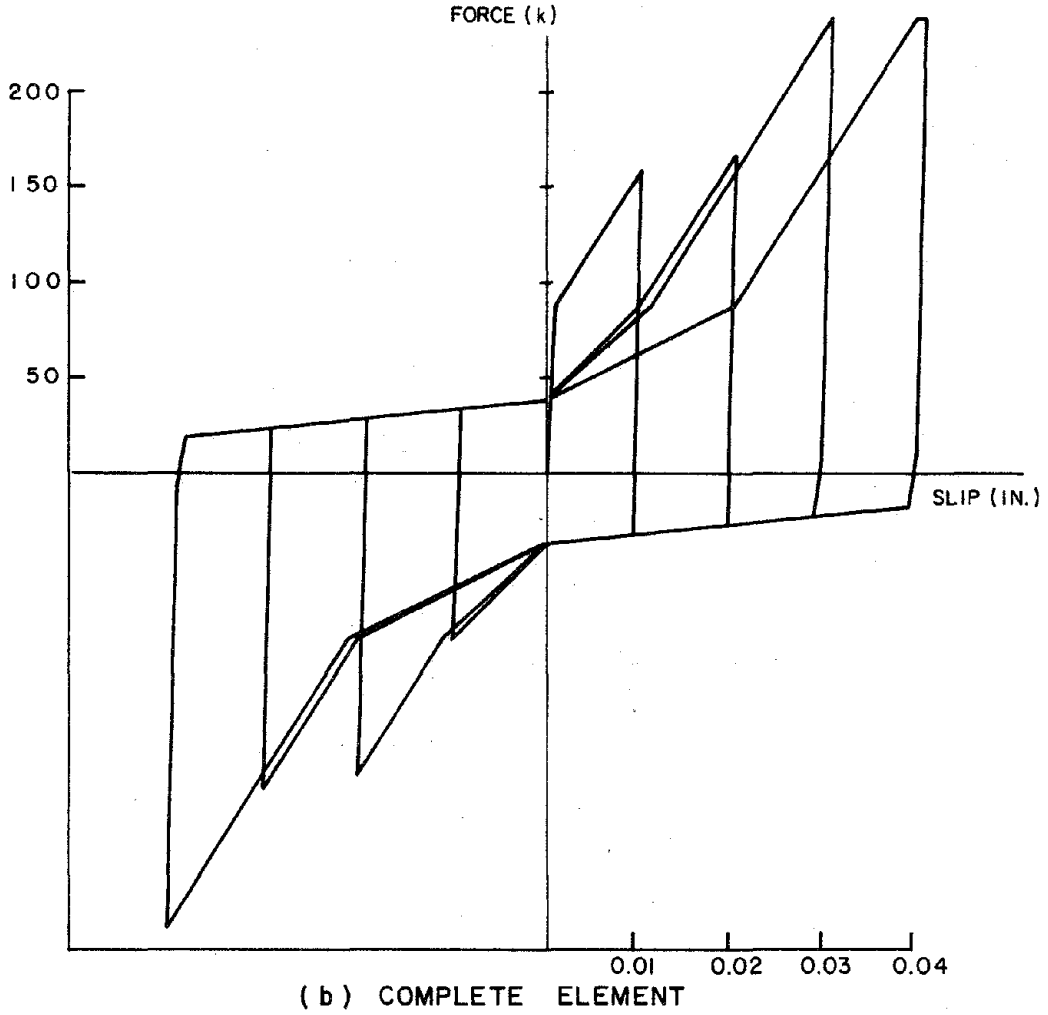

(b) COMPLETE ELEMENT

FIG. 4.9.5 CYCLIC BEHAVIOR OF SHEAR FRICTION ELEMENT

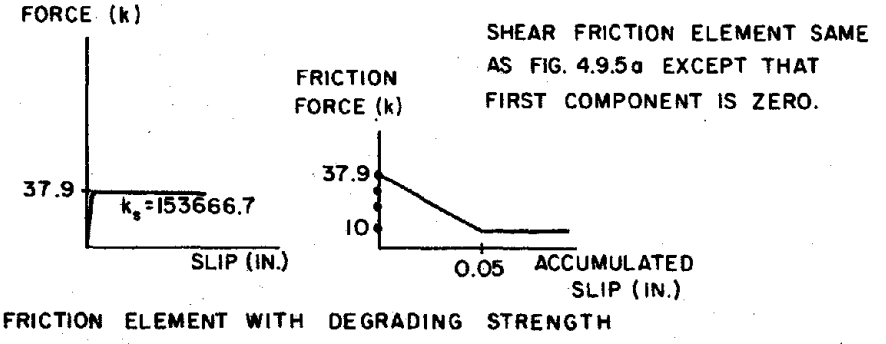

(a) PROPERTIES OF TWO ELEMENTS IN PARALLEL

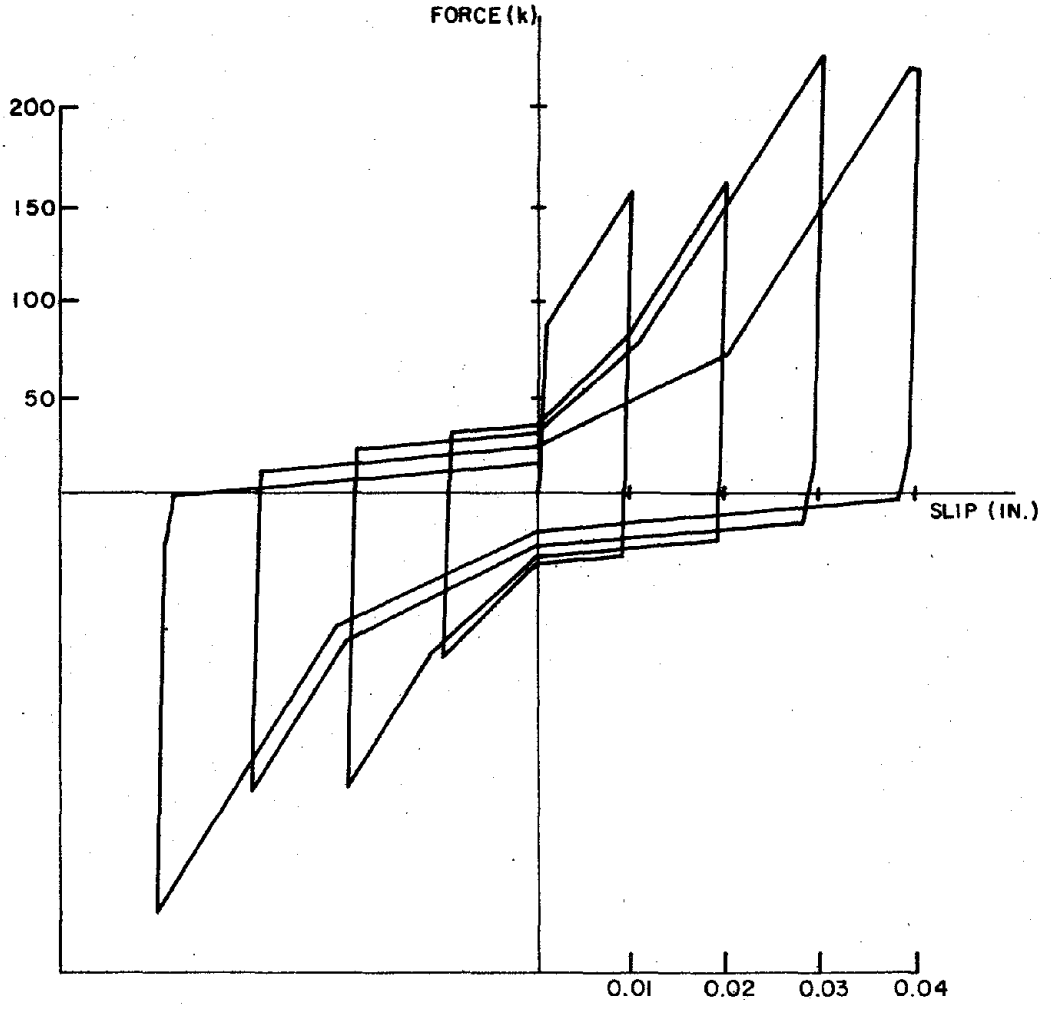

(b) COMPLETE ELEMENT

FIG. 4.9.6 SHEAR FRICTION BEHAVIOR WITH PINCHING EFFECT

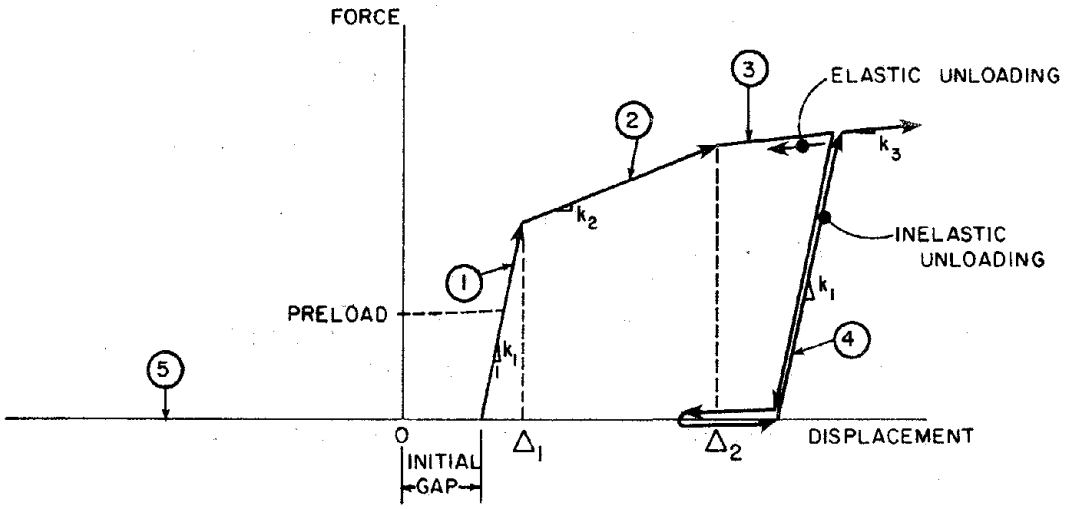

FIG. 4.10.1 LINK ELEMENT: FORCE-DISPLACEMENT RELATIONSHIP

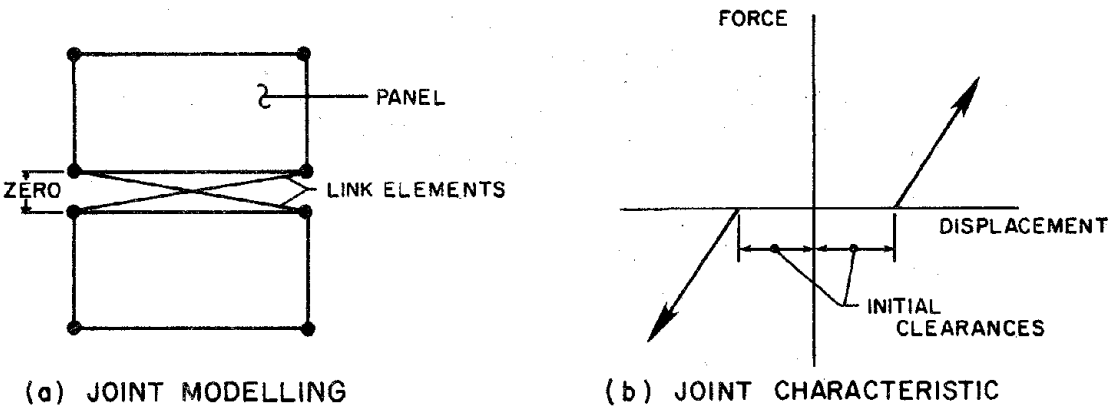

FIG. 4.10.2 STOP ELEMENT IN A HORIZONTAL JOINT

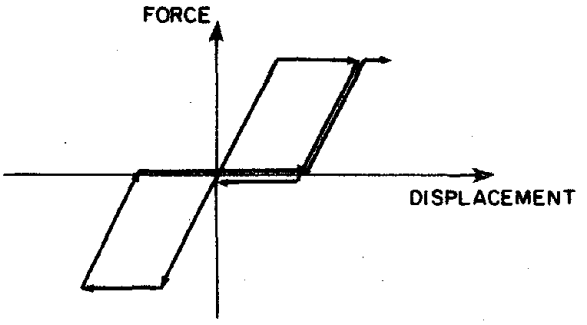

FIG. 4.10.3 TWO LINK ELEMENTS WITH $K_2 = 0$ AND $\Delta_2 = \infty$

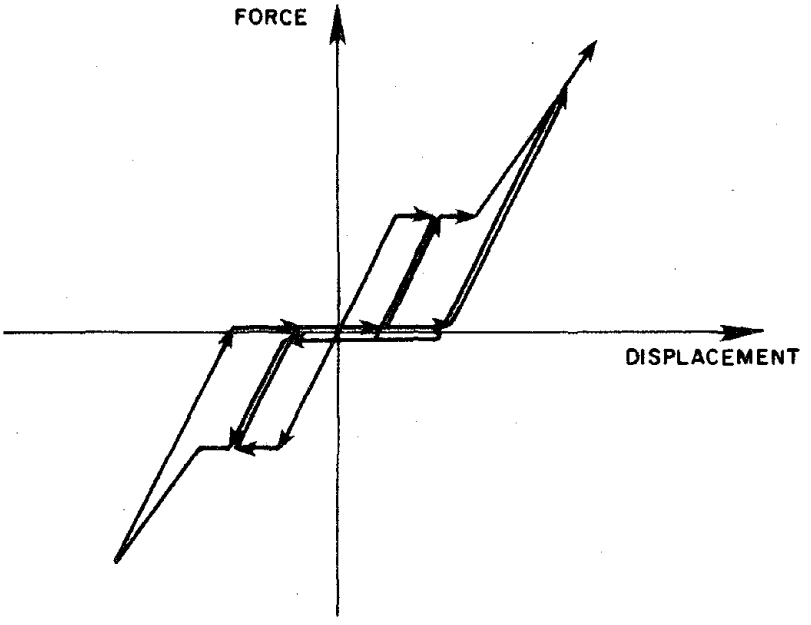

FIG. 4.10.4 TWO LINK ELEMENTS WITH $K_2 = 0$ AND $K_3 < K_1$

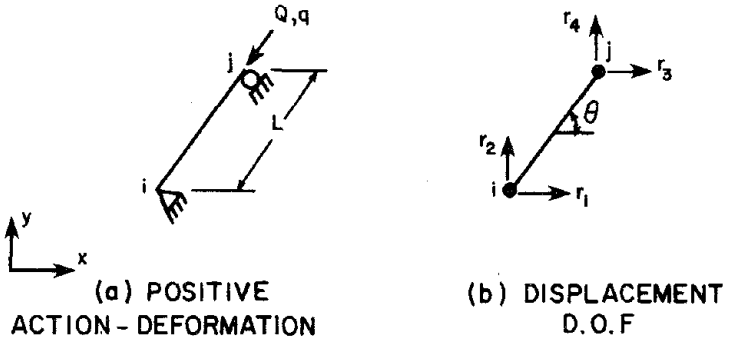

FIG. 4.10.5 DEGREES OF FREEDOM FOR LINK ELEMENT

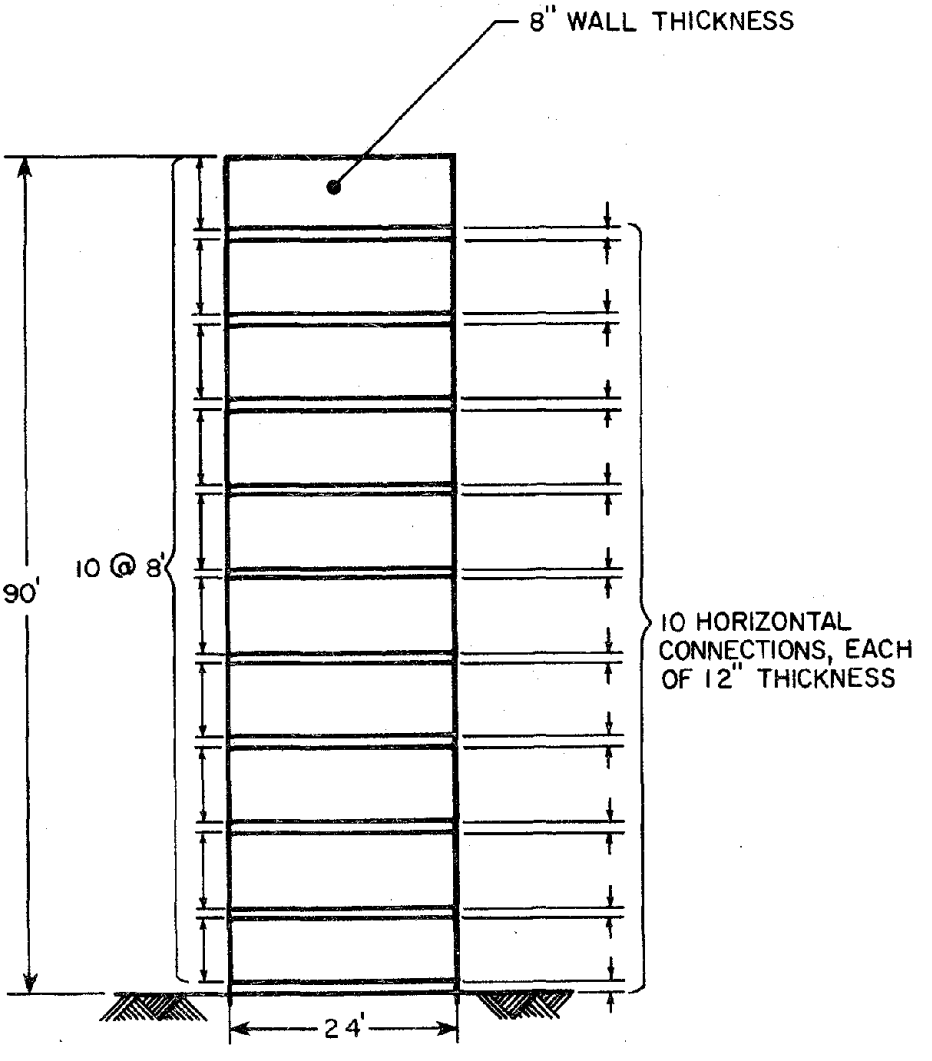

FIG. 5.2.1 TYPICAL LARGE PANEL WALL

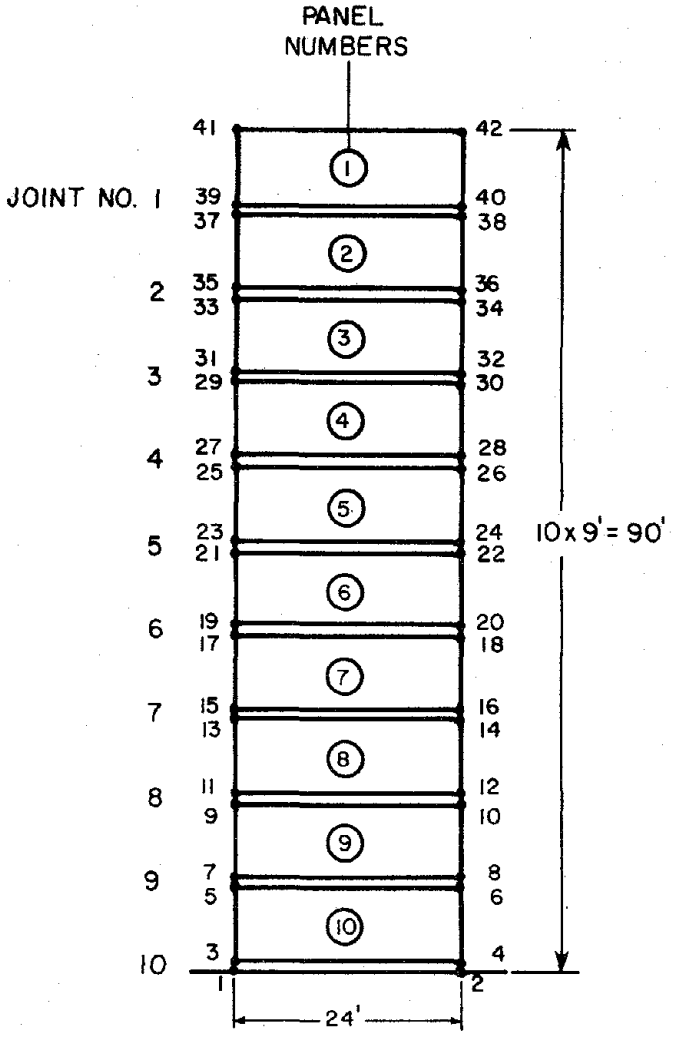

FIG. 5.3.1 BEAM MODEL

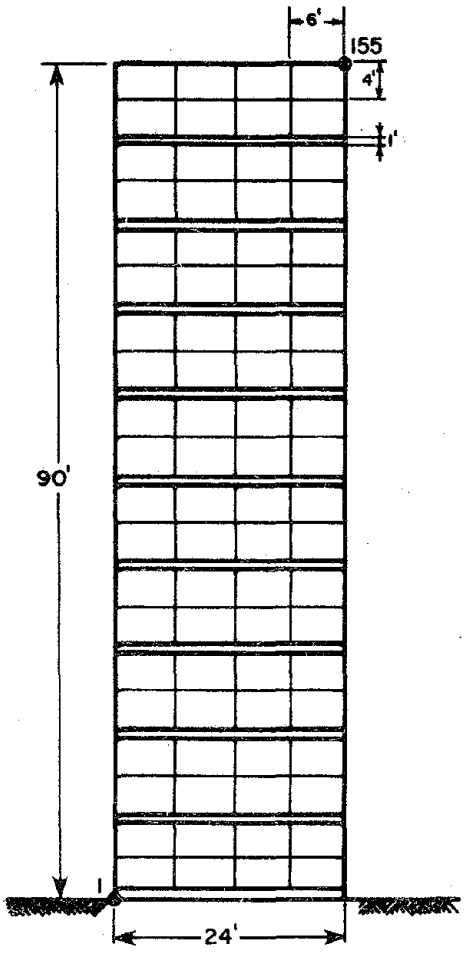

FIG. 5.3.2 FINITE ELEMENT MODEL

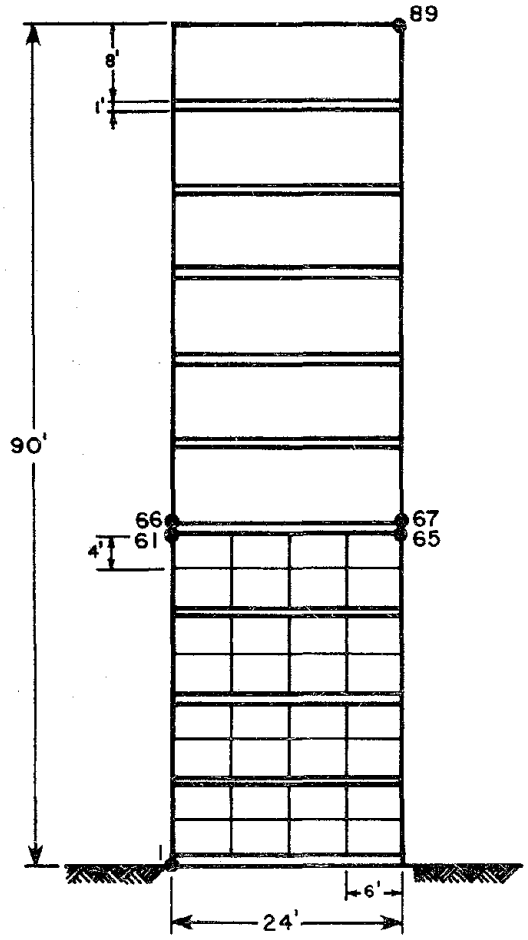

FIG. 5.3.3 BEAM-FINITE ELEMENT MODEL

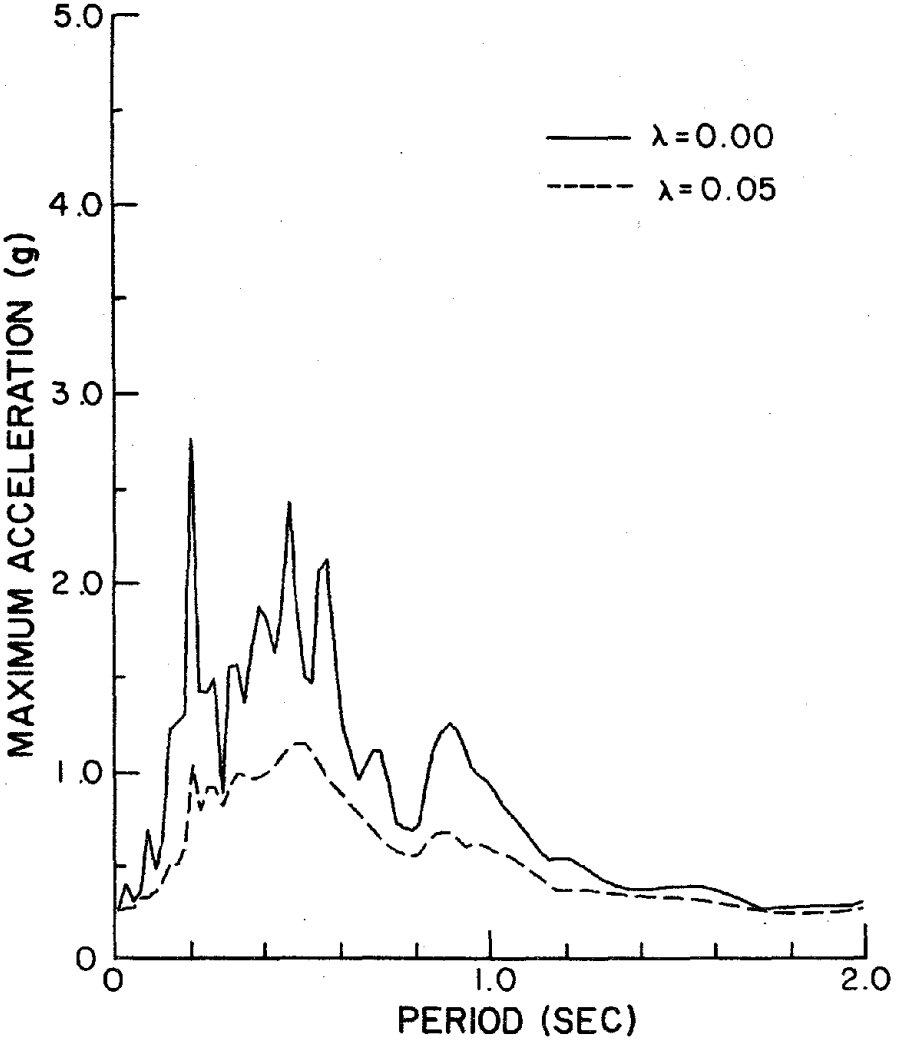

FIG. 5.5.1 ACCELERATION RESPONSE SPECTRUM
EC MOTION

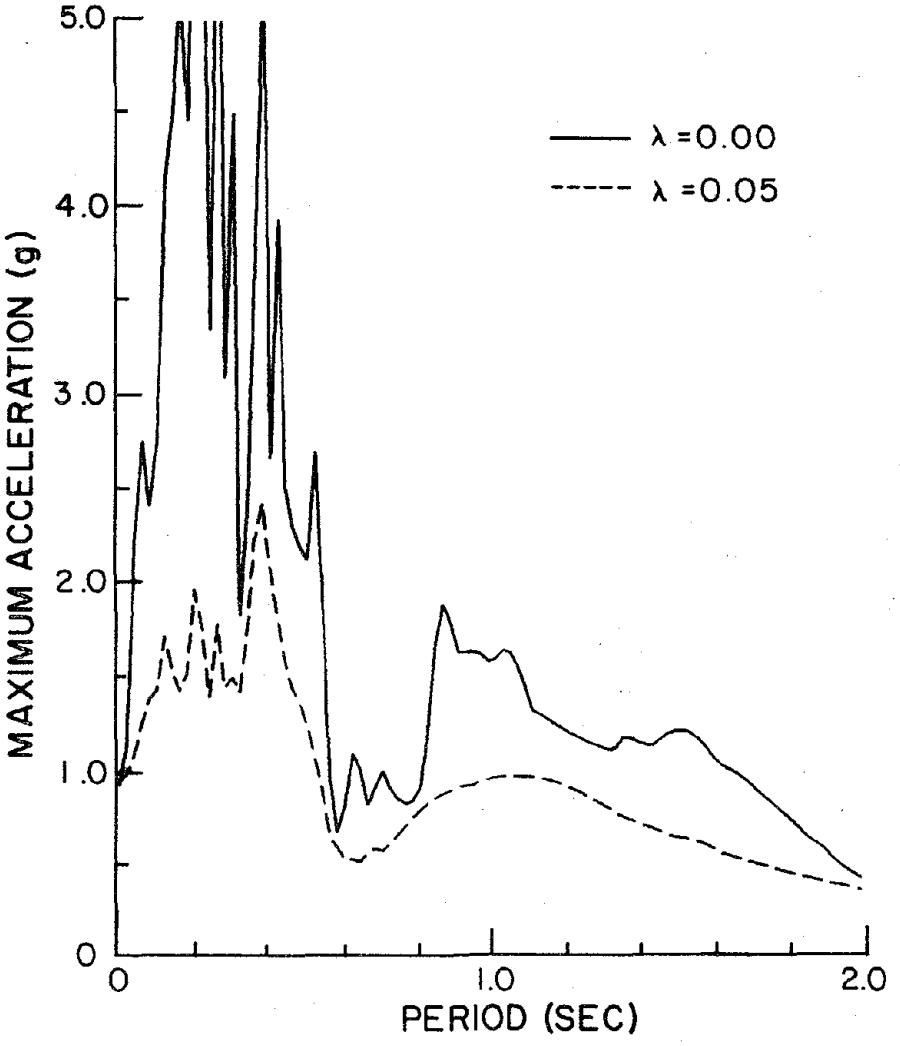

FIG. 5.5.2 ACCELERATION RESPONSE SPECTRUM
PD MOTION

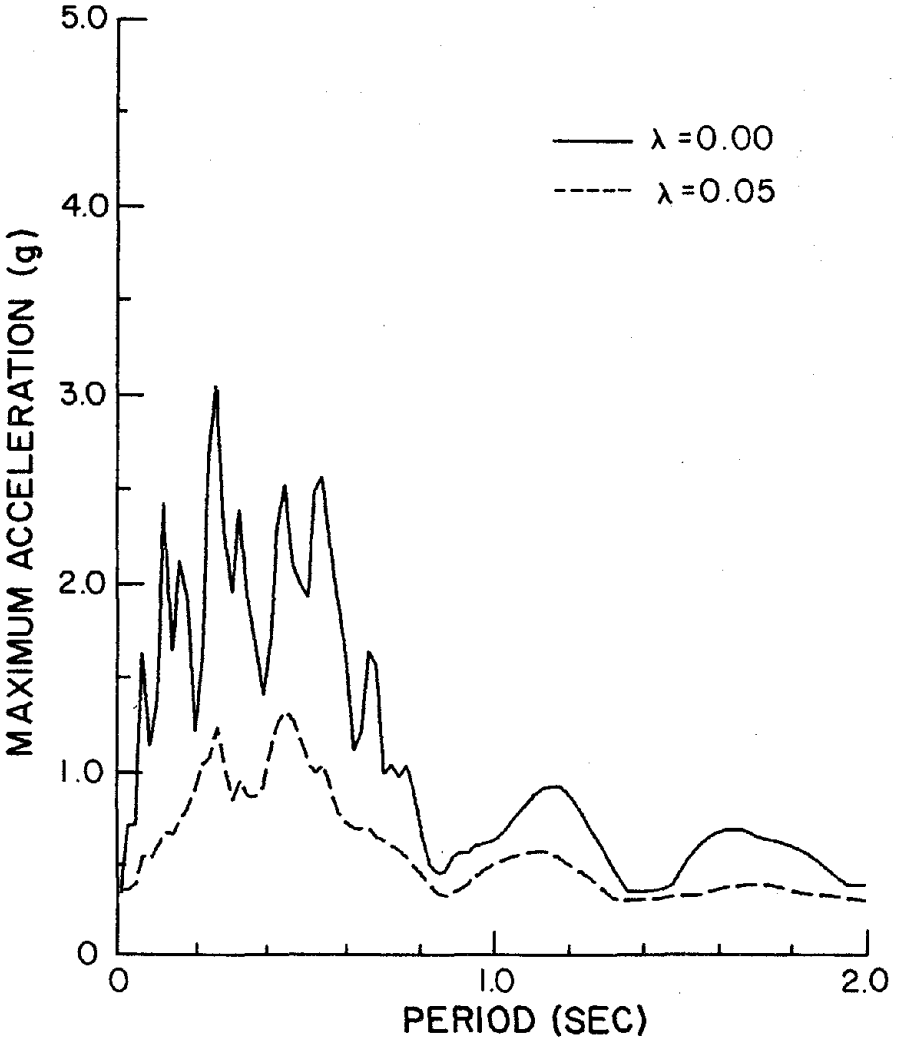

FIG. 5.5.3 ACCELERATION RESPONSE SPECTRUM
AA MOTION

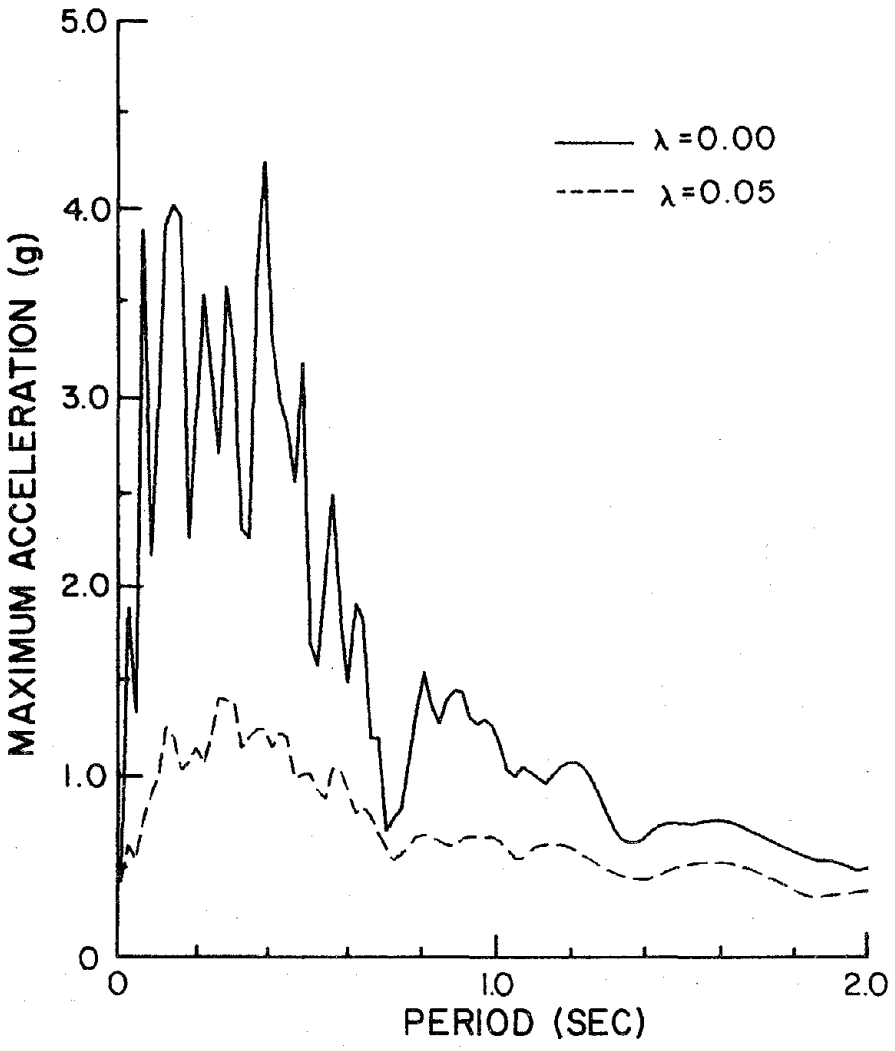

FIG. 5.5.4 ACCELERATION RESPONSE SPECTRUM
AB MOTION

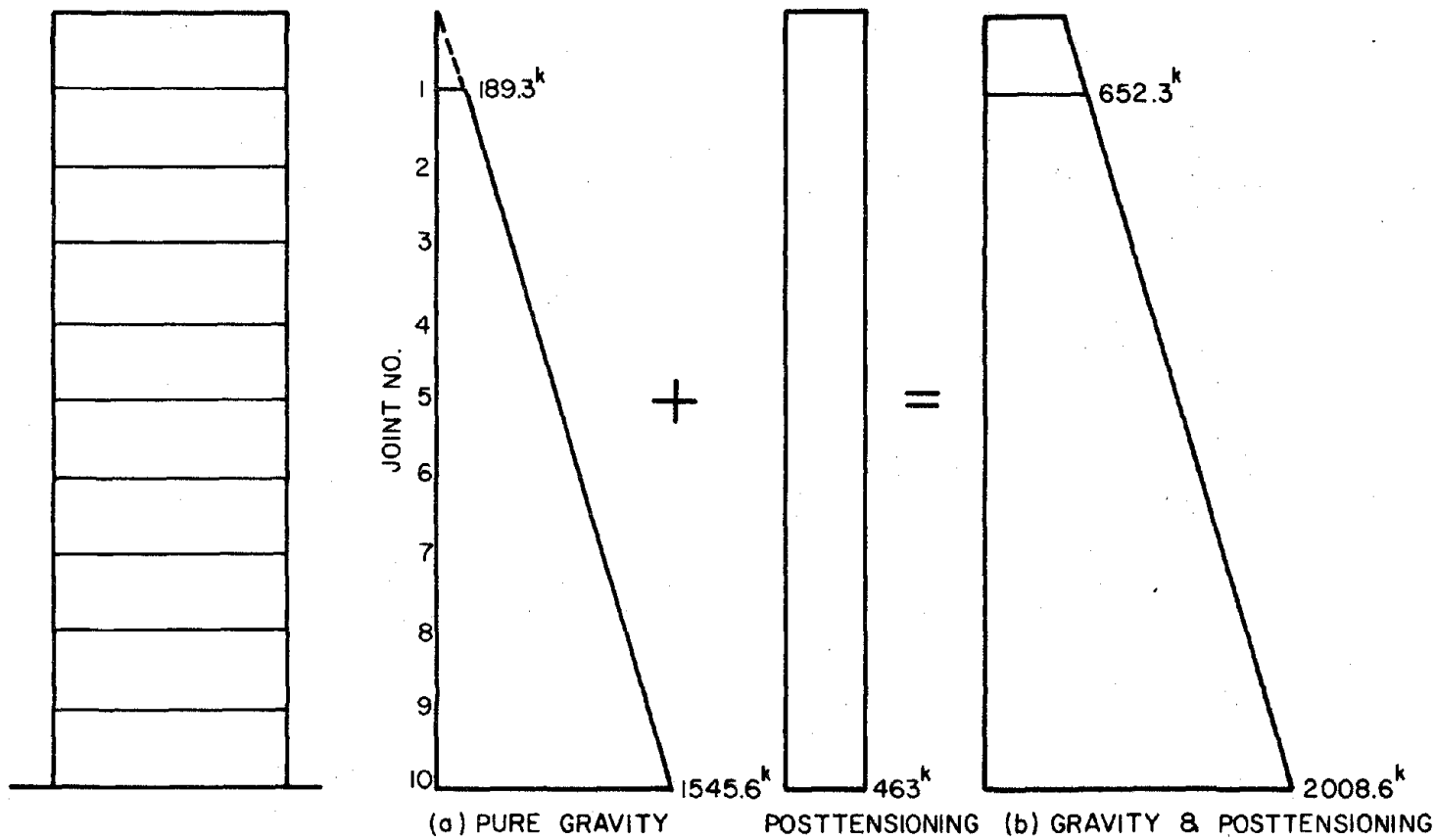

FIG. 5.6.1 VERTICAL LOADS ON JOINTS

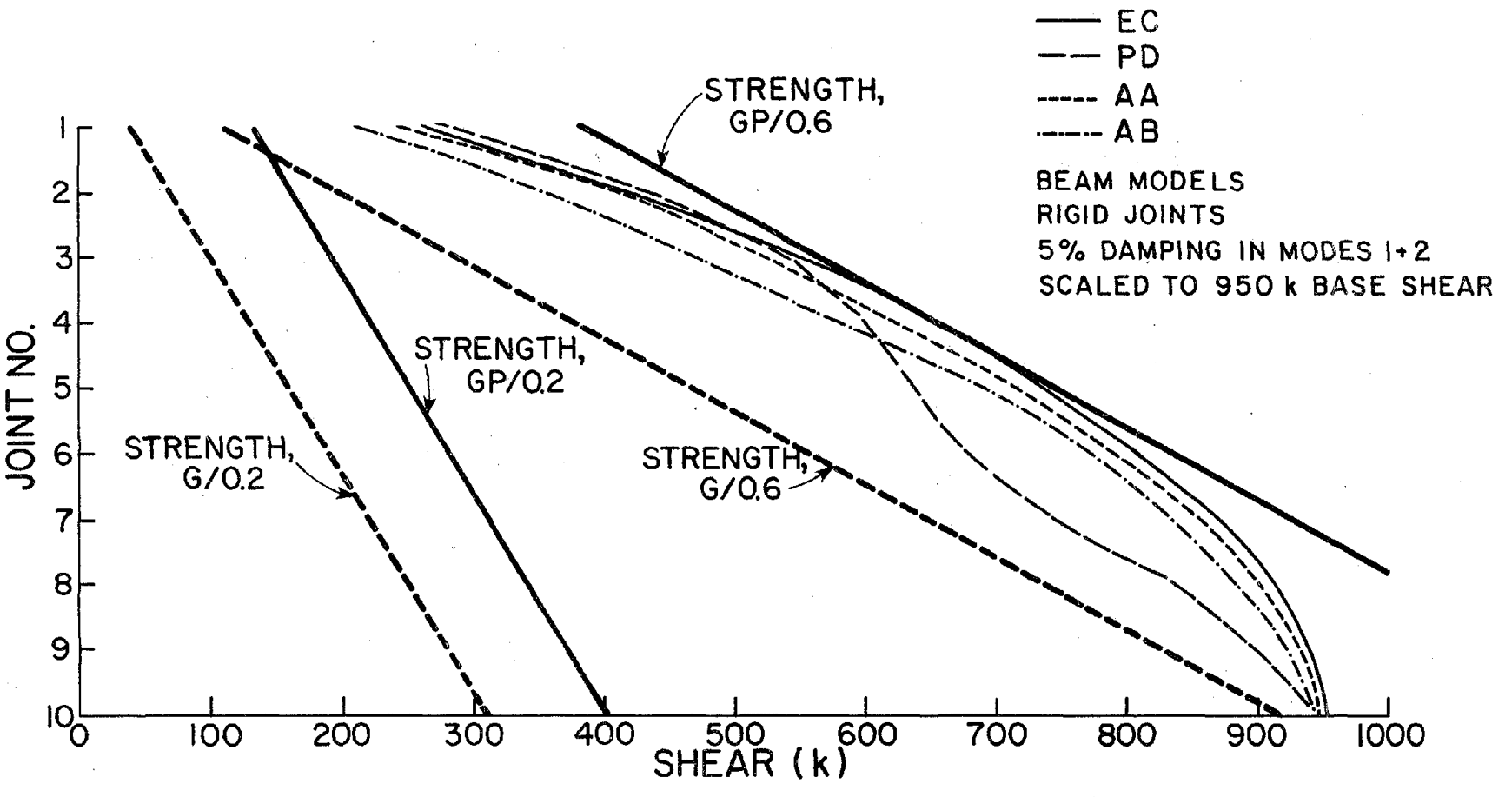

FIG. 5.8.1 CALCULATED JOINT SHEARS AND SHEAR STRENGTHS

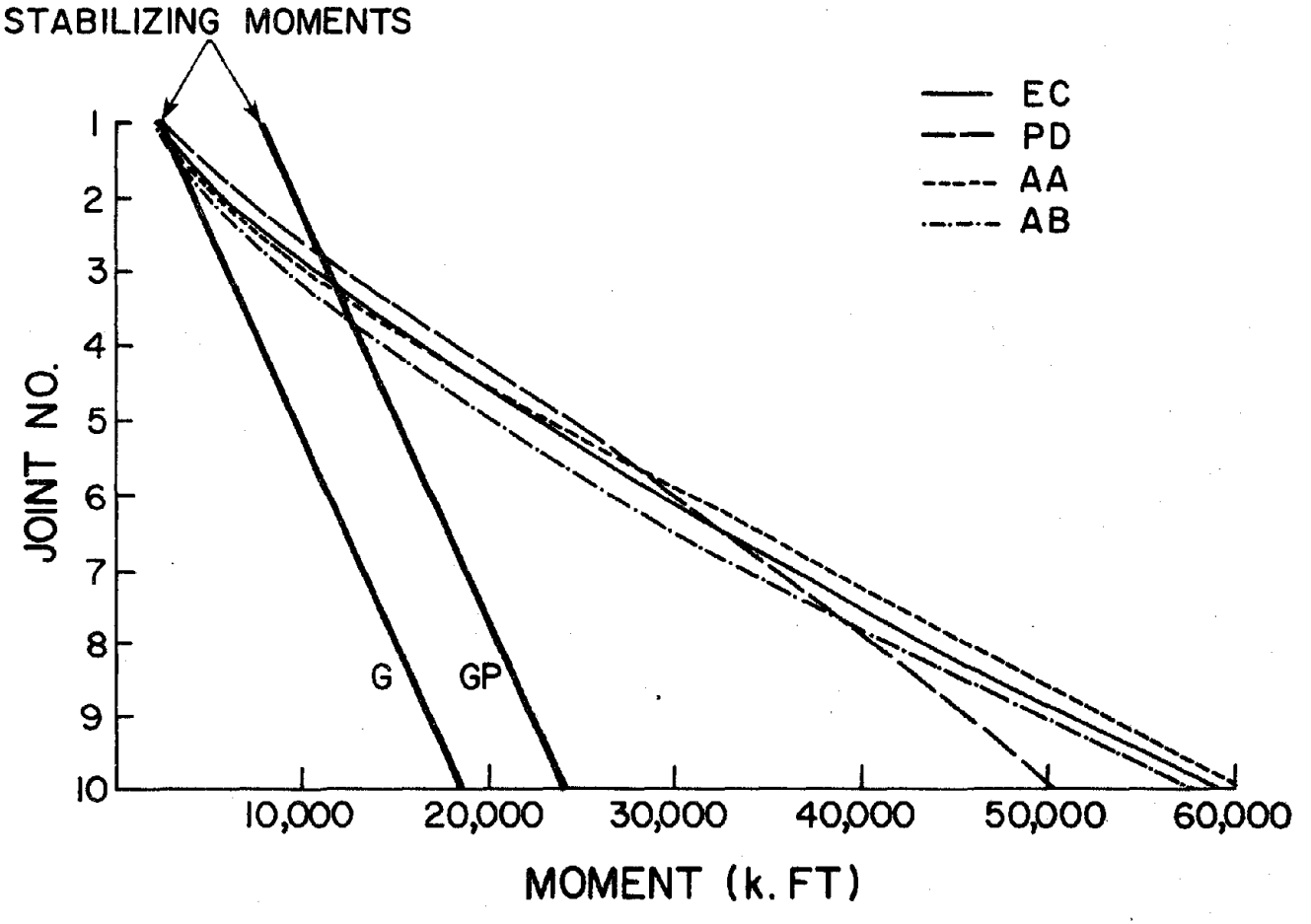

FIG. 5.8.2 CALCULATED OVERTURNING MOMENTS AND STABILIZING MOMENTS

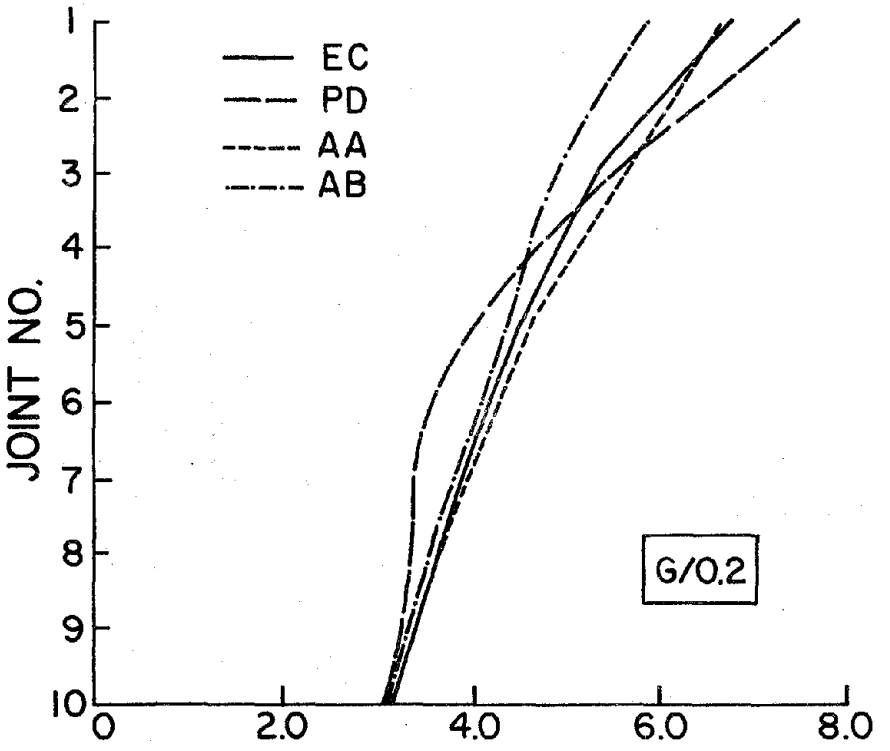

FIG. 5.9.1 RATIO OF MAXIMUM SHEAR TO JOINT SHEAR STRENGTH. G/0.2 CASES.

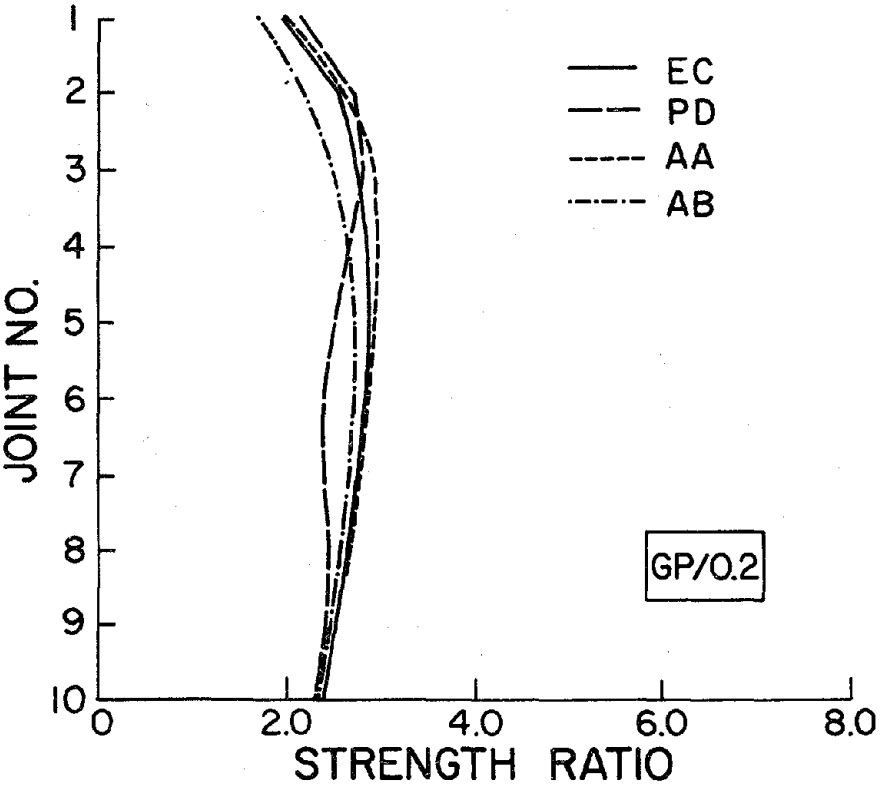

FIG. 5.9.2 RATIO OF MAXIMUM SHEAR TO JOINT SHEAR STRENGTH. GP/0.2 CASES.

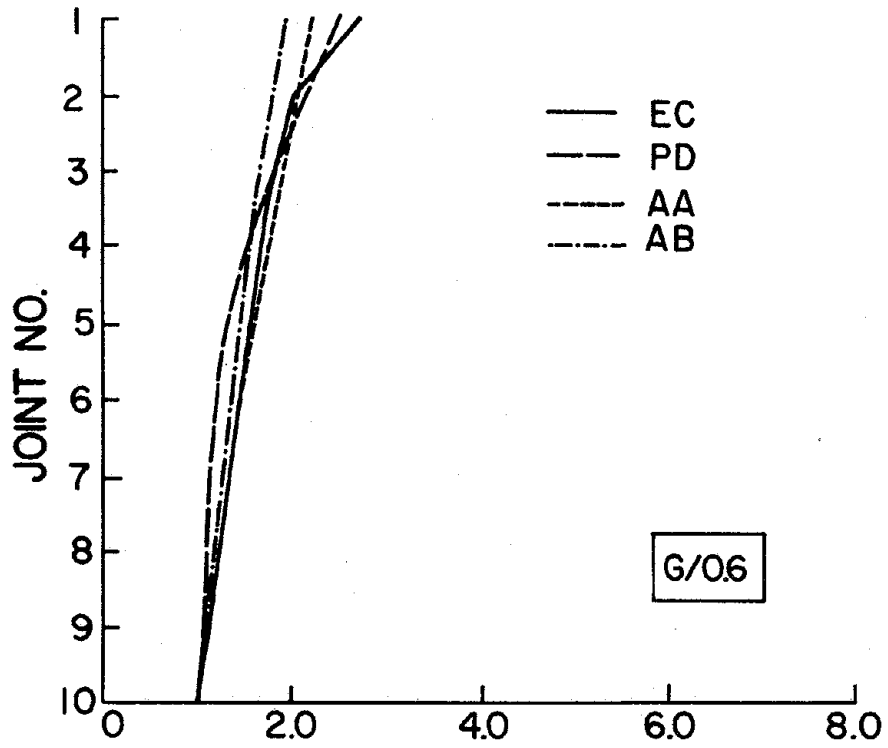

FIG. 5.9.3 RATIO OF MAXIMUM SHEAR TO JOINT SHEAR STRENGTH. G/0.6 CASES.

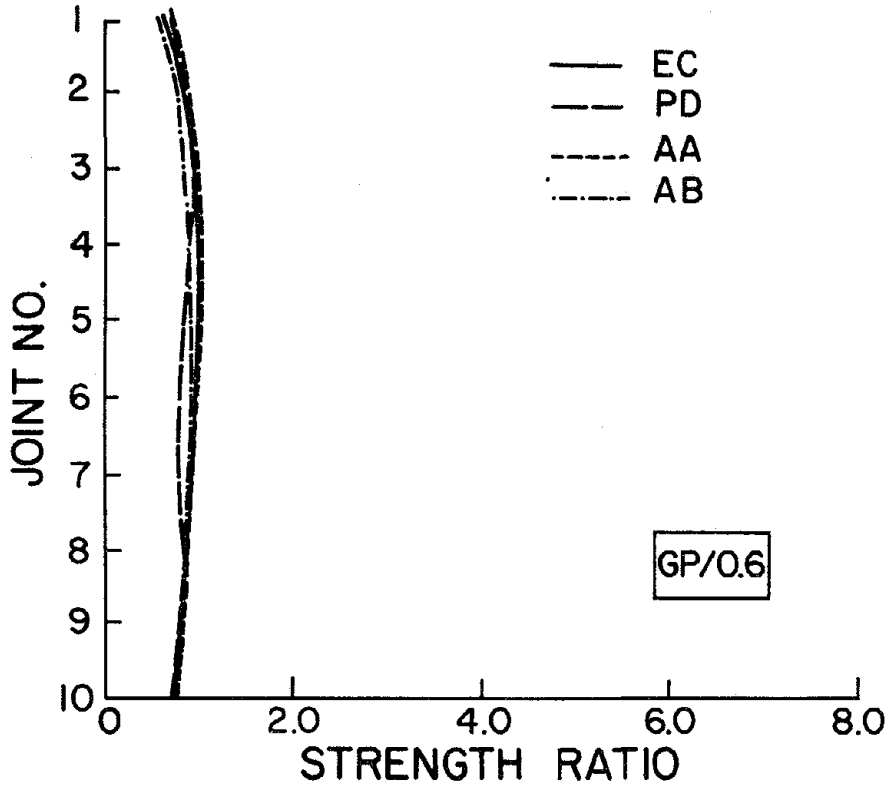

FIG. 5.9.4 RATIO OF MAXIMUM SHEAR TO JOINT SHEAR STRENGTH. GP/0.6 CASES.

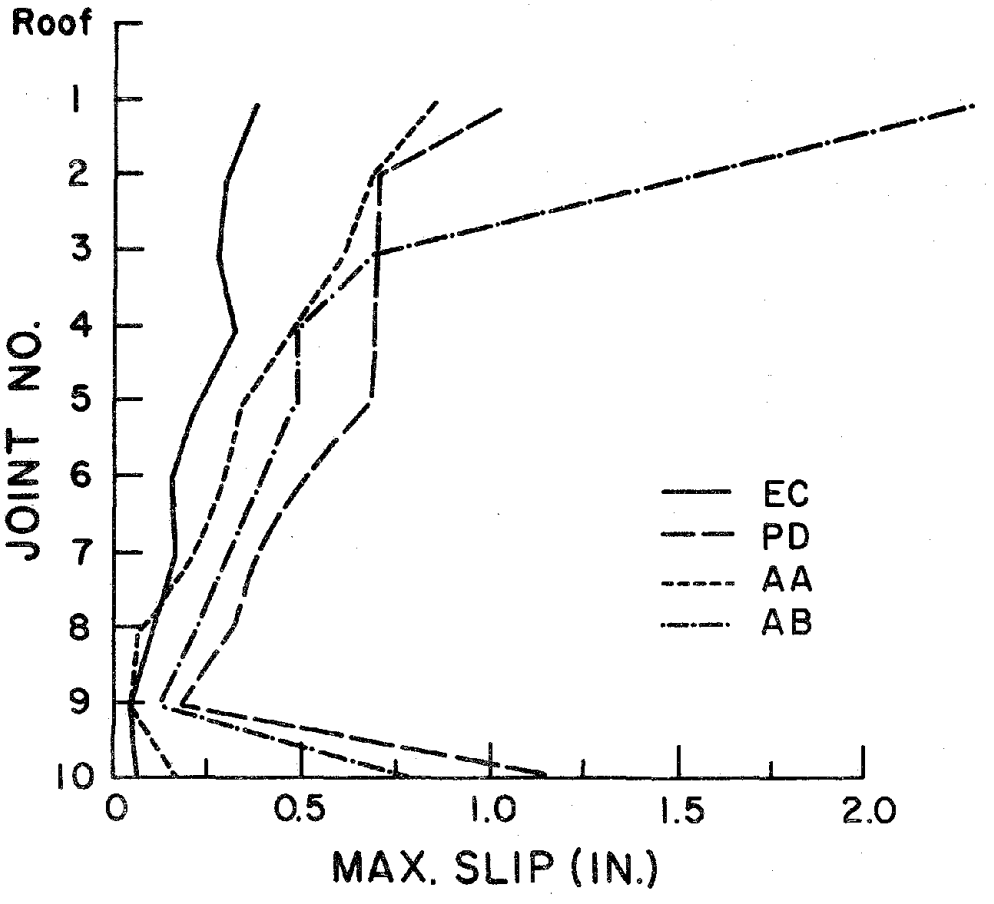

FIG. 5.10.1 CASE G/0.2: SIMPLE FRICTION ELEMENT WITH ZERO STRAIN HARDENING. MAXIMUM SLIP.

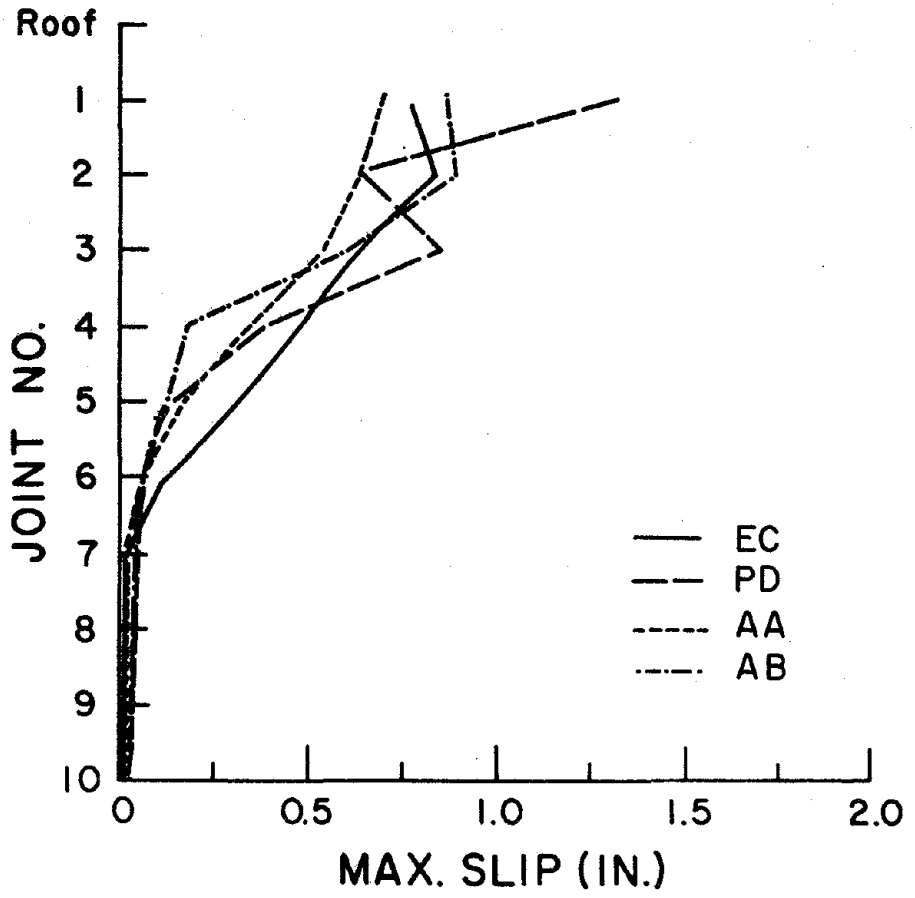

FIG. 5.10.2 CASE G/0.6 : SIMPLE FRICTION ELEMENT WITH ZERO STRAIN HARDENING. MAXIMUM SLIP.

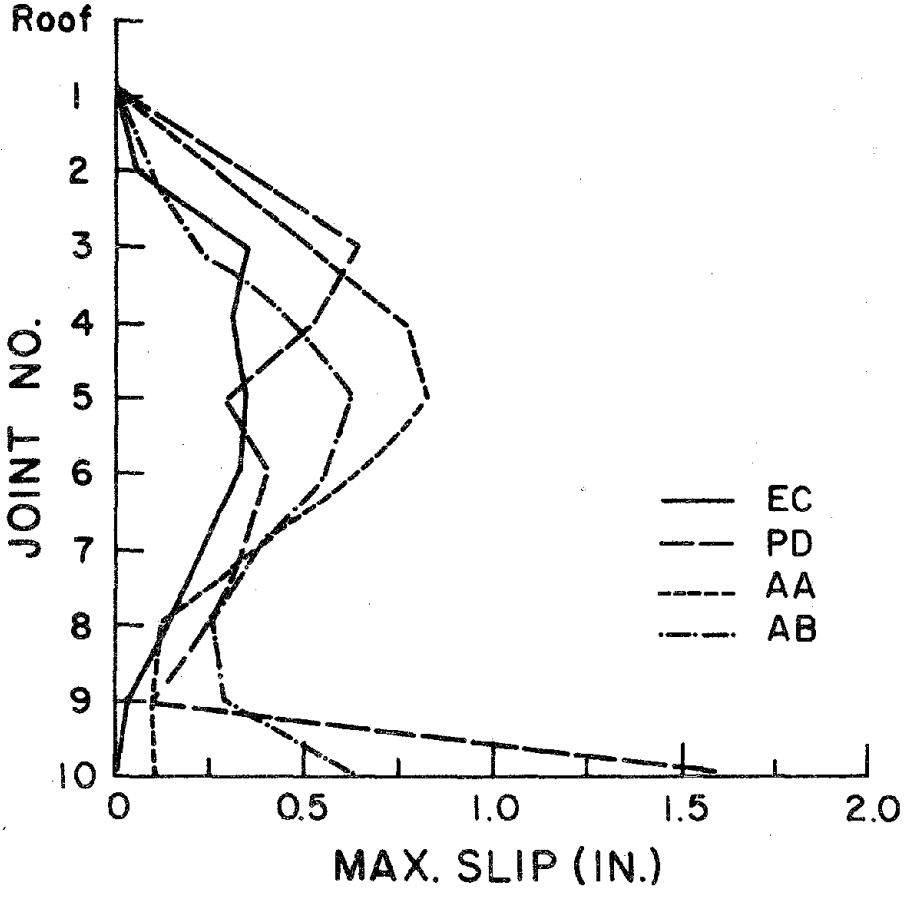

FIG. 5.10.3 CASE GP/0.2 : SIMPLE FRICTION ELEMENT WITH ZERO STRAIN HARDENING. MAXIMUM SLIP.

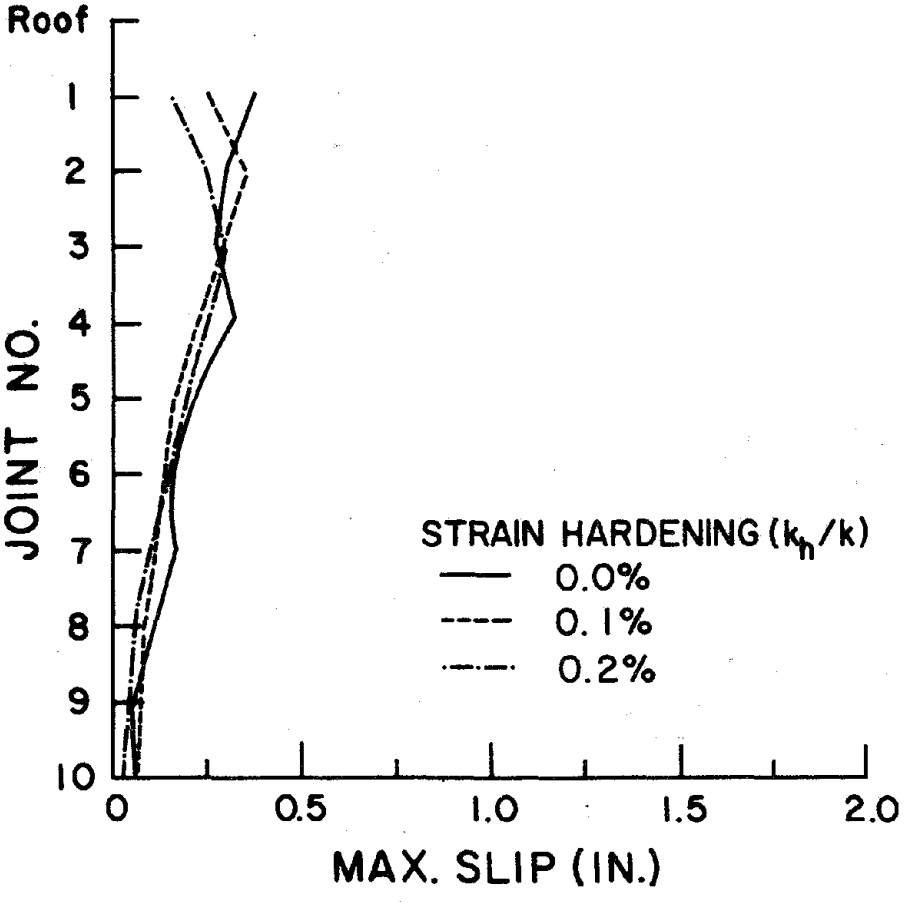

FIG. 5.10.4 CASE G/0.2/EC: SIMPLE FRICTION ELEMENT WITH STRAIN HARDENING. MAXIMUM SLIP.

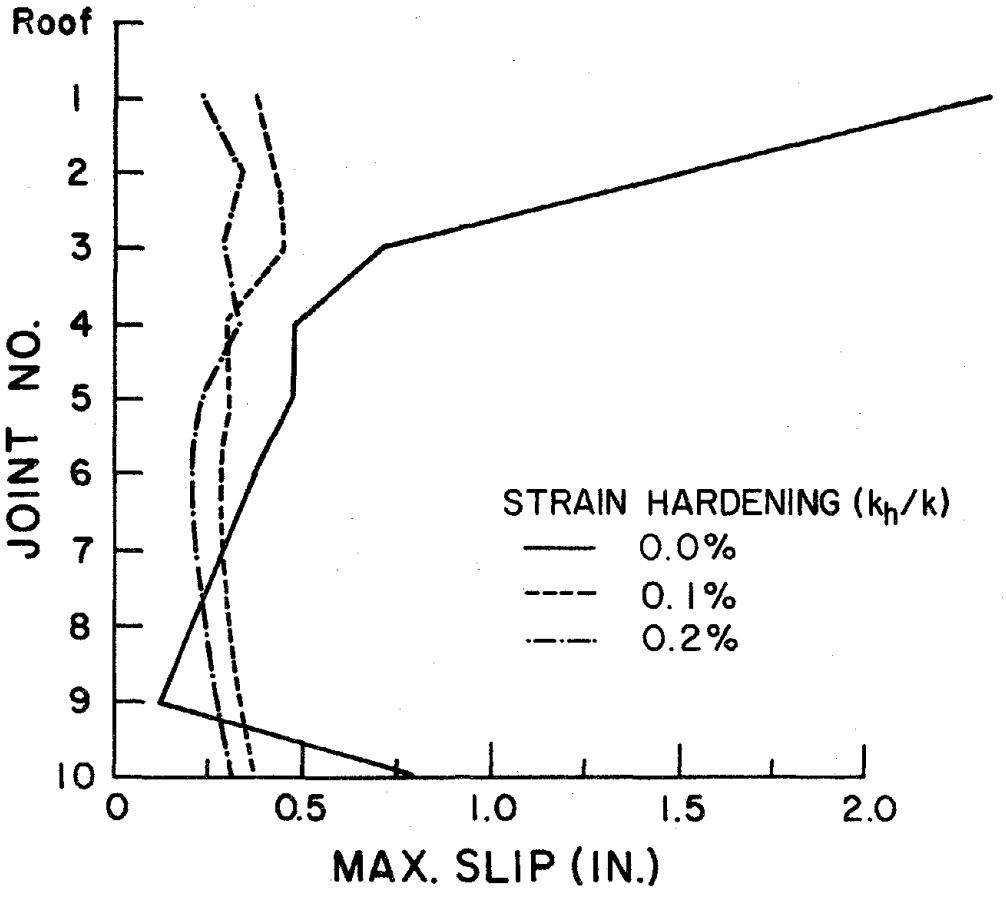

FIG. 5.10.5 CASE G/0.2/AB: SIMPLE FRICTION ELEMENT WITH STRAIN HARDENING. MAXIMUM SLIP.

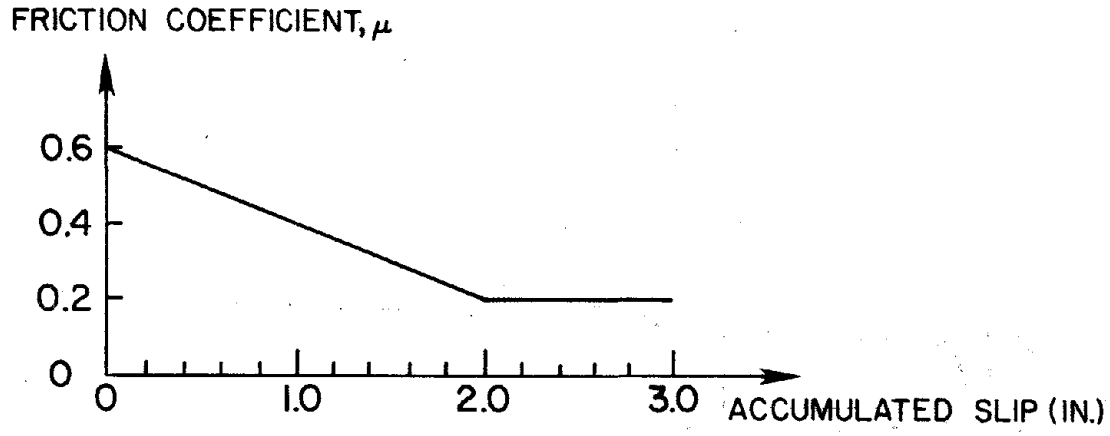

FIG. 5.10.6 DEGRADATION OF FRICTION COEFFICIENT

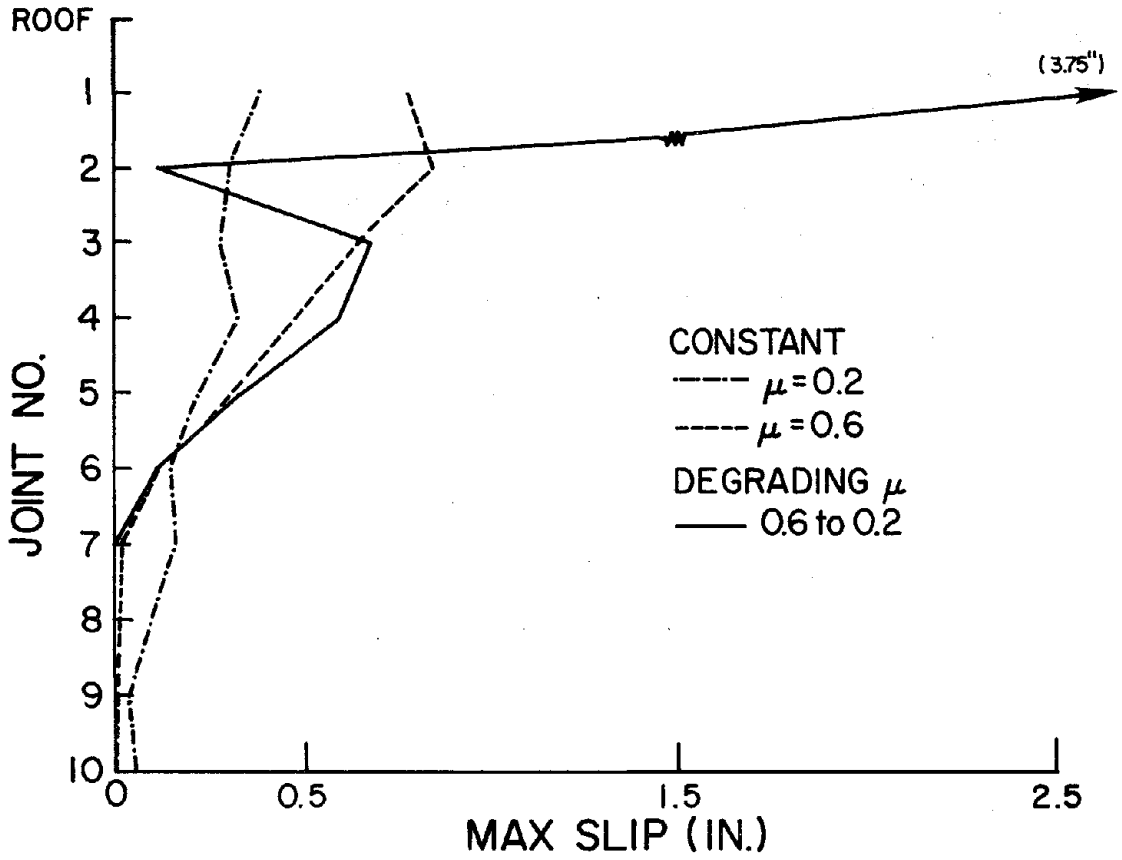

FIG. 5.10.7 CASE G/μ/EC: FRICTION ELEMENT WITH DEGRADING STRENGTH. MAXIMUM SLIP.

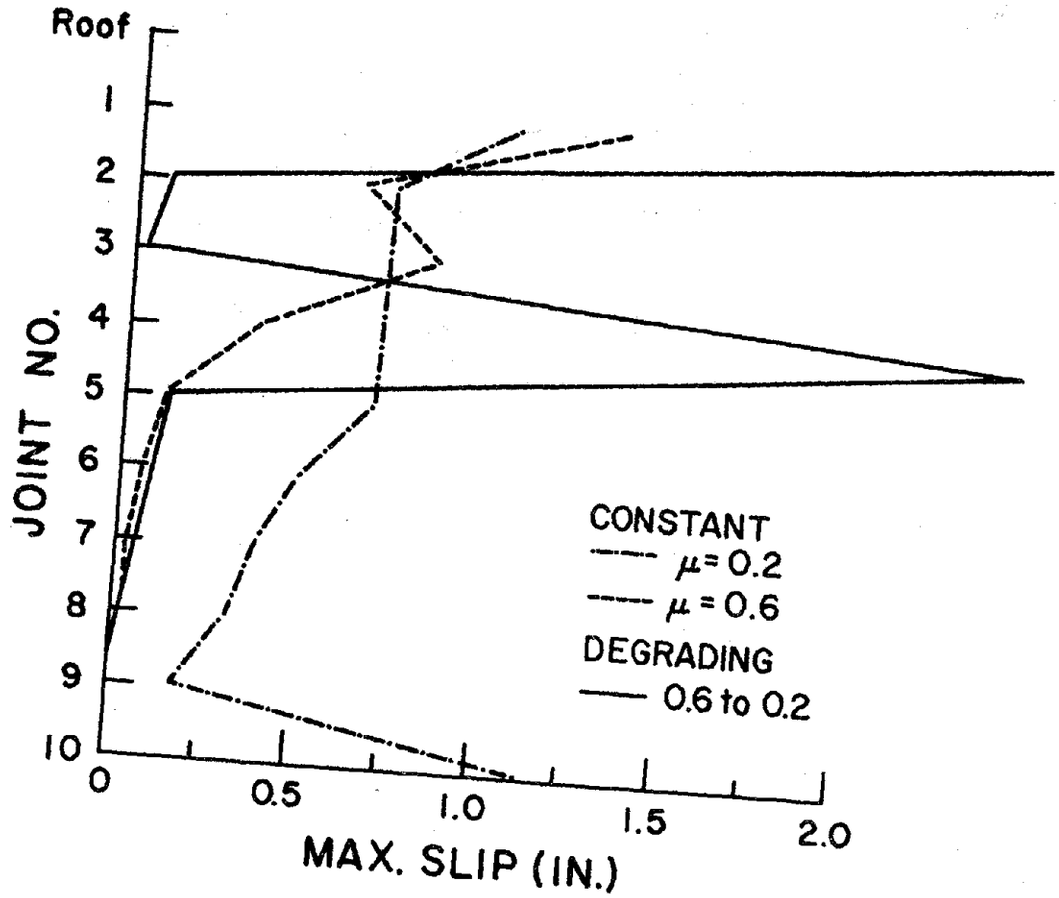

FIG. 5.10.8 CASE G/μ/PD: FRICTION ELEMENT WITH DEGRADING STRENGTH. MAXIMUM SLIP.

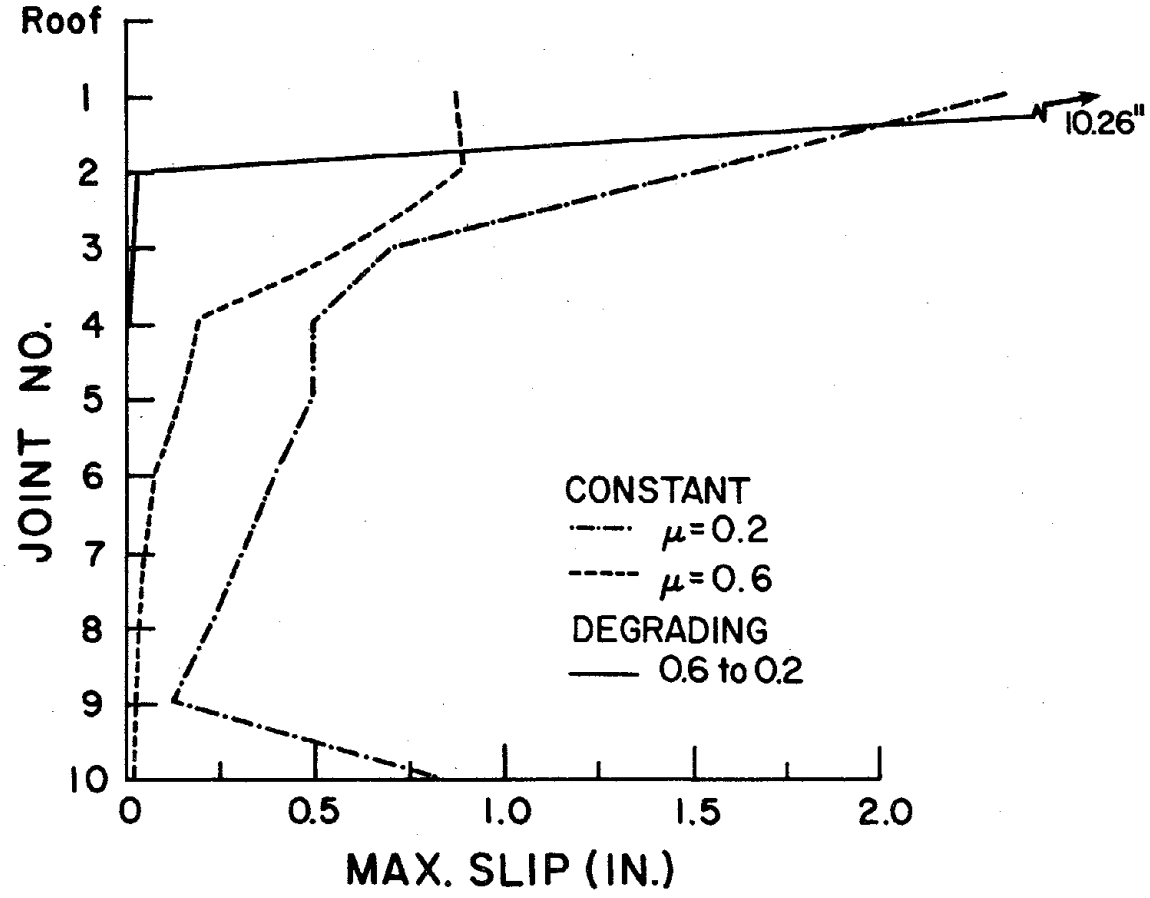

FIG. 5.10.9 CASE G/μ/AB: FRICTION ELEMENT WITH DEGRADING STRENGTH. MAXIMUM SLIP.

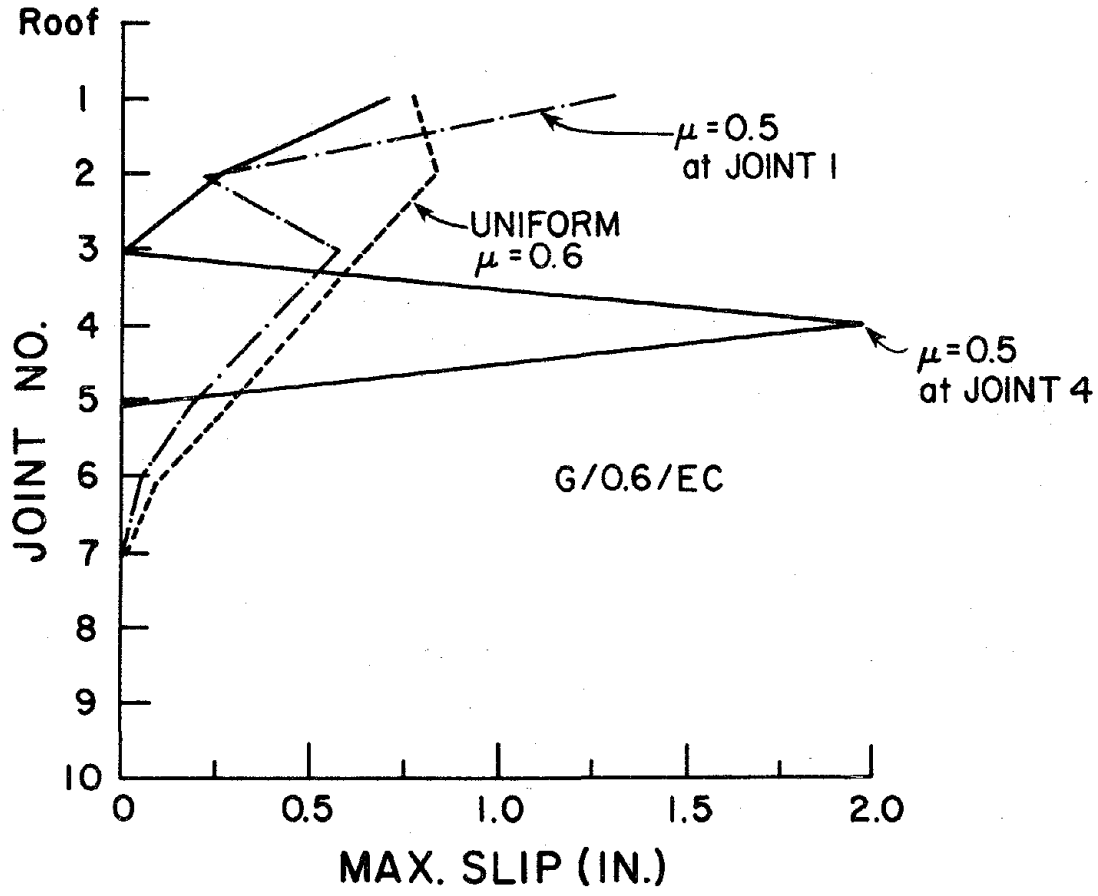

FIG. 5.10.10 EFFECT OF LOCAL JOINT WEAKNESS.
CASES G/0.6 WITH ONE WEAK JOINT.

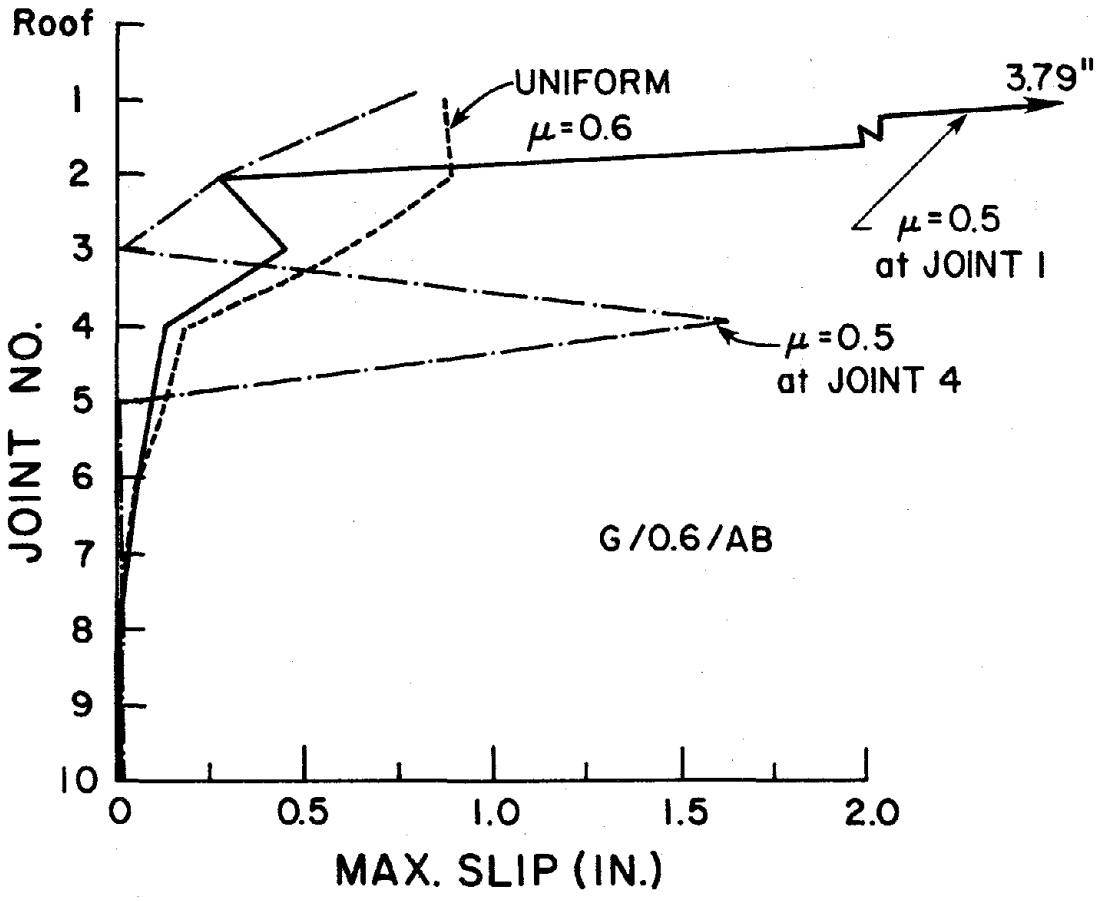

FIG. 5.10.10 (CONTINUED)

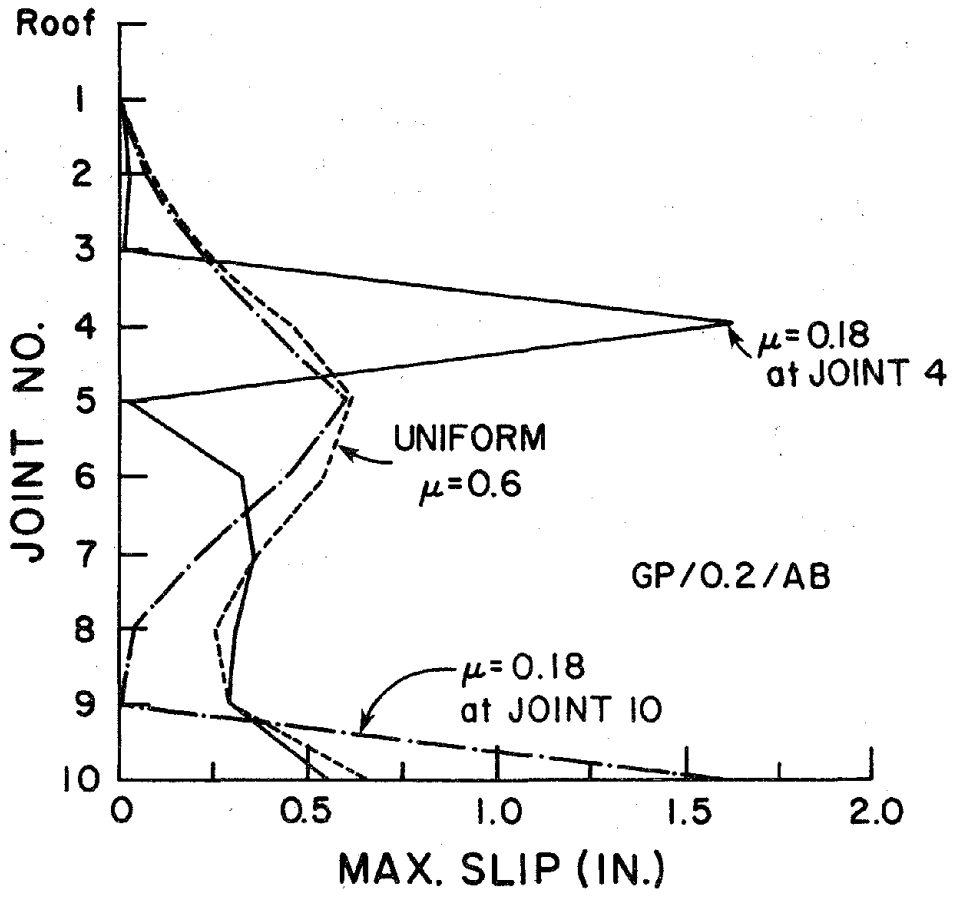

FIG. 5.10.11 EFFECT OF LOCAL JOINT WEAKNESS.
CASES GP/0.2/AB WITH ONE WEAK JOINT

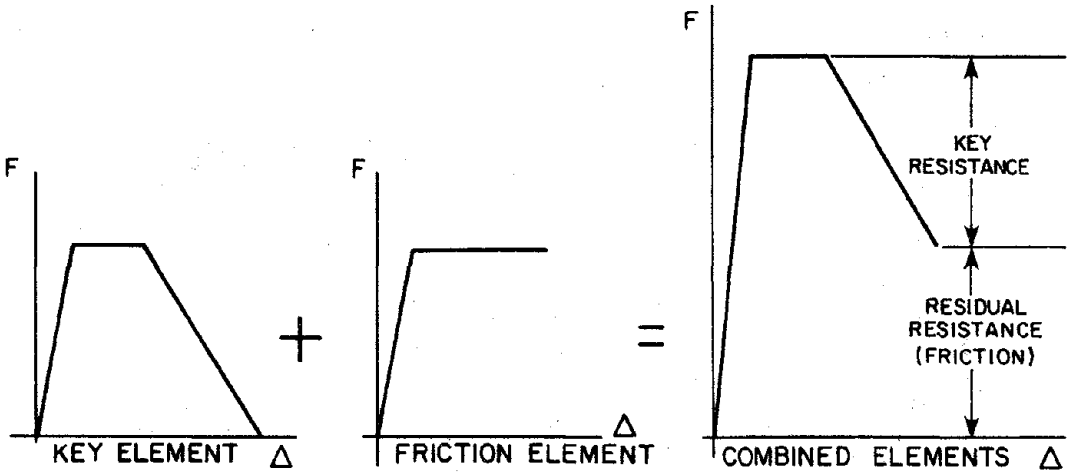

FIG. 5.10.12 SHEAR-SLIP RELATIONSHIP FOR KEYED CONNECTIONS

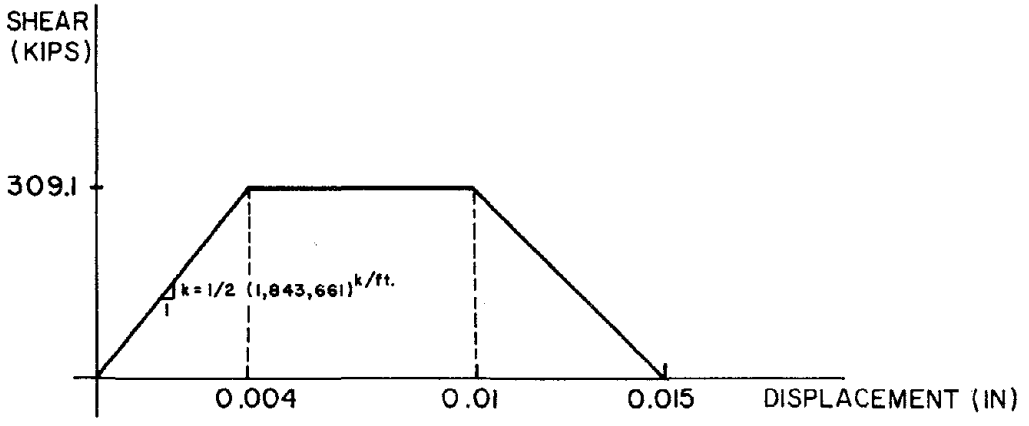

FIG. 5.10.13 FORCE-DISPLACEMENT RELATIONSHIP FOR KEY ELEMENTS

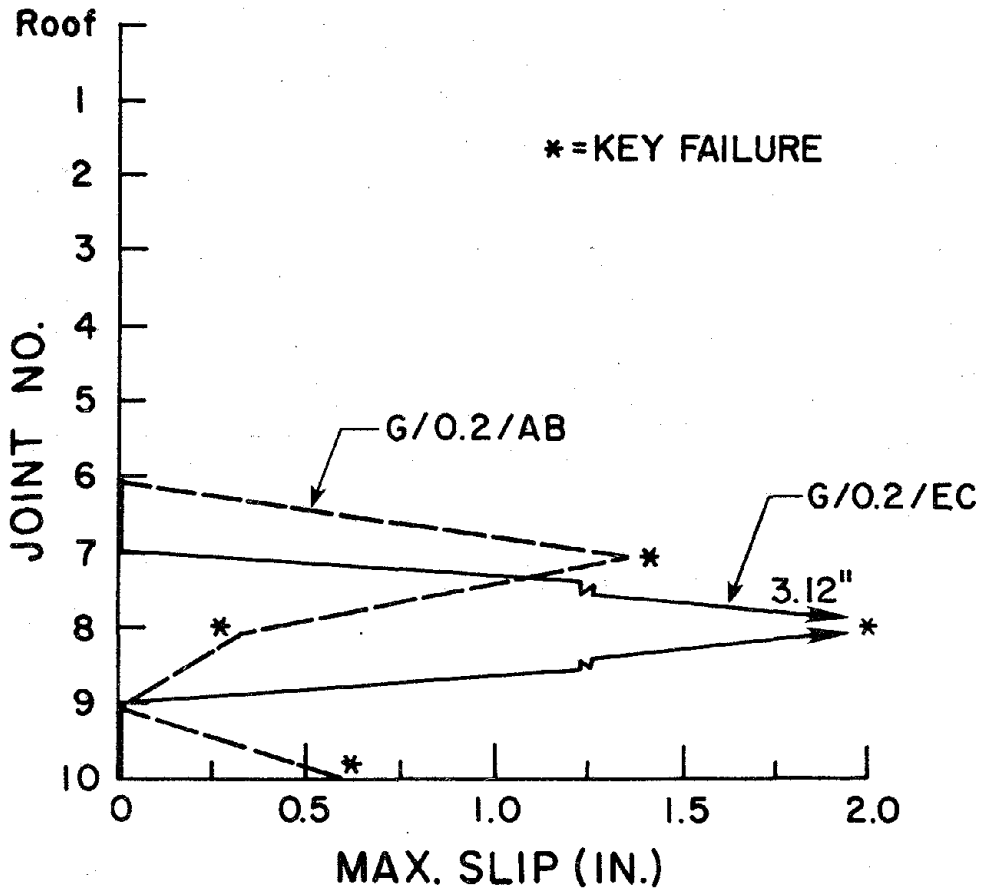

FIG. 5.10.14 CASE G/0.2. KEYED CONNECTIONS. MAXIMUM SLIP.

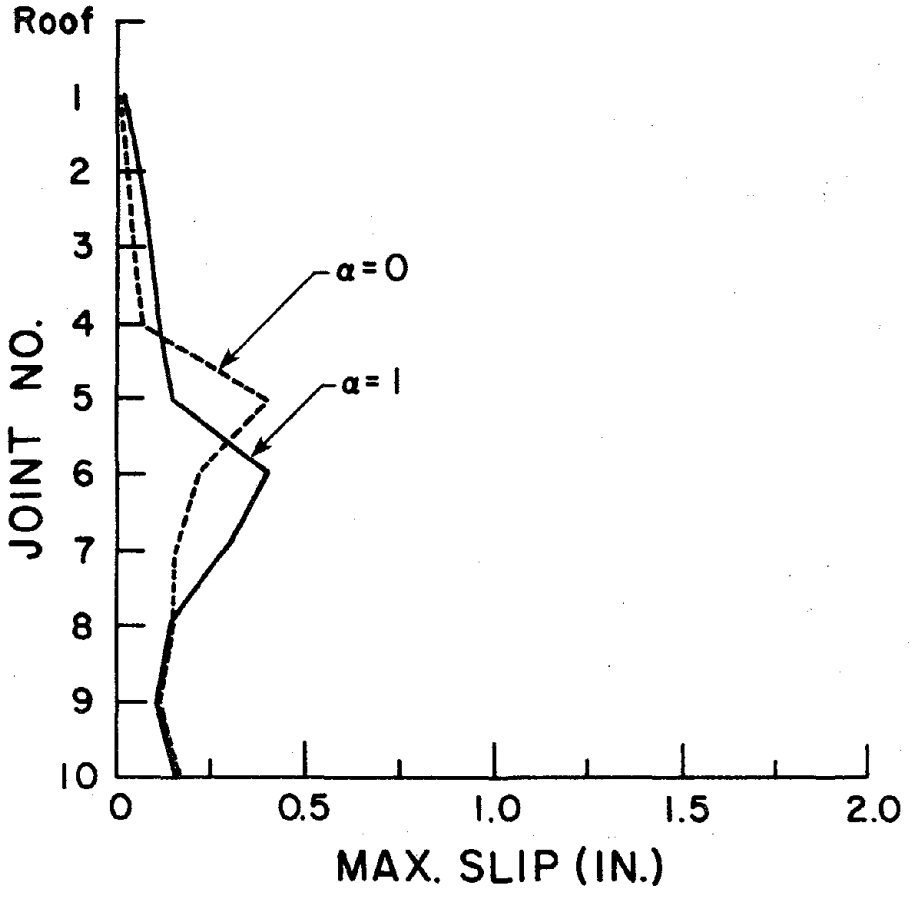

FIG. 5.10.15 CASE G/0.2/EC: SHEAR FRICTION ELEMENT. MAXIMUM SLIP.

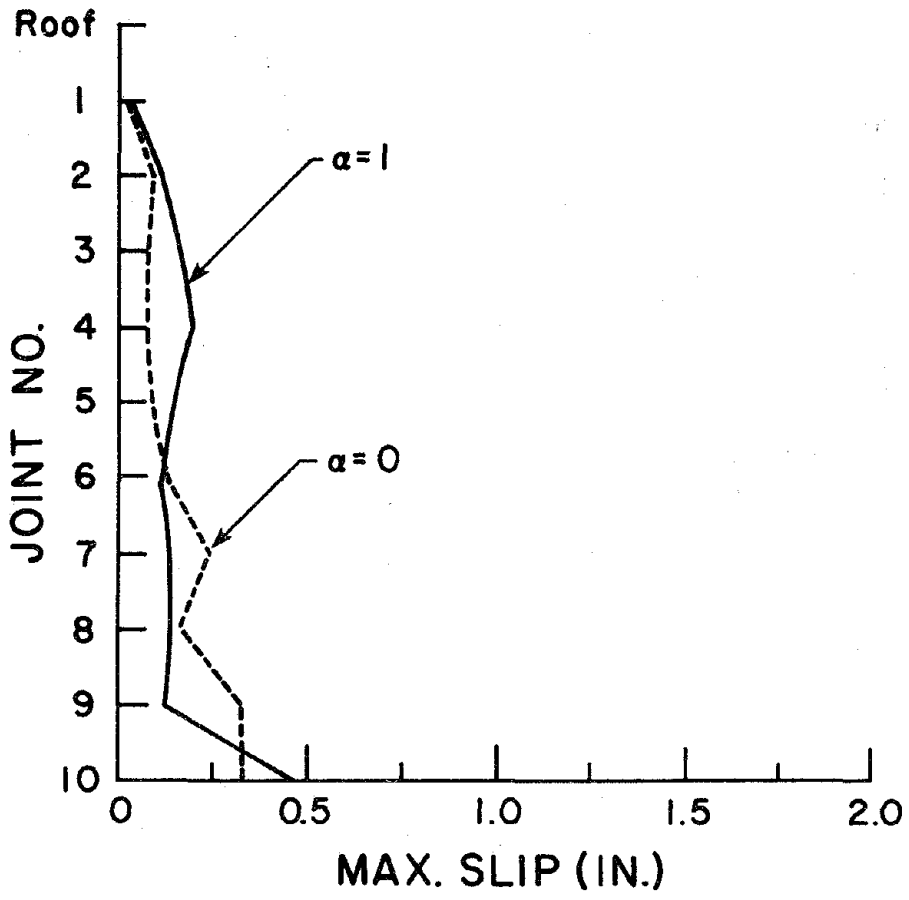

FIG. 5.10.16 CASE G/0.2/AB: SHEAR FRICTION ELEMENT. MAXIMUM SLIP.

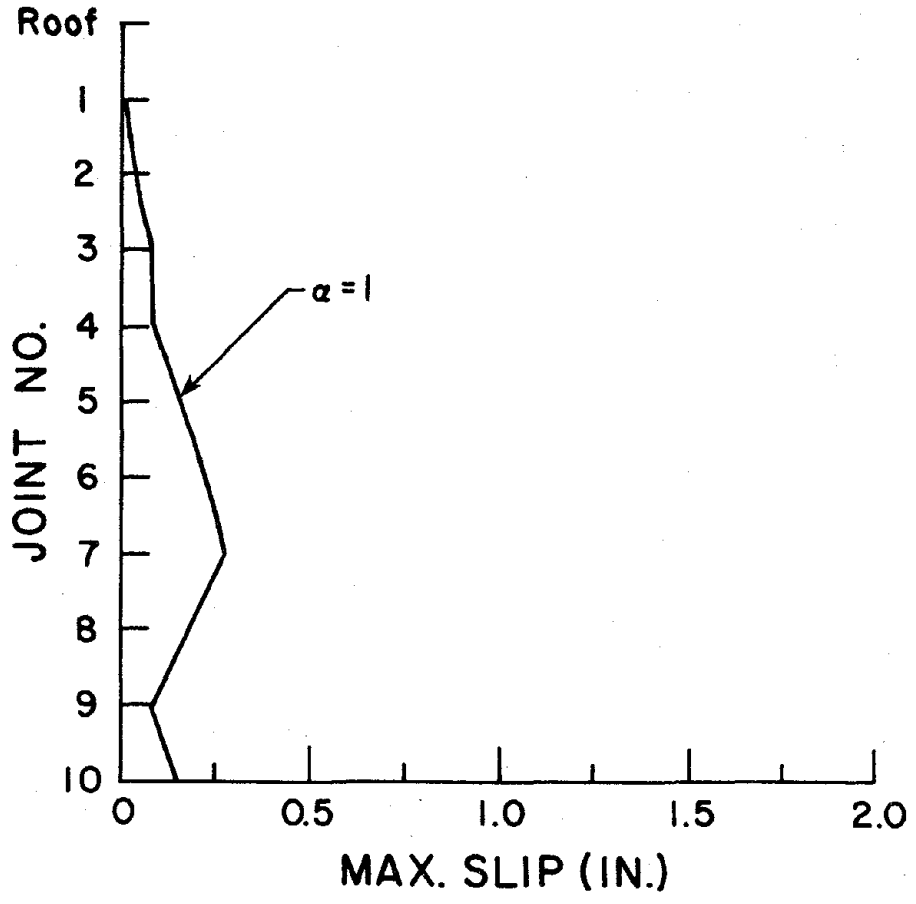

FIG. 5.10.17 CASE GP/0.2/EC: SHEAR FRICTION ELEMENT. MAXIMUM SLIP.

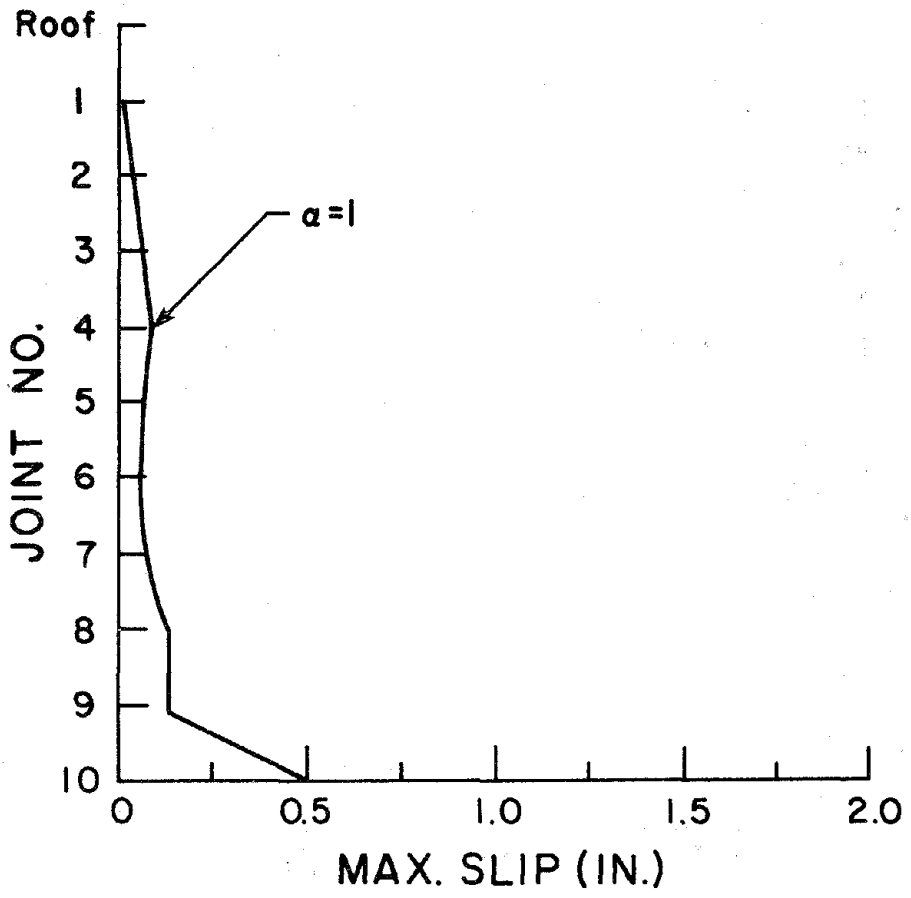

FIG. 5.10.18 CASE GP/0.2/AB: SHEAR FRICTION ELEMENT. MAXIMUM SLIP.

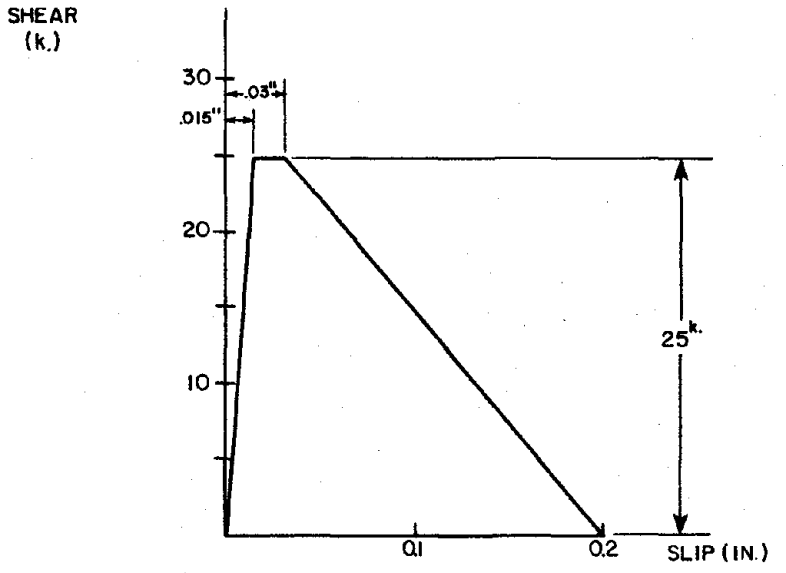

(a) KEY ELEMENT

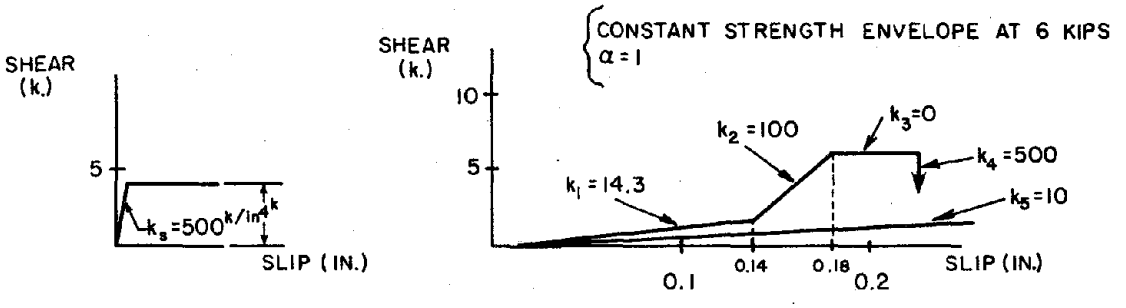

(b) SHEAR FRICTION ELEMENT

FIG. 5.10.19 FORCE-DISPLACEMENT RELATIONSHIPS FOR COMPOUND SHEAR-FRICTION JOINT

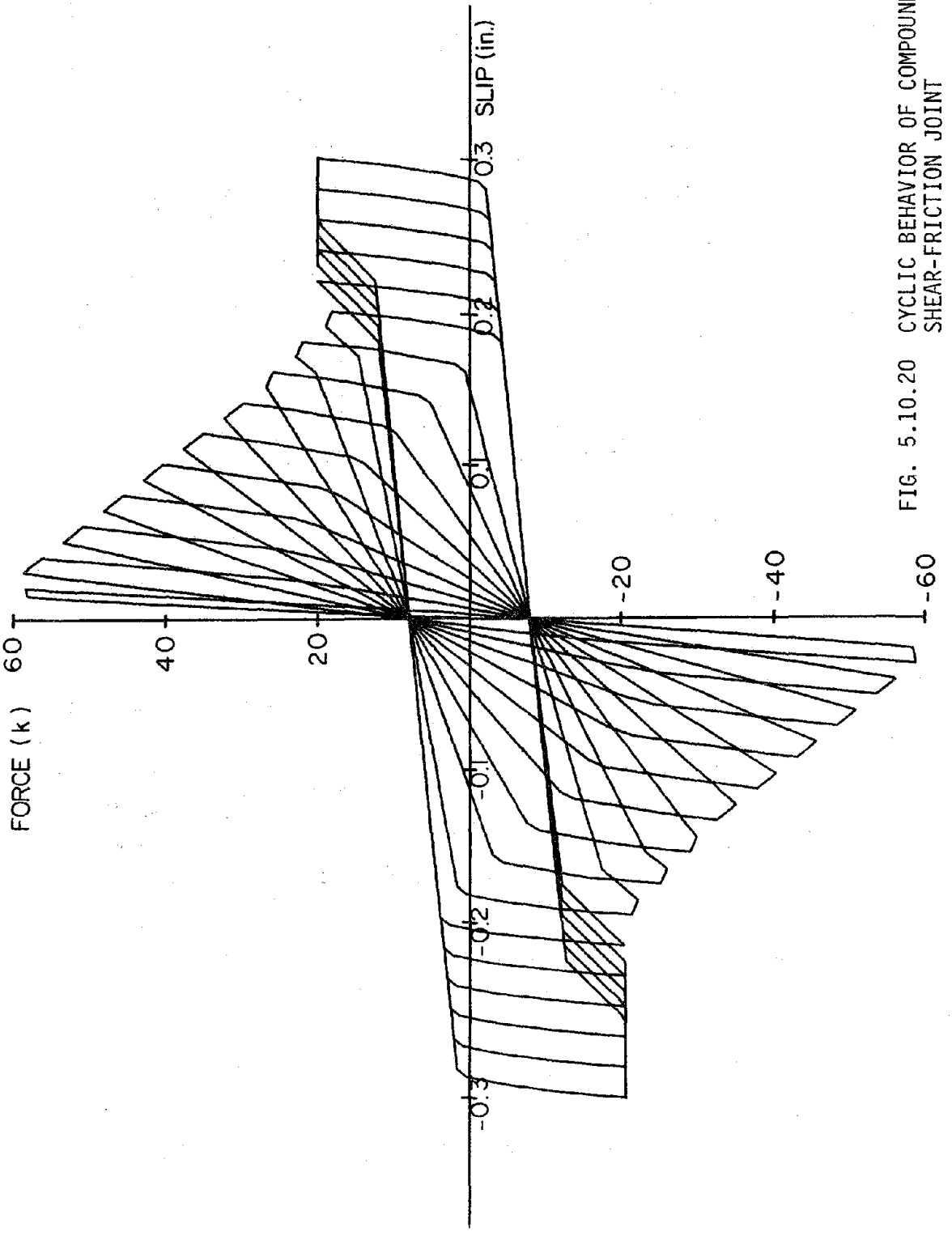

FIG. 5.10.20 CYCLIC BEHAVIOR OF COMPOUND SHEAR-FRICTION JOINT

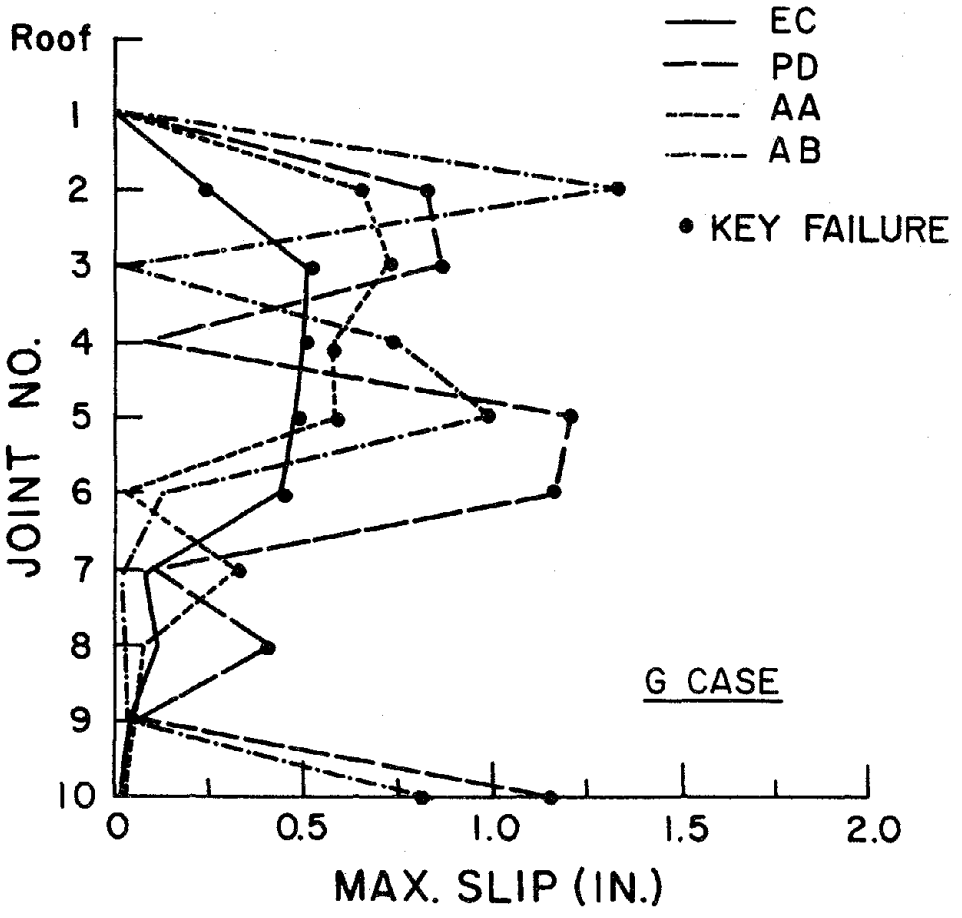

FIG. 5.10.21 JOINTS WITH COMPOUND SHEAR-FRICTION BEHAVIOR. G CASES. MAXIMUM SLIP.

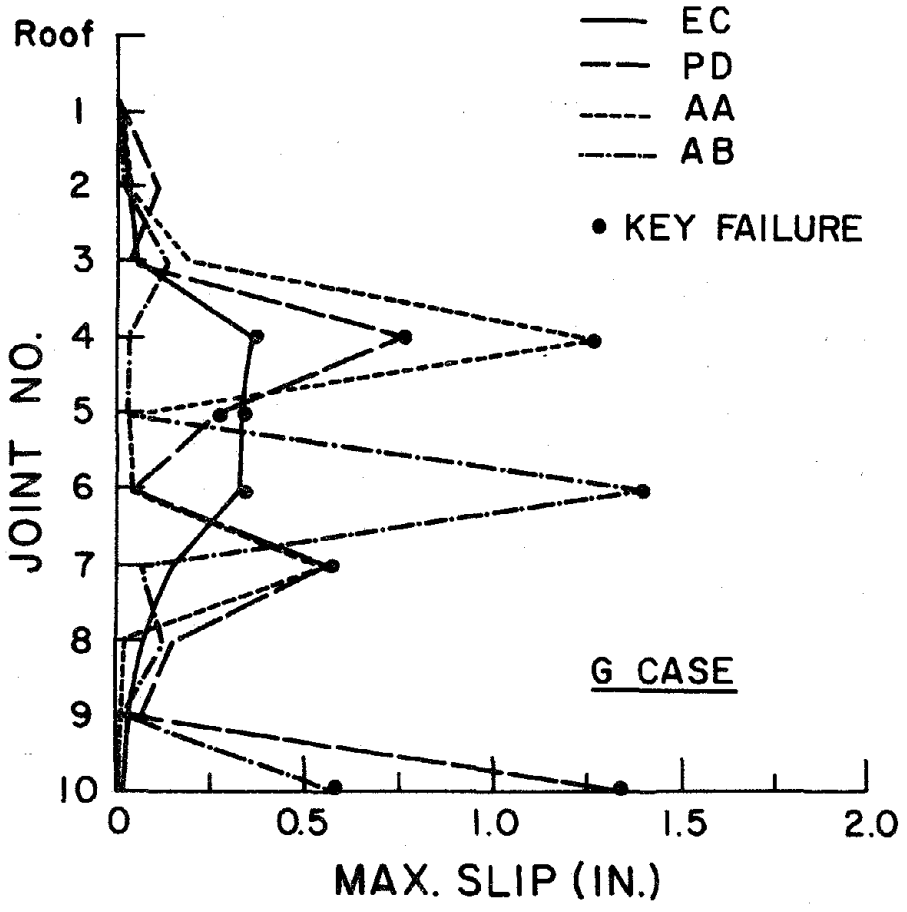

FIG. 5.10.22 JOINTS WITH COMPOUND SHEAR-FRICTION BEHAVIOR. GP CASES. MAXIMUM SLIP.

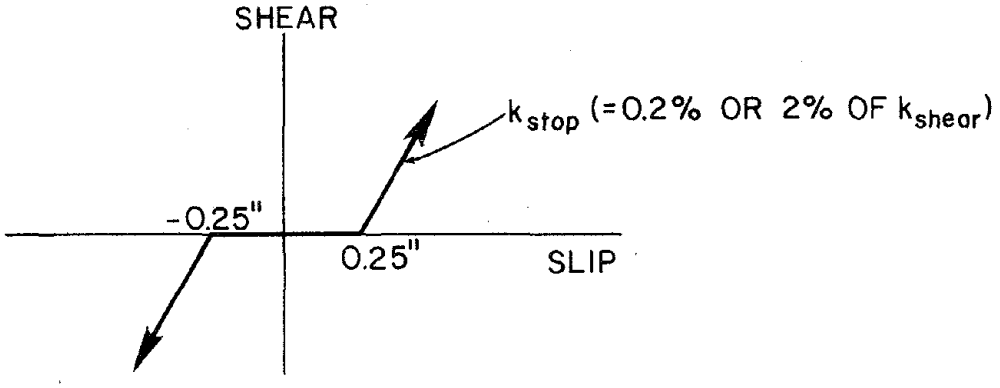

FIG. 5.10.23 STOP ELEMENT CHARACTERISTICS

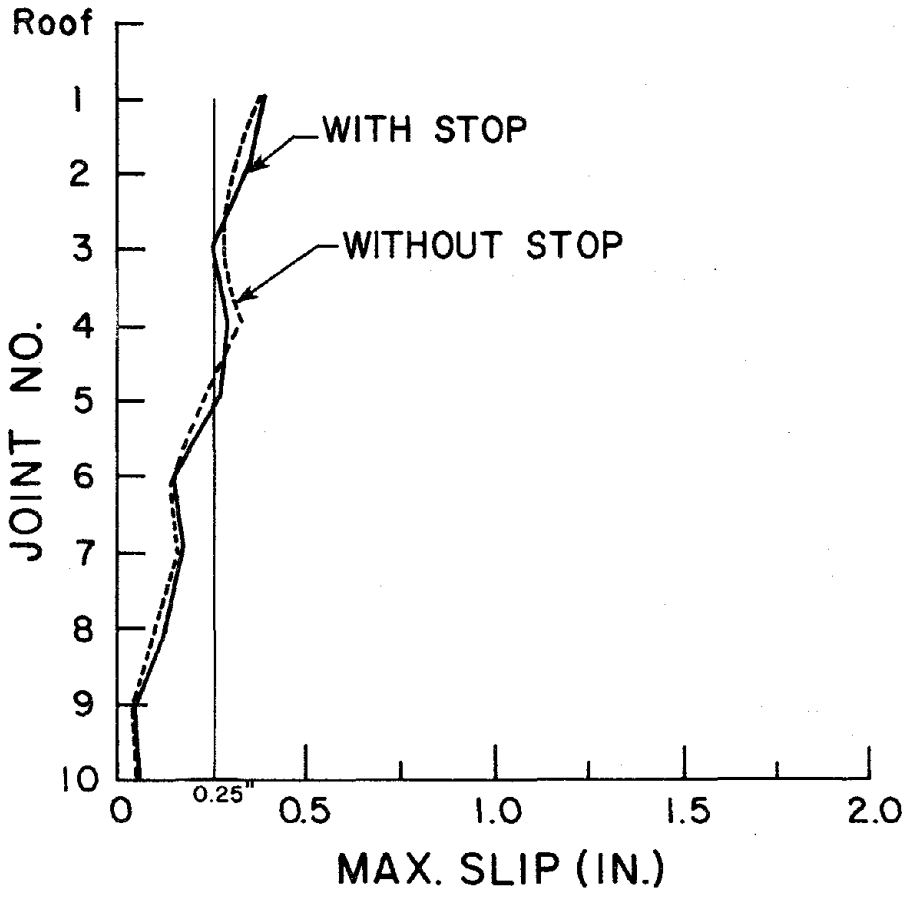

FIG. 5.10.24 CASE G/0.2/EC: SIMPLE FRICTION ELEMENT WITH STOP. MAXIMUM SLIP.

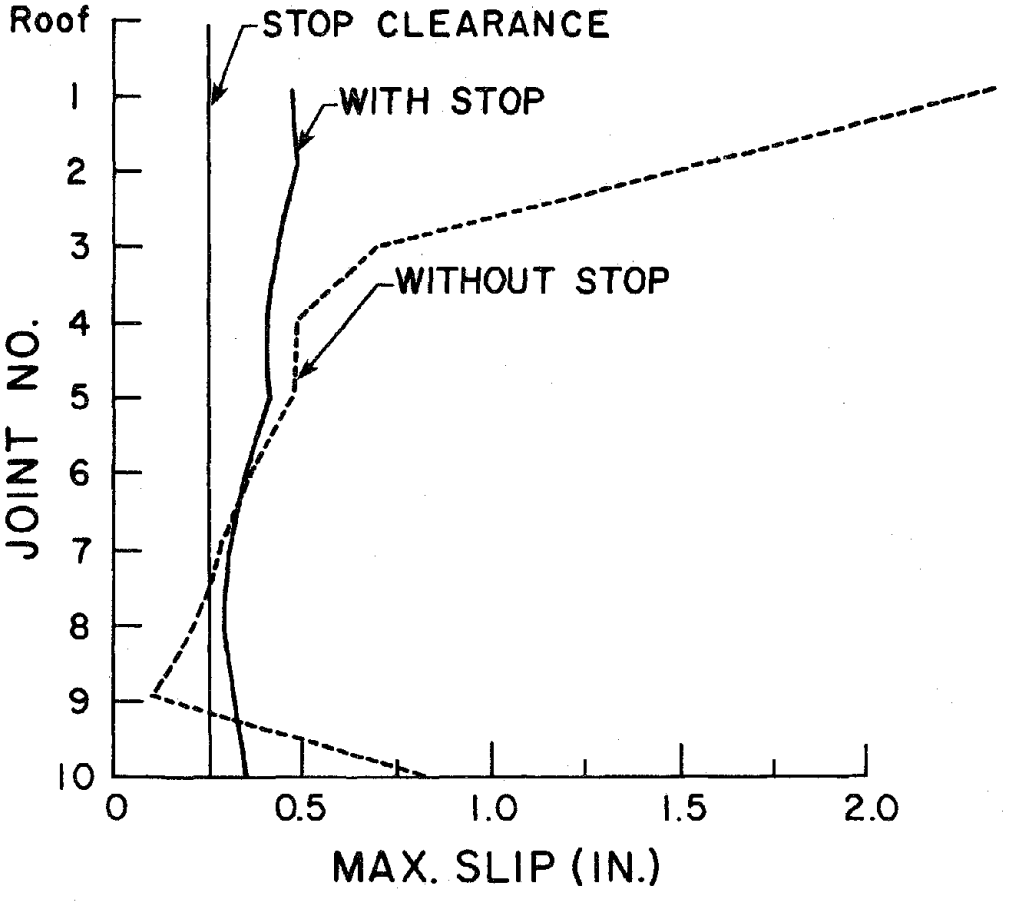

FIG. 5.10.25 CASE G/0.2/AB: SIMPLE FRICTION ELEMENT WITH STOP. MAXIMUM SLIP.

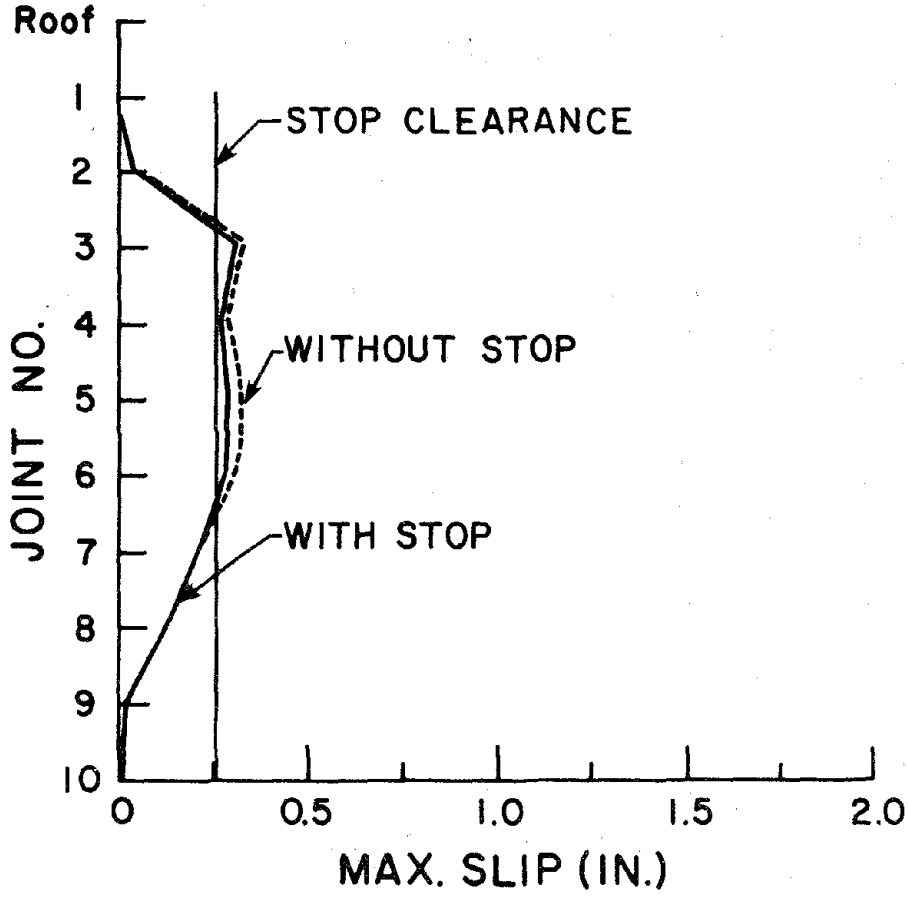

FIG. 5.10.26 CASE GP/0.2/EC: SIMPLE FRICTION ELEMENT WITH STOP. MAXIMUM SLIP.

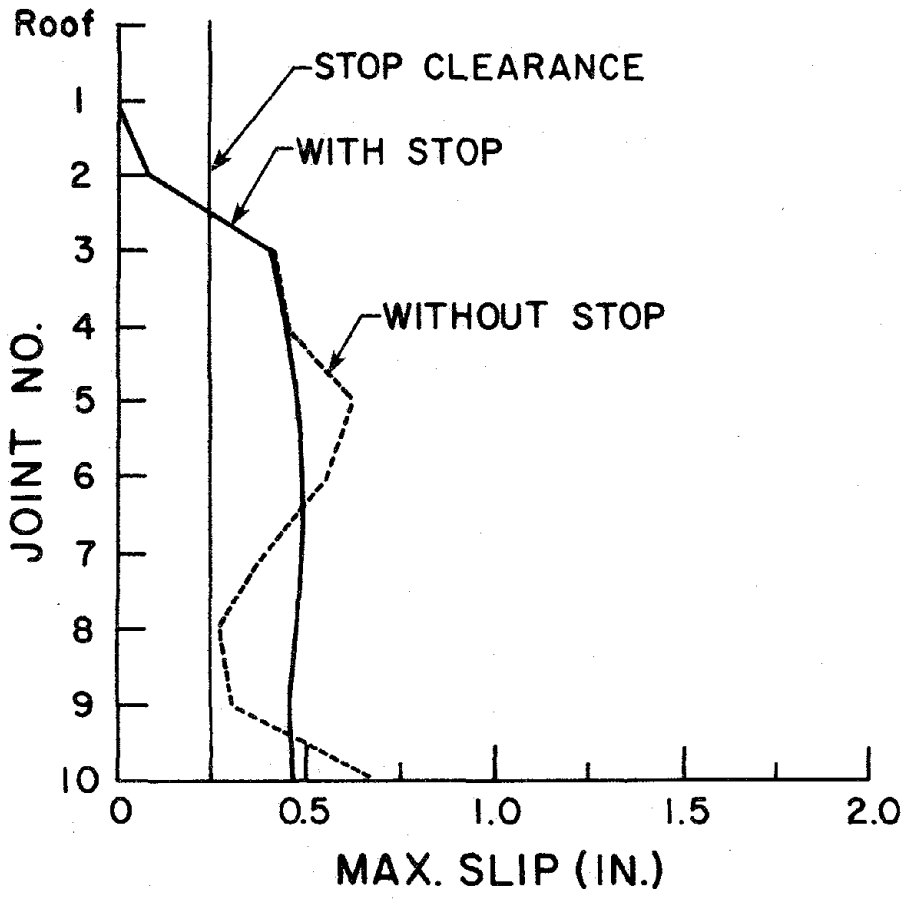

FIG. 5.10.27 CASE GP/0.2/AB: SIMPLE FRICTION ELEMENT WITH STOP. MAXIMUM SLIP.

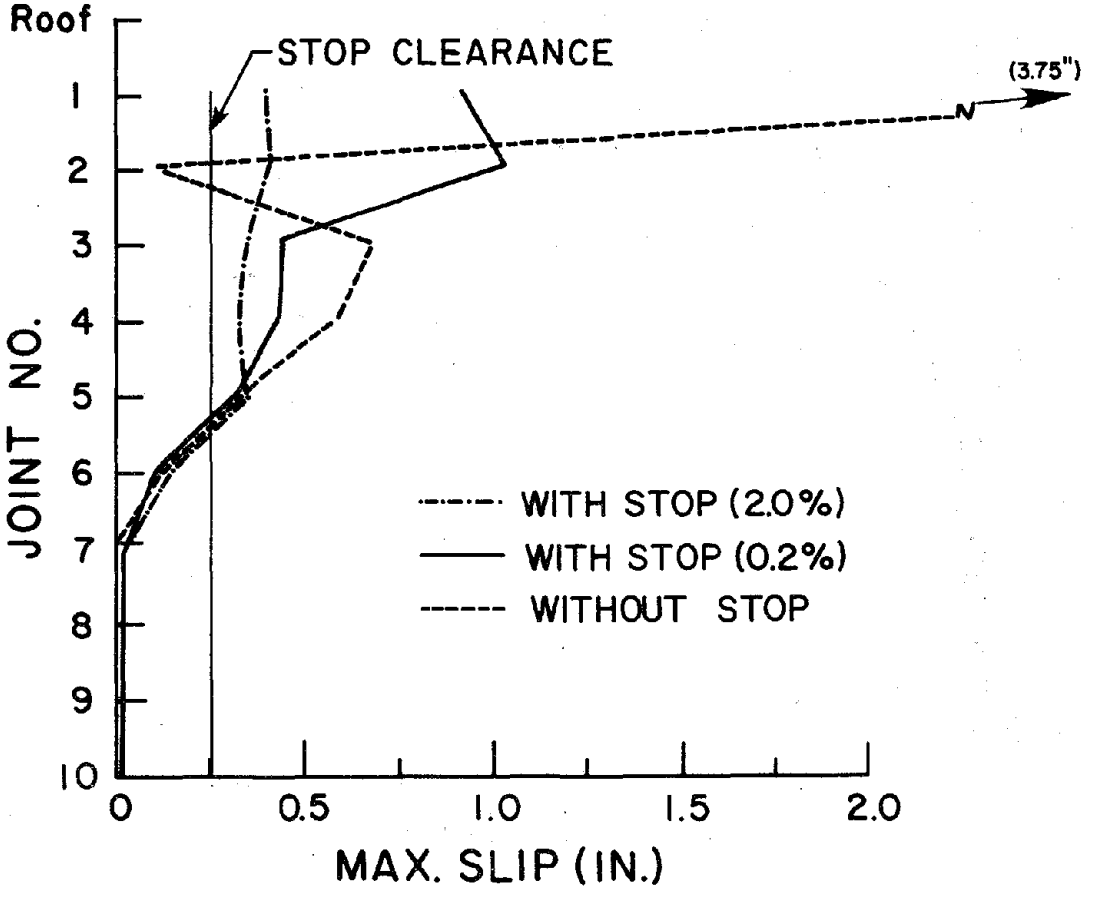

FIG. 5.10.28 CASE G/μ/EC: FRICTION ELEMENT WITH DEGRADING STRENGTH AND STOP. MAXIMUM SLIP.

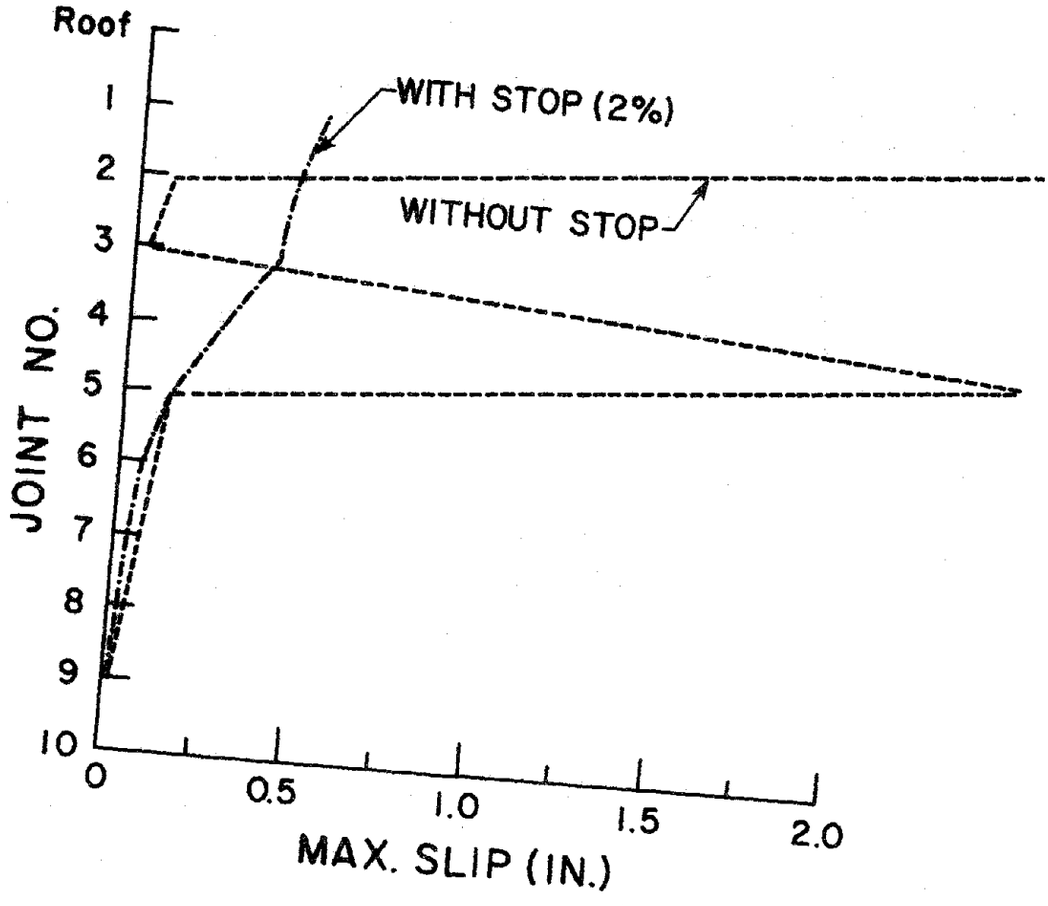

FIG. 5.10.29 CASE G/μ/PD: FRICTION ELEMENT WITH DEGRADING STRENGTH AND STOP. MAXIMUM SLIP.

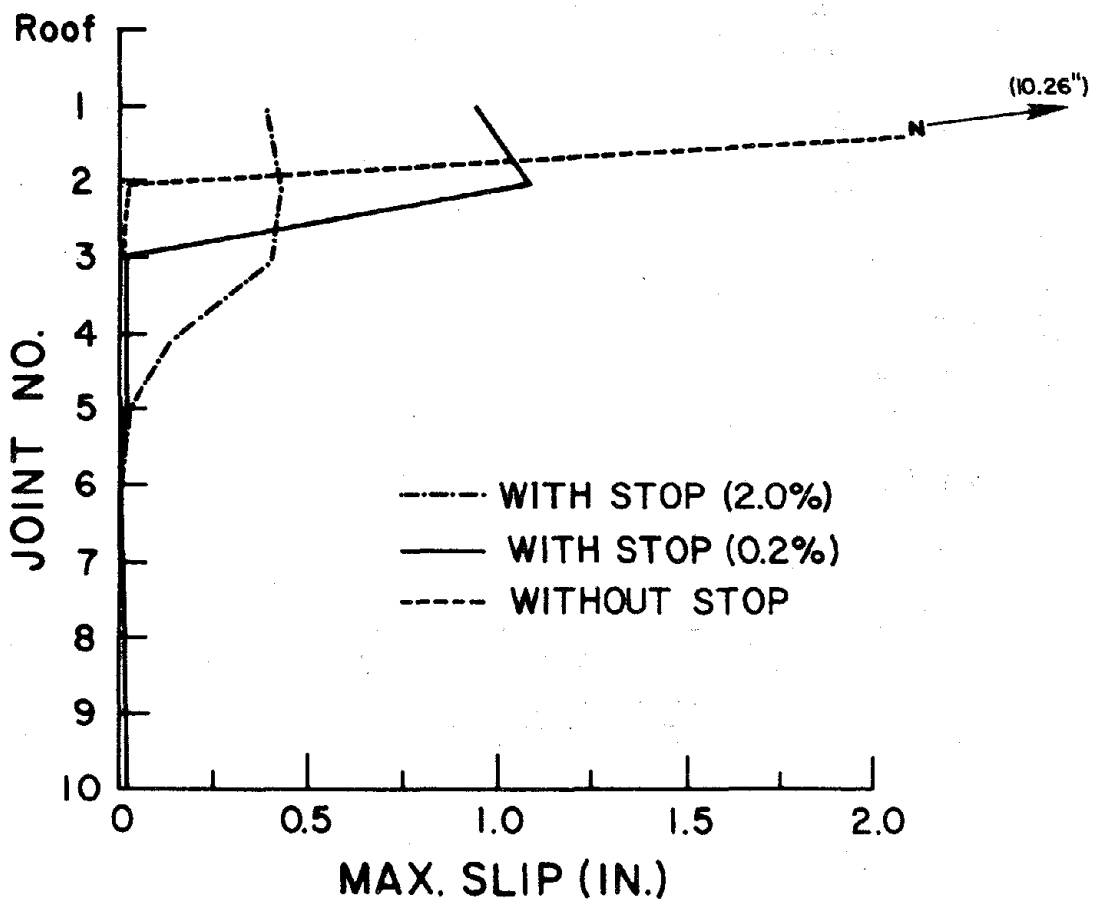

FIG. 5.10.30 CASE G/μ/AB: FRICTION ELEMENT WITH DEGRADING STRENGTH AND STOP. MAXIMUM SLIP.

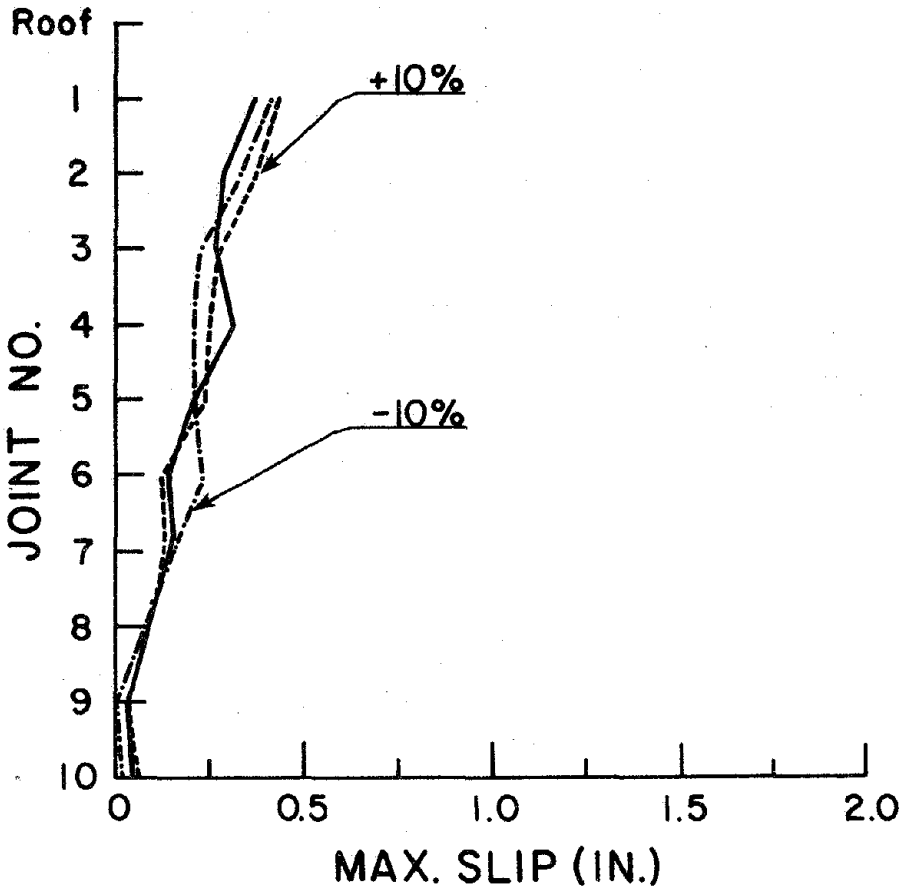

FIG. 5.10.31 EFFECT OF PANEL STIFFNESSES CHANGE. CASE G/0.2/EC.

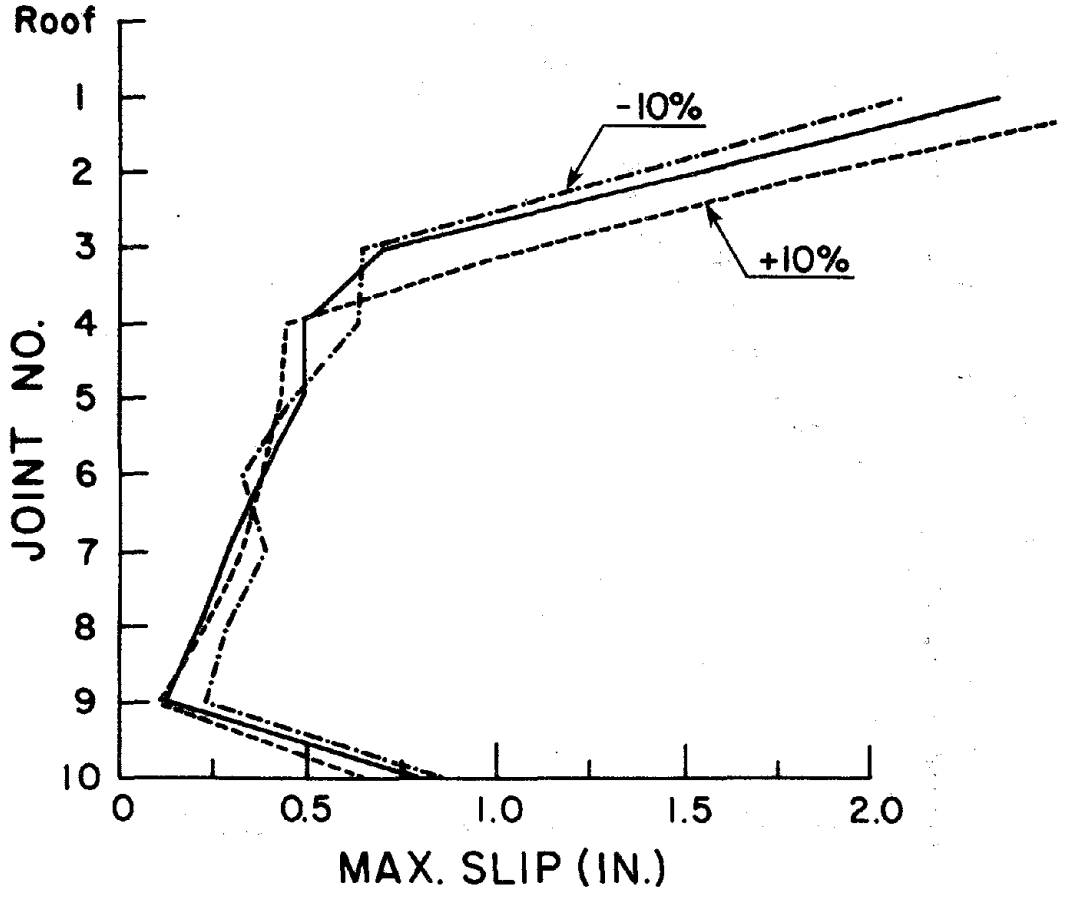

FIG. 5.10.32 EFFECT OF PANEL STIFFNESSES CHANGE. CASE G/0.2/AB.

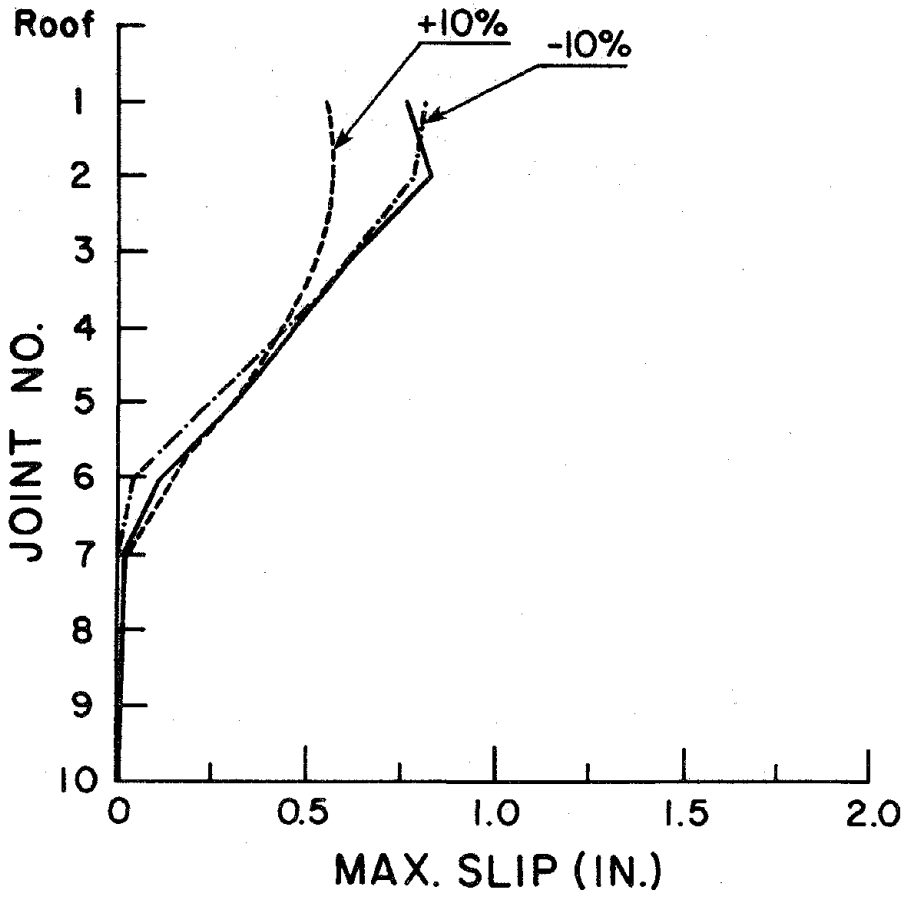

FIG. 5.10.33 EFFECT OF PANEL STIFFNESSES CHANGE. CASE G/0.6/EC.

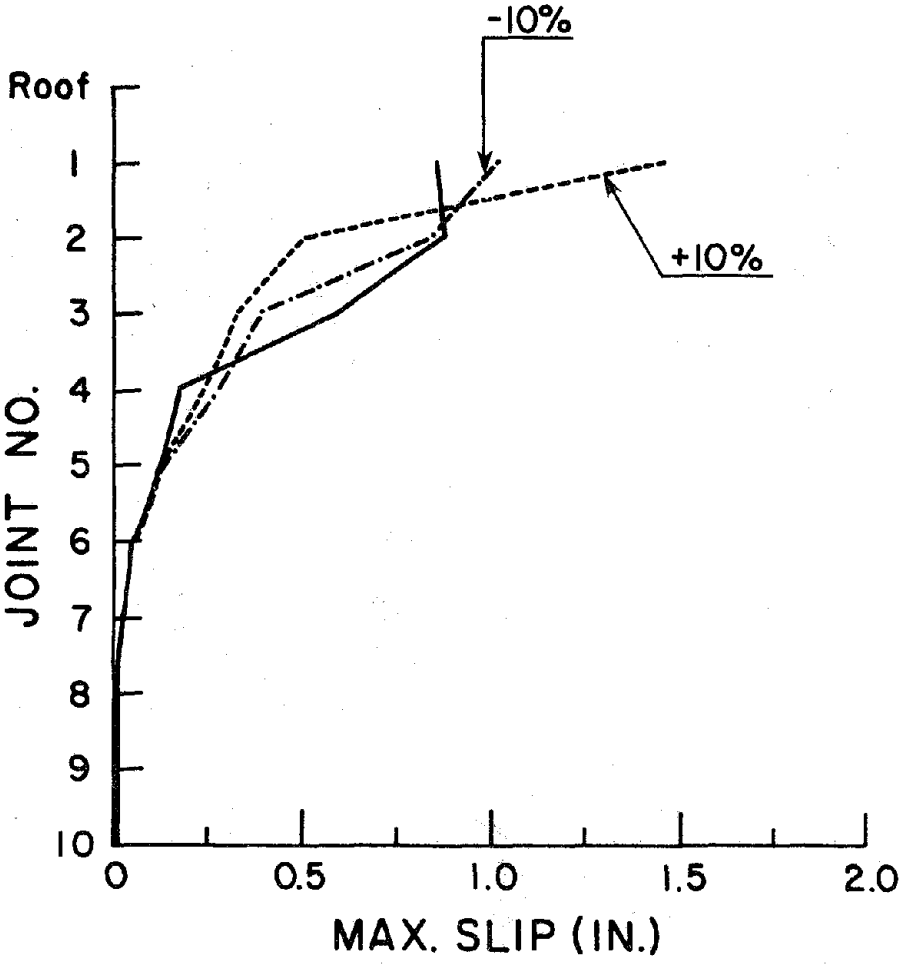

FIG. 5.10.34 EFFECT OF PANEL STIFFNESSES CHANGE. CASE G/0.6/AB.

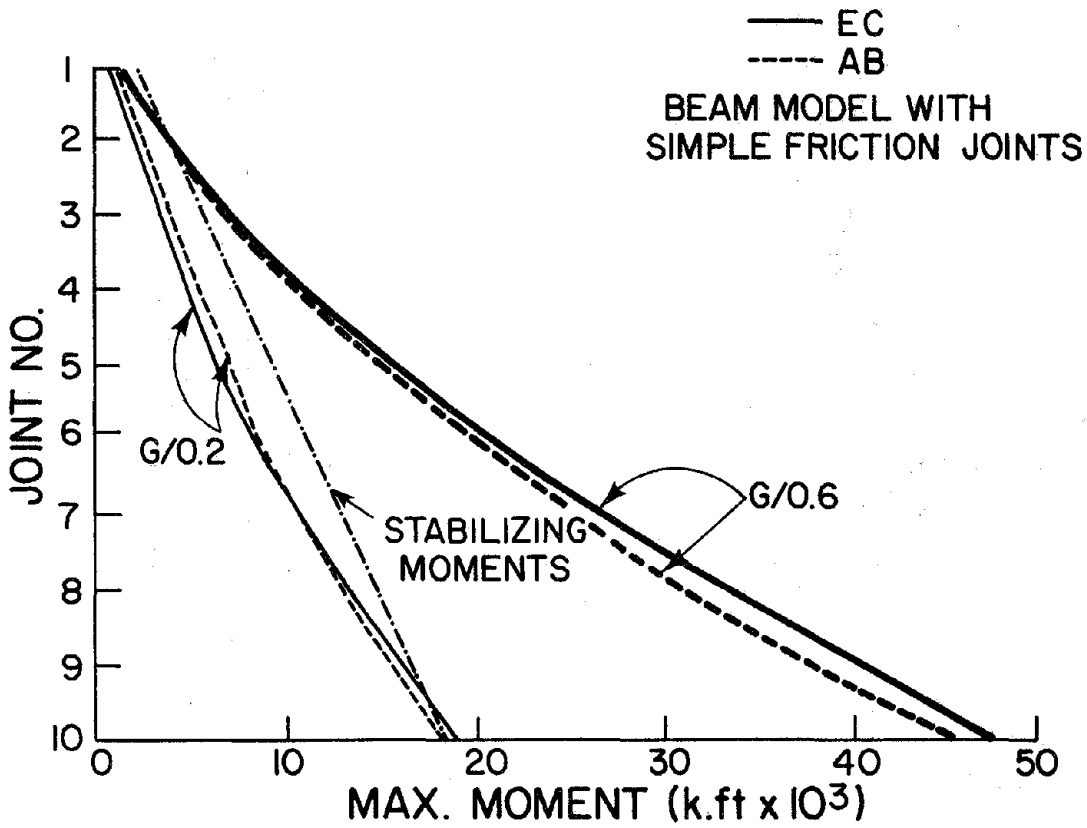

FIG. 5.11.1 OVERTURNING MOMENTS AND JOINT STABILIZING MOMENTS. G CASES.

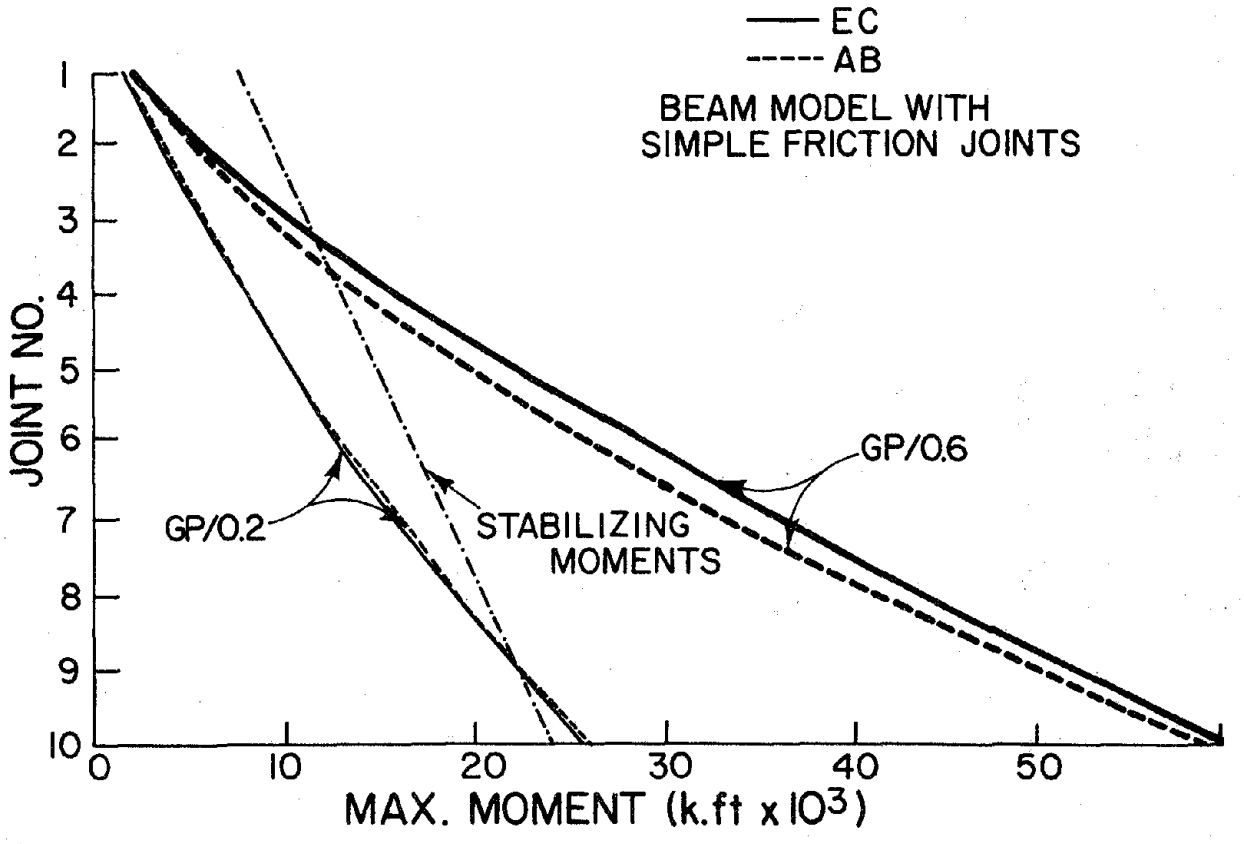

FIG. 5.11.2 OVERTURNING MOMENTS AND JOINT STABILIZING MOMENTS.
GP CASES.

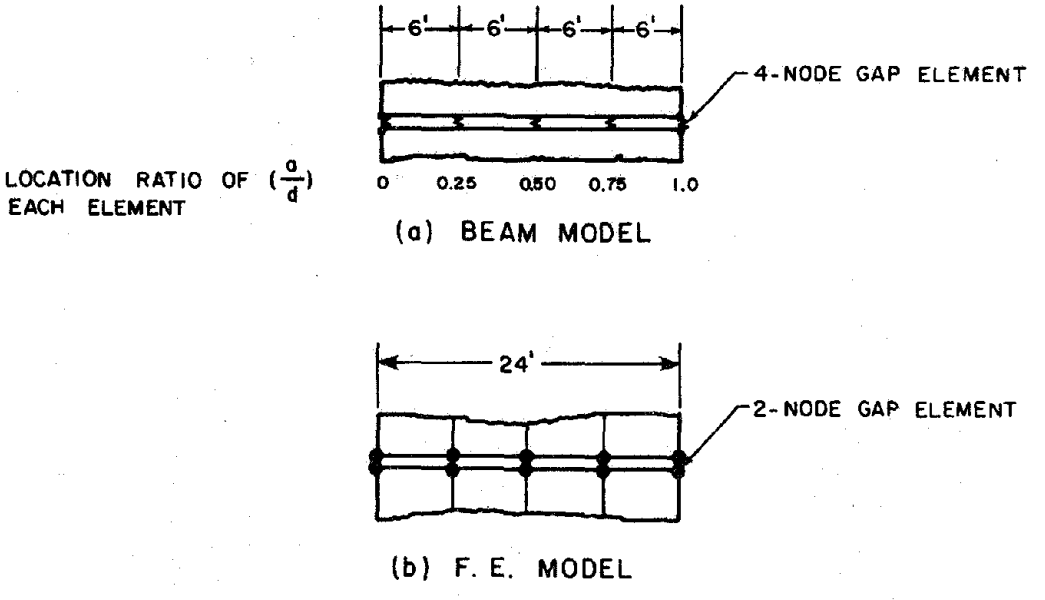

FIG. 5.11.3 IDEALIZATION WITH FIVE GAP ELEMENTS PER JOINT

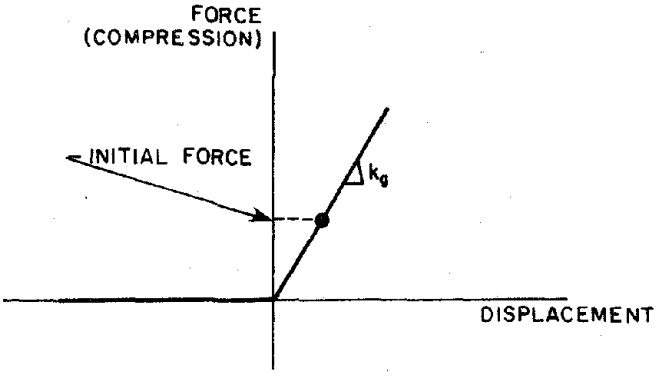

5 GAP ELEMENTS / JOINT : $k_g = 0.517 \cdot 10^6$ k/ft FOR OUTER ELEMENTS
$k_g = 1.034 \cdot 10^6$ k/ft FOR INNER ELEMENTS

2 GAP ELEMENTS/JOINT : $k_g = 2.068 \cdot 10^6$ k/ft

FIG. 5.11.4 FORCE-DISPLACEMENT RELATIONSHIP OF EACH GAP ELEMENT

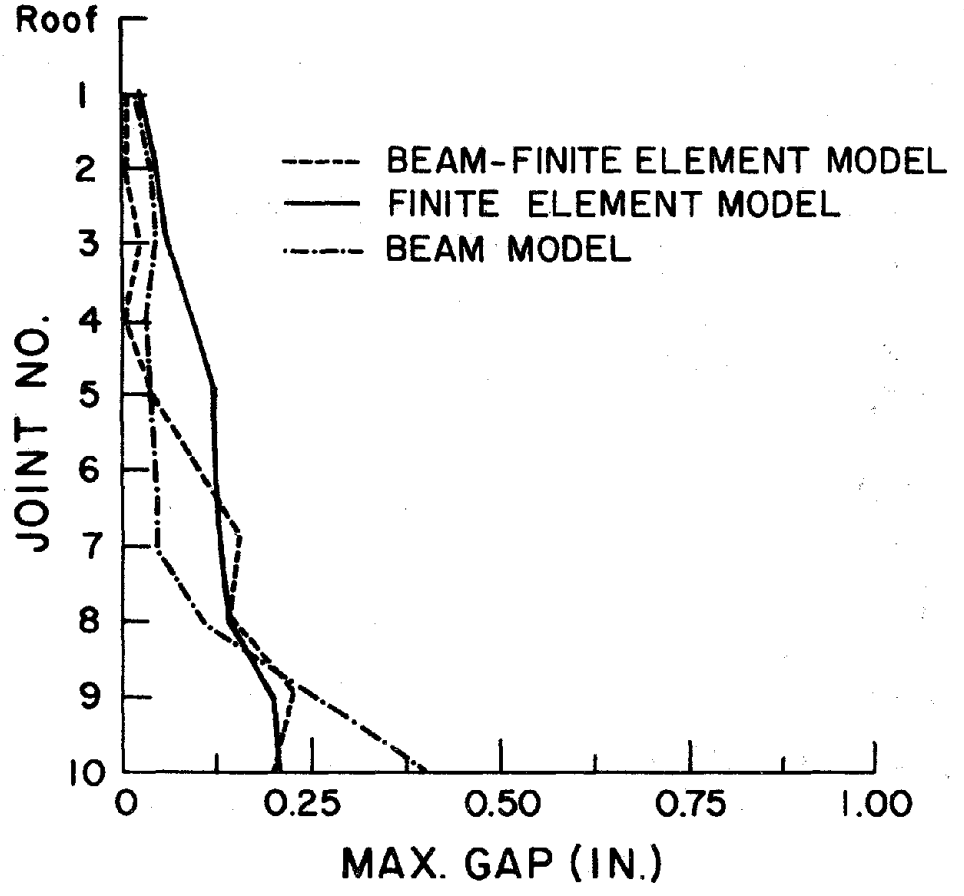

FIG. 5.11.5 CASE G/EC. MAXIMUM JOINT OPENING.

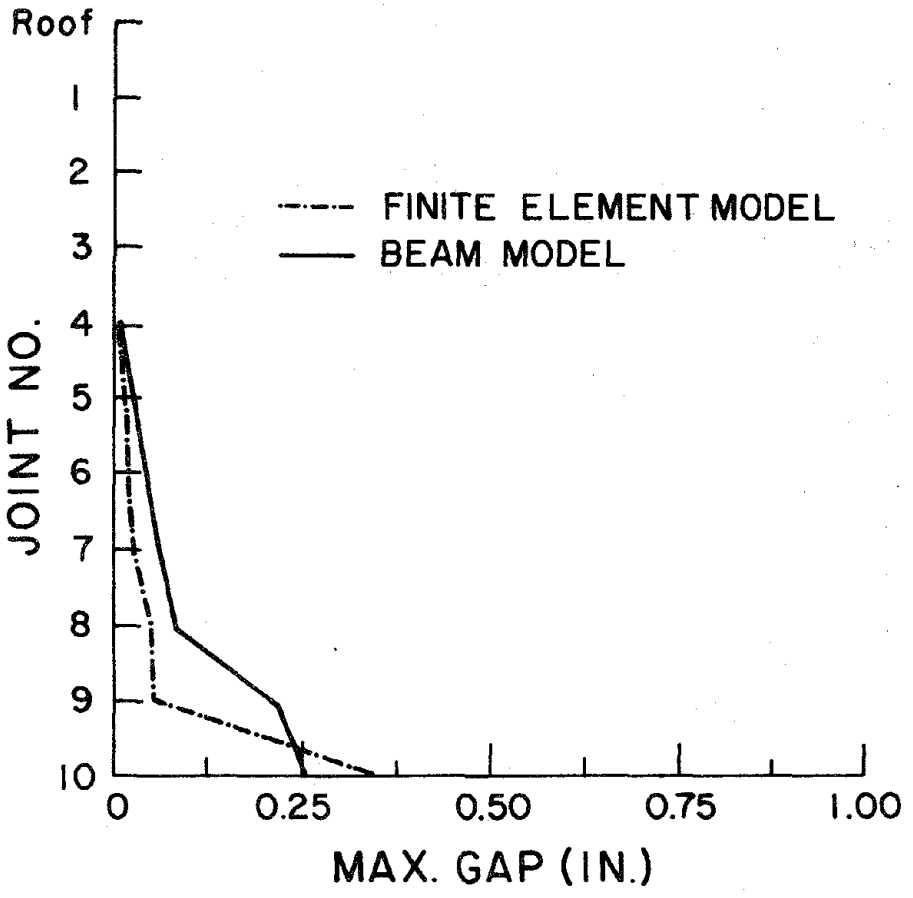

FIG. 5.11.6 CASE GP/EC. MAXIMUM JOINT OPENING.

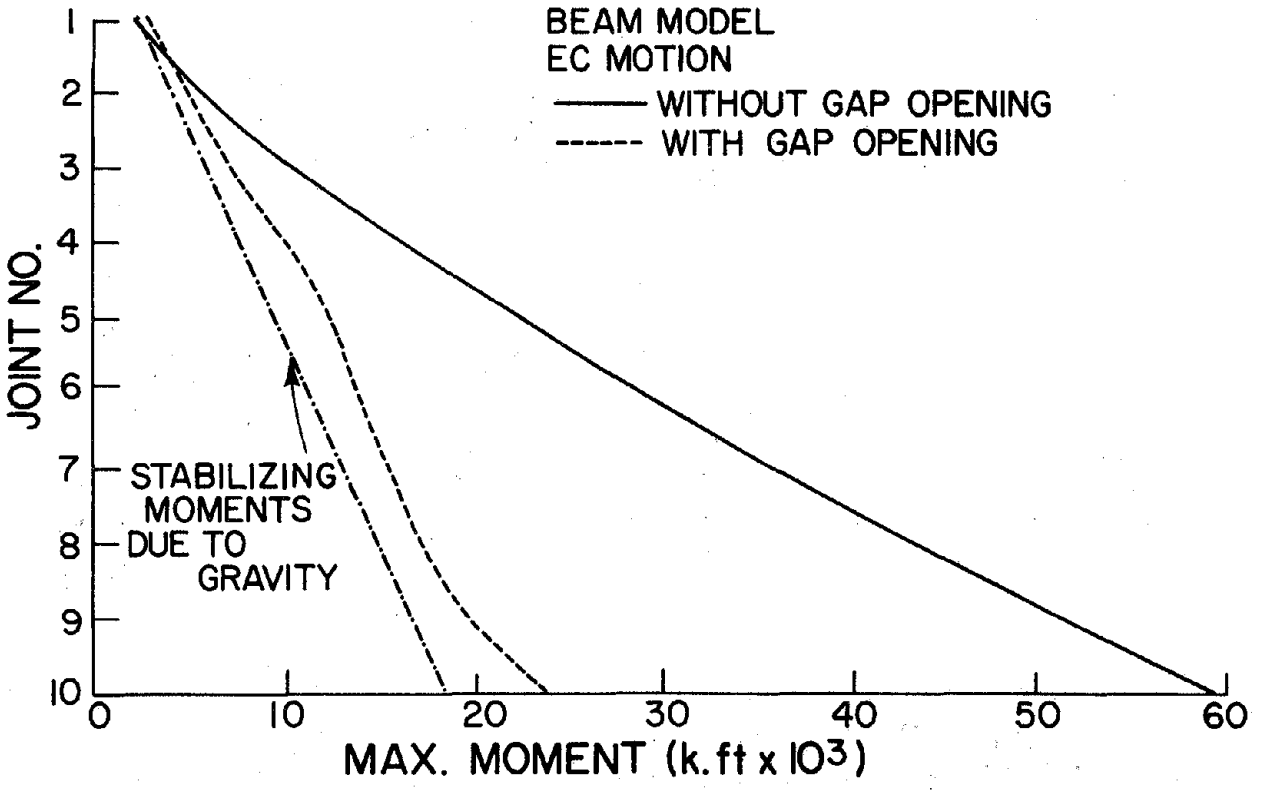

FIG. 5.11.7 OVERTURNING MOMENTS FOR G CASE.

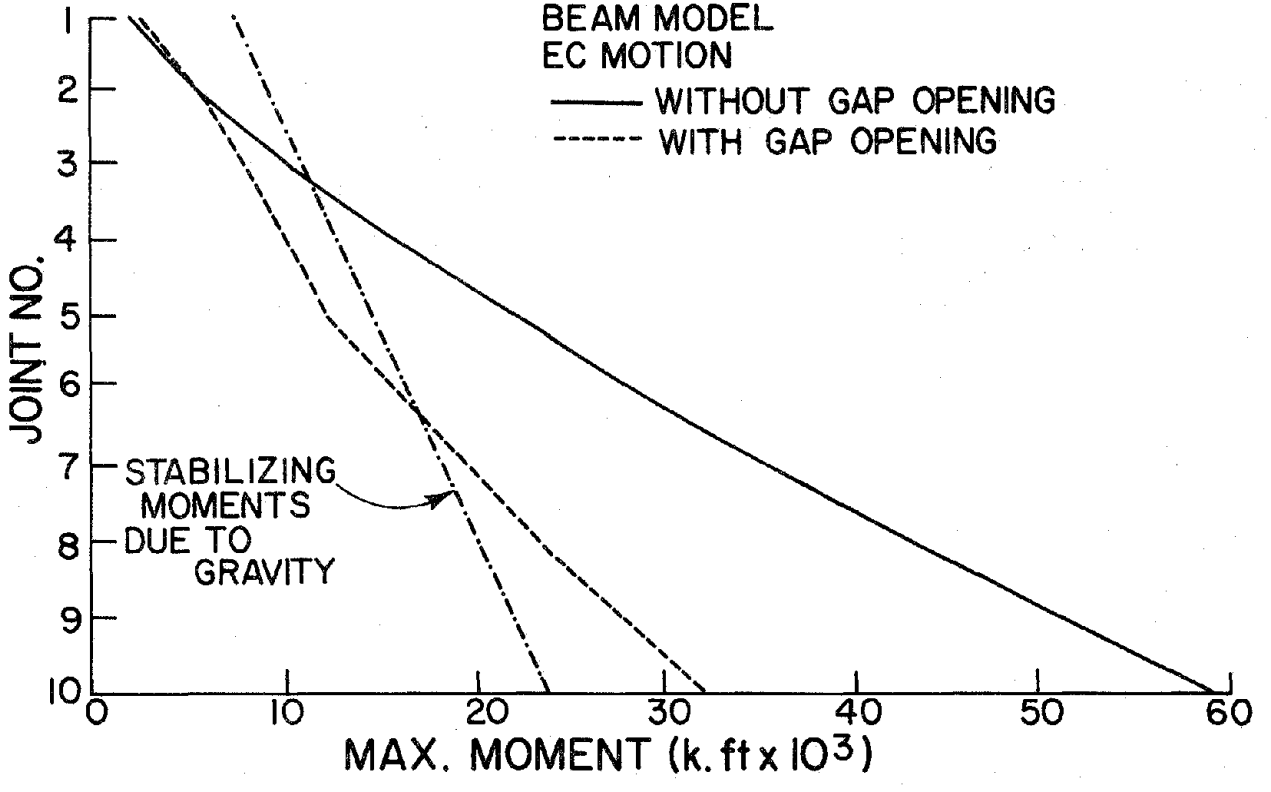

FIG. 5.11.8 OVERTURNING MOMENTS FOR GP CASE.

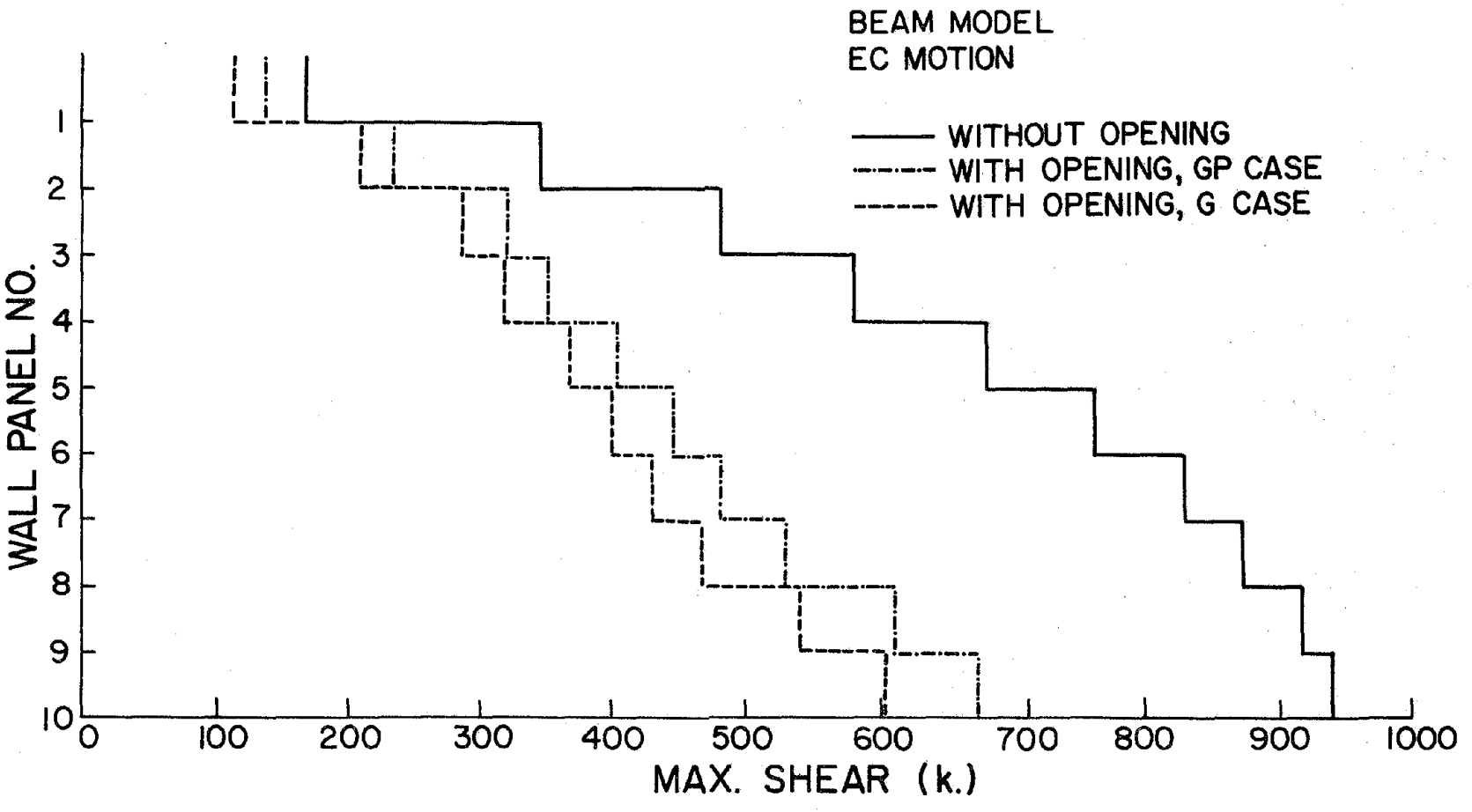

FIG. 5.11.9 STORY SHEARS FOR G AND GP CASES

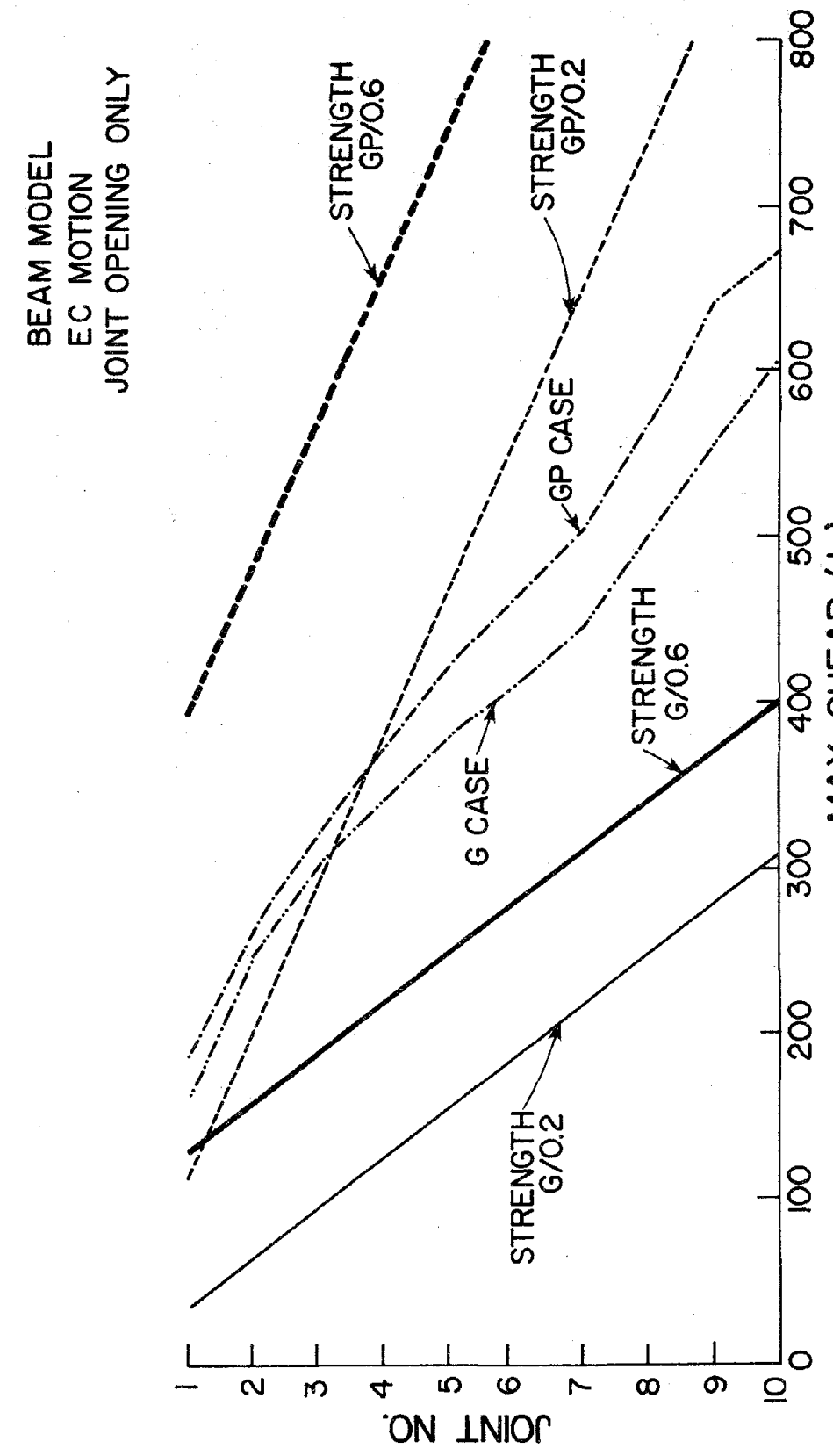

FIG. 5.11.10 COMPARISON OF MAXIMUM JOINT SHEARS WITH JOINT SHEAR STRENGTHS

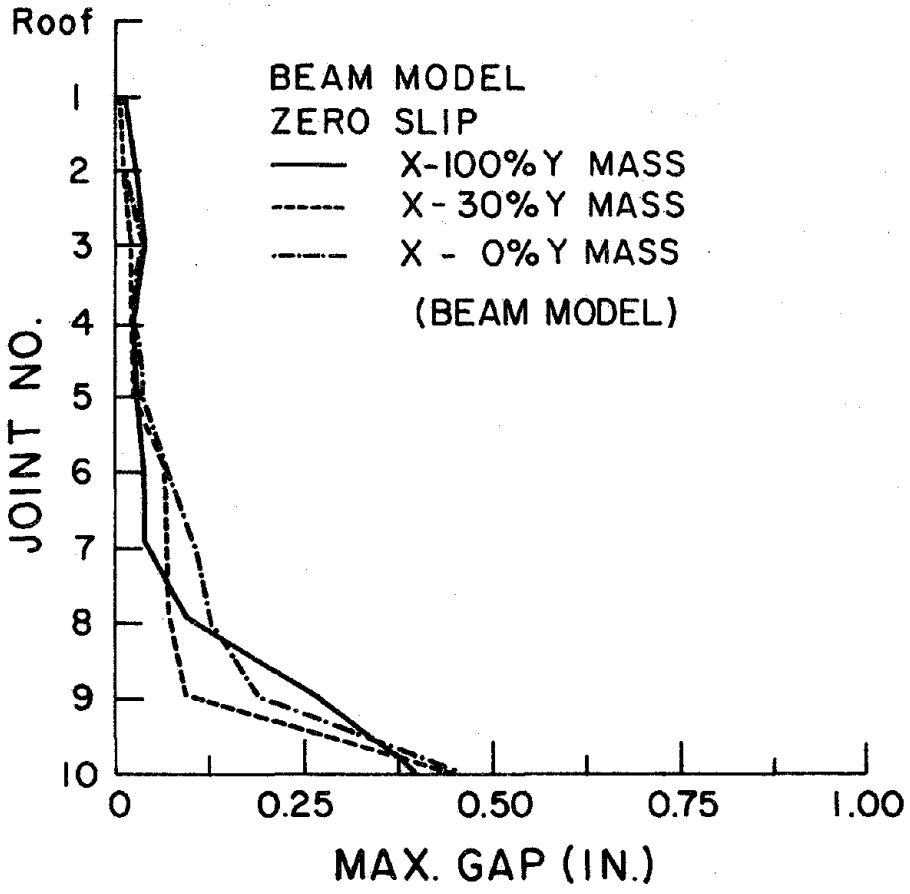

FIG. 5.11.11 CASE G/EC. MAXIMUM JOINT OPENING

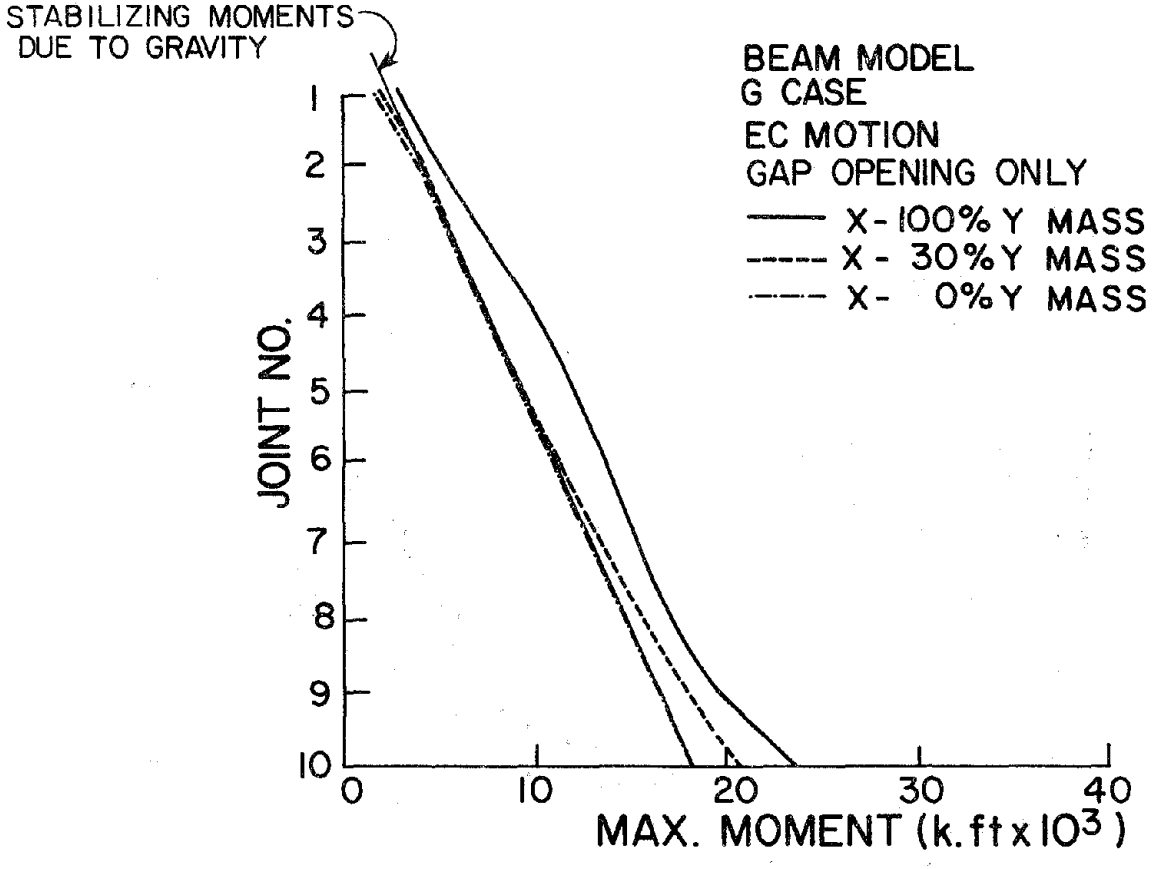

FIG. 5.11.12 CASE G/∞/EC. EFFECT OF VERTICAL INERTIA ON OVERTURNING MOMENTS

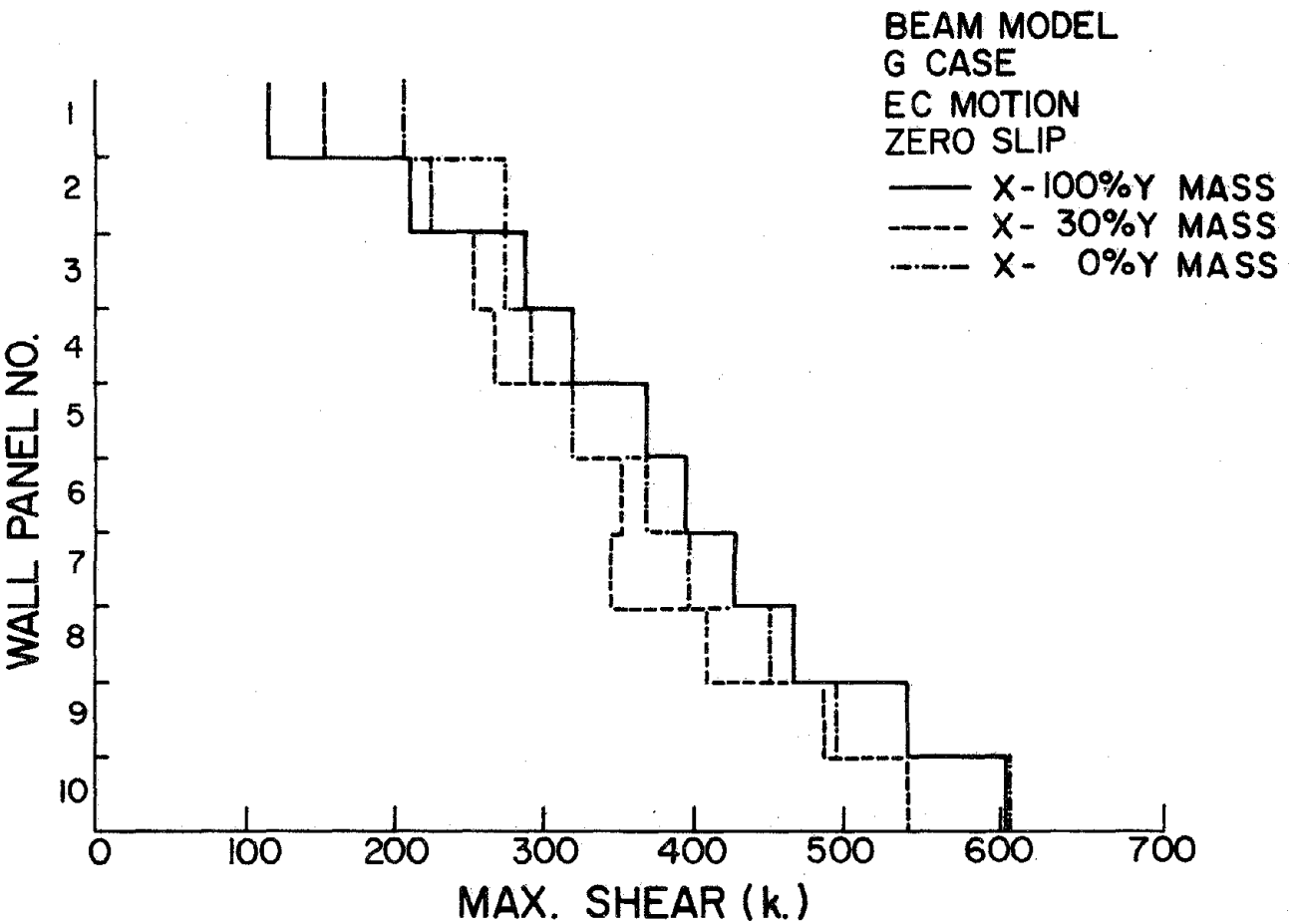

FIG. 5.11.13 CASE G/∞/EC. EFFECT OF VERTICAL INERTIA ON STORY SHEARS

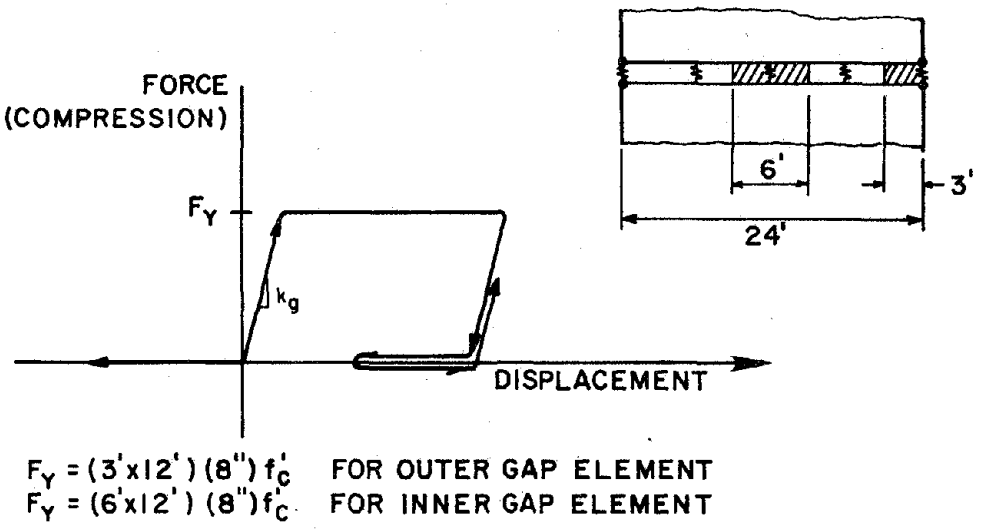

FIG. 5.11.14 PROPERTIES ASSUMED FOR JOINTS WITH CRUSHING

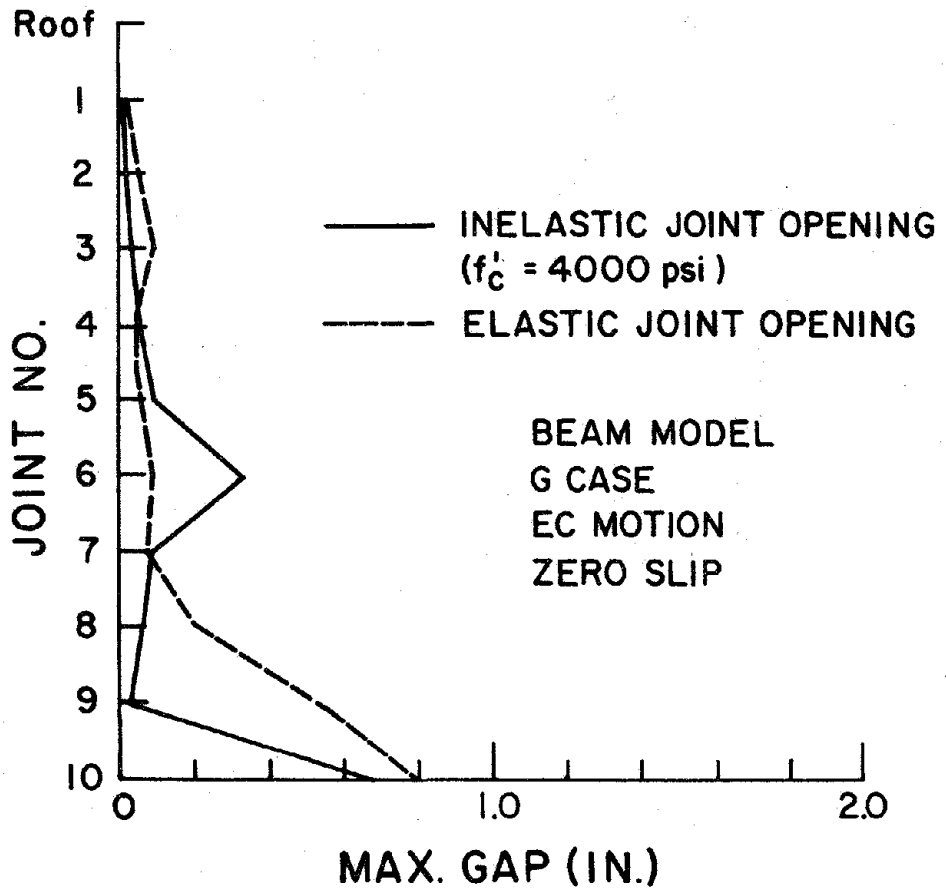

FIG. 5.11.15 CASE G/∞/EC. EFFECT OF JOINT CRUSHING ON GAP OPENING

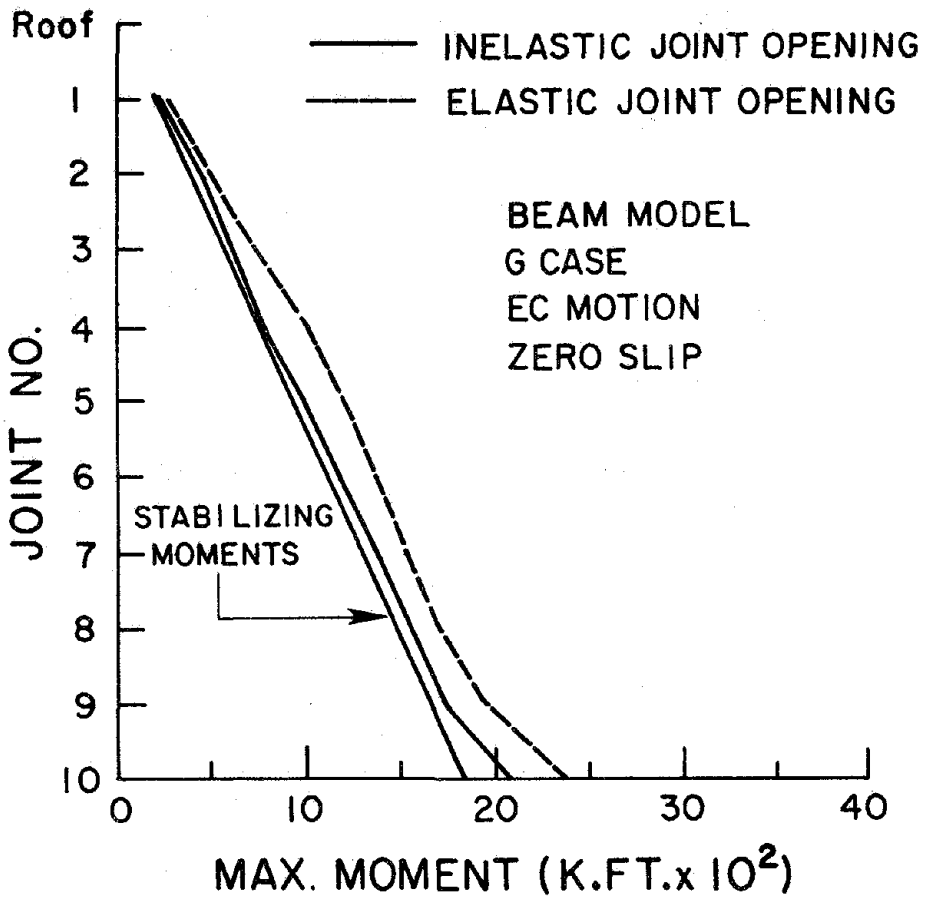

FIG. 5.11.16 CASE G/∞/EC. EFFECT OF JOINT CRUSHING ON OVERTURNING MOMENTS

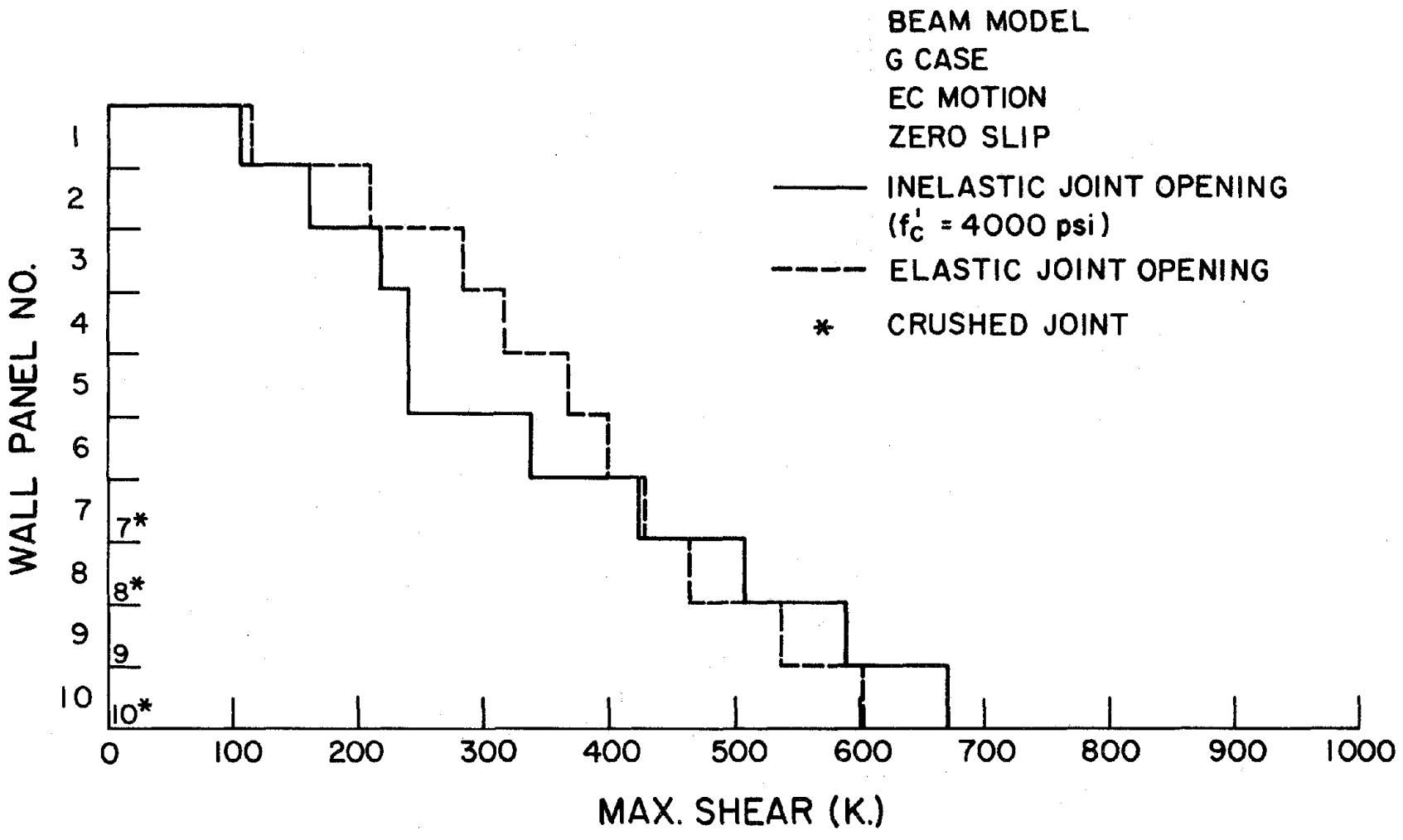

FIG. 5.11.17 CASE G/∞/EC. EFFECT OF JOINT CRUSHING ON STORY SHEARS

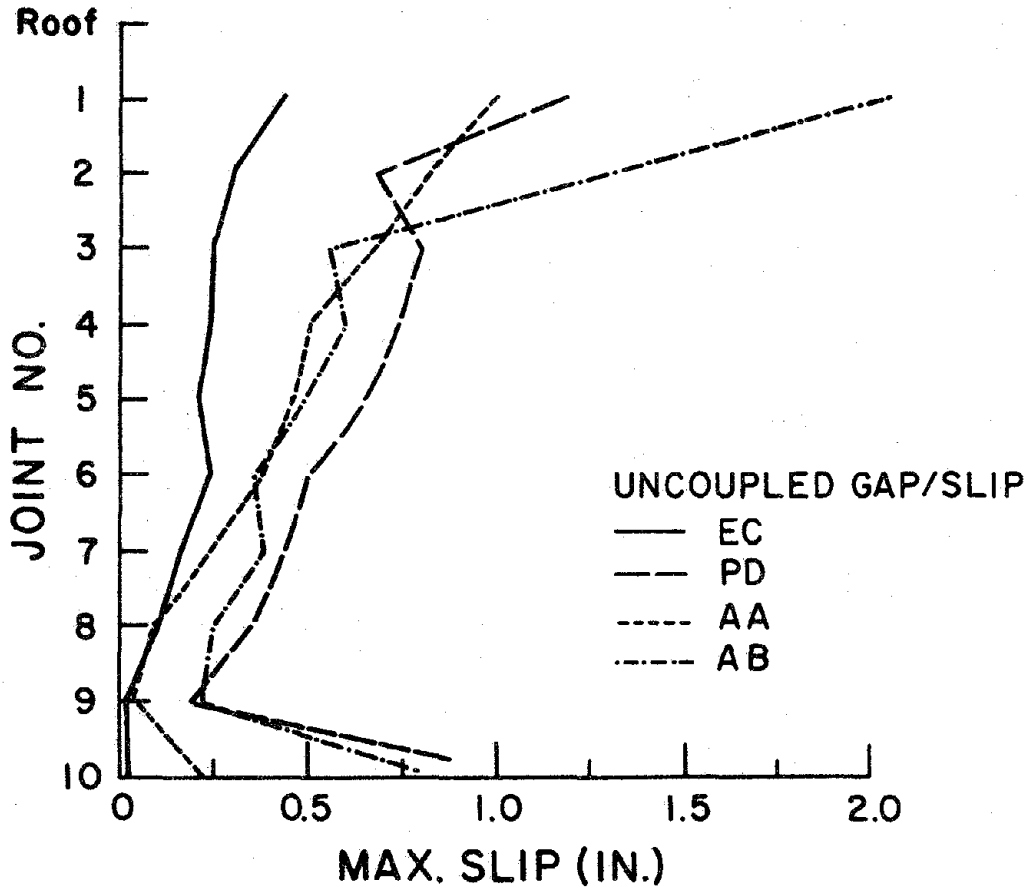

FIG. 5.12.1 CASE G/0.2 UNCOUPLED SLIP AND GAP OPENING. MAXIMUM SLIP

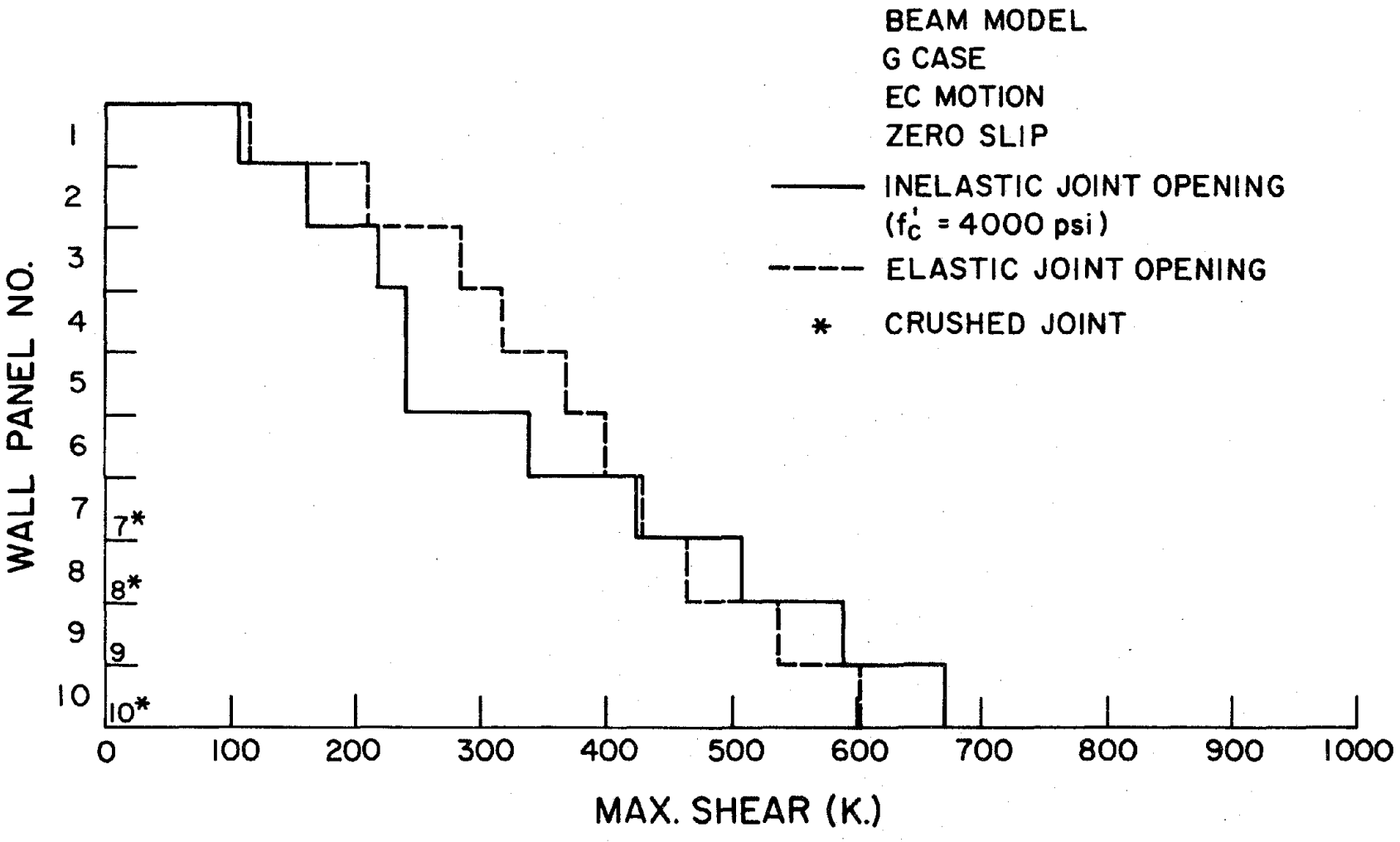

FIG. 5.11.17 CASE G/∞/EC. EFFECT OF JOINT CRUSHING ON STORY SHEARS

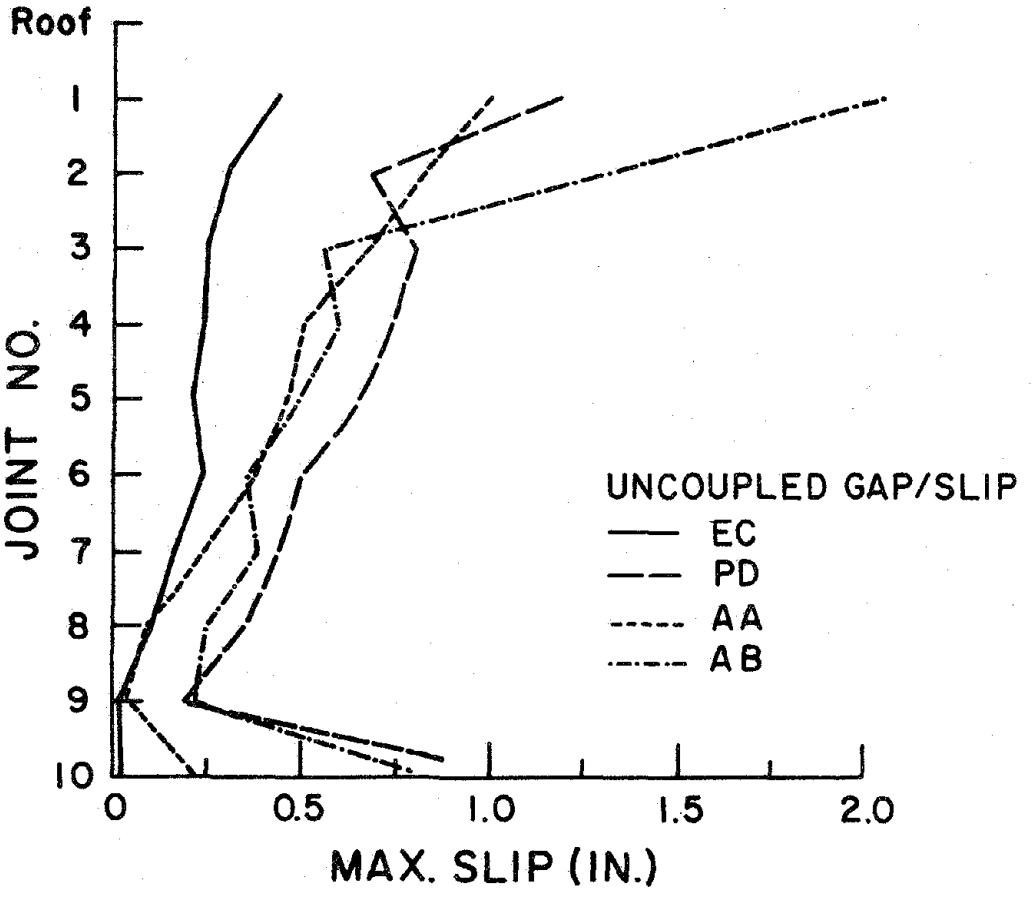

FIG. 5.12.1 CASE G/0.2 UNCOUPLED SLIP AND GAP OPENING. MAXIMUM SLIP

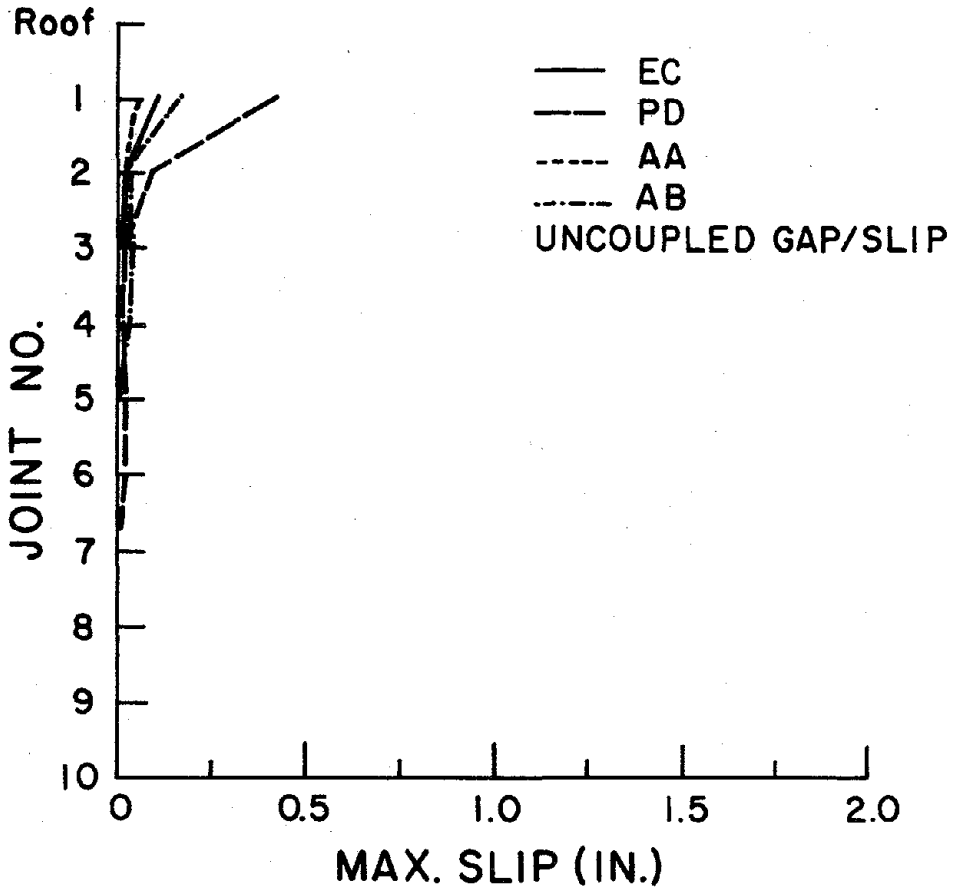

FIG. 5.12.2 CASE G/0.6 UNCOUPLED SLIP AND GAP OPENING. MAXIMUM SLIP

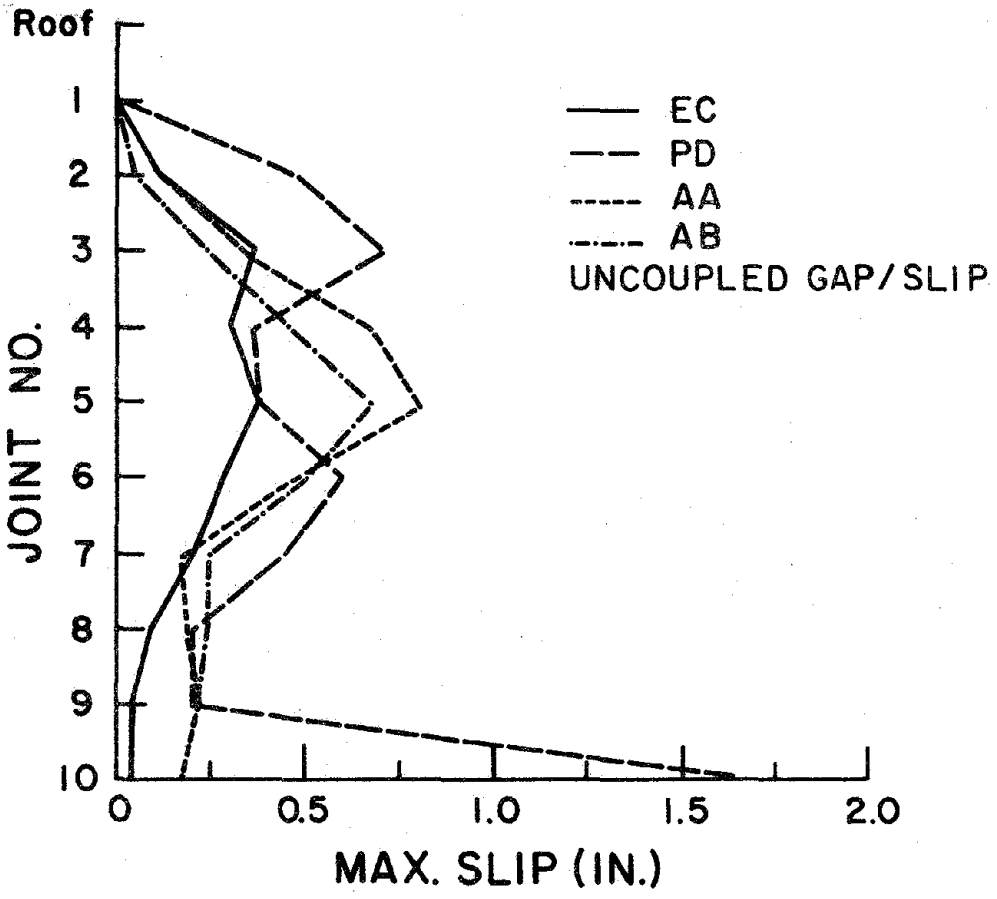

FIG. 5.12.3 CASE GP/0.2 UNCOUPLED SLIP AND GAP OPENING. MAXIMUM SLIP

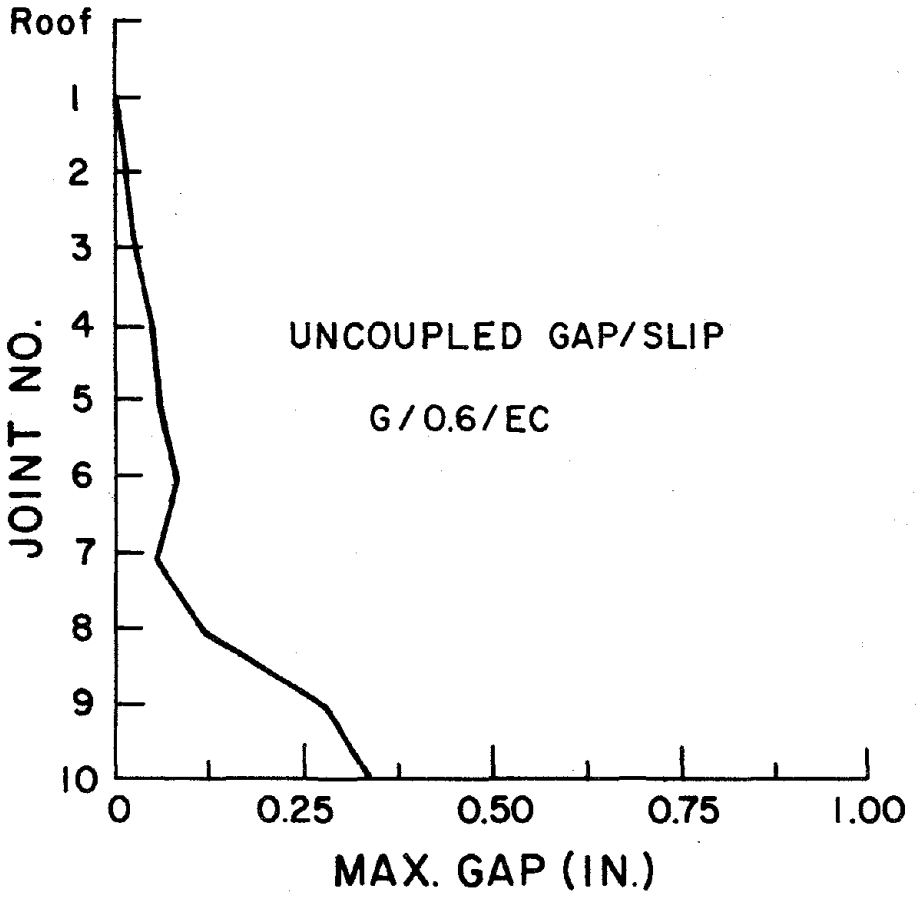

FIG. 5.12.4 CASE G/0.6/EC. UNCOUPLED SLIP AND GAP OPENING. MAXIMUM GAP.

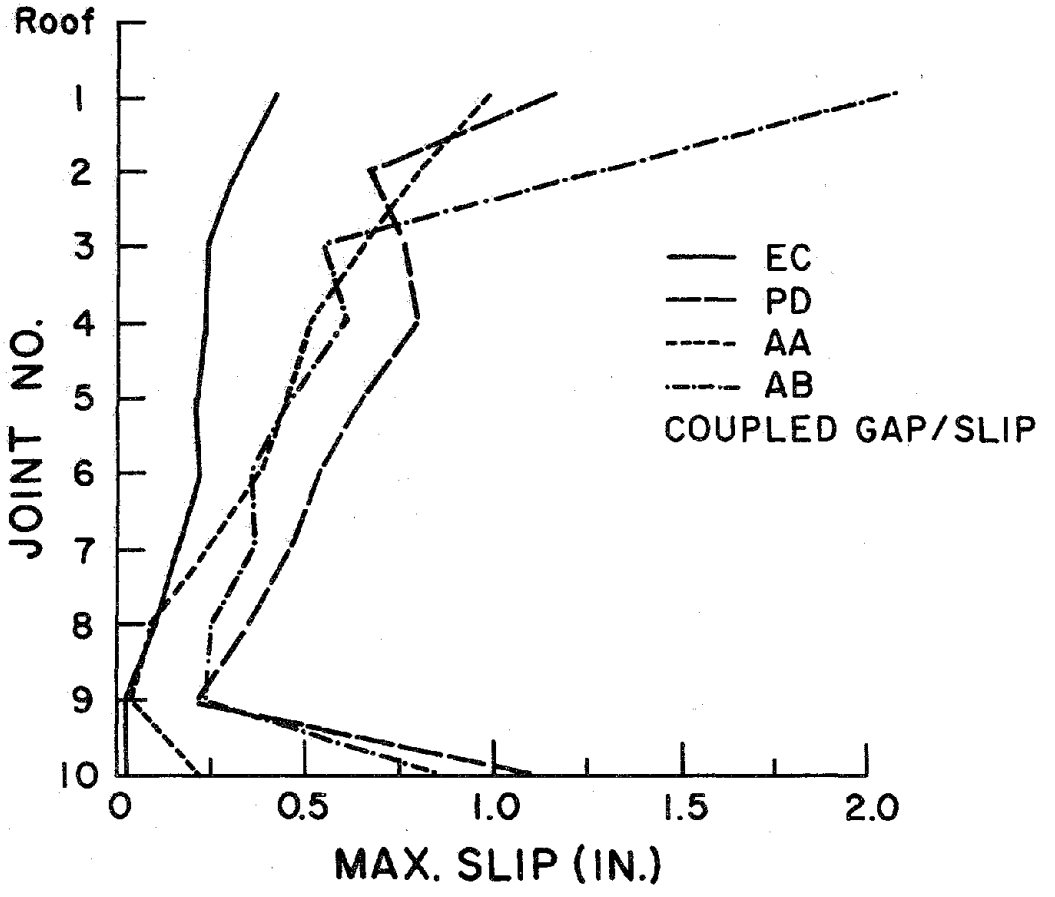

FIG. 5.12.5 CASE G/0.2 COUPLED SLIP AND GAP OPENING. MAXIMUM SLIP

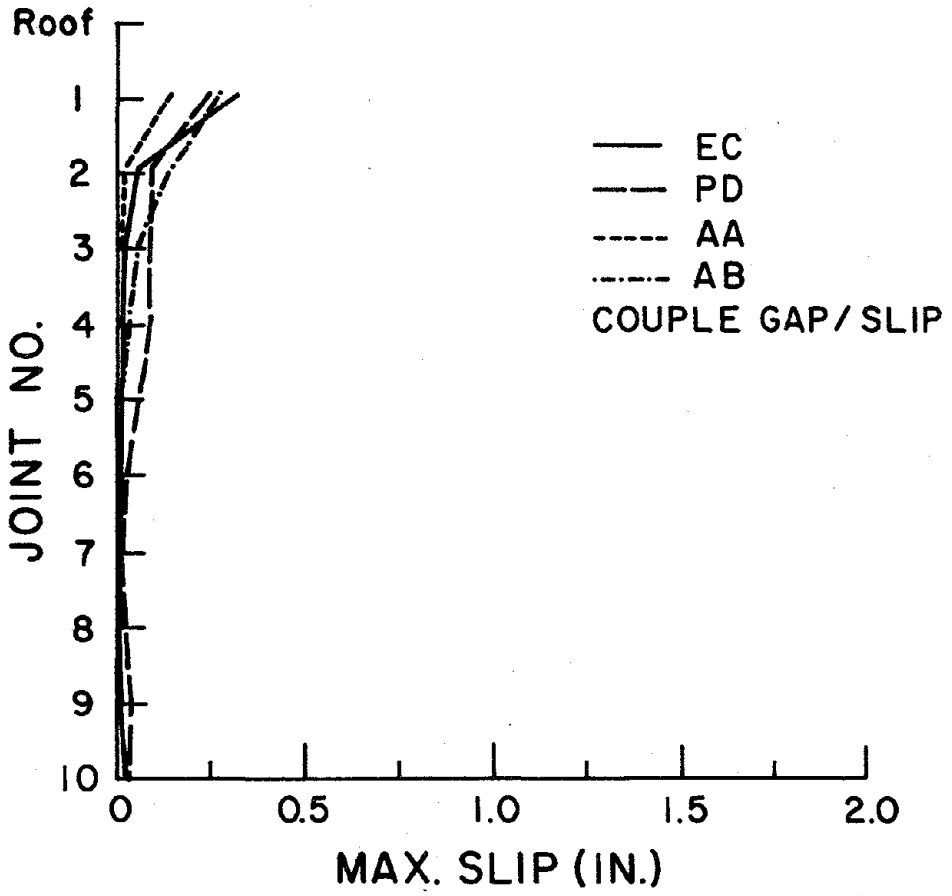

FIG. 5.12.6 CASE G/0.6 COUPLED SLIP AND GAP OPENING. MAXIMUM SLIP

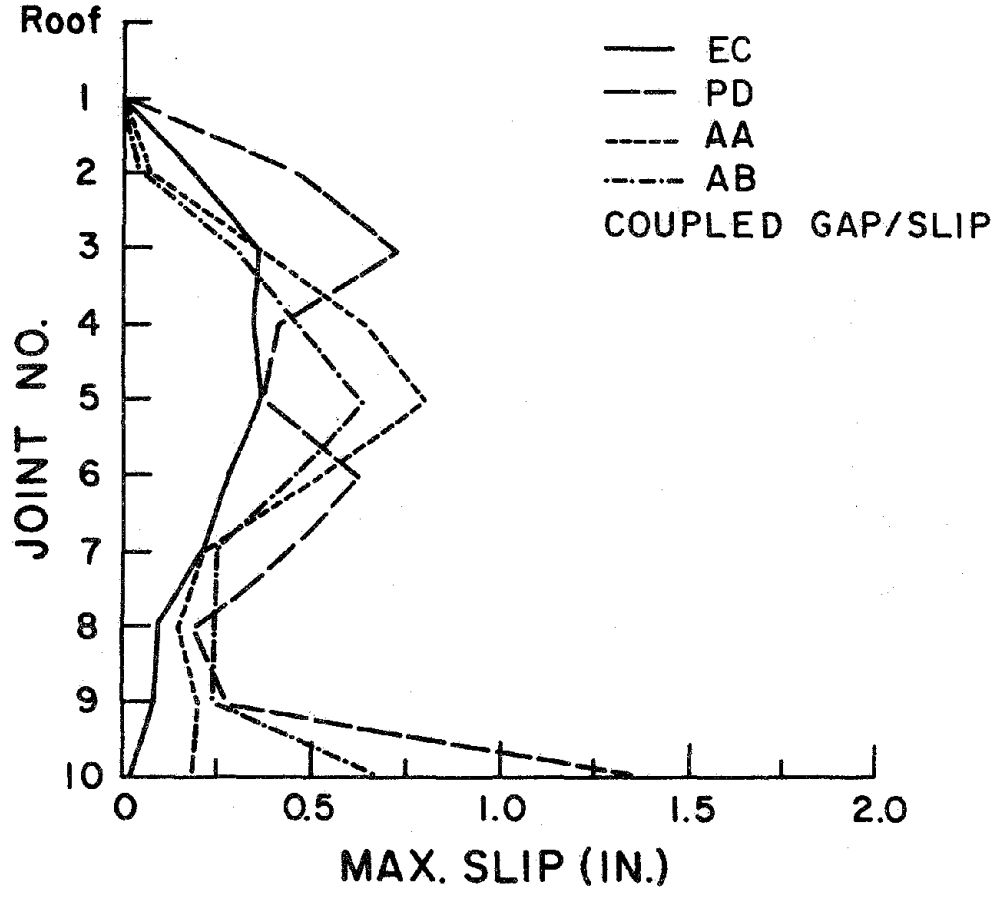

FIG. 5.12.7 CASE GP/0.2 COUPLED SLIP AND GAP OPENING. MAXIMUM SLIP

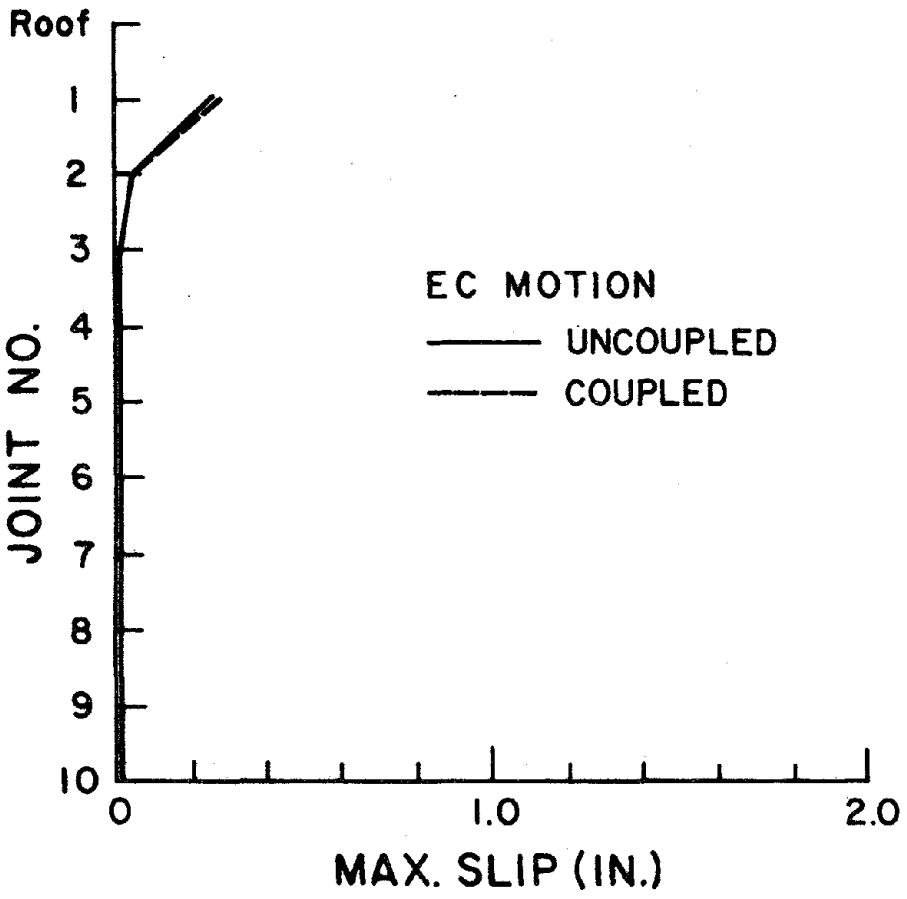

FIG. 5.12.8a CASE G/0.6/EC. MAXIMUM SLIP FOR UNCOUPLED AND COUPLED ANALYSES

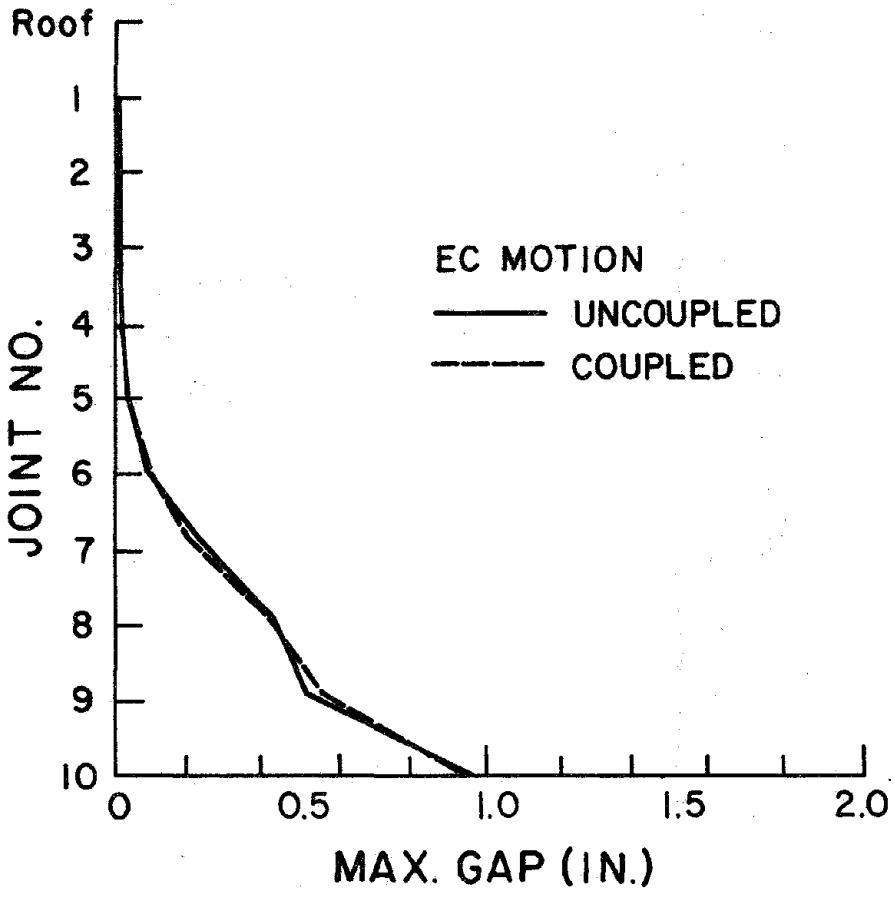

FIG. 5.12.8b CASE G/0.6/EC. MAXIMUM GAP OPENING FOR UNCOUPLED AND COUPLED ANALYSES

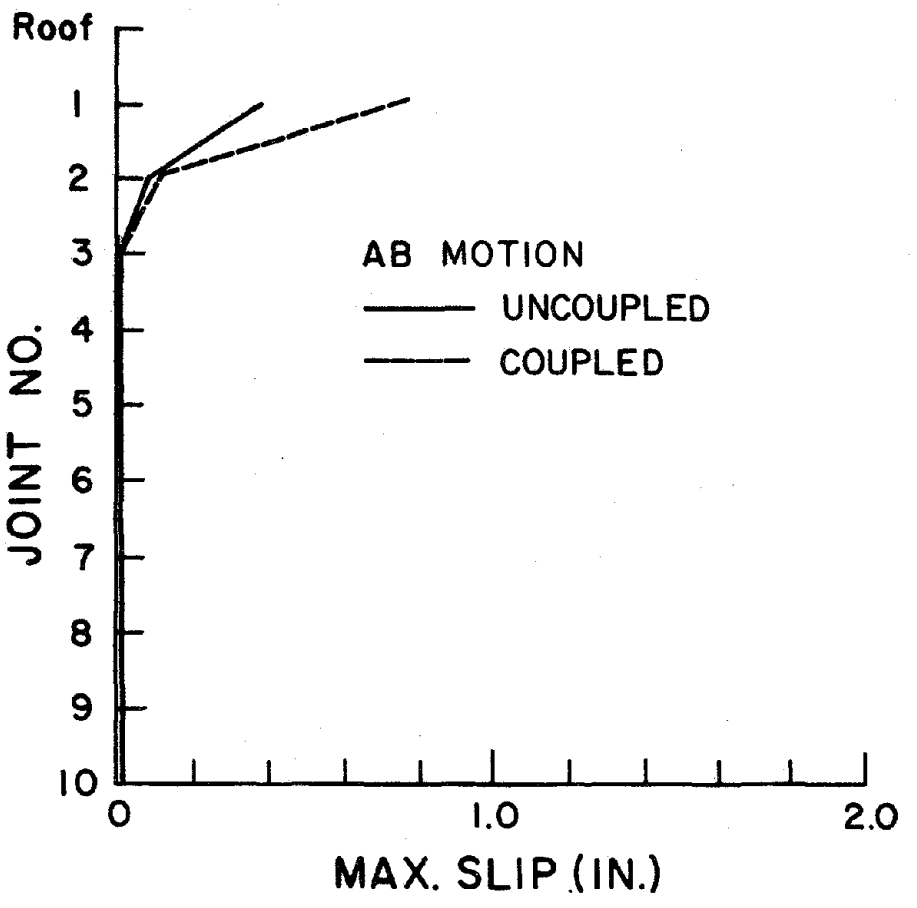

FIG. 5.12.9a CASE G/0.6/AB MAXIMUM SLIP FOR COUPLED AND UNCOUPLED ANALYSES

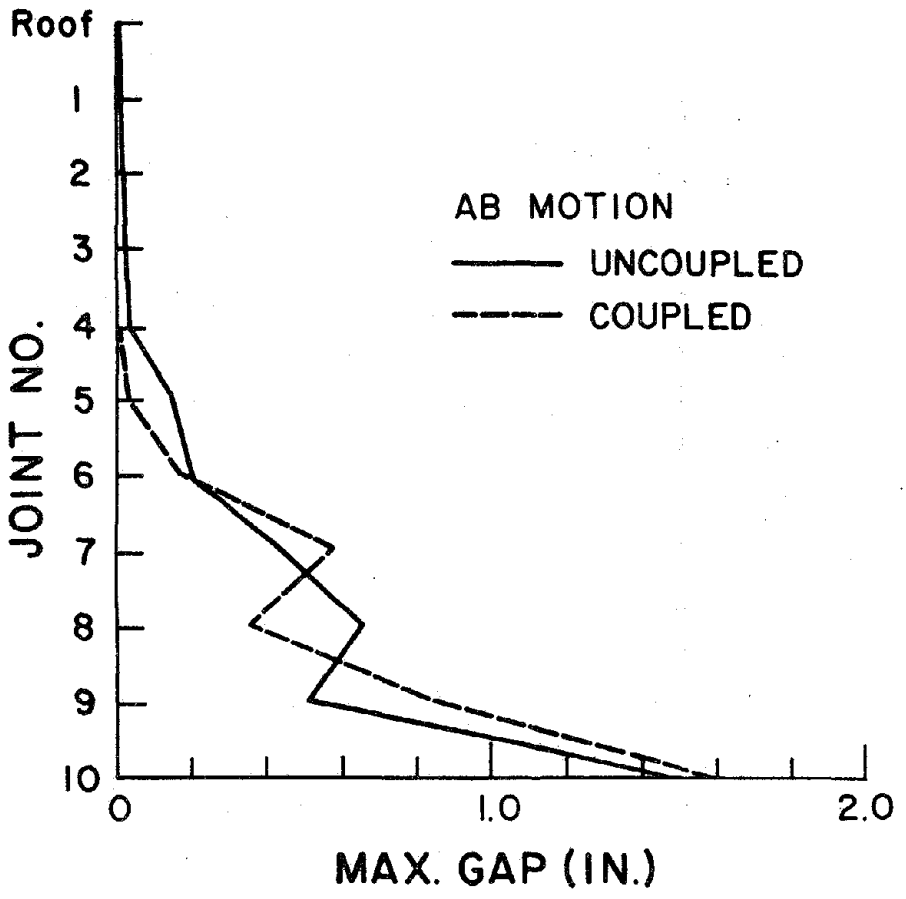

FIG. 5.12.9b CASE G/0.6/AB MAXIMUM GAP OPENING FOR COUPLED AND UNCOUPLED ANALYSES

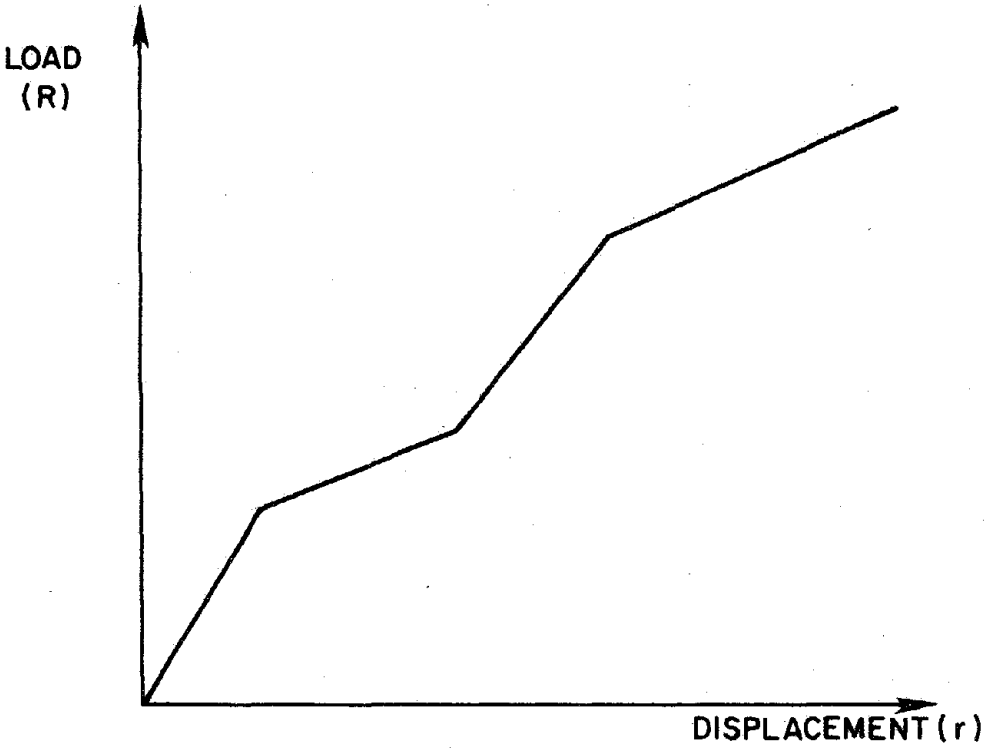

FIG. A.1 PIECEWISE LINEAR BEHAVIOR

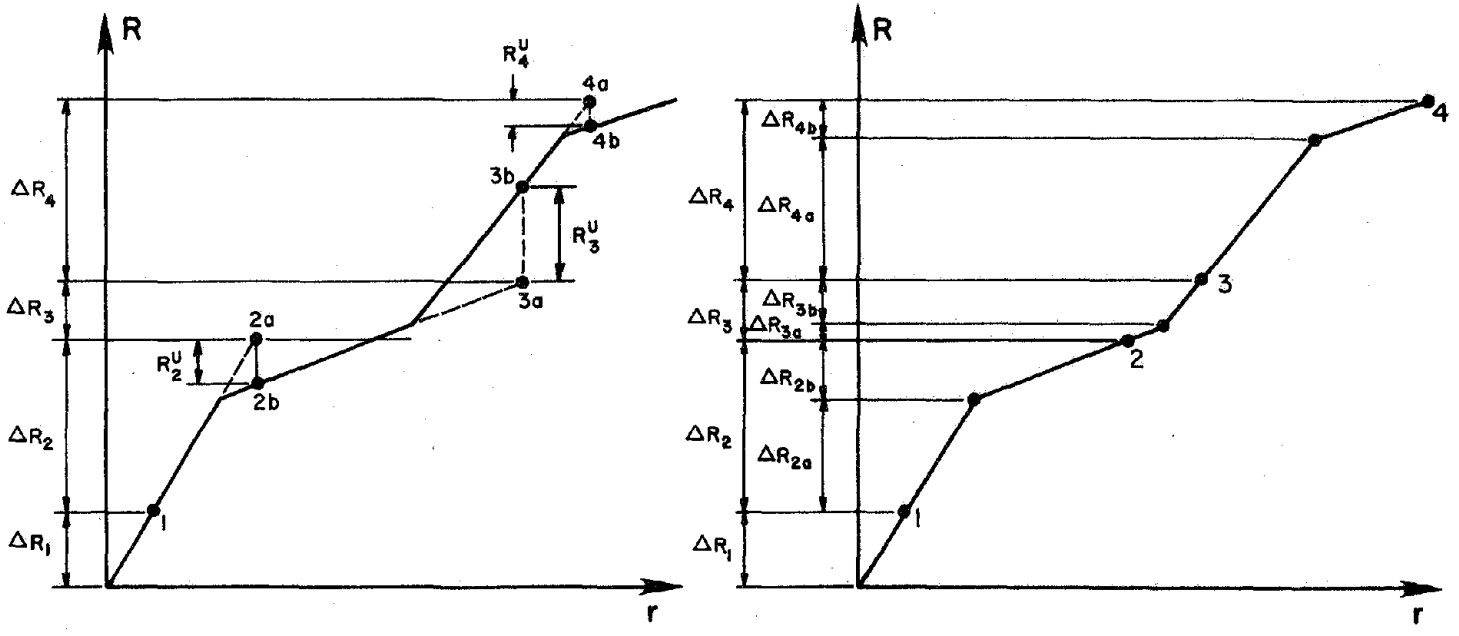

FIG. A.2 SOLUTION STRATEGIES

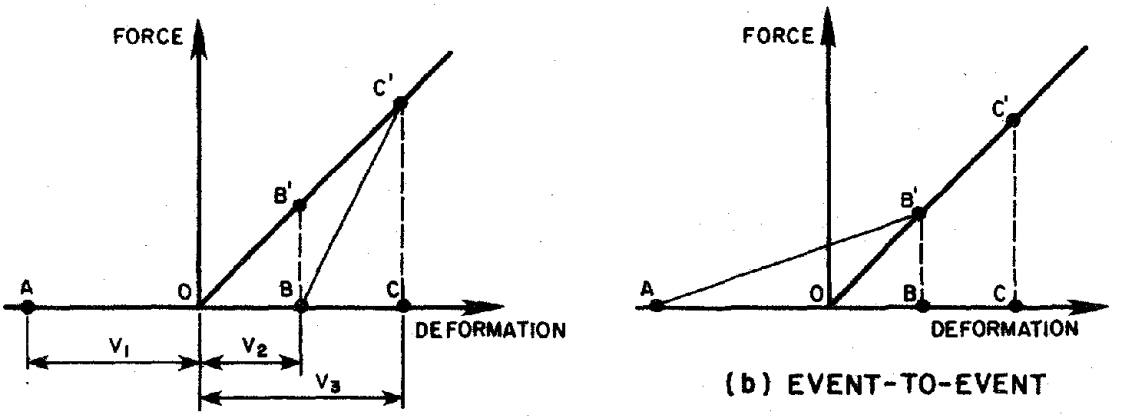

(a) EQUILIBRIUM CORRECTION

(b) EVENT-TO-EVENT

FIG. A.3 ENERGY ERRORS

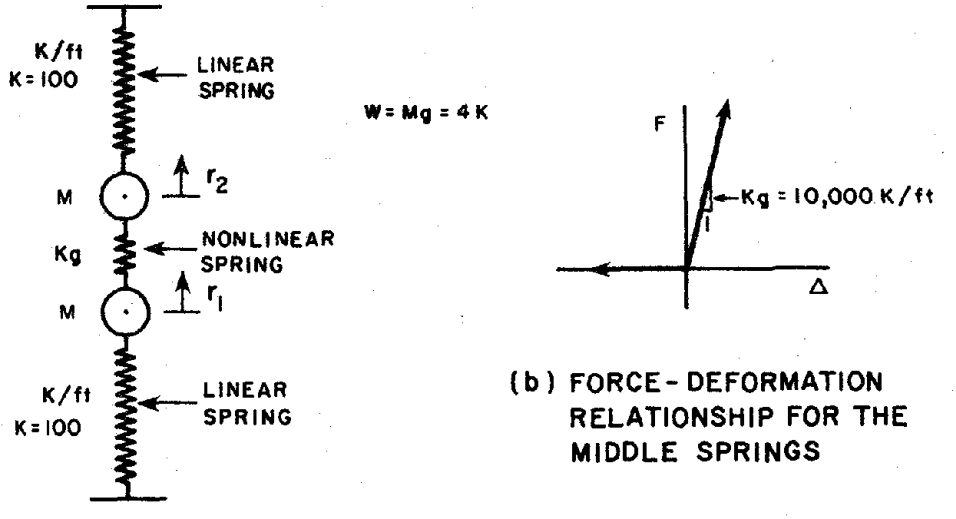

(a) TWO d.o.f. SYSTEM

(b) FORCE-DEFORMATION RELATIONSHIP FOR THE MIDDLE SPRINGS

FIG. A.4 EXAMPLE: 3-SPRING NONLINEAR SYSTEM

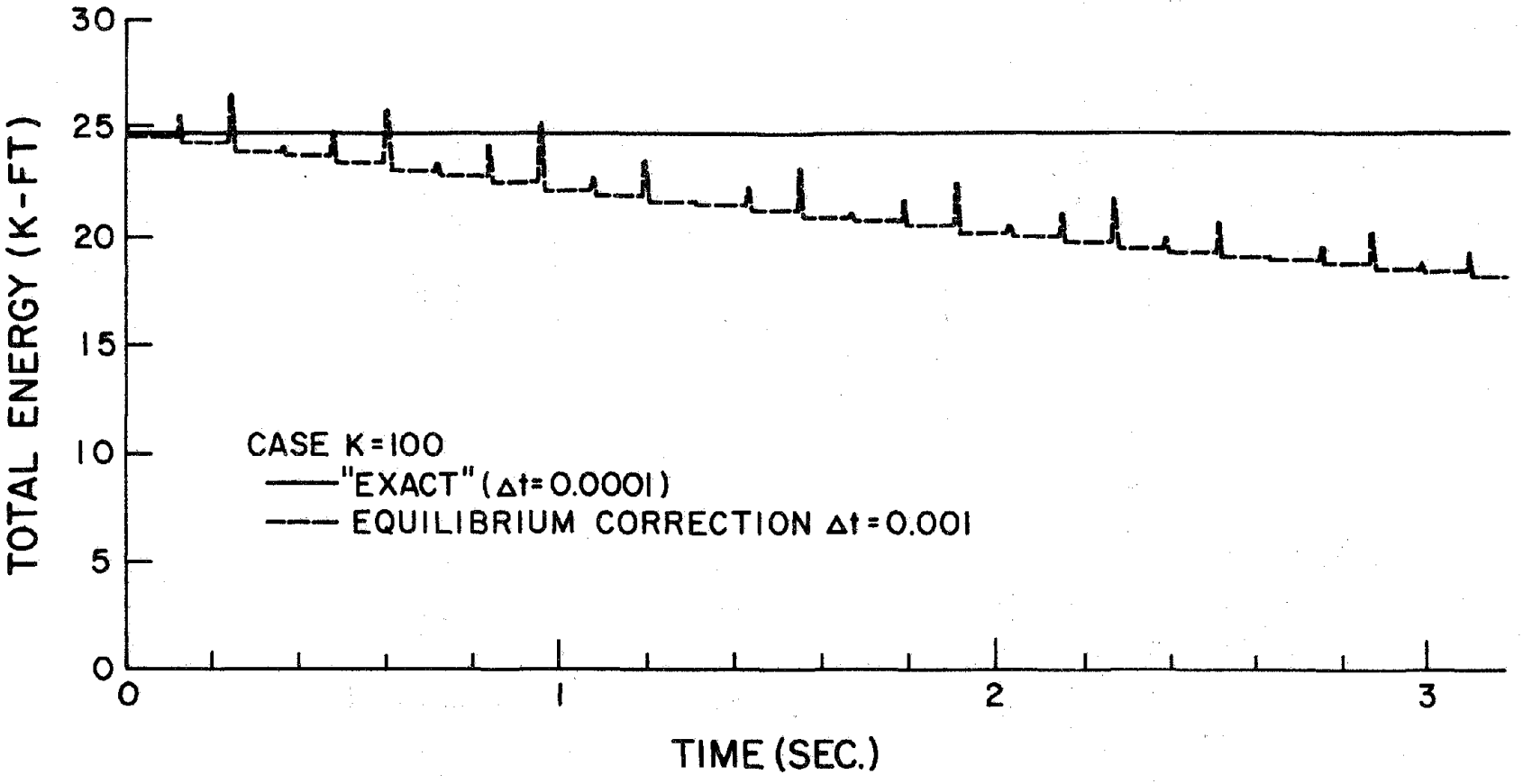

FIG. A.5a ENERGY FLUCTUATIONS FOR EQUILIBRIUM CORRECTION STRATEGY

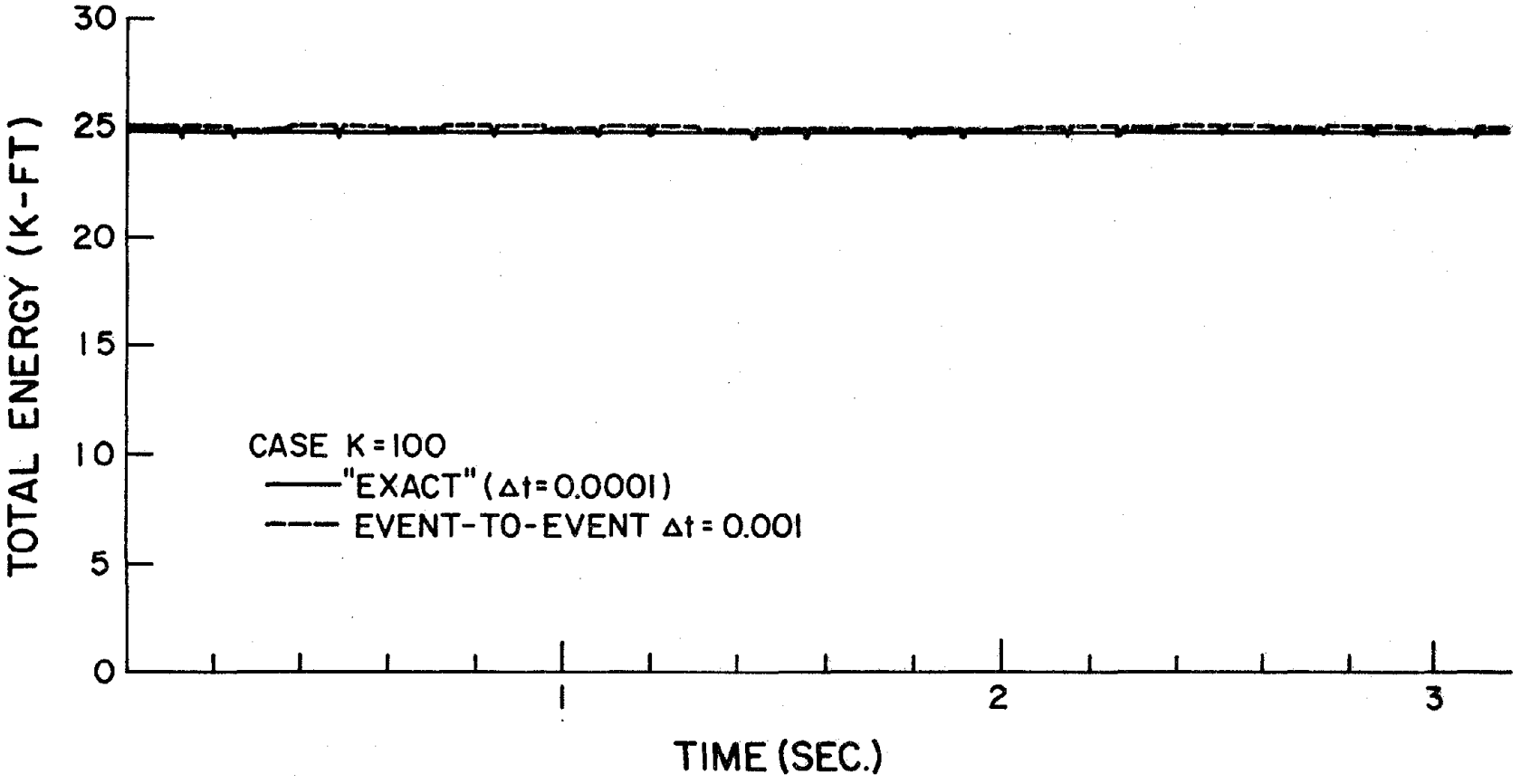

FIG. A.5b ENERGY FLUCTUATIONS FOR EVENT-TO-EVENT STRATEGY

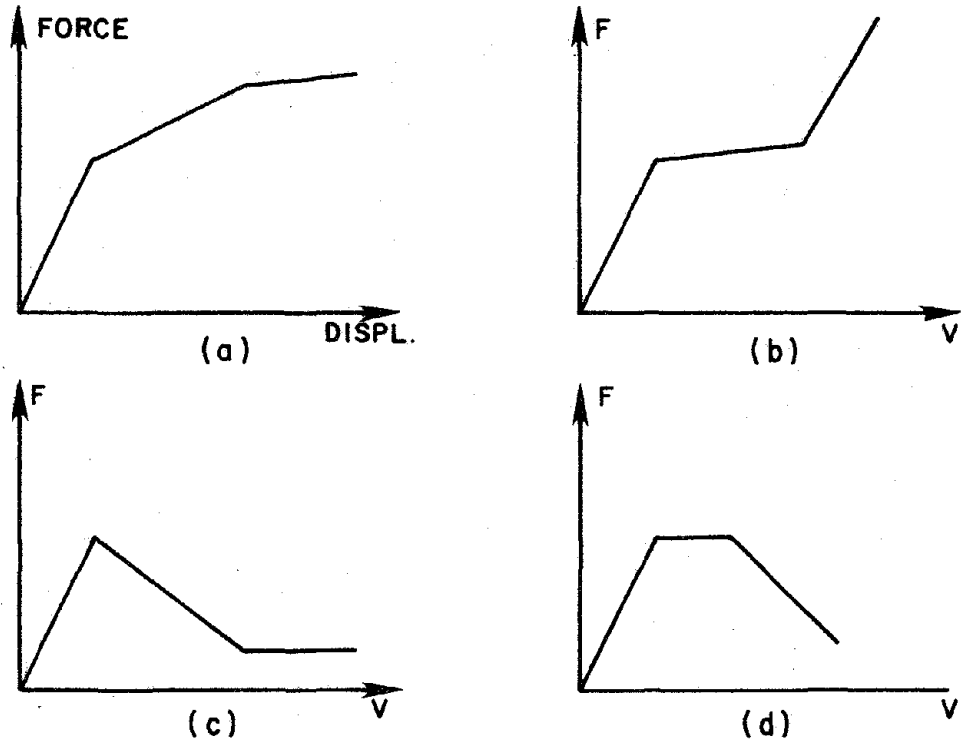

FIG. B.1 TRILINEAR FORCE-DISPLACEMENT RELATIONSHIPS

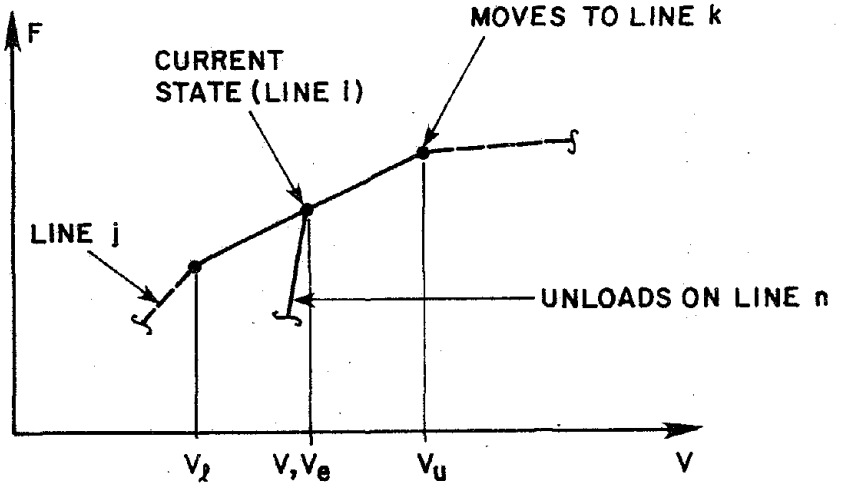

FIG. B.2 LOGIC FOR MULTILINEAR APPROXIMATION

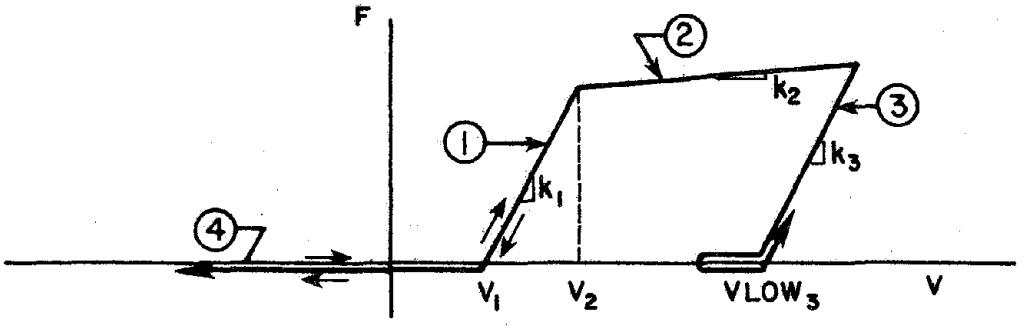

LINE	VUP	VLOW	IUP	ILOW	STIFFNESS
1	V_2	V_1	2	4	k_1
2	$+\infty$	V	2	3	k_2
3	V	COMPUTE VLOW3	2	4	k_3
4	V_1	$-\infty$	1	4	0

FIG. B.3 EXAMPLE FOR COMPUTER LOGIC

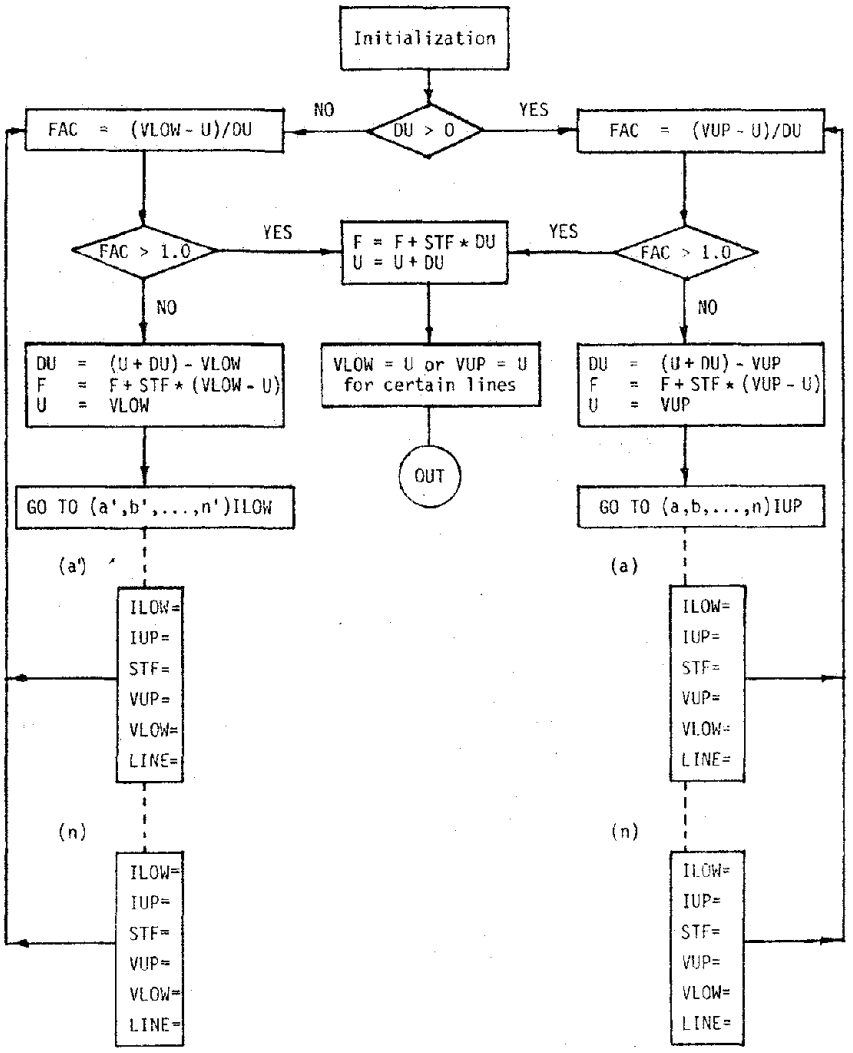

FIG. B.4 FLOW DIAGRAM FOR COMPUTER LOGIC

APPENDIX A

MODIFIED DYNAMIC SOLUTION TECHNIQUE

A.1 EQUILIBRIUM CORRECTION AND EVENT-TO-EVENT STRATEGIES

Most elements developed for DRAIN-2D have been modelled using piecewise linear force-deformation relationships. As a result, the load-displacement relationship of the assembled structure will also typically be piecewise linear (Fig. A.1).

Consider, for the purpose of discussion, the analysis of a piecewise linear structure under static load. For the load-displacement relationship shown in Fig. A.1, and a series of load increments, the solution strategy used in the basic DRAIN-2D program is the equilibrium correction strategy in Fig. A.2(a). In this strategy, the unbalanced load (R^U) at the end of each load increment is calculated, and added to the load increment (ΔR) for the following step. Unless very small load increments are used, it is possible for the solution path to depart substantially from the true load-displacement path.

An alternative strategy is illustrated in Fig. A.2(b). In this strategy the load increments are subdivided into subincrements, so that the solution proceeds from "event" (i.e., stiffness change) to event. The size of the load subincrements can be determined by the computer program. There is never any unbalanced load, and the solution follows the exact load-deflection relationship. This strategy has the disadvantage of being more expensive computationally, but the additional cost is large only if the number of events is large.

The modified DRAIN-2D program uses a combination of the equilibrium correction and event-to-event strategies. Events (and hence load substeps)

are recognized for certain elements only, specifically those in which large stiffness changes, and hence large equilibrium errors, can occur. Events are ignored in other elements, and any resulting errors are taken into account by applying equilibrium corrections.

The strategy in DRAIN-2D must, however, consider not static load but dynamic load. This requires further assumptions and leads to further approximations.

A.2 EVENT-BY-EVENT STRATEGY IN A DYNAMIC ANALYSIS

For a time step, Δt, the linearized incremental equations of motion can be written as

$$\underline{M}\,\Delta\ddot{\underline{r}} + \underline{C}\,\Delta\dot{\underline{r}} + \underline{K}\,\Delta\underline{r} = \Delta\underline{R} \qquad (A.1)$$

in which $\Delta\ddot{\underline{r}}$, $\Delta\dot{\underline{r}}$, $\Delta\underline{r}$ and $\Delta\underline{R}$ are the increments of acceleration, velocity, displacement and applied load, respectively; $\underline{M}$ is the mass matrix; and $\underline{C}$ and $\underline{K}$ are the tangent damping and stiffness matrices, respectively, at the beginning of the time step.

If the damping matrix is assumed to be proportional to the mass and stiffness matrices (i.e., $\underline{C} = \alpha\underline{M} + \beta\underline{K}$), and the constant average acceleration method (Newmark $\beta = 1/4$) is used, the equilibrium equation can be written as

$$\underline{K}^*\,\Delta\underline{r} = \Delta\underline{R}^* \qquad (A.2)$$

in which $\underline{K}^*$ and $\Delta\underline{R}^*$ are effective stiffness and load values, defined by

$$\underline{K}^* = \left(\frac{4}{\Delta t^2} + \frac{2\alpha}{\Delta t}\right)\underline{M} + \left(\frac{2\beta}{\Delta t} + 1\right)\underline{K} \qquad (A.3)$$

$$\Delta\underline{R}^* = \Delta\underline{R} + \underline{M}\left[2\ddot{\underline{r}}_o + \left(\frac{4}{\Delta t} + 2\alpha\right)\dot{\underline{r}}_o\right] + 2\beta\underline{K}\,\dot{\underline{r}}_o \qquad (A.4)$$

and $\dot{\underline{r}}_o$, $\ddot{\underline{r}}_o$ are the velocities and accelerations at the beginning of the

step. Dynamic analysis is thus similar to static analysis, except that effective stiffness and load matrices are used. These matrices depend on the time step.

In the modified DRAIN-2D program, the event-to-event strategy has been applied to the dynamic problem as though it were a static problem. In particular, the event factors are calculated assuming linear displacement variation with load (and hence, by implication, with time). The significance of equating dynamic behavior to static behavior has not been explored in detail (this will be a topic for future study). One important aspect of the method is, however, its effect on energy balance.

A.3 ENERGY BALANCE

Fig. A.3 shows the force-deformation relationship for a gap element. With the equilibrium correction strategy, let the calculated deformations after three successive time steps be v_1, v_2 and v_3 (Fig. A.3a). At deformation v_2 there is an equilibrium error which implies application of an external load, F_u, on the structure. The need for this load develops during the time step from v_1 to v_2. The load is actually applied, however, during the following step, when the equilibrium correction is made. The resistance developed by the mathematical model thus follows path A-B-C', and the work done is the area BCC'. The true resistance path, however, is A-O-C', and the stored strain energy is the area OCC'. The system has thus gained energy (the gained energy can be recovered when the element unloads along line C'O). By similar reasoning, it can be shown that when the gap re-opens, energy is lost.

The corresponding situation for the event-to-event strategy is shown in Fig. A.3b. Again, the successive deformations are v_1, v_2 and v_3, but the strategy ensures that equilibrium is satisfied at deformation v_2. The

resistance path developed by the mathematical model is thus A-B'-C', whereas the true path is again A-O-C'. The stored strain energy is thus less than the external work, and energy is lost. By similar reasoning, energy is gained when the gap re-opens.

The energy loss-gain characteristics of the event-to-event strategy are thus the opposite of the equilibrium correction strategy. In an actual analysis, the energy losses and gains will, with luck, balance out. Occasionally, however, the gains (or losses) will consistently dominate, and grossly incorrect results can be obtained.

A.4 EXAMPLE

The energy loss-gain characteristics of the two strategies have been explored using the nonlinear spring-mass system shown in Fig. A.4. The variation of total energy with time are shown in Fig. A.5a for the event-to-event strategy and in Fig. A.5b for the equilibrium correction strategy.

In Fig. A.5a, each "spike" corresponds to impact followed shortly afterwards by separation. The energy decreases at impact, then increases at separation. The fluctuations are small. In Fig. A.5b, each spike again corresponds to impact followed by separation, with energy gain followed by energy loss. The fluctuations are substantial and systematic, leading to a progressive loss in energy in the first few seconds (beyond 5 seconds, the computation showed a progressive gain in energy).

This example suggests that the event-to-event strategy is superior to the equilibrium correction strategy. Other analyses of the system in Fig. A.4, together with experience in the use of DRAIN-2D, have confirmed that this is generally the case.

A.4 CONTINUING WORK

Work is continuing on improving the strategy. A scheme proposed by

Hughes et al [46], which introduces additional external forces to improve the energy balance, has been studied, but has been found to be too complex for general purpose use. A procedure proposed by Hibbitt and Karlsson [71], which automatically varies the time step, is being studied, and shows a great deal of promise.

APPENDIX B

PROGRAMMING LOGIC FOR MULTILINEAR FORCE-DEFORMATION RELATIONSHIPS

B.1 MULTILINEAR REPRESENTATION

For one dimensional elements, multilinear action-deformation relationships have advantages over curvilinear ones. Probably the most important advantage is that a multilinear formulation allows the user greater flexibility in choosing the shape of the force-displacement relationship. For example, a trilinear curve can represent any of the four characteristics shown in Fig. B.1.

Also, for a computer code such as DRAIN-2D, which uses a simple step-by-step solution strategy, the solution time will usually be reduced when a multilinear formulation is used. This is because the element tangent stiffness is constant along any linear segment, and hence the structure stiffness matrix will generally remain unchanged over several time steps. Further, when the element tangent stiffness is piecewise constant the computational effort for the state determination calculation will usually be small. This is important, because the state determination phase can consume a majority of the total computer time.

B.2 PROGRAMMING LOGIC

Complex multilinear relationships can be considered in DRAIN-2D using simple logic. A convenient procedure for keeping track of the element state is illustrated in Fig. B.2 for a multilinear, hysteretic, uniaxial element. The current state is on line i at total deformation V. If the increment of deformation, DV, is positive, an "event" (corresponding to a change in tangent stiffness) occurs at deformation V_u, and the relationship moves to line k. If DV is negative, unloading occurs

immediately along line n. The parameters i, n, k, V and V_u serve both to define the current state of the element and to define the next event. When an event occurs, these parameters can be updated to correspond to the new linear segment, and the event calculation process can continue.

In general, it is necessary to define a set of rules such that the following parameters can be specified:

(1) LINE = current line no.

(2) ILOW = next line if deformation decreases.

(3) IUP = next line if deformation increases.

(4) VLOW = deformation at which state moves to next line if extension decreases.

(5) VUP = deformation at which state moves to next line if extension increases.

Fig. B.3 shows an example of how the parameters are defined for a simple force-deformation relationship.

A flow diagram of the logic is shown in Fig. B.4. An essential feature of the logic is the calculation of the factor, FAC, which is the proportion of the deformation increment at which the next event occurs. If FAC is less than one, then an event occurs in the current time step. If FAC is less than one, a part of DV (i.e., FAC*DV) is applied to reach the event, the state is updated, and the remaining portion of DV is applied in the new state. The computer logic is formulated to allow for any number of events in a single time step, although typically at most one event will occur. If several events occur in a step, the time step has probably been made too large. In a practical computer program, a warning message might be printed when this occurs, to alert the analyst to a possible error.

APPENDIX C

ELEMENT USER GUIDES

I. PANEL ELEMENT: MODIFIED BEAM MODEL

See Section 4.2 for description of element.

Number of words of information per element = 35.

(a) CONTROL INFORMATION (3I5) - One card.

Columns	
5	Element group indicator. Punch 8.
6 - 10	Number of elements in group.
11 - 15	Number of different element stiffness types (max. 40).

(b) STIFFNESS TYPES (I5, 3F10.0) - One card for each stiffness type.

Columns	
1 - 5	Stiffness type number, in sequence beginning with 1.
6 - 15	Effective EA for vertical extension.
16 - 25	Effective EI for symmetrical bending.
26 - 35	Effective GA' for shear racking.

(c) ELEMENT GENERATION COMMANDS (8I5) - One card for each generation command. Elements must be specified in increasing numerical order. Cards for the first and last elements must be included.

Columns	
1 - 5	Element number, or number of first element in a sequentially numbered series to be generated by this card.
6 - 10	Node number i (top left).
11 - 15	Node number j (top right).
16 - 20	Node number k (bottom left).
21 - 25	Node number ℓ (bottom right).

(c) ELEMENT GENERATION COMMANDS (Continued)

26 - 30	Node number increment for element generation. Default = 1.
31 - 35	Stiffness type number.
40	Time history output code. Leave blank or punch zero for no time history. Punch 1 if time history is required.

RESULTS PRINTOUT

The printed results consist of the top and bottom moments, shear force, and axial force on each element, as shown in Fig. 4.2.8.

II. PANEL ELEMENT: FINITE ELEMENT MODEL

See Section 4.3 for description of element.

Number of words of information per element = 75.

(a) CONTROL INFORMATION (3I5) - One Card

Columns

5	Element group indicator. Punch 4.
6 - 10	Number of elements in group.
11 - 15	Number of different element stiffness types (max. 40).

(b) STIFFNESS TYPES (I5, 2F10.0) - One Card for each stiffness type.

Columns

1 - 5	Stiffness type number, in sequence, beginning with 1.
6 - 15	Young's Modulus of Elasticity, E.
16 - 25	Poisson's Ratio, ν.

(c) ELEMENT GENERATION COMMANDS (8I5, 4F10.0) - One card for each generation command. Elements must be specified in increasing numerical order. Cards for the first and last elements must be included.

Columns

1 - 5	Element number, or number of first element in a sequentially numbered series to be generated by this card.
6 - 10	Node number i (bottom left).
11 - 15	Node number j (top left).
16 - 20	Node number k (top right).

(c) ELEMENT GENERATION COMMANDS (Continued)

21 - 25	Node number ℓ (bottom right).
26 - 30	Node number increment for element generation. Default = 1.
31 - 35	Stiffness type number.
40	Time history output code. Leave blank or punch zero for no time history. Punch 1 if time history is required.
41 - 50	Element thickness.
51 - 60	Initial horizontal stress, σ_{0xx}. See Fig. (b) for sign convention.
61 - 70	Initial vertical stress, σ_{0yy}.
71 - 80	Initial shear stress, σ_{0xy}.

RESULTS PRINTOUT

The printed results consist of the stresses σ_{xx}, σ_{yy} and σ_{xy} at the midpoints of the element edges (points A, B, C, and D, as shown in Fig. (a)). The sign convention is as shown in Fig. (b)).

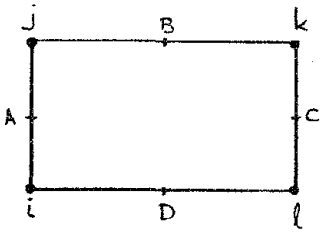

(a) Element Nodes

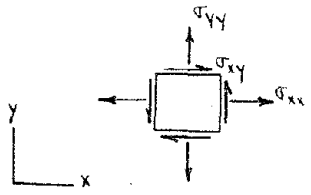

(b) Positive stresses

III. SIMPLE FRICTION ELEMENT

See Section 4.4 for description of element.

Number of words of information per element = 26.

(a) CONTROL INFORMATION (3I5, 30X, I5) - One card.

Columns

5	Element group indicator. Punch 9.
6 - 10	Number of elements in group.
11 - 15	Number of different element stiffness types (max. 40).
50	Punch 1 if time-step repetititon technique is to be used. Otherwise leave blank.

(b) STIFFNESS TYPES (I5, 3F10.0) - One card for each stiffness type (See Fig. 4.4.2).

Columns

1 - 5	Stiffness type number, in sequence beginning with 1.
6 - 15	Shear stiffness, k_s.
16 - 25	Strain hardening modulus, as a proportion of k_s (i.e., k_h/k_s). Must be < 1.
26 - 35	Shear strength, F_{so}.

(c) ELEMENT GENERATION COMMANDS (10I5) - One card for each generation command. Elements must be specified in increasing numerical order. Cards for the first and last elements must be included.

Columns

1 - 5	Element number or number of first element in a sequentially numbered series to be generated by

(c) ELEMENT GENERATION COMMANDS (Continued)

this card.

10	Punch zero for a horizontal joint; one for a vertical joint.
11 - 15	Node number i (see Fig. 4.4.1).
16 - 20	Node number j.. May be same as i.
21 - 25	Node number k. Must have same coordinates as node i.
26 - 30	Node number ℓ. May be same as k. Must have same coordinate as node j.
31 - 35	Node number increment for element generation. Default = 1.
36 - 40	Stiffness type number.
45	Time history output code. Leave blank or punch zero for no time history. Punch 1 if time history is required.
50	Unloading code. Leave blank or punch zero for unloading as in Fig. 4.4.3b. Punch 1 for unloading as in Fig. 4.4.3a.

RESULTS PRINTOUT

The printed results consist of the slip code (zero = elastic; 1 = slipping), shear force, shear deformation, positive accumulated slip, and negative accumulated slip. The sign convention is shwon in Fig. 4.4.4.

IV. FRICTION ELEMENT WITH DEGRADING STRENGTH

See Section 4.5 for description of element.

Number of words of information per element = 31.

(a) CONTROL INFORMATION (3I5, 30X, I5) - One Card

Columns

5	Element group indicator. Punch 9.
6 - 10	Number of elements in group.
11 - 15	Number of different element stiffness types (max. 40).
50	Punch 1 if time-step repetition technique is to be used. Otherwise leave blank.

(b) STIFFNESS TYPES (I5, 7F10.0) - One card for each stiffness type (see Fig. 4.5.1).

Columns

1 - 5	Stiffness type number, in sequence beginning with 1.
6 - 15	Shear stiffness, k_s.
16 - 25	Strain hardening modulus, as a proportion of k_s (i.e., k_h/k_s). Must be < 1.
26 - 35	Shear strength, F_{s0}.
36 - 45	Shear force, F_{s1}, for friction degradation.
46 - 55	Shear force, F_{s2}.
56 - 65	Accumulated slip, S_1.
66 - 75	Accumulated slip, S_2.

(c) ELEMENT GENERATION COMMANDS (10I5) - One card for each generation command. Elements must be specified in increasing numerical order. Cards for the first and last elements must be

(c) ELEMENT GENERATION COMMANDS (Continued)

included.

Columns

1 - 5	Element number, of number of first element in a sequentially numbered series to be generated by this card.
10	Punch zero for a horizontal joint; one for a vertical joint.
11 - 15	Node number i (see Fig. 4.4.1)
16 - 20	Node number j. May be same as i.
21 - 25	Node number k. Must have same coordinates as node i.
26 - 30	Node number ℓ. May be same as k. Must have same coordinate as node j.
31 - 35	Node number increment for element generation.
36 - 40	Stiffness type number.
45	Time history output code. Leave blank or punch zero for no time history. Punch 1 if time history is required.
50	Unloading code. Leave blank or punch zero for unloading as in Fig. 4.4.3b. Punch 1 for unloading as in Fig. 4.4.3a.

RESULTS PRINTOUT

The printed results consist of the slip code (zero = elastic; 1 = slipping), shear force, shear deformation, positive accumulated slip, and negative accumulated slip. The sign convention is shown in Fig. 4.4.4.

V. GAP ELEMENT

See Section 4.6 for the description of element.

Number of words of information per element = 36.

(a) CONTROL INFORMATION (3I5, 30X, I5) - One card.

Columns

4 - 5	Element group indicator. Punch 10.
6 - 10	Number of element in group.
11 - 15	Number of different element stiffness types (max. 40).
50	Punch 1 if time-step repetition technqiue is to be used. Otherwise leave blank.

(b) STIFFNESS TYPES (I5, 6F10.0) - One card for each stiffness type (see Fig. 4.6.1).

Columns

1 - 5	Stiffness type number, in sequence beginning with 1.
6 - 15	Displacment limit Δ_1.
16 - 25	Displacement limit Δ_2.
26 - 35	Stiffness k_1.
36 - 45	Stiffness k_2.
46 - 55	Stiffness k_3.
56 - 65	Stiffness k_4. Leave blank or punch zero for elastic unloading. Must not be less than the largest of k_1, k_2, and k_3,

(c) ELEMENT GENERATION COMMANDS (7I5, F10.0, 2I5, 2F10.0) - One card for each generation command. Elements must be specified in increasing numerical order. Cards for the first and last

(c) ELEMENT GENERATION COMMANDS (Continued)

elements must be included.

Columns

1 - 5	Element number, or number of first element in a sequentially numbered series to be generated by this card.
10	Punch zero for a horizontal joint; one for a vertical joint.
11 - 15	Node number i (see Fig. 4.6.2).
16 - 20	Node number j. May be same as i.
21 - 25	Node number k.
26 - 30	Node number ℓ. May be same as k.
31 - 35	Stiffness type number.
36 - 45	Initial bearing force (input as a positive number).
46 - 50	Node number increment for element generation. Default = 1.
55	Time history output code. Leave blank or punch zero for no time history. Punch 1 if time history is required.
56 - 65	Element location ratio, a_1/L_1 (see Fig. 4.6.2).
66 - 75	Element location ratio, a_2/L_2.

RESULTS PRINTOUT

The printed results consist of the line number in the force-deformation relationship (Fig. 4.6.1), the bearing force, and the normal deformation on the element. Compressive normal force and corresponding normal deformation are positive. Negative normal deformation indicates the amount of gap opening.

VI. COMBINED GAP-FRICTION ELEMENT

See Section 4.7 for description of element.

Number of words of information per element = 47.

(a) CONTROL INFORMATION (3I5, 30X, I5) - One card.

Columns

5	Element group indicator. Punch 2.
6 - 10	Number of elements in group.
11 - 15	Number of different element stiffness types (max. 40).
50	Punch 1 if time-step repetition technique is to be used. Otherwise leave blank.

(b) STIFFNESS TYPES (I5, 6F10.0, F5.0, F10.0) - One card for each stiffness type (see Fig. 4.7.3).

Columns

1 - 5	Stiffness type number, in sequence beginning with 1.
6 - 15	Displacement limit Δ_1.
16 - 25	Displacement limit Δ_2.
26 - 35	Stiffness k_1.
36 - 45	Stiffness k_2.
46 - 55	Stiffness k_3.
56 - 65	Stiffness k_4. Leave blank or punch zero for elastic unloading. Must not be less than the largest of k_1, k_2 and k_3.
66 - 70	Coefficient of friction, μ.
71 - 80	Shear stiffness, k_s.

(c) ELEMENT GENERATION COMMANDS (5I5, F10.0, 3I5) - One card for each generation command. Elements must be specified in increasing numerical order. Cards for the first and last elements must be included.

Columns

1 - 5	Element number, or number of first element in a sequentially numbered series to be generated by this card.
10	Punch zero for a horizontal joint; one for a vertical joint.
11 - 15	Node number i (see Fig. 4.7.2).
16 - 20	Node number j. Must have same coordinates as node i.
21 - 25	Stiffness type number.
26 - 35	Initial bearing force (input as a positive number).
36 - 40	Node number increment for element generation. Default = 1.
45	Time history output code. Leave blank or punch zero for no time history. Punch 1 if time history is required.
50	Unloading code for shear component. Leave blank or punch zero for unloading as in Fig. 4.4.3b. Punch 1 for unloading as in Fig. 4.4.3a.

RESULTS PRINTOUT

The printed results consits of the bearing force and corresponding deformation for the gap component (compressive positive);

the line number in the force-deformation relationship (Fig. 4.7.3b); and the slip code (zero = elastic; 1 = slipping), shear force and shear deformation for the shear component (positive directions are shown in Fig. 4.4.4).

VII. KEY ELEMENT

See Section 4.8 for description of element.

Number of words of information per element = 30.

(a) CONTROL INFORMATION (3I5) - One card.

Columns

5	Element group indicator. Punch 7.
6 - 10	Number of elements in group.
11 - 15	Number of different element stiffness types (max. 40).

(b) STIFFNESS TYPES (I5, 4F10.0) - One card for each stiffness type (see Fig. 4.8.1).

Columns

1 - 5	Stiffness type number, in sequence beginning with 1.
6 - 15	Displacement limit Δ_1.
16 - 25	Displacement limit Δ_2.
26 - 35	Displacement limit Δ_3.
36 - 45	Yield strength, F_{yp}.

(c) ELEMENT GENERATION COMMANDS (7I5) - One card for each generation command. Elements must be specified in increasing numerical order. Cards for the first and last elements must be included.

Columns

1 - 5	Element number, or number of first element in a sequentially numbered series to be generated by this card.

(c) ELEMENT GENERATION COMMANDS (Continued)

10	Punch zero for a horizontal joint; one for a vertical joint.
11 - 15	Node number i (see Fig. 4.8.3).
16 - 20	Node number j. Must have same coordinates as node i.
21 - 25	Node number increment for element generation. Default = 1.
26 - 30	Stiffness type number.
35	Time history output code. Leave blank or punch zero for no time history. Punch 1 if time history is required.

RESULTS PRINTOUT

The printed results consist of the line number in the force-deformation relationship (Fig. 4.8.1b), shear force, and shear deformation. The sign convention is as shown in Fig. 4.8.1a.

VIII. SHEAR FRICTION ELEMENT

See Section 4.9 for description of element.

Number of words of information per element = 55.

(a) CONTROL INFORMATION (3I5, 30X, I5) - One card.

Columns

5	Element group indicator. Punch 5.
6 - 10	Number of elements in group.
11 - 15	Number of different element stiffness types (max. 40).
50	Punch 1 if time-step repetition technique is to be used. Otherwise leave blank.

(b) STIFFNESS TYPES (I5, 6F10.0/7F10.0) - Two cards for each stiffness type (see Fig. 4.9.2).

FIRST CARD

Columns

1 - 5	Stiffness type number, in sequence beginning with 1.
6 - 15	Stiffness k_0.
16 - 25	Stiffness k_1.
26 - 35	Stiffness k_2.
36 - 45	Stiffness k_3.
46 - 55	Stiffness k_4. Must not be less than the largest of k_1, k_2, and k_3.
56 - 65	Stiffness k_5.

SECOND CARD

Columns

1 - 10	Slip force, F_f.

11 - 20 Displacement limit Δ_1.

21 - 30 Displacement limit Δ_2.

31 - 40 Force limit P_1 (see Fig. 4.9.4) for strength envelope.

41 - 50 Force limit P_2.

51 - 60 Slip limit, S_1.

61 - 70 Slip limit S_2.

(c) ELEMENT GENERATION COMMANDS (9I5, F10.0) - One card for each generation command. Elements must be specified in increasing numerical order. Cards for the first and last elements must be included.

Columns

1 - 5 Element number, or number of first element in a sequentially numbered series to be generated by this card.

10 Punch zero for a horizontal joint; one for a vertical joint.

11 - 15 Node number i (see Fig. 4.9.1)

16 - 20 Node number j. May be same as i.

21 - 25 Node number k. Must have same coordinates as node i.

26 - 30 Node number ℓ. May be same as k. Must have same coordinates as node j.

31 - 35 Node number increment for element generation. Default = 1.

36 - 40 Stiffness type number.

45 Time history output code. Leave blank or punch

(c) ELEMENT GENERATION COMMANDS (Continued)

zero for no time history. Punch 1 if time history is required.

46 - 55 Degrading factor, $\alpha(\geq 0.)$ See Section 4.9.3.

RESULTS PRINTOUT

The printed results consist of the shear force and corresponding deformation (positive directions as shown in Fig. 4.4.4); positive and negative accumulated slips and the slip code for the simple friction component; and the line number in the force-deformation relationship of the shear friction component (Fig. 4.9.2).

IX. LINK ELEMENT

See Section 4.10 for description of element.

Number of words of information per element = 34.

(a) CONTROL INFORMATION (3I5) - One card.

Columns

5	Element group indicator. Punch 6.
6 - 10	Number of elements in group.
11 - 15	Number of different element stiffness types (max. 40).

(b) STIFFNESS TYPES (2I5, 5F10.0) - One card for each stiffness type (see Fig. 4.10.1).

Columns

1 - 5	Stiffness type number, in sequence beginning with 1.
10	Leave blank or punch zero for inelastic unloading. Punch 1 for elastic unloading.
11 - 20	Displacement limit Δ_1.
21 - 30	Displacement limit Δ_2.
31 - 40	Stiffness k_1.
41 - 50	Stiffness k_2.
51 - 60	Stiffness k_3.

(c) ELEMENT GENERATION COMMANDS (4I5, F10.0, 2I5) - One card for each generation command. Elements must be specified in increasing numerical order. Cards for the first and last elements must be included.

(c) ELEMENT GENERATION COMMANDS (Continued)

Columns

1 - 5	Element number, or number of first element in a sequentially numbered series to be generated by this card.
6 - 10	Node number i.
11 - 15	Node number j. Must not have the same coordinates as in node i.
16 - 20	Stiffness type number.
21 - 30	Initial bearing force if input as a positive number. Initial gap if input as a negative number.
31 - 35	Node number increment for element generation. Default = 1.
40	Time history output code. Leave blank or punch zero for no time history. Punch 1 if time history is required.

RESULTS PRINTOUT

The printed results consist of the force and corresponding deformation in the element, and the line number in the force-deformation relationship (Fig. 4.10.1). The sign convention is as shown in Fig. 4.10.5a.

EARTHQUAKE ENGINEERING RESEARCH CENTER REPORTS

NOTE: Numbers in parenthesis are Accession Numbers assigned by the National Technical Information Service; these are followed by a price code. Copies of the reports may be ordered from the National Technical Information Service, 5285 Port Royal Road, Springfield, Virginia, 22161. Accession Numbers should be quoted on orders for reports (PB --- ---) and remittance must accompany each order. Reports without this information were not available at time of printing. Upon request, EERC will mail inquirers this information when it becomes available.

EERC 67-1 "Feasibility Study Large-Scale Earthquake Simulator Facility," by J. Penzien, J.G. Bouwkamp, R.W. Clough and D. Rea - 1967 (PB 187 905)A07

EERC 68-1 Unassigned

EERC 68-2 "Inelastic Behavior of Beam-to-Column Subassemblages Under Repeated Loading," by V.V. Bertero - 1968 (PB 184 888)A05

EERC 68-3 "A Graphical Method for Solving the Wave Reflection-Refraction Problem," by H.D. McNiven and Y. Mengi - 1968 (PB 187 943)A03

EERC 68-4 "Dynamic Properties of McKinley School Buildings," by D. Rea, J.G. Bouwkamp and R.W. Clough - 1968 (PB 187 902)A07

EERC 68-5 "Characteristics of Rock Motions During Earthquakes," by H.B. Seed, I.M. Idriss and F.W. Kiefer - 1968 (PB 188 338)A03

EERC 69-1 "Earthquake Engineering Research at Berkeley," - 1969 (PB 187 906)A11

EERC 69-2 "Nonlinear Seismic Response of Earth Structures," by M. Dibaj and J. Penzien - 1969 (PB 187 904)A08

EERC 69-3 "Probabilistic Study of the Behavior of Structures During Earthquakes," by R. Ruiz and J. Penzien - 1969 (PB 187 886)A06

EERC 69-4 "Numerical Solution of Boundary Value Problems in Structural Mechanics by Reduction to an Initial Value Formulation," by N. Distefano and J. Schujman - 1969 (PB 187 942)A02

EERC 69-5 "Dynamic Programming and the Solution of the Biharmonic Equation," by N. Distefano - 1969 (PB 187 941)A03

EERC 69-6 "Stochastic Analysis of Offshore Tower Structures," by A.K. Malhotra and J. Penzien - 1969 (PB 187 903)A09

EERC 69-7 "Rock Motion Accelerograms for High Magnitude Earthquakes," by H.B. Seed and I.M. Idriss - 1969 (PB 187 940)A02

EERC 69-8 "Structural Dynamics Testing Facilities at the University of California, Berkeley," by R.M. Stephen, J.G. Bouwkamp, R.W. Clough and J. Penzien - 1969 (PB 189 111)A04

EERC 69-9 "Seismic Response of Soil Deposits Underlain by Sloping Rock Boundaries," by H. Dezfulian and H.B. Seed 1969 (PB 189 114)A03

EERC 69-10 "Dynamic Stress Analysis of Axisymmetric Structures Under Arbitrary Loading," by S. Ghosh and E.L. Wilson 1969 (PB 189 026)A10

EERC 69-11 "Seismic Behavior of Multistory Frames Designed by Different Philosophies," by J.C. Anderson and V. V. Bertero - 1969 (PB 190 662)A10

EERC 69-12 "Stiffness Degradation of Reinforcing Concrete Members Subjected to Cyclic Flexural Moments," by V.V. Bertero, B. Bresler and H. Ming Liao - 1969 (PB 202 942)A07

EERC 69-13 "Response of Non-Uniform Soil Deposits to Travelling Seismic Waves," by H. Dezfulian and H.B. Seed - 1969 (PB 191 023)A03

EERC 69-14 "Damping Capacity of a Model Steel Structure," by D. Rea, R.W. Clough and J.G. Bouwkamp - 1969 (PB 190 663)A06

EERC 69-15 "Influence of Local Soil Conditions on Building Damage Potential during Earthquakes," by H.B. Seed and I.M. Idriss - 1969 (PB 191 036)A03

EERC 69-16 "The Behavior of Sands Under Seismic Loading Conditions," by M.L. Silver and H.B. Seed - 1969 (AD 714 982)A07

EERC 70-1 "Earthquake Response of Gravity Dams," by A.K. Chopra - 1970 (AD 709 640)A03

EERC 70-2 "Relationships between Soil Conditions and Building Damage in the Caracas Earthquake of July 29, 1967," by H.B. Seed, I.M. Idriss and H. Dezfulian - 1970 (PB 195 762)A05

EERC 70-3 "Cyclic Loading of Full Size Steel Connections," by E.P. Popov and R.M. Stephen - 1970 (PB 213 545)A04

EERC 70-4 "Seismic Analysis of the Charaima Building, Caraballeda, Venezuela," by Subcommittee of the SEAONC Research Committee: V.V. Bertero, P.F. Fratessa, S.A. Mahin, J.H. Sexton, A.C. Scordelis, E.L. Wilson, L.A. Wyllie, H.B. Seed and J. Penzien, Chairman - 1970 (PB 201 455)A06

EERC 70-5 "A Computer Program for Earthquake Analysis of Dams," by A.K. Chopra and P. Chakrabarti - 1970 (AD 723 994)A05

EERC 70-6 "The Propagation of Love Waves Across Non-Horizontally Layered Structures," by J. Lysmer and L.A. Drake 1970 (PB 197 896)A03

EERC 70-7 "Influence of Base Rock Characteristics on Ground Response," by J. Lysmer, H.B. Seed and P.B. Schnabel 1970 (PB 197 897)A03

EERC 70-8 "Applicability of Laboratory Test Procedures for Measuring Soil Liquefaction Characteristics under Cyclic Loading," by H.B. Seed and W.H. Peacock - 1970 (PB 198 016)A03

EERC 70-9 "A Simplified Procedure for Evaluating Soil Liquefaction Potential," by H.B. Seed and I.M. Idriss - 1970 (PB 198 009)A03

EERC 70-10 "Soil Moduli and Damping Factors for Dynamic Response Analysis," by H.B. Seed and I.M. Idriss - 1970 (PB 197 869)A03

EERC 71-1 "Koyna Earthquake of December 11, 1967 and the Performance of Koyna Dam," by A.K. Chopra and P. Chakrabarti 1971 (AD 731 496)A06

EERC 71-2 "Preliminary In-Situ Measurements of Anelastic Absorption in Soils Using a Prototype Earthquake Simulator," by R.D. Borcherdt and P.W. Rodgers - 1971 (PB 201 454)A03

EERC 71-3 "Static and Dynamic Analysis of Inelastic Frame Structures," by F.L. Porter and G.H. Powell - 1971 (PB 210 135)A06

EERC 71-4 "Research Needs in Limit Design of Reinforced Concrete Structures," by V.V. Bertero - 1971 (PB 202 943)A04

EERC 71-5 "Dynamic Behavior of a High-Rise Diagonally Braced Steel Building," by D. Rea, A.A. Shah and J.G. Bouwkamp 1971 (PB 203 584)A06

EERC 71-6 "Dynamic Stress Analysis of Porous Elastic Solids Saturated with Compressible Fluids," by J. Ghaboussi and E. L. Wilson - 1971 (PB 211 396)A06

EERC 71-7 "Inelastic Behavior of Steel Beam-to-Column Subassemblages," by H. Krawinkler, V.V. Bertero and E.P. Popov 1971 (PB 211 335)A14

EERC 71-8 "Modification of Seismograph Records for Effects of Local Soil Conditions," by P. Schnabel, H.B. Seed and J. Lysmer - 1971 (PB 214 450)A03

EERC 72-1 "Static and Earthquake Analysis of Three Dimensional Frame and Shear Wall Buildings," by E.L. Wilson and H.H. Dovey - 1972 (PB 212 904)A05

EERC 72-2 "Accelerations in Rock for Earthquakes in the Western United States," by P.B. Schnabel and H.B. Seed - 1972 (PB 213 100)A03

EERC 72-3 "Elastic-Plastic Earthquake Response of Soil-Building Systems," by T. Minami - 1972 (PB 214 868)A08

EERC 72-4 "Stochastic Inelastic Response of Offshore Towers to Strong Motion Earthquakes," by M.K. Kaul - 1972 (PB 215 713)A05

EERC 72-5 "Cyclic Behavior of Three Reinforced Concrete Flexural Members with High Shear," by E.P. Popov, V.V. Bertero and H. Krawinkler - 1972 (PB 214 555)A05

EERC 72-6 "Earthquake Response of Gravity Dams Including Reservoir Interaction Effects," by P. Chakrabarti and A.K. Chopra - 1972 (AD 762 330)A08

EERC 72-7 "Dynamic Properties of Pine Flat Dam," by D. Rea, C.Y. Liaw and A.K. Chopra - 1972 (AD 763 928)A05

EERC 72-8 "Three Dimensional Analysis of Building Systems," by E.L. Wilson and H.H. Dovey - 1972 (PB 222 438)A06

EERC 72-9 "Rate of Loading Effects on Uncracked and Repaired Reinforced Concrete Members," by S. Mahin, V.V. Bertero, D. Rea and M. Atalay - 1972 (PB 224 520)A08

EERC 72-10 "Computer Program for Static and Dynamic Analysis of Linear Structural Systems," by E.L. Wilson, K.-J. Bathe, J.E. Peterson and H.H.Dovey - 1972 (PB 220 437)A04

EERC 72-11 "Literature Survey - Seismic Effects on Highway Bridges," by T. Iwasaki, J. Penzien and R.W. Clough - 1972 (PB 215 613)A19

EERC 72-12 "SHAKE-A Computer Program for Earthquake Response Analysis of Horizontally Layered Sites," by P.B. Schnabel and J. Lysmer - 1972 (PB 220 207)A06

EERC 73-1 "Optimal Seismic Design of Multistory Frames," by V.V. Bertero and H. Kamil - 1973

EERC 73-2 "Analysis of the Slides in the San Fernando Dams During the Earthquake of February 9, 1971," by H.B. Seed, K.L. Lee, I.M. Idriss and F. Makdisi - 1973 (PB 223 402)A14

EERC 73-3 "Computer Aided Ultimate Load Design of Unbraced Multistory Steel Frames," by M.B. El-Hafez and G.H. Powell 1973 (PB 248 315)A09

EERC 73-4 "Experimental Investigation into the Seismic Behavior of Critical Regions of Reinforced Concrete Components as Influenced by Moment and Shear," by M. Celebi and J. Penzien - 1973 (PB 215 884)A09

EERC 73-5 "Hysteretic Behavior of Epoxy-Repaired Reinforced Concrete Beams," by M. Celebi and J. Penzien - 1973 (PB 239 568)A03

EERC 73-6 "General Purpose Computer Program for Inelastic Dynamic Response of Plane Structures," by A. Kanaan and G.H. Powell - 1973 (PB 221 260)A08

EERC 73-7 "A Computer Program for Earthquake Analysis of Gravity Dams Including Reservoir Interaction," by P. Chakrabarti and A.K. Chopra - 1973 (AD 766 271)A04

EERC 73-8 "Behavior of Reinforced Concrete Deep Beam-Column Subassemblages Under Cyclic Loads," by O. Küstü and J.G. Bouwkamp - 1973 (PB 246 117)A12

EERC 73-9 "Earthquake Analysis of Structure-Foundation Systems," by A.K. Vaish and A.K. Chopra - 1973 (AD 766 272)A07

EERC 73-10 "Deconvolution of Seismic Response for Linear Systems," by R.B. Reimer - 1973 (PB 227 179)A08

EERC 73-11 "SAP IV: A Structural Analysis Program for Static and Dynamic Response of Linear Systems," by K.-J. Bathe, E.L. Wilson and F.E. Peterson - 1973 (PB 221 967)A09

EERC 73-12 "Analytical Investigations of the Seismic Response of Long, Multiple Span Highway Bridges," by W.S. Tseng and J. Penzien - 1973 (PB 227 816)A10

EERC 73-13 "Earthquake Analysis of Multi-Story Buildings Including Foundation Interaction," by A.K. Chopra and J.A. Gutierrez - 1973 (PB 222 970)A03

EERC 73-14 "ADAP: A Computer Program for Static and Dynamic Analysis of Arch Dams," by R.W. Clough, J.M. Raphael and S. Mojtahedi - 1973 (PB 223 763)A09

EERC 73-15 "Cyclic Plastic Analysis of Structural Steel Joints," by R.B. Pinkney and R.W. Clough - 1973 (PB 226 843)A08

EERC 73-16 "QUAD-4: A Computer Program for Evaluating the Seismic Response of Soil Structures by Variable Damping Finite Element Procedures," by I.M. Idriss, J. Lysmer, R. Hwang and H.B. Seed - 1973 (PB 229 424)A05

EERC 73-17 "Dynamic Behavior of a Multi-Story Pyramid Shaped Building," by R.M. Stephen, J.P. Hollings and J.G. Bouwkamp - 1973 (PB 240 718)A06

EERC 73-18 "Effect of Different Types of Reinforcing on Seismic Behavior of Short Concrete Columns," by V.V. Bertero, J. Hollings, O. Küstü, R.M. Stephen and J.G. Bouwkamp - 1973

EERC 73-19 "Olive View Medical Center Materials Studies, Phase I," by B. Bresler and V.V. Bertero - 1973 (PB 235 986)A06

EERC 73-20 "Linear and Nonlinear Seismic Analysis Computer Programs for Long Multiple-Span Highway Bridges," by W.S. Tseng and J. Penzien - 1973

EERC 73-21 "Constitutive Models for Cyclic Plastic Deformation of Engineering Materials," by J.M. Kelly and P.P. Gillis 1973 (PB 226 024)A03

EERC 73-22 "DRAIN - 2D User's Guide," by G.H. Powell - 1973 (PB 227 016)A05

EERC 73-23 "Earthquake Engineering at Berkeley - 1973," (PB 226 033)A11

EERC 73-24 Unassigned

EERC 73-25 "Earthquake Response of Axisymmetric Tower Structures Surrounded by Water," by C.Y. Liaw and A.K. Chopra 1973 (AD 773 052)A09

EERC 73-26 "Investigation of the Failures of the Olive View Stairtowers During the San Fernando Earthquake and Their Implications on Seismic Design," by V.V. Bertero and R.G. Collins - 1973 (PB 235 106)A13

EERC 73-27 "Further Studies on Seismic Behavior of Steel Beam-Column Subassemblages," by V.V. Bertero, H. Krawinkler and E.P. Popov - 1973 (PB 234 172)A06

EERC 74-1 "Seismic Risk Analysis," by C.S. Oliveira - 1974 (PB 235 920)A06

EERC 74-2 "Settlement and Liquefaction of Sands Under Multi-Directional Shaking," by R. Pyke, C.K. Chan and H.B. Seed 1974

EERC 74-3 "Optimum Design of Earthquake Resistant Shear Buildings," by D. Ray, K.S. Pister and A.K. Chopra - 1974 (PB 231 172)A06

EERC 74-4 "LUSH - A Computer Program for Complex Response Analysis of Soil-Structure Systems," by J. Lysmer, T. Udaka, H.B. Seed and R. Hwang - 1974 (PB 236 796)A05

EERC 74-5 "Sensitivity Analysis for Hysteretic Dynamic Systems: Applications to Earthquake Engineering," by D. Ray 1974 (PB 233 213)A06

EERC 74-6 "Soil Structure Interaction Analyses for Evaluating Seismic Response," by H.B. Seed, J. Lysmer and R. Hwang 1974 (PB 236 519)A04

EERC 74-7 Unassigned

EERC 74-8 "Shaking Table Tests of a Steel Frame - A Progress Report," by R.W. Clough and D. Tang - 1974 (PB 240 869)A03

EERC 74-9 "Hysteretic Behavior of Reinforced Concrete Flexural Members with Special Web Reinforcement," by V.V. Bertero, E.P. Popov and T.Y. Wang - 1974 (PB 236 797)A07

EERC 74-10 "Applications of Reliability-Based, Global Cost Optimization to Design of Earthquake Resistant Structures," by E. Vitiello and K.S. Pister - 1974 (PB 237 231)A06

EERC 74-11 "Liquefaction of Gravelly Soils Under Cyclic Loading Conditions," by R.T. Wong, H.B. Seed and C.K. Chan 1974 (PB 242 042)A03

EERC 74-12 "Site-Dependent Spectra for Earthquake-Resistant Design," by H.B. Seed, C. Ugas and J. Lysmer - 1974 (PB 240 953)A03

EERC 74-13 "Earthquake Simulator Study of a Reinforced Concrete Frame," by P. Hidalgo and R.W. Clough - 1974 (PB 241 944)A13

EERC 74-14 "Nonlinear Earthquake Response of Concrete Gravity Dams," by N. Pal - 1974 (AD/A 006 583)A06

EERC 74-15 "Modeling and Identification in Nonlinear Structural Dynamics - I. One Degree of Freedom Models," by N. Distefano and A. Rath - 1974 (PB 241 548)A06

EERC 75-1 "Determination of Seismic Design Criteria for the Dumbarton Bridge Replacement Structure, Vol. I: Description, Theory and Analytical Modeling of Bridge and Parameters," by F. Baron and S.-H. Pang - 1975 (PB 259 407)A15

EERC 75-2 "Determination of Seismic Design Criteria for the Dumbarton Bridge Replacement Structure, Vol. II: Numerical Studies and Establishment of Seismic Design Criteria," by F. Baron and S.-H. Pang - 1975 (PB 259 408)A11 (For set of EERC 75-1 and 75-2 (PB 259 406))

EERC 75-3 "Seismic Risk Analysis for a Site and a Metropolitan Area," by C.S. Oliveira - 1975 (PB 248 134)A09

EERC 75-4 "Analytical Investigations of Seismic Response of Short, Single or Multiple-Span Highway Bridges," by M.-C. Chen and J. Penzien - 1975 (PB 241 454)A09

EERC 75-5 "An Evaluation of Some Methods for Predicting Seismic Behavior of Reinforced Concrete Buildings," by S.A. Mahin and V.V. Bertero - 1975 (PB 246 306)A16

EERC 75-6 "Earthquake Simulator Study of a Steel Frame Structure, Vol. I: Experimental Results," by R.W. Clough and D.T. Tang - 1975 (PB 243 981)A13

EERC 75-7 "Dynamic Properties of San Bernardino Intake Tower," by D. Rea, C.-Y. Liaw and A.K. Chopra - 1975 (AD/A008 406) A05

EERC 75-8 "Seismic Studies of the Articulation for the Dumbarton Bridge Replacement Structure, Vol. I: Description, Theory and Analytical Modeling of Bridge Components," by F. Baron and R.E. Hamati - 1975 (PB 251 539)A07

EERC 75-9 "Seismic Studies of the Articulation for the Dumbarton Bridge Replacement Structure, Vol. 2: Numerical Studies of Steel and Concrete Girder Alternates," by F. Baron and R.E. Hamati - 1975 (PB 251 540)A10

EERC 75-10 "Static and Dynamic Analysis of Nonlinear Structures," by D.P. Mondkar and G.H. Powell - 1975 (PB 242 434)A08

EERC 75-11 "Hysteretic Behavior of Steel Columns," by E.P. Popov, V.V. Bertero and S. Chandramouli - 1975 (PB 252 365)A11

EERC 75-12 "Earthquake Engineering Research Center Library Printed Catalog," - 1975 (PB 243 711)A26

EERC 75-13 "Three Dimensional Analysis of Building Systems (Extended Version)," by E.L. Wilson, J.P. Hollings and H.H. Dovey - 1975 (PB 243 989)A07

EERC 75-14 "Determination of Soil Liquefaction Characteristics by Large-Scale Laboratory Tests," by P. De Alba, C.K. Chan and H.B. Seed - 1975 (NUREG 0027)A08

EERC 75-15 "A Literature Survey - Compressive, Tensile, Bond and Shear Strength of Masonry," by R.L. Mayes and R.W. Clough - 1975 (PB 246 292)A10

EERC 75-16 "Hysteretic Behavior of Ductile Moment Resisting Reinforced Concrete Frame Components," by V.V. Bertero and E.P. Popov - 1975 (PB 246 388)A05

EERC 75-17 "Relationships Between Maximum Acceleration, Maximum Velocity, Distance from Source, Local Site Conditions for Moderately Strong Earthquakes," by H.B. Seed, R. Murarka, J. Lysmer and I.M. Idriss - 1975 (PB 248 172)A03

EERC 75-18 "The Effects of Method of Sample Preparation on the Cyclic Stress-Strain Behavior of Sands," by J. Mulilis, C.K. Chan and H.B. Seed - 1975 (Summarized in EERC 75-28)

EERC 75-19 "The Seismic Behavior of Critical Regions of Reinforced Concrete Components as Influenced by Moment, Shear and Axial Force," by M.B. Atalay and J. Penzien - 1975 (PB 258 842)A11

EERC 75-20 "Dynamic Properties of an Eleven Story Masonry Building," by R.M. Stephen, J.P. Hollings, J.G. Bouwkamp and D. Jurukovski - 1975 (PB 246 945)A04

EERC 75-21 "State-of-the-Art in Seismic Strength of Masonry - An Evaluation and Review," by R.L. Mayes and R.W. Clough 1975 (PB 249 040)A07

EERC 75-22 "Frequency Dependent Stiffness Matrices for Viscoelastic Half-Plane Foundations," by A.K. Chopra, P. Chakrabarti and G. Dasgupta - 1975 (PB 248 121)A07

EERC 75-23 "Hysteretic Behavior of Reinforced Concrete Framed Walls," by T.Y. Wong, V.V. Bertero and E.P. Popov - 1975

EERC 75-24 "Testing Facility for Subassemblages of Frame-Wall Structural Systems," by V.V. Bertero, E.P. Popov and T. Endo - 1975

EERC 75-25 "Influence of Seismic History on the Liquefaction Characteristics of Sands," by H.B. Seed, K. Mori and C.K. Chan - 1975 (Summarized in EERC 75-28)

EERC 75-26 "The Generation and Dissipation of Pore Water Pressures during Soil Liquefaction," by H.B. Seed, P.P. Martin and J. Lysmer - 1975 (PB 252 648)A03

EERC 75-27 "Identification of Research Needs for Improving Aseismic Design of Building Structures," by V.V. Bertero 1975 (PB 248 136)A05

EERC 75-28 "Evaluation of Soil Liquefaction Potential during Earthquakes," by H.B. Seed, I. Arango and C.K. Chan - 1975 (NUREG 0026)A13

EERC 75-29 "Representation of Irregular Stress Time Histories by Equivalent Uniform Stress Series in Liquefaction Analyses," by H.B. Seed, I.M. Idriss, F. Makdisi and N. Banerjee - 1975 (PB 252 635)A03

EERC 75-30 "FLUSH - A Computer Program for Approximate 3-D Analysis of Soil-Structure Interaction Problems," by J. Lysmer, T. Udaka, C.-F. Tsai and H.B. Seed - 1975 (PB 259 332)A07

EERC 75-31 "ALUSH - A Computer Program for Seismic Response Analysis of Axisymmetric Soil-Structure Systems," by E. Berger, J. Lysmer and H.B. Seed - 1975

EERC 75-32 "TRIP and TRAVEL - Computer Programs for Soil-Structure Interaction Analysis with Horizontally Travelling Waves," by T. Udaka, J. Lysmer and H.B. Seed - 1975

EERC 75-33 "Predicting the Performance of Structures in Regions of High Seismicity," by J. Penzien - 1975 (PB 248 130)A03

EERC 75-34 "Efficient Finite Element Analysis of Seismic Structure - Soil - Direction," by J. Lysmer, H.B. Seed, T. Udaka, R.N. Hwang and C.-F. Tsai - 1975 (PB 253 570)A03

EERC 75-35 "The Dynamic Behavior of a First Story Girder of a Three-Story Steel Frame Subjected to Earthquake Loading," by R.W. Clough and L.-Y. Li - 1975 (PB 248 841)A05

EERC 75-36 "Earthquake Simulator Study of a Steel Frame Structure, Volume II - Analytical Results," by D.T. Tang - 1975 (PB 252 926)A10

EERC 75-37 "ANSR-I General Purpose Computer Program for Analysis of Non-Linear Structural Response," by D.P. Mondkar and G.H. Powell - 1975 (PB 252 386)A08

EERC 75-38 "Nonlinear Response Spectra for Probabilistic Seismic Design and Damage Assessment of Reinforced Concrete Structures," by M. Murakami and J. Penzien - 1975 (PB 259 530)A05

EERC 75-39 "Study of a Method of Feasible Directions for Optimal Elastic Design of Frame Structures Subjected to Earthquake Loading," by N.D. Walker and K.S. Pister - 1975 (PB 257 781)A06

EERC 75-40 "An Alternative Representation of the Elastic-Viscoelastic Analogy," by G. Dasgupta and J.L. Sackman - 1975 (PB 252 173)A03

EERC 75-41 "Effect of Multi-Directional Shaking on Liquefaction of Sands," by H.B. Seed, R. Pyke and G.R. Martin - 1975 (PB 258 781)A03

EERC 76-1 "Strength and Ductility Evaluation of Existing Low-Rise Reinforced Concrete Buildings - Screening Method," by T. Okada and B. Bresler - 1976 (PB 257 906)A11

EERC 76-2 "Experimental and Analytical Studies on the Hysteretic Behavior of Reinforced Concrete Rectangular and T-Beams," by S.-Y.M. Ma, E.P. Popov and V.V. Bertero - 1976 (PB 260 843)A12

EERC 76-3 "Dynamic Behavior of a Multistory Triangular-Shaped Building," by J. Petrovski, R.M. Stephen, E. Gartenbaum and J.G. Bouwkamp - 1976 (PB 273 279)A07

EERC 76-4 "Earthquake Induced Deformations of Earth Dams," by N. Serff, H.B. Seed, F.I. Makdisi & C.-Y. Chang - 19[illegible] (PB 292 065)A08

EERC 76-5 "Analysis and Design of Tube-Type Tall Building Structures," by H. de Clercq and G.H. Powell - 1976 (PB 252 220) A10

EERC 76-6 "Time and Frequency Domain Analysis of Three-Dimensional Ground Motions, San Fernando Earthquake," by T. Kubo and J. Penzien (PB 260 556)A11

EERC 76-7 "Expected Performance of Uniform Building Code Design Masonry Structures," by R.L. Mayes, Y. Omote, S.W. Chen and R.W. Clough - 1976 (PB 270 098)A05

EERC 76-8 "Cyclic Shear Tests of Masonry Piers, Volume 1 - Test Results," by R.L. Mayes, Y. Omote, R.W. Clough - 1976 (PB 264 424)A06

EERC 76-9 "A Substructure Method for Earthquake Analysis of Structure - Soil Interaction," by J.A. Gutierrez and A.K. Chopra - 1976 (PB 257 783)A08

EERC 76-10 "Stabilization of Potentially Liquefiable Sand Deposits using Gravel Drain Systems," by H.B. Seed and J.R. Booker - 1976 (PB 258 820)A04

EERC 76-11 "Influence of Design and Analysis Assumptions on Computed Inelastic Response of Moderately Tall Frames," by G.H. Powell and D.G. Row - 1976 (PB 271 409)A06

EERC 76-12 "Sensitivity Analysis for Hysteretic Dynamic Systems: Theory and Applications," by D. Ray, K.S. Pister and E. Polak - 1976 (PB 262 859)A04

EERC 76-13 "Coupled Lateral Torsional Response of Buildings to Ground Shaking," by C.L. Kan and A.K. Chopra - 1976 (PB 257 907)A09

EERC 76-14 "Seismic Analyses of the Banco de America," by V.V. Bertero, S.A. Mahin and J.A. Hollings - 1976

EERC 76-15 "Reinforced Concrete Frame 2: Seismic Testing and Analytical Correlation," by R.W. Clough and J. Gidwani - 1976 (PB 261 323)A08

EERC 76-16 "Cyclic Shear Tests of Masonry Piers, Volume 2 - Analysis of Test Results," by R.L. Mayes, Y. Omote and R.W. Clough - 1976

EERC 76-17 "Structural Steel Bracing Systems: Behavior Under Cyclic Loading," by E.P. Popov, K. Takanashi and C.W. Roeder - 1976 (PB 260 715)A05

EERC 76-18 "Experimental Model Studies on Seismic Response of High Curved Overcrossings," by D. Williams and W.G. Godden - 1976 (PB 269 548)A08

EERC 76-19 "Effects of Non-Uniform Seismic Disturbances on the Dumbarton Bridge Replacement Structure," by F. Baron and R.E. Hamati - 1976 (PB 282 981)A16

EERC 76-20 "Investigation of the Inelastic Characteristics of a Single Story Steel Structure Using System Identification and Shaking Table Experiments," by V.C. Matzen and H.D. McNiven - 1976 (PB 258 453)A07

EERC 76-21 "Capacity of Columns with Splice Imperfections," by E.P. Popov, R.M. Stephen and R. Philbrick - 1976 (PB 260 378)A04

EERC 76-22 "Response of the Olive View Hospital Main Building during the San Fernando Earthquake," by S. A. Mahin, V.V. Bertero, A.K. Chopra and R. Collins - 1976 (PB 271 425)A14

EERC 76-23 "A Study on the Major Factors Influencing the Strength of Masonry Prisms," by N.M. Mostaghel, R.L. Mayes, R. W. Clough and S.W. Chen - 1976 (Not published)

EERC 76-24 "GADFLEA - A Computer Program for the Analysis of Pore Pressure Generation and Dissipation during Cyclic or Earthquake Loading," by J.R. Booker, M.S. Rahman and H.B. Seed - 1976 (PB 263 947)A04

EERC 76-25 "Seismic Safety Evaluation of a R/C School Building," by B. Bresler and J. Axley - 1976

EERC 76-26 "Correlative Investigations on Theoretical and Experimental Dynamic Behavior of a Model Bridge Structure," by K. Kawashima and J. Penzien - 1976 (PB 263 388)A11

EERC 76-27 "Earthquake Response of Coupled Shear Wall Buildings," by T. Srichatrapimuk - 1976 (PB 265 157)A07

EERC 76-28 "Tensile Capacity of Partial Penetration Welds," by E.P. Popov and R.M. Stephen - 1976 (PB 262 899)A03

EERC 76-29 "Analysis and Design of Numerical Integration Methods in Structural Dynamics," by H.M. Hilber - 1976 (PB 264 410)A06

EERC 76-30 "Contribution of a Floor System to the Dynamic Characteristics of Reinforced Concrete Buildings," by L.E. Malik and V.V. Bertero - 1976 (PB 272 247)A13

EERC 76-31 "The Effects of Seismic Disturbances on the Golden Gate Bridge," by F. Baron, M. Arikan and R.E. Hamati - 1976 (PB 272 279)A09

EERC 76-32 "Infilled Frames in Earthquake Resistant Construction," by R.E. Klingner and V.V. Bertero - 1976 (PB 265 892)A13

UCB/EERC-77/01 "PLUSH - A Computer Program for Probabilistic Finite Element Analysis of Seismic Soil-Structure Interaction," by M.P. Romo Organista, J. Lysmer and H.B. Seed - 1977

UCB/EERC-77/02 "Soil-Structure Interaction Effects at the Humboldt Bay Power Plant in the Ferndale Earthquake of June 7, 1975," by J.E. Valera, H.B. Seed, C.F. Tsai and J. Lysmer - 1977 (PB 265 795)A04

UCB/EERC-77/03 "Influence of Sample Disturbance on Sand Response to Cyclic Loading," by K. Mori, H.B. Seed and C.K. Chan - 1977 (PB 267 352)A04

UCB/EERC-77/04 "Seismological Studies of Strong Motion Records," by J. Shoja-Taheri - 1977 (PB 269 655)A10

UCB/EERC-77/05 "Testing Facility for Coupled-Shear Walls," by L. Li-Hyung, V.V. Bertero and E.P. Popov - 1977

UCB/EERC-77/06 "Developing Methodologies for Evaluating the Earthquake Safety of Existing Buildings," by No. 1 - B. Bresler; No. 2 - B. Bresler, T. Okada and D. Zisling; No. 3 - T. Okada and B. Bresler; No. 4 - V.V. Bertero and B. Bresler - 1977 (PB 267 354)A08

UCB/EERC-77/07 "A Literature Survey - Transverse Strength of Masonry Walls," by Y. Omote, R.L. Mayes, S.W. Chen and R.W. Clough - 1977 (PB 277 933)A07

UCB/EERC-77/08 "DRAIN-TABS: A Computer Program for Inelastic Earthquake Response of Three Dimensional Buildings," by R. Guendelman-Israel and G.H. Powell - 1977 (PB 270 693)A07

UCB/EERC-77/09 "SUBWALL: A Special Purpose Finite Element Computer Program for Practical Elastic Analysis and Design of Structural Walls with Substructure Option," by D.Q. Le, H. Peterson and E.P. Popov - 1977 (PB 270 567)A05

UCB/EERC-77/10 "Experimental Evaluation of Seismic Design Methods for Broad Cylindrical Tanks," by D.P. Clough (PB 272 280)A13

UCB/EERC-77/11 "Earthquake Engineering Research at Berkeley - 1976," - 1977 (PB 273 507)A09

UCB/EERC-77/12 "Automated Design of Earthquake Resistant Multistory Steel Building Frames," by N.D. Walker, Jr. - 1977 (PB 276 526)A09

UCB/EERC-77/13 "Concrete Confined by Rectangular Hoops Subjected to Axial Loads," by J. Vallenas, V.V. Bertero and E.P. Popov - 1977 (PB 275 165)A06

UCB/EERC-77/14 "Seismic Strain Induced in the Ground During Earthquakes," by Y. Sugimura - 1977 (PB 284 201)A04

UCB/EERC-77/15 "Bond Deterioration under Generalized Loading," by V.V. Bertero, E.P. Popov and S. Viwathanatepa - 1977

UCB/EERC-77/16 "Computer Aided Optimum Design of Ductile Reinforced Concrete Moment Resisting Frames," by S.W. Zagajeski and V.V. Bertero - 1977 (PB 280 137)A07

UCB/EERC-77/17 "Earthquake Simulation Testing of a Stepping Frame with Energy-Absorbing Devices," by J.M. Kelly and D.F. Tsztoo - 1977 (PB 273 506)A04

UCB/EERC-77/18 "Inelastic Behavior of Eccentrically Braced Steel Frames under Cyclic Loadings," by C.W. Roeder and E.P. Popov - 1977 (PB 275 526)A15

UCB/EERC-77/19 "A Simplified Procedure for Estimating Earthquake-Induced Deformations in Dams and Embankments," by F.I. Makdisi and H.B. Seed - 1977 (PB 276 820)A04

UCB/EERC-77/20 "The Performance of Earth Dams during Earthquakes," by H.B. Seed, F.I. Makdisi and P. de Alba - 1977 (PB 276 821)A04

UCB/EERC-77/21 "Dynamic Plastic Analysis Using Stress Resultant Finite Element Formulation," by P. Lukkunapvasit and J.M. Kelly - 1977 (PB 275 453)A04

UCB/EERC-77/22 "Preliminary Experimental Study of Seismic Uplift of a Steel Frame," by R.W. Clough and A.A. Huckelbridge 1977 (PB 278 769)A08

UCB/EERC-77/23 "Earthquake Simulator Tests of a Nine-Story Steel Frame with Columns Allowed to Uplift," by A.A. Huckelbridge - 1977 (PB 277 944)A09

UCB/EERC-77/24 "Nonlinear Soil-Structure Interaction of Skew Highway Bridges," by M.-C. Chen and J. Penzien - 1977 (PB 276 176)A07

UCB/EERC-77/25 "Seismic Analysis of an Offshore Structure Supported on Pile Foundations," by D.D.-N. Liou and J. Penzien 1977 (PB 283 180)A06

UCB/EERC-77/26 "Dynamic Stiffness Matrices for Homogeneous Viscoelastic Half-Planes," by G. Dasgupta and A.K. Chopra - 1977 (PB 279 654)A06

UCB/EERC-77/27 "A Practical Soft Story Earthquake Isolation System," by J.M. Kelly, J.M. Eidinger and C.J. Derham - 1977 (PB 276 814)A07

UCB/EERC-77/28 "Seismic Safety of Existing Buildings and Incentives for Hazard Mitigation in San Francisco: An Exploratory Study," by A.J. Meltsner - 1977 (PB 281 970)A05

UCB/EERC-77/29 "Dynamic Analysis of Electrohydraulic Shaking Tables," by D. Rea, S. Abedi-Hayati and Y. Takahashi 1977 (PB 282 569)A04

UCB/EERC-77/30 "An Approach for Improving Seismic - Resistant Behavior of Reinforced Concrete Interior Joints," by B. Galunic, V.V. Bertero and E.P. Popov - 1977 (PB 290 870)A06

UCB/EERC-78/01 "The Development of Energy-Absorbing Devices for Aseismic Base Isolation Systems," by J.M. Kelly and D.F. Tsztoo - 1978 (PB 284 978)A04

UCB/EERC-78/02 "Effect of Tensile Prestrain on the Cyclic Response of Structural Steel Connections, by J.G. Bouwkamp and A. Mukhopadhyay - 1978

UCB/EERC-78/03 "Experimental Results of an Earthquake Isolation System using Natural Rubber Bearings," by J.M. Eidinger and J.M. Kelly - 1978 (PB 281 686)A04

UCB/EERC-78/04 "Seismic Behavior of Tall Liquid Storage Tanks," by A. Niwa - 1978 (PB 284 017)A14

UCB/EERC-78/05 "Hysteretic Behavior of Reinforced Concrete Columns Subjected to High Axial and Cyclic Shear Forces," by S.W. Zagajeski, V.V. Bertero and J.G. Bouwkamp - 1978 (PB 283 858)A13

UCB/EERC-78/06 "Inelastic Beam-Column Elements for the ANSR-I Program," by A. Riahi, D.G. Row and G.H. Powell - 1978

UCB/EERC-78/07 "Studies of Structural Response to Earthquake Ground Motion," by O.A. Lopez and A.K. Chopra - 1978 (PB 282 790)A05

UCB/EERC-78/08 "A Laboratory Study of the Fluid-Structure Interaction of Submerged Tanks and Caissons in Earthquakes," by R.C. Byrd - 1978 (PB 284 957)A08

UCB/EERC-78/09 "Model for Evaluating Damageability of Structures," by I. Sakamoto and B. Bresler - 1978

UCB/EERC-78/10 "Seismic Performance of Nonstructural and Secondary Structural Elements," by I. Sakamoto - 1978

UCB/EERC-78/11 "Mathematical Modelling of Hysteresis Loops for Reinforced Concrete Columns," by S. Nakata, T. Sproul and J. Penzien - 1978

UCB/EERC-78/12 "Damageability in Existing Buildings," by T. Blejwas and B. Bresler - 1978

UCB/EERC-78/13 "Dynamic Behavior of a Pedestal Base Multistory Building," by R.M. Stephen, E.L. Wilson, J.G. Bouwkamp and M. Button - 1978 (PB 286 650)A08

UCB/EERC-78/14 "Seismic Response of Bridges - Case Studies," by R.A. Imbsen, V. Nutt and J. Penzien - 1978 (PB 286 503)A10

UCB/EERC-78/15 "A Substructure Technique for Nonlinear Static and Dynamic Analysis," by D.G. Row and G.H. Powell - 1978 (PB 288 077)A10

UCB/EERC-78/16 "Seismic Risk Studies for San Francisco and for the Greater San Francisco Bay Area," by C.S. Oliveira - 1978

UCB/EERC-78/17 "Strength of Timber Roof Connections Subjected to Cyclic Loads," by P. Gülkan, R.L. Mayes and R.W. Clough - 1978

UCB/EERC-78/18 "Response of K-Braced Steel Frame Models to Lateral Loads," by J.G. Bouwkamp, R.M. Stephen and E.P. Popov - 1978

UCB/EERC-78/19 "Rational Design Methods for Light Equipment in Structures Subjected to Ground Motion," by J.L. Sackman and J.M. Kelly - 1978 (PB 292 357)A04

UCB/EERC-78/20 "Testing of a Wind Restraint for Aseismic Base Isolation," by J.M. Kelly and D.E. Chitty - 1978 (PB 292 833)A03

UCB/EERC-78/21 "APOLLO - A Computer Program for the Analysis of Pore Pressure Generation and Dissipation in Horizontal Sand Layers During Cyclic or Earthquake Loading," by P.P. Martin and H.B. Seed - 1978 (PB 292 835)A04

UCB/EERC-78/22 "Optimal Design of an Earthquake Isolation System," by M.A. Bhatti, K.S. Pister and E. Polak - 1978 (PB 294 735)A06

UCB/EERC-78/23 "MASH - A Computer Program for the Non-Linear Analysis of Vertically Propagating Shear Waves in Horizontally Layered Deposits," by P.P. Martin and H.B. Seed - 1978 (PB 293 101)A05

UCB/EERC-78/24 "Investigation of the Elastic Characteristics of a Three Story Steel Frame Using System Identification," by I. Kaya and H.D. McNiven - 1978

UCB/EERC-78/25 "Investigation of the Nonlinear Characteristics of a Three-Story Steel Frame Using System Identification," by I. Kaya and H.D. McNiven - 1978

UCB/EERC-78/26 "Studies of Strong Ground Motion in Taiwan," by Y.M. Hsiung, B.A. Bolt and J. Penzien - 1978

UCB/EERC-78/27 "Cyclic Loading Tests of Masonry Single Piers: Volume 1 - Height to Width Ratio of 2," by P.A. Hidalgo, R.L. Mayes, H.D. McNiven and R.W. Clough - 1978

UCB/EERC-78/28 "Cyclic Loading Tests of Masonry Single Piers: Volume 2 - Height to Width Ratio of 1," by S.-W.J. Chen, P.A. Hidalgo, R.L. Mayes, R.W. Clough and H.D. McNiven - 1978

UCB/EERC-78/29 "Analytical Procedures in Soil Dynamics," by J. Lysmer - 1978

UCB/EERC-79/01 "Hysteretic Behavior of Lightweight Reinforced Concrete Beam-Column Subassemblages," by B. Forzani, E.P. Popov, and V.V. Bertero - 1979

UCB/EERC-79/02 "The Development of a Mathematical Model to Predict the Flexural Response of Reinforced Concrete Beams to Cyclic Loads, Using System Identification," by J.F. Stanton and H.D. McNiven - 1979

UCB/EERC-79/03 "Linear and Nonlinear Earthquake Response of Simple Torsionally Coupled Systems," by C.L. Kan and A.K. Chopra - 1979

UCB/EERC-79/04 "A Mathematical Model of Masonry for Predicting Its Linear Seismic Response Characteristics," by Y. Mengi and H.D. McNiven - 1979

UCB/EERC-79/05 "Mechanical Behavior of Lightweight Concrete Confined by Different Types of Lateral Reinforcement," by M.A. Manrique, V.V. Bertero and E.P. Popov - 1979

UCB/EERC-79/06 "Static Tilt Tests of a Tall Cylindrical Liquid Storage Tank," by R.W. Clough and A. Niwa - 1979

UCB/EERC-79/07 "The Design of Steel Energy Absorbing Restrainers and Their Incorporation Into Nuclear Power Plants for Enhanced Safety: Volume 1 - Summary Report," by P.N. Spencer, V.F. Zackay, and E.R. Parker - 1979

UCB/EERC-79/08 "The Design of Steel Energy Absorbing Restrainers and Their Incorporation Into Nuclear Power Plants for Enhanced Safety: Volume 2 - The Development of Analyses for Reactor System Piping," "Simple Systems" by M.C. Lee, J. Penzien, A.K. Chopra, and K. Suzuki "Complex Systems" by G.H. Powell, E.L. Wilson,R.W. Clough and D.G. Row - 1979

UCB/EERC-79/09 "The Design of Steel Energy Absorbing Restrainers and Their Incorporation Into Nuclear Power Plants for Enhanced Safety: Volume 3 - Evaluation of Commerical Steels," by W.S. Owen, R.M.N. Pelloux, R.O. Ritchie, M. Faral, T. Ohhashi, J. Toplosky, S.J. Hartman, V.F. Zackay, and E.R. Parker - 1979

UCB/EERC-79/10 "The Design of Steel Energy Absorbing Restrainers and Their Incorporation Into Nuclear Power Plants for Enhanced Safety: Volume 4 - A Review of Energy-Absorbing Devices," by J.M. Kelly and M.S. Skinner - 1979

UCB/EERC-79/11 "Conservatism In Summation Rules for Closely Spaced Modes," by J.M. Kelly and J.L. Sackman - 1979

UCB/EERC-79/12 "Cyclic Loading Tests of Masonry Single Piers Volume 3 - Height to Width Ratio of 0.5," by P.A. Hidalgo, R.L. Mayes, H.D. McNiven and R.W. Clough - 1979

UCB/EERC-79/13 "Cyclic Behavior of Dense Coarse-Grained Materials in Relation to the Seismic Stability of Dams," by N.G. Banerjee, H.B. Seed and C.K. Chan - 1979

UCB/EERC-79/14 "Seismic Behavior of Reinforced Concrete Interior Beam-Column Subassemblages," by S. Viwathanatepa, E.P. Popov and V.V. Bertero - 1979

UCB/EERC-79/15 "Optimal Design of Localized Nonlinear Systems with Dual Performance Criteria Under Earthquake Excitations," by M.A. Bhatti - 1979

UCB/EERC-79/16 "OPTDYN - A General Purpose Optimization Program for Problems with or without Dynamic Constraints," by M.A. Bhatti, E. Polak and K.S. Pister - 1979

UCB/EERC-79/17 "ANSR-II, Analysis of Nonlinear Structural Response, Users Manual," by D.P. Mondkar and G.H. Powell - 1979

UCB/EERC-79/18 "Soil Structure Interaction in Different Seismic Environments," A. Gomez-Masso, J. Lysmer, J.-C. Chen and H.B. Seed - 1979

UCB/EERC-79/19 "ARMA Models for Earthquake Ground Motions," by M.K. Chang, J.W. Kwiatkowski, R.F. Nau, R.M. Oliver and K.S. Pister - 1979

UCB/EERC-79/20 "Hysteretic Behavior of Reinforced Concrete Structural Walls," by J.M. Vallenas, V.V. Bertero and E.P. Popov - 1979

UCB/EERC-79/21 "Studies on High-Frequency Vibrations of Buildings I: The Column Effects," by J. Lubliner - 1979

UCB/EERC-79/22 "Effects of Generalized Loadings on Bond Reinforcing Bars Embedded in Confined Concrete Blocks," by S. Viwathanatepa, E.P. Popov and V.V. Bertero - 1979

UCB/EERC-79/23 "Shaking Table Study of Single-Story Masonry Houses, Volume 1: Test Structures 1 and 2," by P. Gülkan, R.L. Mayes and R.W. Clough - 1979

UCB/EERC-79/24 "Shaking Table Study of Single-Story Masonry Houses, Volume 2: Test Structures 3 and 4," by P. Gülkan, R.L. Mayes and R.W. Clough - 1979

UCB/EERC-79/25 "Shaking Table Study of Single-Story Masonry Houses, Volume 3: Summary, Conclusions and Recommendations," by R.W. Clough, R.L. Mayes and P. Gülkan - 1979

UCB/EERC-79/26 "Recommendations for a U.S.-Japan Cooperative Research Program Utilizing Large-Scale Testing Facilities," by U.S.-Japan Planning Group - 1979

UCB/EERC-79/27 "Earthquake-Induced Liquefaction Near Lake Amatitlan, Guatemala," by H.B. Seed, I. Arango, C.K. Chan, A. Gomez-Masso and R. Grant de Ascoli - 1979

UCB/EERC-79/28 "Infill Panels: Their Influence on Seismic Response of Buildings," by J.W. Axley and V.V. Bertero - 1979

UCB/EERC-79/29 "3D Truss Bar Element (Type 1) for the ANSR-II Program," by D.P. Mondkar and G.H. Powell - 1979

UCB/EERC-79/30 "2D Beam-Column Element (Type 5 - Parallel Element Theory) for the ANSR-II Program," by D.G. Row, G.H. Powell and D.P. Mondkar

UCB/EERC-79/31 "3D Beam-Column Element (Type 2 - Parallel Element Theory) for the ANSR-II Program," by A. Riahi, G.H. Powell and D.P. Mondkar - 1979

UCB/EERC-79/32 "On Response of Structures to Stationary Excitation," by A. Der Kiureghian - 1979

UCB/EERC-79/33 "Undisturbed Sampling and Cyclic Load Testing of Sands," by S. Singh, H.B. Seed and C.K. Chan - 1979

UCB/EERC-79/34 "Interaction Effects of Simultaneous Torsional and Compressional Cyclic Loading of Sand," by P.M. Griffin and W.N. Houston - 1979

UCB/EERC-80/01 "Earthquake Response of Concrete Gravity Dams Including Hydrodynamic and Foundation Interaction Effects," by A.K. Chopra, P. Chakrabarti and S. Gupta - 1980

UCB/EERC-80/02 "Rocking Response of Rigid Blocks to Earthquakes," by C.S. Yim, A.K. Chopra and J. Penzien - 1980

UCB/EERC-80/03 "Optimum Inelastic Design of Seismic-Resistant Reinforced Concrete Frame Structures," by S.W. Zagajeski and V.V. Bertero - 1980

UCB/EERC-80/04 "Effects of Amount and Arrangement of Wall-Panel Reinforcement on Hysteretic Behavior of Reinforced Concrete Walls," by R. Iliya and V.V. Bertero - 1980

UCB/EERC-80/05 "Shaking Table Research on Concrete Dam Models," by A. Niwa and R.W. Clough - 1980

UCB/EERC-80/06 "Piping With Energy Absorbing Restrainers: Parameter Study on Small Systems," by G.H. Powell, C. Oughourlian and J. Simons - 1980

UCB/EERC-80/07 "Inelastic Torsional Response of Structures Subjected to Earthquake Ground Motions," by Y. Yamazaki - 1980

UCB/EERC-80/08 "Study of X-Braced Steel Frame Structures Under Earthquake Simulation," by Y. Ghanaat - 1980

UCB/EERC-80/09 "Hybrid Modelling of Soil-Structure Interaction," by S. Gupta, T.W. Lin, J. Penzien and C.S. Yeh - 1980

UCB/EERC-80/10 "General Applicability of a Nonlinear Model of a One Story Steel Frame," by B.I. Sveinsson and H. McNiven - 1980

UCB/EERC-80/11 "A Green-Function Method for Wave Interaction with a Submerged Body," by W. Kioka - 1980

UCB/EERC-80/12 "Hydrodynamic Pressure and Added Mass for Axisymmetric Bodies," by F. Nilrat - 1980

UCB/EERC-80/13 "Treatment of Non-Linear Drag Forces Acting on Offshore Platforms," by B.V. Dao and J. Penzien - 1980

UCB/EERC-80/14 "2D Plane/Axisymmetric Solid Element (Type 3 - Elastic or Elastic-Perfectly Plastic) for the ANSR-II Program," by D.P. Mondkar and G.H. Powell - 1980

UCB/EERC-80/15 "A Response Spectrum Method for Random Vibrations," by A. Der Kiureghian - 1980

UCB/EERC-80/16 "Cyclic Inelastic Buckling of Tubular Steel Braces," by V.A. Zayas, E.P. Popov and S.A. Mahin - June 1980

UCB/EERC-80/17 "Dynamic Response of Simple Arch Dams Including Hydrodynamic Interaction," by C.S. Porter and A.K. Chopra - July 1980

UCB/EERC-80/18 "Experimental Testing of a Friction Damped Aseismic Base Isolation System with Fail-Safe Characteristics," by J.M. Kelly, K.E. Beucke and M.S. Skinner - July 1980

UCB/EERC-80/19 "The Design of Steel Energy-Absorbing Restrainers and their Incorporation into Nuclear Power Plants for Enhanced Safety (Vol 1B): Stochastic Seismic Analyses of Nuclear Power Plant Structures and Piping Systems Subjected to Multiple Support Excitations," by M.C. Lee and J. Penzien - 1980

UCB/EERC-80/20 "The Design of Steel Energy-Absorbing Restrainers and their Incorporation into Nuclear Power Plants for Enhanced Safety (Vol 1C): Numerical Method for Dynamic Substructure Analysis," by J.M. Dickens and E.L. Wilson - 1980

UCB/EERC-80/21 "The Design of Steel Energy-Absorbing Restrainers and their Incorporation into Nuclear Power Plants for Enhanced Safety (Vol 2): Development and Testing of Restraints for Nuclear Piping Systems," by J.M. Kelly and M.S. Skinner - 1980

UCB/EERC-80/22 "3D Solid Element (Type 4-Elastic or Elastic-Perfectly-Plastic) for the ANSR-II Program," by D.P. Mondkar and G.H. Powell - 1980

UCB/EERC-80/23 "Gap-Friction Element (Type 5) for the ANSR-II Program," by D.P. Mondkar and G.H. Powell - 1980

UCB/EERC-80/24 "U-Bar Restraint Element (Type 11) for the ANSR-II Program," C. Oughourlian and G.H. Powell - 1980

UCB/EERC-80/25 "Testing of a Natural Rubber Base Isolation System by an Explosively Simulated Earthquake," by J.M. Kelly 1980

UCB/EERC-80/26 "Input Identification from Structural Vibrational Response," by Y. Hu - 1980

UCB/EERC-80/27 "Cyclic Inelastic Behavior of Steel Offshore Structures," by V.A. Zayas, S.A. Mahin and E.P. Popov - 1980

UCB/EERC-80/28 "Shaking Table Testing of a Reinforced Concrete Frame with Biaxial Response," M.G. Oliva and R.W. Clough 1980

UCB/EERC-80/29 "Dynamic Properties of a Twelve-Story Prefabricated Panel Building," by J.G. Bouwkamp, J.P. Kollegger and R.M. Stephen - 1980

UCB/EERC-80/30 "Dynamic Properties of a Eight-Story Prefabricated Panel Building," by J.G. Bouwkamp, J.P. Kollegger and R.M. Stephen - 1980

UCB/EERC-80/31 "Predictive Dynamic Response of Panel Type Structures Under Earthquakes," by J.P. Kollegger and J.G. Bouwkamp 1980

UCB/EERC-80/32 "The Design of Steel Energy-Absorbing Restrainers and their Incorporation into Nuclear Power Plants for Enhanced Safety: Vol 3, Testing of Commercial Steels in Low-Cycle Torsional Fatigue," by P. Spencer, E.R. Parker, E. Jongewaard and M. Drory - 1980

UCB/EERC-80/33 "The Design of Steel Energy-Absorbing Restrainers and their Incorporation into Nuclear Power Plants for Enhanced Safety: Vol 4, Shaking Table Tests of Piping Systems with Energy-Absorbing Restrainers," by S.F. Stiemer and W.G. Godden - 1980

UCB/EERC-80/34 "The Design of Steel Energy-Absorbing Restrainers and their Incorporation into Nuclear Power Plants for Enhanced Safety: Vol 5, Summary Report," by P. Spencer 1980

UCB/EERC-80/35 "Experimental Testing of an Energy Absorbing Base Isolation System," by J. Kelly, M.S. Skinner and K.E. Beucke - 1980

UCB/EERC-80/36 "Simulating and Analyzing Artificial Non-Stationary Earthquake Ground Motions," by R.F. Nau, R.M. Oliver and K.S. Pister - 1980

UCB/EERC-80/37 "Stochastic Seismic Analysis of Nuclear Power Plant Structures and Piping Systems Subjected to Multiple Support Excitations," by M.C. Lee and J. Penzien - 1980

UCB/EERC-80/38 "Inelastic Seismic Analysis of Large Panel Buildings," by V. Schricker and G.H. Powell - 1980